ISSN 1732-9353
eISSN 2543-7496

Scientific Review

Engineering and Environmental Sciences

Przegląd Naukowy
Inżynieria i Kształtowanie Środowiska

Vol. 30 (2) 2021 Issue 92
Quarterly

Scientific Review Engineering and Environmental Sciences Vol. 30 (2) 2021 Issue 92

SCIENTIFIC REVIEW
ENGINEERING AND ENVIRONMENTAL SCIENCES
Quarterly

The list of reviewers is published in the last issue of the volume and on the http://iks_pn.sggw.pl

EDITORIAL OFFICE ADDRESS
Wydział Budownictwa i Inżynierii Środowiska SGGW
ul. Nowoursynowska 159, 02-776 Warsaw, Poland
tel. (+48 22) 59 35 363, 59 35 210, 59 35 302
e-mail: srees@sggw.edu.pl
http://iks_pn.sggw.pl

ISSN 1732-9353
e-ISSN 2543-7496

Printed version of the Scientific Review Engineering and Environmental Sciences is primary version

All papers are indexed in the data bases as follows: AGRO(Poznań), BazTech, Biblioteka Nauki, **CrossRef**, **DOAJ**, **Google Scholar**, **Index Copernicus**, INFONA, POL-Index, **SCOPUS**, SIGŻ(CBR)

Scientific Review

Engineering and Environmental Sciences

Przegląd Naukowy

Inżynieria i Kształtowanie Środowiska

Vol. 30 (2) 2021 Issue 92

Contents

Editorial work – Anna Dołomisiewicz, Elżbieta Wojnarowska

ISSN 1732-9353 eISSN 2543-7496

Printing: Libra-Print, al. Legionów 114B, 18-400 Łomża

Scientific Review – Engineering and Environmental Sciences (2021), 30 (2), 221–235
Sci. Rev. Eng. Env. Sci. (2021), 30 (2)
Przegląd Naukowy – Inżynieria i Kształtowanie Środowiska (2021), 30 (2), 221–235
Prz. Nauk. Inż. Kszt. Środ. (2021), 30 (2)
http://iks.pn.sggw.pl
DOI 10.22630/PNIKS.2021.30.2.19

Alaa M. Al-LAMI, Yaseen K. Al-TIMIMI, Hasanain K.A. Al-SHAMARTI

Mustansiriyah University, College of Science

Spatiotemporal analysis of some extreme rainfall indices over Iraq (1981–2017)

Key words: extreme precipitation, RClimDex, ETCCDI, climate change, OLS, Iraq

Introduction

Global warming influences the global average increase in temperature which has a significant effect on regional precipitation by changing the thermodynamic properties of both sea and land (Lee, Lee & Julien, 2018; Ding, Lu & Wang, 2019). Regional and local flooding, droughts, and snowstorms caused by extreme weather conditions have environmental impacts on the progress of forests, animals, agriculture, and socio-economic (Knapp et al., 2008; Xiong et al., 2019). Precipitation is one of the most significant environmental factors for diagnosing climate change and may also determine the regional-scale eco-environmental approach to climate change (Subba, Ma & Ma, 2019).

A great deal of research work has been done around the world to study extreme weather events based on some extreme indices. These extreme indices can be defined either based on the probability of occurrence of given quantities or according to threshold exceedances (Seneviratne, Pal, Eltahir & Schär, 2002; Bartolomeu, Carvalho, Marta-Almeida, Melo-Gonçalves & Rocha, 2018). The indices suggested by the Expert Team on Climate Change Detection Monitoring and Indices are commonly used (Parracho, Melo-Gonçalves & Rocha, 2016). Globally, the fluctuations and trends of extreme precipitations have shown substantial spatial variation (Alexander et al., 2006; Li & Hu, 2019). Asadieh and Krakauer (2015) study the patterns of global average precipitation. They noticed that 66.2% of their examined gridded points displayed a positive pattern in South America, Australia, and India over the past 110 years, 18% of which were statistically relevant at the 95% confidence levels (Asadieh & Krakauer, 2015). Many studies from different re-

gions indicated though, that extreme events in precipitation did not have the same regional continuity as extreme temperatures (Lovino, Garcia & Baethgen, 2014; Tan, Ibrahim, Cracknell & Yusop, 2017; Forestieri et al., 2018). Alexander et al. (2006) suggested that alterations in precipitation were significantly globally risen and prevalent. CMIP3 and CMIP5 model output suggested an increase in the global average of daily precipitation levels from about 6 to 7% over 20-year period (Dai, 2006). Several researchers have also illustrated the important role of patterns of large-scale circulation in the optimistic pattern in rainfall anomaly events (Kenyon & Hegerl, 2010). In the Middle East, several studies investigated extreme rainfall patterns (Balling, Keikhosravi, Kiany, Sen Roy & Khoshhal, 2016; Gado, El-Hagrsy & Rashwan, 2019; Tongal, 2019). Alijani, O'Brien and Yarnal (2008) noticed that about 20% of the land area was at significant rainfall risk. The most intense heavy rainfall events were faced primarily by the warm, dry southern coast and the western slopes of the major north-south chain, the Zagros Mountains. Sensoy et al. (2013) show that there are strong consistent warming trends throughout Turkey impacting both high and minimum temperatures, but precipitation shifts are far more complex. Using long-term average rainfall data (1965–2015), Salman with research colleagues investigated the unidirectional patterns in rainfall and rainfall-related extremes in Iraq. The findings indicated that the region has suffered a long period of drought (Salman et al., 2018).

This research work aimed to study the behavior of extreme rainfall phenomena in Iraq. The proposed approach firstly divided the area of study into three distinguished regions. Then a spatiotemporal distribution of 10 extreme precipitation indices was analyzed for Iraq by using the daily data time series 1981–2017. The analyses were done using the RClimDex package and ArcMap 10.4 software.

Material and methods

The study area and data source

Iraq is located in the southwestern part of Asia, with an estimated area of 438,320 km^2. It is surrounded by many countries, Turkey at the north, Iran in the eastern part, the southwestern part with Kuwait, and the Persian Gulf, and the southern part with Saudi Arabia. Also, it is located between the latitudes 37°22′N in the northern part with Turkey and 29°5′N in the southern part with Saudi Arabia, also, Iraq is located between the longitudes 38°45′E, which bordered the Syrian desert and 48°45′E nearly to Shatt Al-Arab (Adeeb & Al-Timimi, 2019; Al--Shamarti, Manji & Albw Jbianah, 2019). The climate of Iraq is generally subtropical and semi-arid, except for the mountainous northern and northern east parts that have a Mediterranean climate. Most of the rainfall occurs between December and April, and the annual average ranges between 100 and 900 mm. The mountainous region in northern Iraq has significantly more rainfall than the central and southern regions. Nearly 90% of the annual precipitation occurs between November and April. Annual average rainfall was measured at 216 mm. Winters are mild and dry, with a daytime

temperature falling to 2°C at night with a chance of frost. Summers are dry and hot to very hot, with shade temperatures reaching 43°C in July and August, but falling to 26°C in the winter (Al-Lami, Al-Timimi & Al-Salihi, 2014). A dataset of daily rainfall of the period 1981 to 2017 for 36 meteorological stations was used in this study. This dataset was obtained from the official website of the NASA with a spatial resolution (0.5° latitude × 0.5° longitude). Figure 1 shows the geographical distribution of the selected station on the Iraq map.

The spatial distribution of rainfall is more realistic and accurate in mountainous terrain when elevation dependence is considered (Al-Ahmadi & Al--Ahmadi, 2013; Song et al., 2019). Since the rainfall average varies from one region to another, the study area was divided into three regions depending on the k-mean method. Region 1 (northern) includes seven stations (Dukcan, Emadia, Sulaymaniyah, Salahaddin, Zakho, Duhook, and Erbil); Region 2 (middle) includes 10 stations (Sinjar, Mosul, Rabiah, Kirkuk, Tel-Afer, Khanaqin, Tuz, Baiji, Tikrit, and Samaraa); Region 3 (southern) includes 19 stations (Amara, Basrah, Anah, Kut, Qaim, Fao, Hai, Hadithah, Nasiriya, Heet, Ramadi, Baghdad, Rutba, Diwaniya, Hella, Samawa, Najaf, Kerbela, and Nukheb) – Figure 2. To test the suitability and accuracy of the study data, the RClimDex package in R software was used to submit all the rainfall data to a high-quality control. The quality control procedures included replacing the missing data with –99.99, label negative data on the average precipitation as erroneous data, and checking the abnormality of selected data by considering all daily data that exceeding

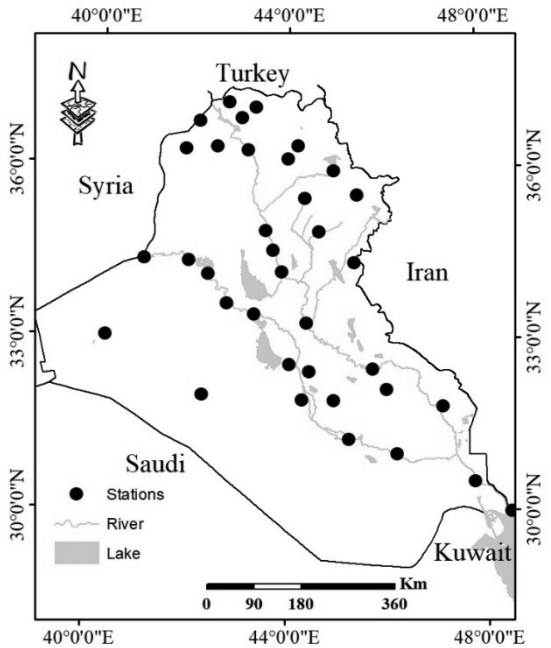

FIGURE 1. The geographical location of grids corresponding to the stations in the study area (Iraq)

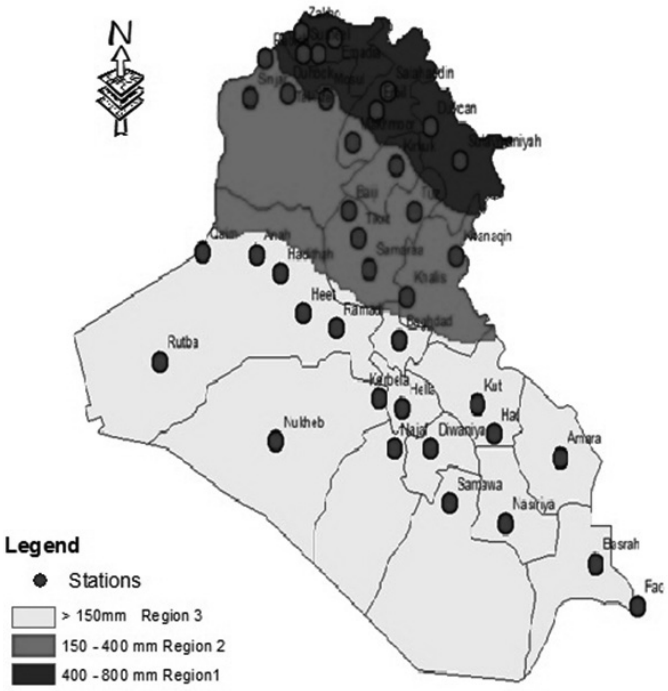

FIGURE 2. Classification of rainfall regions of the study area (Iraq)

the standard deviation for five times as (not available). An analysis of the visual data graphs was established to check the abnormal values. Abnormal values were omitted and adjusted based on statistical analyses and data from neighboring stations (Zhang & Yang, 2004).

Rainfall indices

The extreme rainfall indices were calculated using RClimDex for the daily rainfall data of 36 meteorological stations in Iraq. This package is recommended by the Expert Team on Climate Change Detection and Indices (ETCCDI). The RClimDex has been developed by Zhang and Yang (2004). Providing easy-to-use software for estimating extreme climate indices. From the 27 indices established by the ETCCDI, 11 indices were assigned to determine indices of extreme rainfall. Ten indices are selected to quantify extreme rainfall events in Iraq, and these indices are widely used to study the spatiotemporal analysis of extreme rainfall. Ten indices were classified into two groups. The first one is rainfall days include (CDD, CWD, R10, and R20). The other group is rainfall total contain (PRCPTOT, SDII, R95, R99, RX1day, and RX5day). The table shows the specific details of these indices.

Trends of the rainfall indices were computed using the ordinary least square method (OLS). To determine the slope magnitude, the OLS used a linear model. Linear *p*-value trends of less than 0.10 were considered statistically significant in this study.

TABLE. List of extreme precipitation indices, as adopted from (Dos Santos, de Brito, Júnior & Dantas, 2012)

Indices	ID	Name	Description
Rainfall total [mm]	PRCPTOT	Annual total wet day rainfall	Annual total from days ≥ 1 mm rainfall
	SDII	Simple daily intensity index	Ratio of annual total to WD in a year
	R95p	Very wet days	Annual total rainfall of days in > 95th percentile
	R99p	Extremely wet days	Annual rainfall of days in > 99th percentile
	RX1day	Max 1-day rainfall amount	Annual maximum 1-day rainfall
	RX5day	Max 5-day rainfall amount	Annual maximum consecutive 5-day rainfall
Rainfall days [mm]	CDD	Consecutive dry days	Maximum number of consecutive dry days (rainfall of < 1 mm)
	CWD	Consecutive wet days	Maximum number of consecutive wet days (rainfall of ≥ 1 mm)
	R10mm	Number of heavy rainfall days	Annual count of days when rainfall is ≥ 10 mm
	R20mm	Number of very heavy rainfall days	Annual count of days when rainfall is ≥ 20 mm

Results and discussion

Temporal analysis of extreme rainfall indices

Depending on the rainfall values of all the considered stations and by using the k-mean algorithm, the study area was divided into three regions, northern, middle, and southern from 1981 to 2017. The annual time series of ten extreme rainfall indices in the study regions (northern, middle, and southern Iraq) are shown in Figures 3–8. In Figures 3 and 4, the rainfall indices in the northern region of Iraq showed an increasing trend during 1981–2017. A significant increase trend was distinguished for PRCPTOT with a rate of change of 2.625 mm per year. This is due to the effects of low-pressure system which cause a high intensity of rainfall especially in the northern regions of Iraq. The trends of SDII significantly increased with a change rate of 0.038 mm per day per year. The regional values of RX1day and RX5day were similar, and the rate of positive trend 0.348 and 0.722 mm per year, respectively. R95p and R99p showed a high value of slope with a rate of 2.54 and 1.38 mm per day, respectively. Regarding rainfall days indices in this northern region, CDD and R10 showed a significant increase in the trend with a rate of change of 0.87 and 0.14 when compared to the trend of SDII

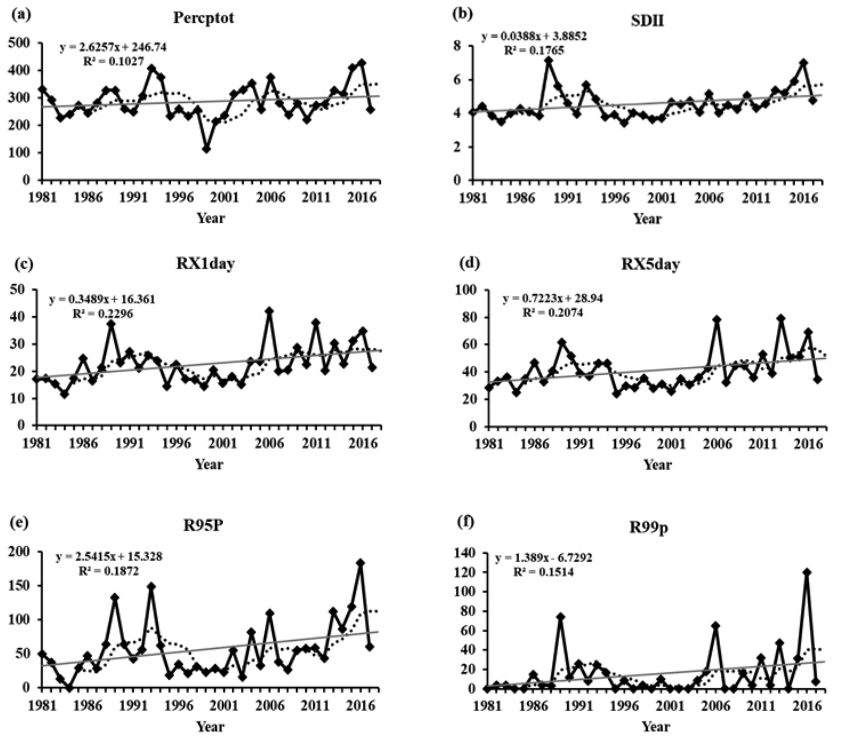

FIGURE 3. Temporal variations for the northern region of extreme rainfall total indices: a – PRCPTOT; b – SDII; c – RX1day; d – RX5day; e – R95; f – R99 respectively. The solid grey line is the linear trend, the solid black line is the annual variations and the dotted black line is the five-year smoothing average

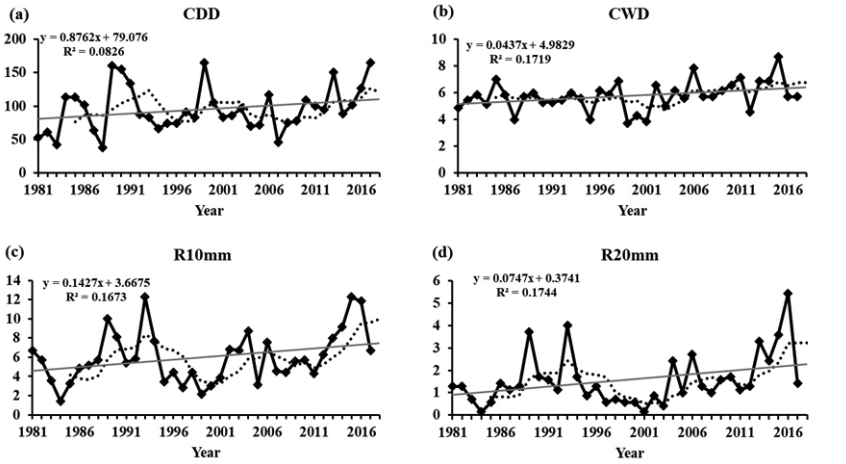

FIGURE 4. Temporal variations for the northern region of extreme rainfall days indices: a – CDD; b – CWD; c – R10; d – R20 respectively. The solid grey line is the linear trend, the solid black line is the annual variations and the dotted black line is the five-year smoothing average

and R20. All indices showed a significant increase during the last 10 years. The reason for this significant increase could be due to the El Niño-Southern Oscillation (ENSO) cold (La Niña) phases in various parts of the world and its impact on the climatic events on these regions. Additionally, the five years moving average slope showed that there were three-clear peaks for most indices that occurred during 2015, 2006, and 1993. The result of the temporal distribution for the ten indices on the surrounding countries like Iran, Turkey and also in China showed an upward trend for all these indices (Sensoy et al., 2013; Balling et al., 2016; Ding et al., 2019).

Figures 5 and 6 illustrate the middle region (Region 2). It can be seen that this region has a positive trend that appeared for all indices. Precipitation total indices showed a high increase in PRCPTOT and R95p with a change rate of 3.26 mm per day per year and 1.61 mm per year, respectively. A low rate of change was noted for other indices, especially in SDII and RX1day. There was no significant increase in the trend in rainfall days' indices, except a high trend that appeared in CDD 0.5 days.

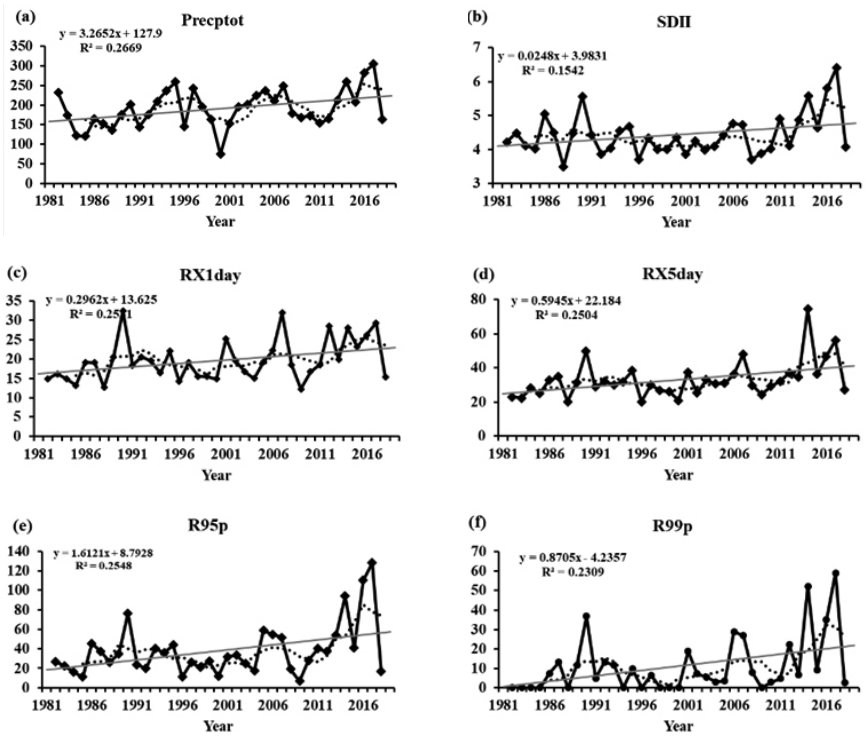

FIGURE 5. Temporal variations for the middle region of extreme rainfall total indices: a – PRCPTOT; b – SDII; c – RX1day; d – RX5day; e – R95; f – R99 respectively. The solid grey line is the linear trend, the solid black line is the annual variations and the dotted black line is the five-year smoothing average

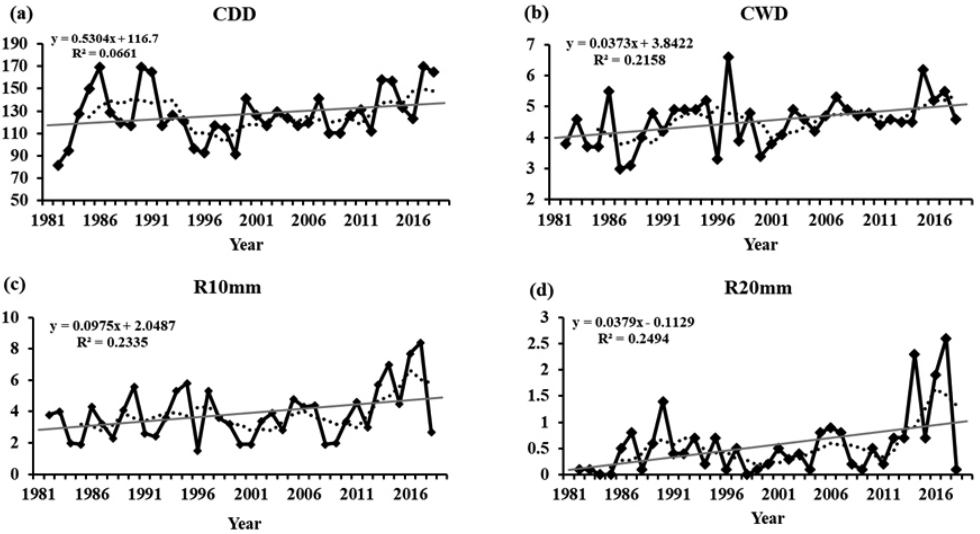

FIGURE 6. Temporal variations for the middle region of extreme rainfall days indices: a – CDD; b – CWD; c – R10; d – R20 respectively. The solid grey line is the linear trend, the solid black line is the annual variations and the dotted black line is the five-year smoothing average

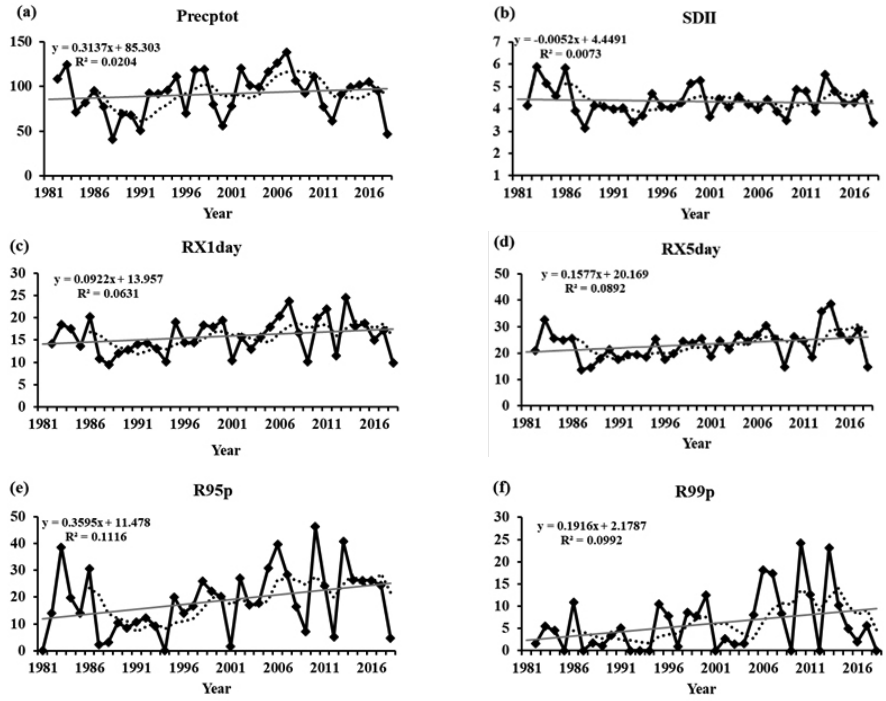

FIGURE 7. Temporal variations for the southern region of extreme rainfall total indices: a – PRCPTOT; b – SDII; c – RX1day; d – RX5day; e – R95; f – R99 respectively. The solid grey line is the linear trend, the solid black line is the annual variations and the dotted black line is the five-year smoothing average

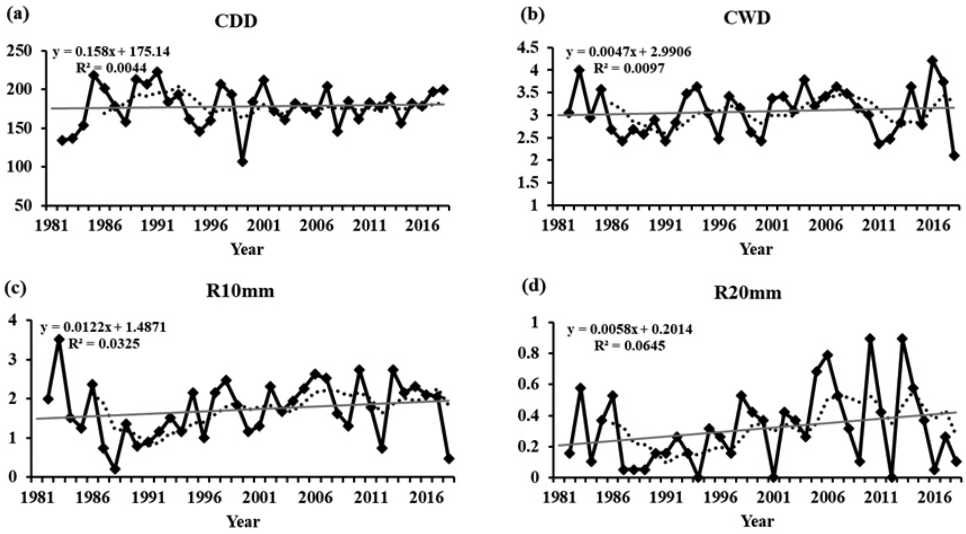

FIGURE 8. Temporal variations for the southern region of extreme rainfall days indices: a – CDD; b – CWD; c – R10; d – R20 respectively. The solid grey line is the linear trend, the solid black line is the annual variations and the dotted black line is the five-year smoothing average

Figures 7 and 8 illustrate Region 3 which represents the southern parts of Iraq, where only SDII showed a negative trend with a rate of –0.0052 mm per year. Other indices showed a less increase in the trend compared to that of the middle and northern regions. Spatial analysis indicated that most western and southerner stations included in this region showed a negative trend for most indices which led to low values of trend increasing in the third region.

Spatial analysis of extreme rainfall indices

Ten rainfall indices were divided into two groups, the first group was (PRCPTOT, SDII, R95, R99, RX1day, and RX5day), and the second group of indices (CDD, CWD, R10, and R20). The spatial distribution of rainfall total indices during 1981–2017 is shown in Figure 9. The high PRCPTOT value occurred mainly in the northwestern region of Iraq, and the low values were distributed primarily in the southwestern regions. The values of PRCPTOT fluctuated between 45.6 mm per year, which appeared in Nukheb station, and 357 mm per year in Zakho station.

Herein 39% of stations showed PRCPTOT values less than 100 mm per year, 22% of stations showed a negative trend of PRCPTOT, and these stations were distributed primarily in the western parts of Iraq, except Basra and Fao stations, in the south of Iraq. A higher positive trend value appeared in Tuz, Khanqinand, and Zakho (4.6, 4.55, and 4.04 mm per year, respectively). The spatial distribution of this index revealed that the wetter region was in northwestern Iraq. Significantly high values of SDII appeared generally in the northern and eastern regions of Iraq, and

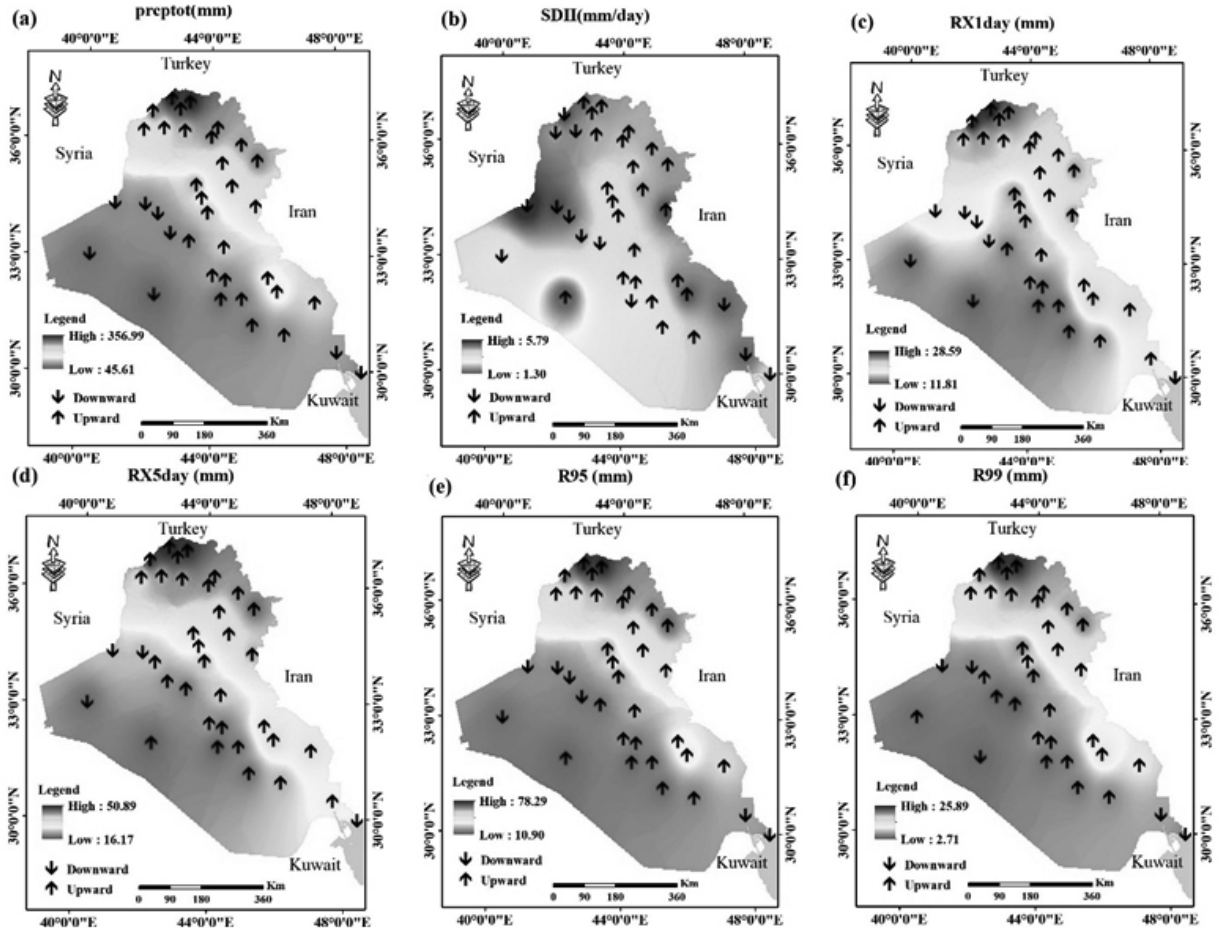

FIGURE 9. Spatial distribution of extreme rainfall total indices: a – PRCPTOT; b – SDII; c – RX1 day; d – RX5day; e – R95; f – R99 respectively over Iraq

approximately 79% of SDII values were more than 4 mm per day per year. A lower SDII value was recorded at Nukheb in the southeastern of Iraq (1.2 mm per day per year), because this site represents the most drier site in Iraq according to records of the total rainfall in this station. A percent of 36% of the stations revealed a negative SDII value, the lowest significant trend was at Qaim –0.054 and the highest trend appeared in Kirkuk 0.067. The values of RX1day and RX5day also indicated a similar distribution, and the highest values of these indices appeared mainly in the stations lies north 36° latitude, while the lowest value was at the western parts of Iraq. Additionally, Najaf station indicated a low value of both indices 11.8 and 16.6 mm per year, respectively. A negative trend appeared in 19.4% of RX1day and 11% of RX5day. Anah and Qaim displayed a significant negative trend for both indices –0.19 and –0.14. The indices of very wet days R95p and extremely wet days R99p ranged from 10.9–78.3 to 2.7–25.9 mm per year, respectively. However, both indices in the northwest part of Iraq were more extreme. The pattern of R95p and R99p distribution also showed similarity, where the lowest value appeared in the western part of Iraq chiefly in Heet, Najaf, and Rutba, but the highest values appeared in both Zakho and Emadiyah. A negative trend indicated only in 11.4% of stations. According to RX1day and RX5day, only five stations showed a negative trend (Anah, Basrah, Fao, Nukheb, and Qaim). Significant positive trends for both indices were indicated in Sulaymaniyah and Dukan. Concerning the above six indices, northern and eastern parts of Iraq showed positive trends with a high probability of extreme rainfall in these regions. The cause can be attributed to the elevation influence of increased relief amplitude on airflow variability, and the elevation of topography has caused the northern parts of Iraq to rainfall more than other regions. Conversely, the low trend appeared mainly in the western and southern parts of Iraq. Another reason for trending in extreme rainfall in this area could be the event ENSO. Recent ENSO studies have established a significant climatic correlation between the anomaly of rainfall and both the Southern Oscillation warm (El Niño) and cold (La Niña) phases in various parts of the world (Ding et al., 2019; Xiong et al., 2019). Regarding the spatial analysis of extreme rainfall days (Fig. 10). The CDD values exhibited a significant increase from the northwestern to the southwestern of Iraq, between 66 days at Samara and 197 days at Najaf. Seventy eight percent of the stations revealed a positive trend, however, only six stations have significant trends increasing, and most of them were distributed in the northern. Samawah and Samara showed low values of CDD due to the extremely low values of rainfall intensity in these two stations. In contrast, the CWD index spatial trend ranged between 2.1 and 6.7 days per year. The largest concentration of CWD was maintained in the northwest of Iraq. The peak values of CWD were recorded in two stations Emadiayia and Zakho (6.7 and 6.6 days, respectively). The concentration was found to increase with the rise in elevation for the northwestern part of Iraq (Al-Ahmadi & Al--Ahmadi 2013; Song et al., 2019). Only four stations showed negative trends

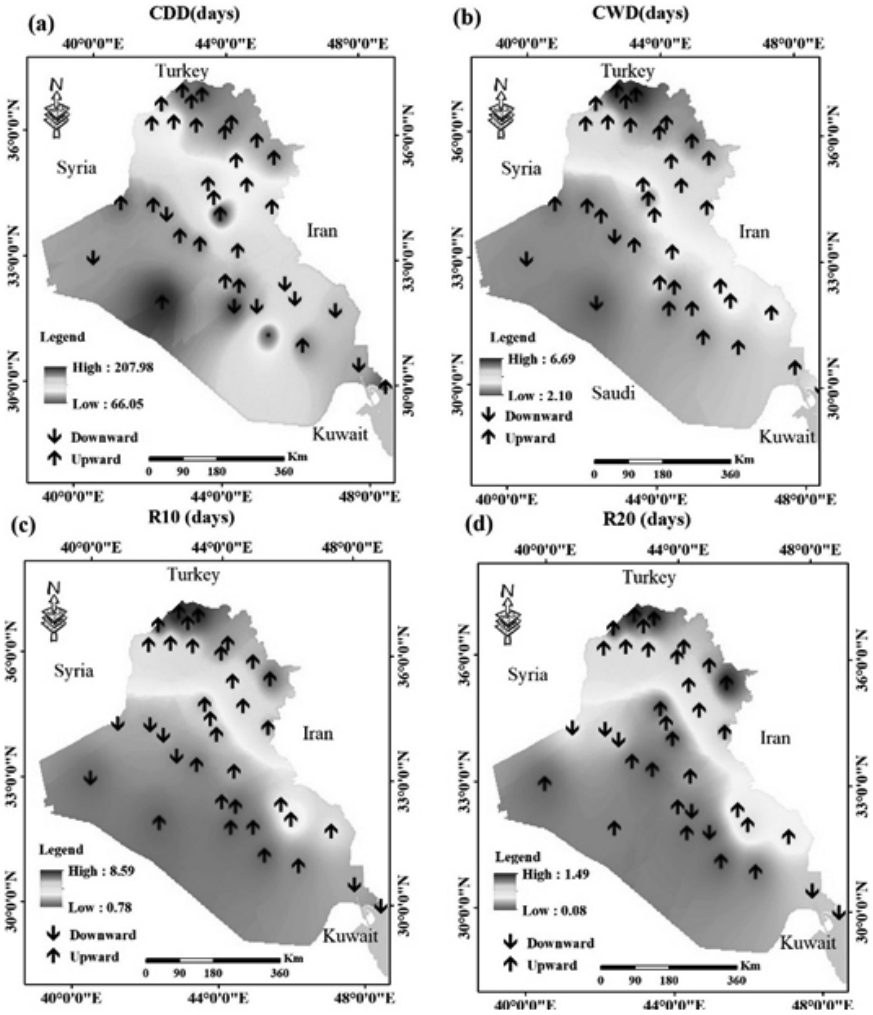

FIGURE 10. Spatial distribution of extreme rainfall days indices: a – CDD; b – CWD; c – R10; d – R20 respectively over Iraq

(Nukheb, Heet, Rutba, and Fao), most of them in the western part of Iraq, except Fao (Fig. 10).

The frequency of annual rainfall day level (R10 mm) index ranged from 0.78 to 8.6 days per year. This index's spatial distribution was close to that of the CWD index, although its higher concentration in northwestern of Iraq. Figure 10 also showed that R10 and R20 values were similar and increased values appeared in the northern parts of Iraq (Hassan, Zeki & Salih, 2018; Al-Nassar, Pelegri, Sangrà, Alarcon & Jansa, 2020). Seven stations for both indices showed a negative trend, most of them dispersed in the west of Iraq. Additionally, all stations showed a non-significant trend increasing,

however, a maximum trend was noted at Khanqin for both indices (0.17 and 0.07 days, respectively).

Conclusions

In this study, we used daily rainfall data from 36 meteorological stations in Iraq to examine the spatiotemporal distribution of extreme rainfall indices using RClimDex package. Ten indices were chosen and divided into two classes: rainfall total (PRCPTOT, SDII, R95, R99, RX1day, and RX5day) and precipitation days (CDD, CWD, R10, and R20). The area of the study was divided into three regions to investigate the temporal characteristics of the time series for extreme rainfall indices. This study came out with several conclusions:

1. High values of rainfall total indices appeared in the northwestern part of Iraq, whereas the lowest values of these indices appeared in western and southern regions. Most of the stations revealed positive trends except seven stations in the western and southern parts of Iraq (Heet, Haditha, Anah, Rutba, Qaim, Nukheb, Fao), which showed a negative trend.
2. Results of rainfall days revealed higher values of consecutive dry days (CDDs) in Najaf and Nukheb stations. Higher values of other indices CWD, R10, R20 appeared mostly at Zakho and Emadiyah in the northern parts of Iraq. The positive trend was non-significant for most rainfall days indices.
3. A high probability of extreme rainfall in the northern and eastern parts of Iraq.
4. Time series analysis of extreme rainfall indices showed a positive increase in the regions under study, except one negative trend appeared in SDII for Region 3. A high rate of change appeared in the north of Iraq, especially for PRCPTOT, R95, and CDD.
5. All indices showed a significant increase during the last 10 years.
6. According to the results of the study we suggest that the Iraqi government needs to take quick actions like designing a national water master plan and implement regional cooperation and coordination.

Acknowledgements

The authors are grateful to the National Aeronautics and Space Administration (NASA) Goddard Earth Sciences Data Information and Services for the provision of the data used in this study.

References

Adeeb, H.Q. & Al-Timimi, Y.K. (2019). GIS techniques for mapping of wind speed over Iraq. *Iraqi Journal of Agricultural Sciences*, *50*(6), 1621-1629.

Al-Ahmadi, K. & Al-Ahmadi, S. (2013). Rainfall-altitude relationship in Saudi Arabia. *Advances in Meteorology*, *2013*, 363029. https://doi.org/10.1155/2013/363029

Alexander, L.V., Zhang, X., Peterson, T.C., Caesar, J., Gleason, B., Klein Tank, A.M.G., Haylock, M., Collins, D., Trewin, B., Rahimzadeh, F., Tagipour, A., Rupa Kumar, K., Revadekar, J., Griffiths, G., Vincent, L., Stephenson, D.B., Burn, Aguilar, E., Brunet, M., Taylor, M., New, M., Zhai, P., Rusticucci, M. & Vazquez-Aguirre, J.L. (2006). Global observed changes in daily climate extremes of temperature and precipitation. *Journal*

of Geophysical Research: Atmospheres, *111*(D5), 1-22.

Alijani, B., O'Brien, J. & Yarnal, B. (2008). Spatial analysis of precipitation intensity and concentration in Iran. *Theoretical and Applied Climatology*, *94*(1), 107-124.

Al-Lami, A.M., Al-Timimi, Y.K. & Al-Salihi, A.M. (2014). The homogeneity analysis of rainfall time series for selected meteorological stations in Iraq. *Diyala Journal for Pure Science*, *10*(2), 60-77.

Al-Nassar, A.R., Pelegrí, J.L., Sangrà, P., Alarcon, M. & Jansa, A. (2020). Cut-off low systems over Iraq: Contribution to annual precipitation and synoptic analysis of extreme events. *International Journal of Climatology*, *40*(2), 908-926.

Al-Shamarti, H.K., Manji, O.B. & Albw Jbianah, M.I.K. (2019). Using monthly rainfall data to estimate rainfall erosivity factor of Iraq. *Scientific Review Engineering and Environmental Sciences*, *28*(3), 444-454.

Asadieh, B. & Krakauer, N.Y. (2015). Global trends in extreme precipitation: climate models versus observations. *Hydrology and Earth System Sciences*, *19*(2), 877-891.

Balling, R.C., Keikhosravi Kiany, M.S., Sen Roy, S. & Khoshhal, J. (2016). Trends in extreme precipitation indices in Iran: 1951–2007. *Advances in Meteorology*, *2016*, 2456809. https://doi.org/10.1155/2016/2456809

Bartolomeu, S., Carvalho, M.J., Marta-Almeida, M., Melo-Gonçalves, P. & Rocha, A. (2016). Recent trends of extreme precipitation indices in the Iberian Peninsula using observations and WRF model results. *Physics and Chemistry of the Earth, Parts A/B/C*, *94*, 10-21.

Dai, A. (2006). Recent climatology, variability, and trends in global surface humidity. *Journal of Climate*, *19*(15), 3589-3606.

Ding, Z., Lu, R. & Wang, Y. (2019). Spatiotemporal variations in extreme precipitation and their potential driving factors in non-monsoon regions of China during 1961-2017. *Environmental Research Letters*, *14*(2), 024005. https://doi.org/10.1088/1748-9326/aaf2ec

Dos Santos, C.A.C., Brito, J.I., de, Júnior, C.H.D.S. & Dantas, L.G. (2012). Trends in precipitation extremes over the northern part of Brazil from Era40 dataset. *Revista Brasileira de Geografia Física*, *5*(4), 836-851.

Forestieri, A., Arnone, E., Blenkinsop, S., Candela, A., Fowler, H. & Noto, L.V. (2018). The impact of climate change on extreme precipitation in Sicily, Italy. *Hydrological Processes*, *32*(3), 332-348.

Gado, T.A., El-Hagrsy, R.M. & Rashwan, I.M.H. (2019). Spatial and temporal rainfall changes in Egypt. *Environmental Science and Pollution Research*, *26*(27), 28228-28242.

Hassan, A.S., Zeki, K.N. & Salih, N.S. (2018). Determination the quantity of extreme rainfall and calculation of the climatology mean for Baghdad City. *Iraqi Journal of Science*, *95*(1B), 447-455.

Kenyon, J. & Hegerl, G.C. (2008). Influence of modes of climate variability on global temperature extremes. *Journal of Climate*, *21*(15), 3872-3889.

Knapp, A.K., Beier, C., Briske, D.D., Classen, A.T., Luo, Y., Reichstein, M., Smith, M.D. & Weng, E. (2008). Consequences of more extreme precipitation regimes for terrestrial ecosystems. *Bioscience*, *58*(9), 811-821.

Lee, J.H., Lee, J.H. & Julien, P.Y. (2018). Global climate teleconnection with rainfall erosivity in South Korea. *Catena*, *167*, 28-43.

Li, X. & Hu, Q. (2019). Spatiotemporal changes in extreme precipitation and its dependence on topography over the Poyang Lake Basin, China. *Advances in Meteorology*, *2019*, 253932. https://doi.org/10.1155/2019/1253932

Lovino, M., García, N.O. & Baethgen, W. (2014). Spatiotemporal analysis of extreme precipitation events in the Northeast region of Argentina (NEA). *Journal of Hydrology: Regional Studies*, *2*, 140-158.

Parracho, A.C., Melo-Gonçalves, P. & Rocha, A. (2016). Regionalisation of precipitation for the Iberian Peninsula and climate change. *Physics and Chemistry of the Earth*, *Parts A/B/C*, *94*, 146-154.

Salman, S.A., Shahid, S., Ismail, T., Rahman, N.B.A., Wang, X. & Chung, E.S. (2018). Unidirectional trends in daily rainfall extremes of Iraq. *Theoretical and Applied Climatology*, *134*(3), 1165-1177.

Seneviratne, S., Pal, J., Eltahir, E. & Schär, C. (2002). Summer dryness in a warmer climate: a process study with a regional climate model. *Climate Dynamics*, *20*(1), 69-85.

Sensoy, S., Türkoğlu, N., Akçakaya, A., Ekici, M., Demircan, M., Ulupinar, Y., Atay, H., Tüvan, A. & Demirbaş, H. (2013). Trends in Turkey climate indices from 1960 to 2010. In *6th International Atmospheric Science Symposium – ATMOS2013. Book of Proceedings*. Istanbul: Istanbul Technical University. Retrieved from http://212.174.109.9/FILES/genel/makale/19_trendsin-turkey.pdf [access 24.06.2020].

Song, L., Chen, M., Gao, F., Cheng, C., Chen, M., Yang, L. & Wang, Y. (2019). Elevation influence on rainfall and a parameterization algorithm in the Beijing area. *Journal of Meteorological Research*, *33*(6), 1143-1156.

Subba, S., Ma, Y. & Ma, W. (2019). Spatial and temporal analysis of precipitation extremities of Eastern Nepal in the last two decades (1997-2016). *Journal of Geophysical Research: Atmospheres*, *124*(14), 7523-7539.

Tan, M.L., Ibrahim, A.L., Cracknell, A.P. & Yusop, Z. (2017). Changes in precipitation extremes over the Kelantan River Basin, Malaysia. *International Journal of Climatology*, *37*(10), 3780-3797.

Tongal, H. (2019). Spatiotemporal analysis of precipitation and extreme indices in the Antalya Basin, Turkey. *Theoretical and Applied Climatology*, *138*(3), 1735-1754.

Xiong, J., Yong, Z., Wang, Z., Cheng, W., Li, Y., Zhang, H., Ye, Ch. & Yang, Y. (2019). Spatial and temporal patterns of the extreme precipitation across the Tibetan Plateau (1986–2015). *Water*, *11*(7), 1453. https://doi.org/10.3390/w11071453

Zhang, X. & Yang, F. (2004). *RClimDex (1.0). User Manual.* Ottawa (ON): Climate Research Branch Environment Canada.

Summary

Spatiotemporal analysis of some extreme rainfall indices over Iraq (1981––2017). Extreme rainfall is one of the environmental hazards with disastrous effects on the human environment. Water resources management is very vulnerable to any changes in rainfall intensities. A spatiotemporal analysis is essential for study the impact of climate change and variability on extreme rainfall. In this study, daily rainfall data for 36 meteorological stations in Iraq during 1981–2017 were used to investigate the spatiotemporal pattern of 10 extreme rainfall indices using RClimDex package. These indices were classified into two categories: rainfall total (PRCPTOT, SDII, R95p, R99p, RX1day, and RX5day) and rainfall days (CDD, CWD, R10, and R20). Depending on the mean annual precipitation data, the study area was divided into three climatic zones to examine the time series features of those 10 indices. Results showed a tendency to increase in precipitation toward the northwestern part of Iraq, and more than 70% of stations achieved a positive trend for most indices. The most frequent negative trend appeared in eight stations distributed in the western and southern parts of Iraq, namely (Heet, Haditha, Anah, Rutba, Qaim, Nukheb, Najaf, and Fao). A significant positive trend appeared obviously in PRCPTOT and R95p with a rate of 0.1–4.6 and 0.5–2.7 mm per year, respectively. Additionally, the least trend increasing appeared in all precipitation days indices specifically in R10 and R20. Time series analyses revealed a positive trend in all regions under study, except SDII in the southern region. The most significant rate of change was noticed in regions one and two (northern and middle parts of Iraq), particularly for PRCPTOT and R95p 3.26 and 2.45 mm per day, respectively. Only the northern and eastern regions of Iraq experienced a high probability of significant extreme rainfall.

Authors' address:
Alaa M. Al-Lami – corresponding author
(https://orcid.org/0000-0003-0641-5015)
Mustansiriyah University
College of Science
Department of Atmospheric Sciences
Palestine Street, 46131 Baghdad
Iraq
e-mail: al.shayia.atmsc@uomustansiriyah.edu.iq

Scientific Review – Engineering and Environmental Sciences (2021), 30 (2), 236–249
Sci. Rev. Eng. Env. Sci. (2021), 30 (2)
Przegląd Naukowy – Inżynieria i Kształtowanie Środowiska (2021), 30 (2), 236–249
Prz. Nauk. Inż. Kszt. Środ. (2021), 30 (2)
http://iks.pn.sggw.pl
DOI 10.22630/PNIKS.2021.30.2.20

Winai SURIYA, Poramate CHUNPANG, Teerawong LAOSUWAN

Mahasarakham University, Faculty Science

Patterns of relationship between PM_{10} from air monitoring quality station and AOT data from MODIS sensor onboard of Terra satellite

Key words: remote sensing, MODIS sensor, PM_{10}, aerosol optical thickness (AOT), air quality index (AQI)

Introduction

Currently, Thailand, especially in the northern region, is encountering air pollutions due to smokes, accumulation of smokes or dust in the air, which are mostly caused by the burning of forest area and open area for agricultural purpose. Also, the terrains in many areas in the northern region are characterized by "pan" shape, with plain areas surrounded by mountains, and the weather is quite still and dry for a long period of time; these are the reason of the accumulation of pollution which cannot be ventilated, therefore, the concentration of pollution is quite high especially in the urban area. This causes such area to encounter the problem of air pollution (Suwanprasit, Charoenpanyanet, Pardthaisong & Sinampol, 2018). Also, there are other causes including more transportation, more burning of forest area and open area (Supasri, Intra, Jomjunyong & Sampattagul, 2018).

Particulate matter (PM) is the particles consisting of nitrogen oxide (NO_x), sulfur dioxide (SO_2), ammonia (NH_3), polycyclic aromatic hydrocarbons (PAHs) which are combined and floating in the air in form of dust; it can be divided by size – the one smaller than 2.5 μm, is called $PM_{2.5}$, and the one smaller than 10 μm is called PM_{10} (Porter & Clarke, 1997; Meng et al., 2019). Dust is the pollution that mostly affects human than other air pollutions. Particulate matter comes from both nature such as soil dust, sand dust, and from the matter on the ground blown by wind, smoke from wild fire, salty particles from seawater

and comes from human activities such as dust from construction, dust from transportation on road, smoke released from exhaust pipe of car and motorcycle, dust and smoke from chimney from crematorium, incinerator of industrial plant, and the burning of agricultural residues in open area (Pollution Control Department [PCD], 2004; Nathapindhu, Sttheetham & Ketkowit, 2011; World Health Organization [WHO], 2017). The danger of dust traveling into the respiratory system depends on the size, quantity, chemical properties, and biological qualities. Dust, once travelling into the respiratory system, would accumulate in various parts of the respiratory system, depending on its size; the rough dust would be filtered by nose hair and thus falling onto the primary respiratory system, and the fine dust and the very fine dust would pass into the bronchus, bronchiole, and deep into the alveoli. If a large quantity of dust is inhaled, it would affect health a lot accordingly (Adams, Greenbaum, Shaikh, van Erp & Russel, 2015; GreenFacts, 2018; United States Environmental Protection Agency [USEPA], 2018).

Particulate matter PM_{10} is the serious problem of air pollution in the northern region, which is mostly caused by the burning of forest area and open area and is clearly seen during January–April of every year (Amphanthong & Busababodhin, 2015). The monitoring of PM_{10} quantity can be done by the inspection performed at the Ground Monitoring Station of Pollution Control Department (PCD) and the Thai Meteorological Department (TMD); it is not possible to install the station in all critical areas due to the fact that the air monitoring device is large, the expense spent in the operation and maintenance is high, and in some monitoring stations it is not possible to perform real-time monitoring which results in the limitation on the monitoring of dust in terms of space and time (Outapa & Ivanovitch, 2019). However, the problem related to dust or PM in the northern region needs to be solved immediately.

According to the related researches, it was found that at present, the remote sensing technology was applied by using data received from the satellite in monitoring and following the air quality situations (Liu, Sarnat, Kilaru, Jacob & Koutrakis, 2005; Kloog, Koutrakis, Coull, Lee & Schwartz, 2011; Nguyen, Cressie & Braverman, 2012; Benas, Beloconi & Chrysoulakis, 2013; Vienneau et al., 2013; Phayungwiwatthanakoon, Suwanwaree & Dasamanda 2014; He & Huang, 2018). The remote sensing is the modern and efficient technology that can be applied to monitor and inspect various phenomena on Earth in time (Sukitpaneenit & Oanh, 2014; Emetere, Sanni, Okoro & Adeyemi, 2018; Rotjanakusol & Laosuwan, 2018, 2019; Uttaruk & Laosuwan, 2019). Due to the importance of monitoring and following up the air quality circumstance, this study aims to find patterns of relationship between PM_{10} from the air quality station and AOT data received from MODIS sensor onboard of Terra satellite in Phrae Province, the northern region of Thailand.

Studying area and satellite data

Studying area. Phrae Province (Fig. 1) is located in the northern region of Thailand, with the area of 6,538.59 km^2, between the latitude of 17.70° to 18.84°N

to the longitude of 99.58° to 100.32°E; it is 155 m high from moderate sea level. The province is surrounded by mountains in four directions; most of the area, about 80%, are mountainous with the plain area of only 20%. The average air temperature in Phrae in the whole year is about 26.4°C, with the average minimum temperature of 21.6°C and with average maximum temperature of 33.2°C.

Data used in the study. Data of Moderate Resolution Imaging Spectroradiometer (MODIS) sensors, the aerosol optical thickness (AOT) on land and ocean would be of the Level 2 Product with the resolution of the image of 10×10 km^2 at and is the near-real-time product data. Therefore, in this study, the data from MODIS sensor onboard of Terra satellite was applied with the code of MODO4_L2 Aerosol Product (Optical_Depth_Land_And_Ocean). The MODO4_L2 Aerosol Product file covers a five-minute time interval. The

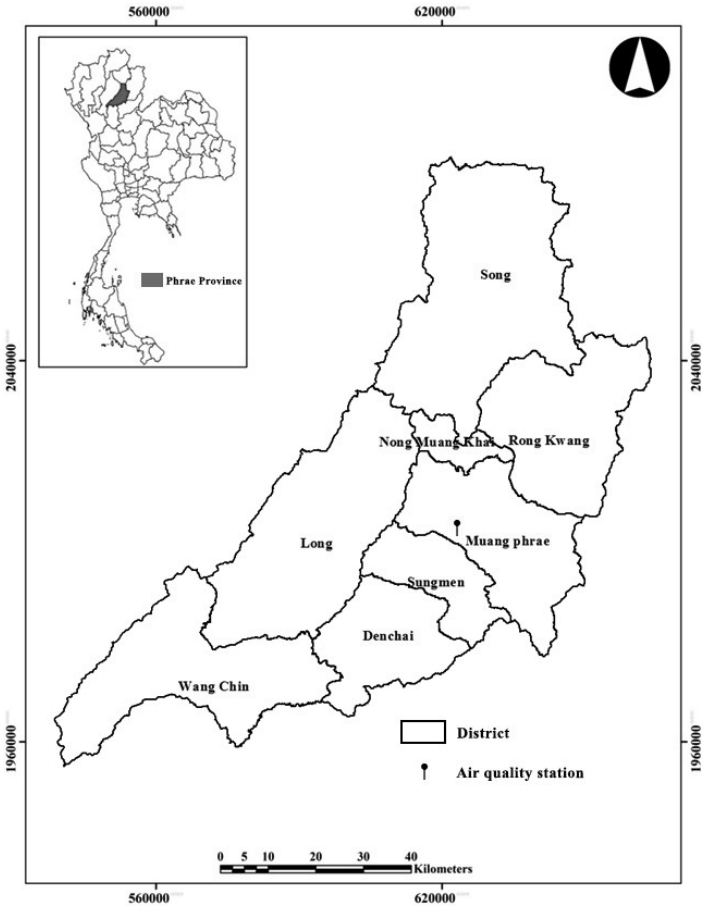

FIGURE 1. Phrae Province, the northern region of Thailand

output grid is 135 pixels in width by 203 pixels in length. Every tenth file has an output grid size of 135 by 204 pixels. The MOD04_L2 Aerosol Product files are stored in hierarchical data format (HDF). The data was downloaded from web interface LAADS DAAC (https://ladsweb.modaps.eosdis.nasa.gov); the duration of 10.00–11.00 am at local time was selected when the MODIS sensor onboard of Terra satellite orbit passes Thailand. Data used were on daily basis from 1st January to 30th April 2018.

Ground temperature data. In this study, the data of PM_{10} on hourly basis was collected in the period from 1st January to 30th April 2018 during 10.00–11.00 am from the air quality station of the air4thai (http://air4thai.pcd.go.th/webV2) located at Mueang District, Phrae Province, located Na Chak Subdistrict, Mueang District, Phrae Province, with the latitude of 18.13°N and longitude of 100.16°E.

Methodology

Since AOT data received from MODIS sensor onboard of Terra satellite is in HDF or granule coverage, so before analyzing AOT data, it is necessary to adjust the projection systems by georeference. In this study, the projection systems were determined to be UTM WGS-84 zone 47; after that, the adjusted data were brought for numerical analysis of AOT further. In this research, the correlation analysis using software package was performed (Eq. 1) to study the relationship between PM_{10} quantity from the air quality station of the air4thai with the AOT data received from Terra MODIS satellite.

$$r = \frac{\sum\left(X_i - \overline{X}\right)\left(Y_i - \overline{Y}\right)}{\sqrt{\sum\left(X_i - \overline{X}\right)^2 \sum\left(Y_i - \overline{Y}\right)^2}} \quad (1)$$

where:
$r = 1$ – perfect positive correlation,
$r = -1$ – perfect negative correlation.

The result of the analysis would yield correlation coefficient (r) which indicated the extent of relationship of the data, for linear regression analysis (Eq. 2), which is one statistical method for examining the relationship between two or more variables; this is divided into independent variable x and dependent variable y. In this research, x is PM_{10} quantity from the air quality station of the air4thai and y is AOT data received from MODIS sensor onboard of Terra satellite at the coordinate of the ground monitoring station.

$$y = ax + b \quad (2)$$

where:
x – independent variable,
y – dependent variable.

Besides, PM_{10} quantity obtained from the monitoring station was brought to replace the value in the linear regression equality of each month in order to see the density of PM_{10} in spatial term. Finally, the distribution map of PM_{10} was created in spatial term under AQI which is the report on the weather in simple and easy-to-understand form in order to disseminate such data to the public so that they could be informed of the air pollution situations. Various countries would have their own AQI – Thailand in this study.

Result of the study

The results of the analysis into the relationship between PM_{10} and AOT by using statistical method that is correlation analysis are shown in Table 1. According to Table 2, it was found that in overall, PM_{10} and AOT are highly related, with the correlation coefficient in January of $r = 0.928$, in February of $r = 0.919$, in March of $r = 0.916$, and in April of $r = 0.927$. The results of the linear regression analysis of duration between January and April are shown in Figures 2–5. In January, the data collection from MODIS sensor onboard of Terra satellite (AOT) and air quality stations (PM_{10}) was shown in Table 2.

TABLE 1. Correlation coefficient (r) between PM_{10} and AOT in Thailand in 2018 in selected months

Month	r
January	0.928
February	0.919
March	0.916
April	0.927

From Figure 2, it shows the relationship between the quantity of PM_{10} and AOT in January of Phrae Province; when PM_{10} increased, AOT would increase accordingly. On the contrary, when PM_{10} decreased, AOT would also decrease. According to the linear regression analysis, it was found that the minimum PM_{10} was 30 $\mu g \cdot m^{-3}$ and maximum PM_{10} was 79 $\mu g \cdot m^{-3}$. The linear regression equality $y = 97.679x - 0.7215$ and the coefficient in making decision of r^2 was 0.983.

In February, the data collection from MODIS sensor onboard of Terra satellite (AOT) and air quality stations (PM_{10}) was shown in Table 3.

TABLE 2. Data collected from MODIS sensor onboard of Terra satellite and the air quality stations in Thailand in January 2018

Date	AOT	PM_{10} [$\mu g \cdot m^{-3}$]	Date	AOT	PM_{10} [$\mu g \cdot m^{-3}$]
5	0.309	30	19	0.408	41
6	0.325	31	20	0.457	46
7	0.358	34	21	0.498	48
8	0.601	59	22	0.553	52
9	0.481	45	23	0.715	71
10	0.449	42	24	0.708	70
11	0.426	41	25	0.562	55
12	0.384	36	26	0.821	79
14	0.393	36	27	0.801	76
15	0.452	44	28	0.547	57
16	0.391	38	29	0.485	49
17	0.486	46	30	0.491	45
18	0.479	43	31	0.624	57

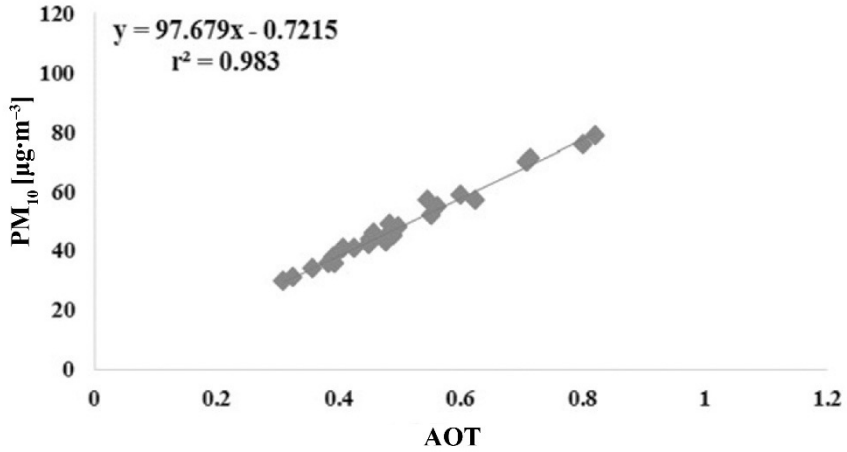

FIGURE 2. Linear regression between PM_{10} and AOT in Thailand in January 2018

TABLE 3. Data collected from MODIS sensor onboard of Terra satellite (AOT) and the air quality stations (PM_{10}) in Thailand in February 2018

Date	AOT	PM_{10} [µg·m^{-3}]	Date	AOT	PM_{10} [µg·m^{-3}]
1	0.603	61	14	0.726	71
2	0.521	51	15	0.887	89
3	0.694	68	16	0.862	84
4	0.635	62	17	0.712	70
5	0.782	75	18	0.631	68
6	0.891	86	19	0.993	97
7	0.973	91	20	0.922	93
8	0.987	96	21	0.876	85
9	1.108	102	23	0.472	44
10	0.921	93	25	0.486	47
11	0.902	94	26	0.553	52
12	0.915	97	28	0.476	48
13	0.841	81			

From Figure 3, it shows the relationship between the quantity of PM_{10} and AOT in February of Phrae Province; when PM_{10} increased, the AOT would increase accordingly. On the contrary, when PM_{10} decreased, AOT would also decrease. According to the linear regression analysis, it was found that the minimum PM_{10} was 44 µg·m^{-3} and maximum PM_{10} was 102 µg·m^{-3}. The linear regression equality $y = 96.643x + 1.3248$ and the coefficient in making decision of r^2 was 0.9719.

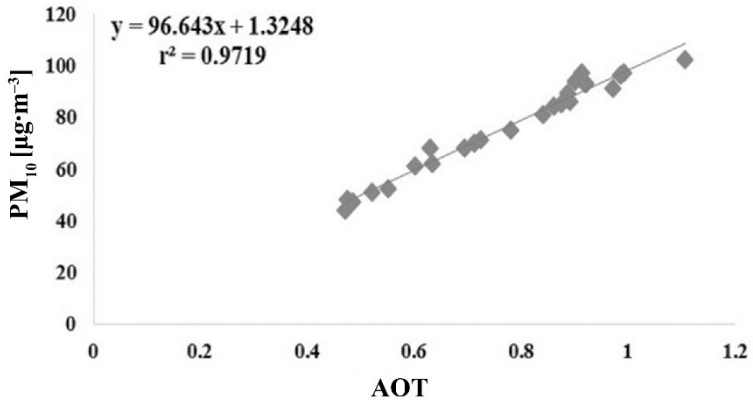

FIGURE 3. Linear regression between PM_{10} and AOT in Thailand in February 2018

In March, the data collection from Terra MODIS satellite (AOT) and air quality stations (PM_{10}) was shown in Table 4.

From Figure 4, it shows the relationship between the quantity of PM_{10} and AOT in March of Phrae Province; when PM_{10} increased, the AOT would increase accordingly. On the contrary, when PM_{10} decreased, AOT would also decrease. According to the linear regression analysis, it was found that the minimum PM_{10} was 58 $\mu g \cdot m^{-3}$ and maximum PM_{10} was

TABLE 4. Data collected from Terra MODIS satellite (AOT) and the air quality stations (PM_{10}) in Thailand in March 2018

Date	AOT	PM_{10} [$\mu g \cdot m^{-3}$]	Date	AOT	PM_{10} [$\mu g \cdot m^{-3}$]
2	0.587	76	18	0.681	86
3	0.596	77	19	0.807	98
4	0.773	93	20	0.954	112
5	1.064	118	21	1.136	132
6	1.663	184	22	0.975	101
7	1.134	139	23	0.682	88
8	0.981	112	24	0.691	88
9	0.394	58	25	0.741	91
11	0.403	59	26	0.809	100
13	0.449	63	27	0.748	92
14	0.561	76	28	0.759	92
15	0.846	107	29	0.862	102
16	0.908	112	30	0.754	93
17	0.795	97	31	0.783	91

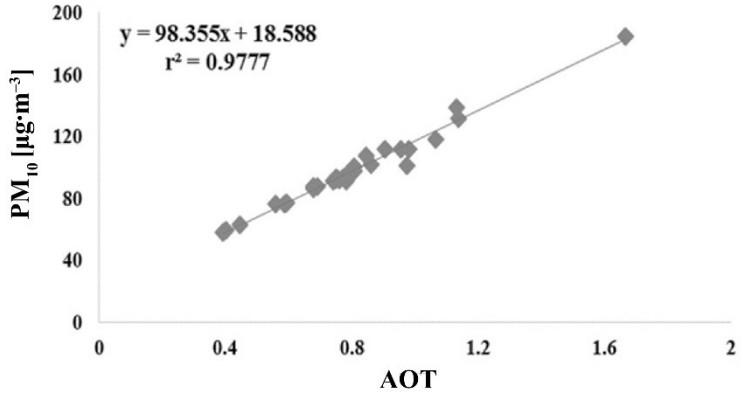

FIGURE 4. Linear regression between PM_{10} and AOT in Thailand in March 2018

184 µg·m^{-3}. The linear regression equality $y = 98.335x + 18.588$ and the coefficient in making decision of r^2 was 0.9777.

In April, the data collection from MODIS sensor onboard of Terra satellite (AOT) and air quality stations (PM_{10}) was shown in Table 5.

From Figure 5, it shows the relationship between the quantity of PM_{10} and AOT in April of Phrae Province; when PM_{10} increased, AOT would increase accordingly. On the contrary, when PM_{10} decreased, AOT would also decrease. According to the linear regression analy-

TABLE 5. Data collected from MODIS sensor onboard of Terra satellite (AOT) and the air quality stations (PM_{10}) in Thailand in March 2018

Date	AOT	PM_{10} [µg·m^{-3}]	Date	AOT	PM_{10} [µg·m^{-3}]
1	0.782	56	17	0.526	32
2	0.754	52	19	0.572	37
3	0.761	50	20	0.754	56
4	0.857	66	21	0.952	74
5	0.731	53	22	1.132	90
7	0.586	37	23	1.053	87
9	0.706	51	24	1.204	99
10	0.701	47	25	1.426	114
11	0.864	65	26	0.857	65
12	0.947	78	27	0.535	32
13	1.065	84	28	0.554	31
14	1.075	82	29	0.493	21
15	1.063	85	30	0.482	24
16	0.725	54			

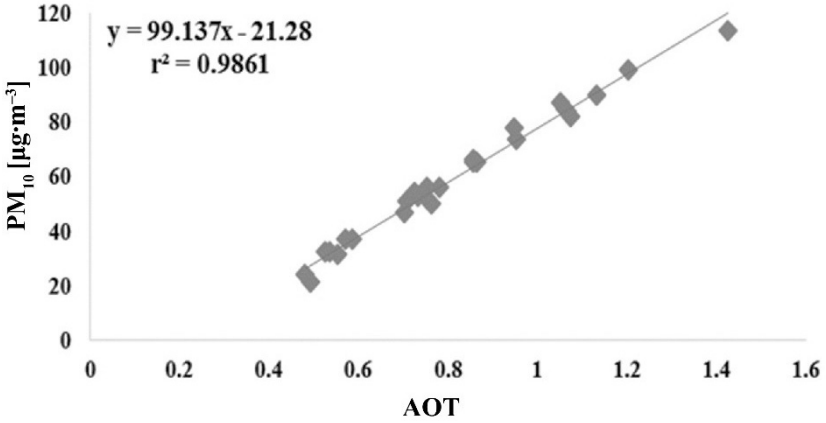

FIGURE 5. Linear regression between PM_{10} and AOT in Thailand in April 2018

sis, it was found that the minimum PM_{10} was 21 $\mu g \cdot m^{-3}$ and maximum PM_{10} was 114 $\mu g \cdot m^{-3}$. The linear regression equality $y = 99.137x - 21.28$ and the coefficient in making decision of r^2 was 0.9861.

Furthermore, the result of the distribution map creation of PM_{10} in spatial term under AQI of Thailand (Table 6) to show that whether PM_{10} has effect on the health or not can be seen from the entire Figure 6. According to Figure 6a, it was found that Phrae Province had air of good quality and moderate quality in January; the people can do outdoor activities and tour normally. From Figure 6b, it was found that Phrae Province had good quality of air and moderate quality of air and the quality of air affected the health in February. The people who live in the blue area and green area can do outdoor activities and tour normally; and the people who live in yellow zone can do outdoor activities normally except for someone who is vulnerable was found to have primary symptom such as cough, being hard to breathe, eye irritation; so, the period of time to do outdoor activities should be reduced. According to Figure 6c, it was found that Phrae Province had moderate quality and the quality of air affected the health in March. The people who live in the blue area and green area can do outdoor activities and tour normally; and the people who live

TABLE 6. Criteria for AQI in Thailand

AQI	PM_{10} [$\mu g \cdot m^{-3}$]	Levels of health concern	Colors
0–25	0–50	very good	blue
26–50	51–80	good	green
51–100	81–120	moderate	yellow
101–200	121–180	unhealthy	orange
> 201	181	very unhealthy	red

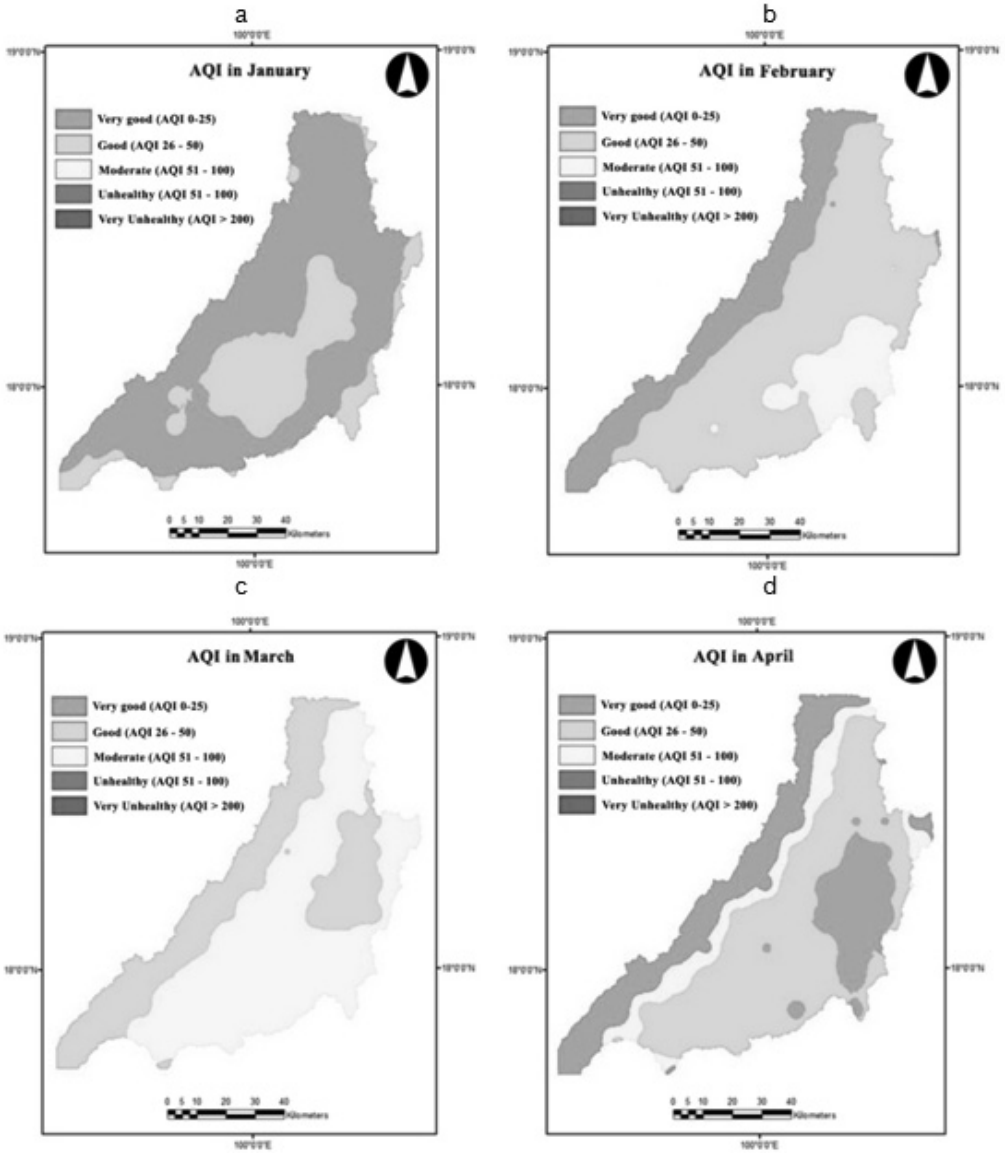

FIGURE 6. The air quality index in Thailand in 2018 in selected months: a – January; b – February; c – March; d – April

in yellow zone can do outdoor activities normally except for someone who is vulnerable was found to have primary symptom such as cough, being hard to breathe, eye irritation; so, the period of time to do outdoor activities should be reduced. From Figure 6d, it was found that Phrae Province had good quality of air and moderate quality of air and the quality of air affected the health in April.

The people who live in the blue area and green area can do outdoor activities and tour normally; and the people who live in yellow zone can do outdoor activities normally except for someone who is vulnerable was found to have primary symptom such as cough, being hard to breathe, eye irritation; so, the period of time to do outdoor activities should be reduced.

In addition, PM_{10} is a major air pollution problem in Northern Thailand. The problem is evident during the dry season from December to April each year. As a result of this study, it was found that the most common problem of PM_{10} was in March, during which time. However, the main causes of PM_{10} in Northern Thailand are caused by open-air burning activities, forest fires, agricultural waste incineration, incineration, and the occurrence of forest fires in neighboring countries.

Conclusions

According to the study into the pattern of relationship between PM_{10} from the ground monitoring station of the air4thai with AOT data received from MODIS sensor onboard of Terra satellite in Phrae Province, the northern region of Thailand during January–April 2018, it was under the objective. It was found from the research that in March, PM_{10} was highest equal to 184 $\mu g \cdot m^{-3}$. In January, where PM_{10} was lowest was equal to 79 $\mu g \cdot m^{-3}$; the change of PM_{10} quantity and AOT was highly related (near 1) in every month. Besides, when the linear regression analysis was performed, it was found that independent variable (x) and dependent variable (y) were consistent, with the coefficient of decision of r^2 being near 1 in every month also. In February–April period in Phrae Province, it was the time when quantity of PM_{10} affected health according to the AQI standard of Thailand. In addition, the result from this research was consistent and was in the same direction with the research on "Satellite measurements of aerosol optical depth and carbon monoxide and comparison with ground data" by Lalitaporn and Mekaumnuaychai (2020), which indicated PM_{10}. High levels of PM_{10} occur more frequently from March to April. Furthermore, PM_{10} is higher in the morning than in the afternoon.

In bringing AOT data obtained from MODIS sensor onboard of Terra satellite to be applied in this research, the advantage was that this was near-real-time data and covered wide area (10×10 km^2 per 1 pixel). However, AOT data were classified by passive remote sensing system, with disadvantage of that in some days, there might be cloud over the area making it impossible to monitor AOT quantity. On part of PM_{10} data from the ground monitoring station, the advantage was that it was PM_{10} which was monitored by direct sensor; but with disadvantage that was that the PM_{10} monitoring tool cannot be installed in the station of all critical area since such air monitoring tool is large and the budget to be spent on the operation and the maintenance is high.

Acknowledgements

This research was financially supported by Mahasarakham University (Grant year 2021).

References

Adams, K., Greenbaum, D.S., Shaikh, R., Erp, A.M. van & Russell, A.G. (2015). Particulate matter components, sources, and health: Systematic approaches to testing effects. *Journal of the Air & Waste Management Association*, *65*(5), 544-558. https://doi.org/10.1080/10962247.2014.1001884

Amphanthong, P. & Busababodhin, P. (2015). Forecasting PM_{10} in the Upper Northern Area of Thailand with Grey System Theory. *Burapha Science Journal*, *20*(1), 15-24.

Benas, N., Beloconi, A. & Chrysoulakis, N. (2013). Estimation of urban PM_{10} concentration, based on MODIS and MERIS/ /AATSR synergistic observations. *Atmospheric Environment*, *79*, 448-454. https://doi.org/10.1016/j.atmosenv.2013.07.012

Emetere, M.E., Sanni, S.E., Okoro, E.E. & Adeyemi, G.A. (2018). Aerosol loading and its effect on respiratory dysfunction disorder over Dapaong-Togo. *Scientific Review Engineering and Environmental Sciences*, *27*(4), 410-424. https://doi.org/10.22630/PNIKS.2018.27.4.40

GreenFacts (2018). *Air pollution particulate matter*. Retrieved from: https://www.greenfacts.org/en/particulate-matter-pm/level-2/01-presentation.htm [access 15.08.2020].

He, Q. & Huang, B. (2018). Satellite-based mapping of daily high-resolution ground $PM_{2.5}$ in China via space-time regression modeling. *Remote Sensing of Environment*, *206*, 72-83. https://doi.org/10.1016/j.rse.2017.12.018

Kloog, I., Koutrakis, P., Coull, B.A., Lee, H.J. & Schwartz, J. (2011). Assessing temporally and spatially resolved $PM_{2.5}$ exposures for epidemiological studies using satellite aerosol optical depth measurements. *Atmospheric Environment*, *45*(35), 6267-6275. https://doi.org/10.1016/j.atmosenv.2011.08.066

Lalitaporn, P. & Mekaumnuaychai, T. (2020). Satellite measurements of aerosol optical depth and carbon monoxide and comparison with ground data. *Environmental Monitoring and Assessment*, *192*, 369. https://doi.org/10.1007/s10661-020-08346-7

Liu, Y., Sarnat, J.A., Kilaru, V., Jacob, D.J. & Koutrakis, P. (2005). Estimating ground-level $PM_{2.5}$ in the eastern United States using satellite remote sensing. *Environmental Science & Technology*, *39*(9), 3269-3278. https://doi.org/10.1021/es049352m

Meng, X., Wu, Y., Pan, Z., Wang, H., Yin, G. & Zhao, H. (2019). Seasonal Characteristics and Particle-size Distributions of Particulate Air Pollutants in Urumqi. *International Journal of Environmental Research and Public Health*, *16*(3), 396. https://doi.org/10.3390/ijerph16030396

Nathapindhu, G., Sttheetham, D. & Ketkowit, K. (2011). Public Participation in Open Burning Control. *KKU Research Journal*, *16*(4), 408-415.

Nguyen, H., Cressie, N. & Braverman, A. (2012). Spatial statistical data fusion for remote sensing applications. *Journal of the American Statistical Association*, *107*(499), 1004-1018. https://doi.org/10.1080/01621459.2012.694717

Outapa, P. & Ivanovitch, K. (2019). The effect of seasonal variation and meteorological data on PM_{10} concentrations in Northern Thailand. *International Journal of GEOMATE*, *16*(56), 46-53. https://doi.org/10.21660/2019.56.4558

Phayungwiwatthanakoon, C., Suwanwaree, P., Dasananda, S. (2014). Application of new MODIS-based Aerosol Index for Air Pollution Severity Assessment and Mapping in Upper Northern Thailand. *Environment Asia*, *7*(2), 133-141. https://doi.org/10.14456/ea.2014.32

Pollution Control Department [PCD] (2004). *Air pollution*. Retrieved from: http://www.pcd.go.th/ info_serv/air_dust.htm [access 04.05.2020].

Porter, J.N. & Clarke, A.D. (1997). Aerosol size distribution models based on in situ measurements. *Journal of Geophysical Research Atmospheres*, *102*(D5), 6035-6045. https://doi.org/10.1029/96JD03403

Rotjanakusol, T. & Laosuwan, T. (2018). Estimation of land surface temperature using Landsat satellite data: a case study of Mueang Maha Sarakham District, Maha Sarakham Province, Thailand for the years 2006 and 2015. *Scientific Review Engineering and Environmental Sciences*, *27*(4), 401-409. https://doi.org/10.22630/PNIKS.2018.27.4.39

Rotjanakusol, T. & Laosuwan, T. (2019). *Drought Evaluation* with *NDVI-Based Standardized Vegetation Index* in *Lower Northeastern Region* of *Thailand. Geographia Technica, 14(1), 118-130*. https://doi.org/10.21163/GT_2019.141.09

Sukitpaneenit, M. & Oanh, N.T.K. (2014). Satellite monitoring for carbon monoxide and particulate matter during forest fire episodes in Northern Thailand. *Environmental Monitoring and Assessment*, *186*(4), 2495-2504. https://doi.org/10.1007/s10661-013-3556-x

Suwanprasit, C., Charoenpanyanet, A., Pardthaisong, L. & Sin-ampol, P. (2018). Spatial and temporal variations of satellite-derived PM_{10} of Chiang Mai: an exploratory analysis. *Procedia Engineering*, *212*, 141-148. https://doi.org/10.1016/j.proeng.2018.01.019

Supasri, T., Intra, P., Jomjunyong, S. & Sampattagul, S. (2018). Evaluation of Particulate Matter Concentration by Using a Wireless Sensor System for Continuous Monitoring of Particulate Air Pollution in Northern of Thailand. *Journal of Innovative Technology Research*, *2*(1), 69-83.

United States Environmental Protection Agency [USEPA] (2018). Particulate Matter (PM) Pollution. Retrieved from: https://www.epa.gov/pm-pollution/particulate-matter-pm-basics [access 20.01.2020].

Uttaruk, Y. & Laosuwan, T. (2019). Drought Analysis Using Satellite-Based Data and Spectral Index in Upper Northeastern Thailand. *Polish Journal of Environmental Studies*, *28*(6), 4447-4454. https://doi.org/10.15244/pjoes/94998

Vienneau, D., Hoogh, K. de, Bechle, M.J., Beelen, R., Donkelaar, A. van, Martin, R.V., Millet, D.B., Hoek, G. & Marshall, J.D. (2013). Western European land use regression incorporating satellite- and ground-based measurements of NO_2 and PM_{10}. *Environmental Science & Technology*, *47*(23), 13555-13564. https://doi.org/10.1021/es403089q

World Health Organization [WHO] (2017). *Air pollution*. Retrieved from: https://www.who.int/docs/default-source/thailand/air-pollution/briefing-on-air-pollution-th-thai.pdf?sfvrsn=408572d4_2 [access 02.10.2020].

Summary

Patterns of relationship between PM_{10} from air monitoring quality station and AOT data from MODIS sensor onboard of Terra satellite. Thailand, especially in the northern region, often encounters the problem of having PM_{10} exceeding the normal standard level, which could do harm to people's health. Mostly, such problem is caused by the burning of forest area and open area; this is clearly seen during January–April of every year. Also, the problem as mentioned is caused by the meteorological conditions and the terrains in the northern region that make it easy for PM_{10} to be accumulated. The aim of this study was to analyze the patterns of relationship between PM_{10} measured from the ground monitoring station and AOT data received from MODIS sensor onboard of Terra satellite in Phrae Province located in the northern region of Thailand. The method performed was by analyzing the correlation between PM_{10} data obtained from the ground monitoring station and the AOT data received from the MODIS sensor onboard of Terra satellite during January–April 2018. It was found from the study that the change of the intensity of PM_{10} and AOT in the climate was highly related; it appeared that the correlation coefficient (r) in January–April was 0.92, 0.91, 0.91 and 0.92, respectively. This research pointed out that during February––April, the areas of Phrae Province had the level of PM_{10} that affected health. Besides, from the method in this research, it revealed AOT data received from MODIS sensor onboard of Terra satellite could be applied in order to follow up, monitor, and notify the spatial changes of PM_{10} efficiently.

Authors' address:
Winai Suriya
(https://orcid.org/0000-0003-2214-4294)
Mahasarakham University
Faculty of Science
Department of Physics
Kham Riang, Kantarawichai

Maha Sarakham, 44150
Thailand
e-mail: kroowinai@hotmail.co.th

Poramate Chunpang
(https://orcid.org/0000-0003-1721-1202)
Mahasarakham University
Faculty of Science
Space Technology and Geoinformatics Research Unit
Kham Riang, Kantarawichai
Maha Sarakham, 44150
Thailand
e-mail: poramate_c@hotmail.com

Teerawong Laosuwan – corresponding author
(https://orcid.org/0000-0002-4231-9285)
Mahasarakham University
Faculty of Science
Department of Physics
Space Technology and Geoinformatics Research Unit
Kham Riang, Kantarawichai
Maha Sarakham, 44150
Thailand
e-mail: teerawong@msu.ac.th

Scientific Review – Engineering and Environmental Sciences (2021), 30 (2), 250–260
Sci. Rev. Eng. Env. Sci. (2021), 30 (2)
Przegląd Naukowy – Inżynieria i Kształtowanie Środowiska (2021), 30 (2), 250–260
Prz. Nauk. Inż. Kszt. Środ. (2021), 30 (2)
http://iks.pn.sggw.pl
DOI 10.22630/PNIKS.2021.30.2.21

Intidhar J. IDAN[1], Jawad K. Al-RIFAIE[2], Hind M. EWADH[3]

[1] University of Babylon, Faculty of Engineering
[2] Al-Furat Al-Awsat Technical University
[3] University of Babylon, Environmental Research and Studies Centre

MgAl-LDH-biochar composites as a green sorbent for lead removal from water

Key words: biochar, cow bones, green sorbent, MgAl-LDH-biochar, lead

Introduction

Environmental pollution is the natural consequence of humankind's activities; therefore, it is impossible to inhibit the pollution of the Earth as long as a single person lives on this planet (Alattabi et al., 2017; Hashim, Shaw & Al-Shamma'a, 2021). The by-products that resulted from the activities of a single person apparently harmless for both environment and public health, but the collective effects of large populations, such as crowded cities, cause extensive pollution phenomena, such as the discharge of liquid and solid wastes to the surrounding environment (Goel, 2006; Abdulla et al., 2020; Khalid et al., 2020a). Unfortunately, there is an irretrievable relationship between the environmental pollution and the existence of humankind because the human needs to use the natural resources to survive and also to develop the infrastructures, which in turn result in the production of different forms of pollutants, including gaseous, liquid and solid pollutants (Salah, Ortega-Martorell, Abdellatif, Gharghan & Ahmed, 2020; Abdulhadi et al., 2021). For instance, the literature shows that the increasing global demand for food has resulted in a dramatic increase in the consumption of fertilizers and pesticides. Zhang et al. (2014) reported that 300 million kg of pesticides are annually used in China to increase crop production, which is 2.5–5 times the average global usage of pesticides, while the usage of fertilizers in China has risen to 2.8–3 times the global average (Han, Currell & Cao, 2016; Alenezi, Hasan, Amoako-Attah,

Gkantou & Abdulhadi, 2020; Al-Marri, AlQuzweeni, AlKizwini, Zubaidi & Al-Khafaji, 2020). The rapid increase in the worldwide population has also resulted in a substantial expansion of industrial activities, such as the textile and pharmaceutical industries, which substantially contributes to the rise of water pollution (Aqeel et al., 2020; Emamjomeh et al., 2020a). In Japan, the literature confirms that concentrations of some heavy metals in the groundwater and soil in Kunugi-yama area also reached alarming levels; zinc concentration in groundwater was about 90 times higher than its reference level, while the concentrations of copper, zinc, and lead in soils were about 2.3–3.4 times higher than their reference levels (Ozaki et al., 2019). Besides the significant water pollution, the planet of Earth faces the dilemma of the increasing generation of municipal solid wastes (MSW) that is seriously polluting both soils and sources of groundwater (Alenazi et al., 2020; Alhendal et al., 2020), and it also generates a substantial amount of greenhouse gases that results in climate changes (Alenazi et al., 2020; Alhendal et al., 2020). This short literature survey indicates that water pollution and the generation of MSW represent direct threats to both eco-system and public health. At the same time, the literature shows many proposed solutions to each one of these dilemmas. For example, a broad spectrum of treatment methods was used to minimize or eliminate water/wastewater pollution, such as electrocoagulation (Hashim et al., 2020b), adsorption (Alyafei et al., 2020), bio-reactors (Khalid et al., 2020a), membranes and chemical precipitations (Al-Saati et al., 2019). In terms of MSW, many solutions were suggested to minimize its impacts on the environment, these solutions mainly focused on the recycle, reuse, sort, incineration, and disposal into landfills (Idowu, Atherton, Alo & Shaw, 2019). It can be seen that the majority of the proposed solutions focused on each dilemma separately. In addition, many of the proposed solutions, especially for water pollution, are expensive and complex, which limits their wide range of applications. Hence, the current study aims at providing a partial solution to these dilemmas by utilizing the wasted cow bones (a kind of MSW) that generated from houses and hospitality facilities to produce a green sorbent that was applied to remediate water from heavy metal pollution (lead as a case study). Heavy metal pollution was considered in the present study as the concentrations of some heavy metals in freshwater bodies have increased by 1,000 folds of the allowable limits.

Methodology

Preparation of the green sorbent

Samples of cow bones were collected from local butcher shops and restaurants, in the city of Babylon, Iraq. Initially, the collected sample was manually cleaned to remove the residuals of meat and fat, then bones were chopped into small pieces (2.0–5.0 cm) (Alquzweeni & Alkizwini, 2020). The cleaned pieces were used to prepare the biochar according to the recommended method by Iriarte-Velasco, Sierra, Zudaire and Ayastuy (2016) as follows: the cleaned

pieces were subjected to a pre-carbonization process at a temperature of 450°C in a nitrogen atmosphere for 1 h to remove any residual of meat and fat. In this step, the heating rate and nitrogen flow were kept constant at 10°C·min^{-1} and 120 cm^3·min^{-1}, respectively, unit the required level was reached. The pre-carbonized sample was cooled down, and then it was sieved to separate particles with a size range of 0.25–0.35 mm. The collected particles were divided into two parts. The first part was subjected to the coating process, while the second part was not further treated to be used later as a reference (for comparison purposes). Analytical grade $MgCl_2 \cdot 6H_2O$, $AlCl_2 \cdot 6H_2O$ and NaOH, provided by Sigma-Aldrich, were used in the preparation of the MgAl-LDH-biochar. Synthetization of the MgAl-LDH-biochar has been carried out according to the stated procedures by Meili et al. (2019) as follows: 3.62 g of $AlCl_2 \cdot 6H_2O$ and 6.09 g of $MgCl_2 \cdot 6H_2O$ were added into a flask containing 20 mL of deionized water, and stirred for 30 min and speed of 150 rpm to ensure that the added chemicals were completely dissolved. Then, 1 g of the biochar was added to this solution; the pH of the solution was increased to 10 by adding 3M of NaOH. The mixture was stirred again for 240 min before centrifuge it using a Sigma machine (model: 3-16 PK) at speed of 3,000 rpm for 5 min. The separated solids were washed with deionized water and dried using an electric oven (model: 101-0BS) at a temperature of 60°C for 16 h. According to the literature, a molar ratio of Mg : Al was kept at 4 : 1 showed a good performance (Meili et al., 2019).

Characterization of the MgAl-LDH--biochar

The physicochemical properties of the MgAl-LDH-biochar were characterized using the X-ray diffractometer (XRD) (Aeris: PANalytical). The characterization process was carried out at λ of 0.1542 nm and a scanning rate of 2°·min^{-1} in 2θ range of 5–65°. Additionally, metals concentration was measured using an Inductively Coupled Plasma-Mass Spectroscopy (ICP-MS) on a Varian Vista Pro.

Batch experiments

A stock lead solution (1,000 mg·L^{-1}) was prepared by dissolving 1.598 g of $Pb(NO_3)_2$ (provided by Sigma-Aldrich) in 1.0 L of deionized water. Fewer concentrations were diluted from this concentrated solution. Batch experiments were carried out by mixing different doses of the MgAl-LDH-biochar (0.1––0.3 g·L^{-1}) with 100 mL of lead solution in a 200 mL flask. The latter was shaken using a mechanical shaker for 3 h at a speed of 150 rpm (Alquzweeni & Alkizwini, 2020). To attain the best removal of lead; the effects of lead concentration (*Lc*) (10–50 mg·L^{-1}), solution initial pH (2.0–7.0), contact time (*Ct*) (5–180 min), and solution temperature (*St*) (15–45°C) on the adsorption efficiency were measured. To measure the residual lead concentration, a 5 mL sample was taken from the mixture at the required time and instantly filtered on a 0.22 nylon membrane filter (provided by Hach-Lange Ltd); the filtrate was examined using a Thermo atomic absorption spectrophotometer (model: ICE 3300). All

experiments were repeated three times. Adsorption isotherm and kinetics of lead on the MgAl-LDH-biochar has been measured by contacting different doses of MgAl-LDH-biochar (0.1–0.3 $g \cdot L^{-1}$) with 100 mL of lead solution (30 $mg \cdot L^{-1}$). The mixture was continuously shaking for 24 h at a speed of 150 rpm to attain the equilibrium condition. The adsorption isotherm experiments were carried out at room temperature. Langmuir isotherm model (Eq. 1) was used to assess the adsorption of lead on the MgAl-LDH--biochar not only because this model is commonly used in such studies, but also because it provides the necessary information to calculate the separation factor (R_L) (Eq. 2), which is a reliable tool to assess the affinity between the absorbates and absorbents. The adsorption process is unfavorable when R_L is more than 1, linear when $R_L = 1$, favorable when the R_L is within the range 1–0 or irreversible when R_L equals 0 (Dada, Olalekan, Olatunya & Dada, 2012).

$$\frac{C_e}{q_e} = \frac{1}{Q_o \cdot b} + \frac{C_e}{Q_o} \tag{1}$$

$$R_L = \frac{1}{1 + b \cdot C_i} \tag{2}$$

where:

q_e – adsorbed amount of lead at equilibrium [$mg \cdot g^{-1}$],

Q_o – hypothetical monolayer adsorption [$mg \cdot g^{-1}$],

b – energy of adsorption [$L \cdot mg^{-1}$].

Additionally, pseudo-second-order model (P-S-O) was also used to examine the adsorption kinetics. Removal efficiency was measured basing on the initial and final concentrations of lead as follows (Emamjomeh et al., 2020b; Hashim, Andrew, Al-Jumeily, Alwash & Aljefery, 2020a):

$$\underset{[\%]}{removal} = \frac{\begin{matrix}initial\ concentration - \\ - final\ concentration \\ of\ lead\end{matrix}}{\begin{matrix}initial\ concentration \\ of\ lead\end{matrix}} \cdot 100\% \tag{3}$$

Results and discussion

Figure 1 shows the XRD patterns of the developed MgAl-LDH-biochar adsorbent and the reference (pure biochar). The XRD pattern of the MgAl-LDH-biochar shows a number of characteristic peaks, in 2θ range of 100–250, which confirm the successful deposition of the MgAl-LDH on the surfaces of the biochar particles as these peaks were absent in the reference. A number of unidenti-

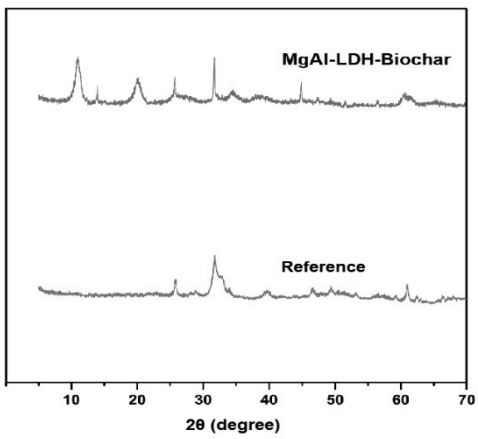

FIGURE 1. X-ray diffraction of MgAl-LDH-biochar and the reference

fied peaks were noticed in the XRD patterns that indicate the presence of minor amounts of other minerals, which are usually detected in biochars that derived from organic origins. Additionally, minor crystallinity was observed in the biochar that could be resulted from the degradation of carbonaceous materials. In summary, the obtained results from the XRD test confirmed the presence of the MgAl-LDH on the surfaces of the biochar particles.

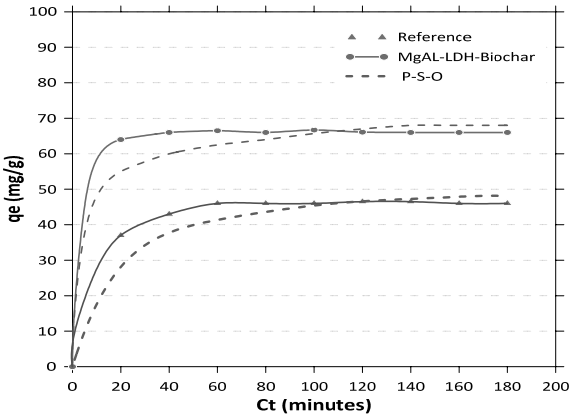

FIGURE 2. Experimental data of the reference and MgAl--LDH-biochar adjusted to the kinetic model of P-S-O

Lead adsorption experiments

Kinetics of lead adsorption on the MgAl-LDH-biochar

To assess the kinetics of lead removal on both MgAl--LDH-biochar and the reference. Figure 2 shows the results of fitting experimental results to the P-S-O, which reveals a set of key facts about the adsorption of lead ions on both MgAl--LDH-biochar and the reference. Firstly, a glance on Figure 2 reveals that the P-O-S is suitable for describing the adsorption of lead on MgAl-LDH-biochar and the reference; R^2 values for the relationships of reference – P-S-O and MgAl-LDH-biochar-P-S-O were 0.947 and 0.932, respectively, which indicate the suitability of P-S-O for describing the adsorption of lead on coated and uncoated adsorbents. Secondly, it can be seen from Figure 2 that the equilibrium condition was attained after 80 min of contact. Finally, the obtained results show that the MgAl-LDH-biochar is superior to the reference (untreated biochar) in terms of lead removal from water. Figure 3 shows the outcomes of Langmuir isotherm model application to the experimental data obtained from mixing different amounts of MgAl-LDH-biochar with the lead solution. It can be seen from this figure that the constant of Langmuir isotherm model

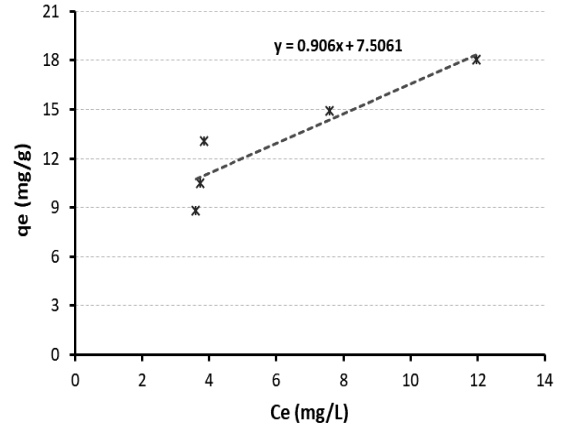

FIGURE 3. Langmuir isotherm for lead adsorption on MgAl-LDH-biochar

was 0.1332, which means that the R_L is 0.07. The latter indicates high affinity between leads ions and MgAl-LDH-biochar (the R_L is within the range 1–0). Basing on the outcomes of this part of the study, the *Ct* will be kept constant at 80 min.

Effects of solution pH on lead removal

Lead adsorption on the MgAl-LDH--biochar has been examined at a pH range of 2.0–7.0 at MgAl-LDH-biochar dose of 0.2 g·L^{-1}, *Ct*: 80 min, *Lc*: 30 mg·L^{-1}, *St*: 25°C, and stirring speed of 150 rpm. Figure 4 indicates that lead adsorption was enhanced with the increase of the initial pH, but a negligible enhancement in the removal of lead when the pH increased from 6.0 to 7.0. At low pH values, the surfaces of the MgAl-LDH-biochar adsorbent develop positive charges that result in a repulsion of the positively charged lead ions, which minimizes the removal efficiency. Additionally, the competition between the accumulated hydrogen/hydronium ions and lead ions for the available active sits also minimizes the removal efficiency. Increasing the pH of the solution to the vicinity of 5 results in the development of positive charges on the surfaces of the MgAl-LDH-biochar adsorbent that helps to develop an electrostatic attraction between the adsorbent and lead ions. It is also believed that the inner surfaces of MgAl-LDH-biochar develop coordinate covalent bonds between the surfaces oxide's oxygen and the metal forming monodentate and bidentate complexes. It noteworthy to highlight that the predominant path of lead removal at neutral or slightly acidic pH range is the precipitation of lead in the form of lead(II) hydroxides. The rest of the batch experiments, therefore; were run at a pH of 5.0.

Effects of *Ct* on lead removal

Effects of *Ct* on the adsorption of lead on the MgAl-LDH-biochar was examined at 10, 20, 30, 40, 50, 60, 70, and 80 min at *St*: 25°C, pH: 5.0; MgAl-LDH--biochar dose: 0.2 g·L^{-1}, *Lc*: 30 mg·L^{-1} and stirring speed: 150 rpm. Lead removal increased from about 59.8 to 92.3% as the *Ct* increased from 20 to 120 min, respectively (Fig. 5). The majority of the lead uptake happened during the first 100 min. Additionally, it was

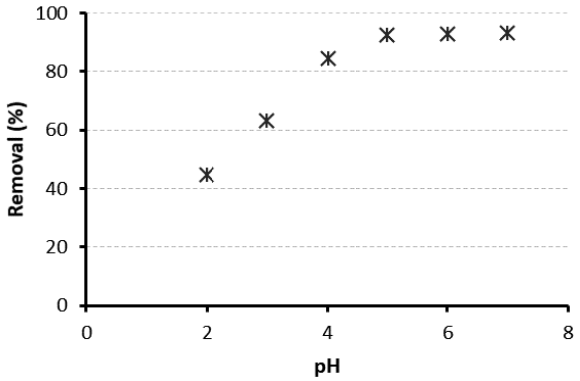

FIGURE 4. Effects of solution pH on lead adsorption on the MgAl-LDH-biochar

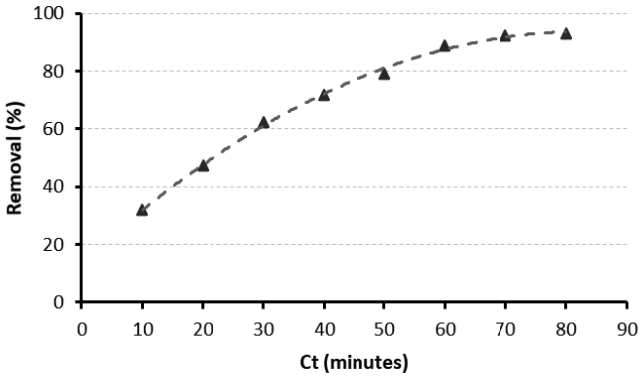

FIGURE 5. Effects of *Ct* on lead adsorption on the MgAl-LDH-biochar

noticed that the uptake rate of lead was rapid during the first 80 min, but it was slowed down during the last 40 min. The rapid uptake rate of lead, during the first 80 min, may be attributed to the fact that the initial uptake of lead mostly happens on the available external sites on the surfaces of MgAl-LDH-biochar. With the progress of the *Ct* the available binding sites became limited, which results in slowing down the uptake rate of lead.

Effects of *St*

Solution temperature (*St*) plays a significant role in the adsorption process not because it governs the driving force of the pollutant ions onto the surface of the MgAl-LDH-biochar, but it also governs other key parameters, such as the strength of the energy barrier of reaction between the adsorbent and the adsorbate and it governs the size of the binding sites. Hence, the effect of the *St* on the uptake of lead by the MgAl-LDH--biochar was investigated by commencing the adsorption experiments at different temperatures. Lead adsorption was examined at *St* of 15, 25, 35, and 45°C keeping the initial pH, MgAl-LDH-biochar dose, *Lc*, *Ct*, and stirring speed constant at 5, 0.2 $g \cdot L^{-1}$, 30 $mg \cdot L^{-1}$, 80 min, and 150 rpm, respectively. The results of these experiments showed that the lead removal was enhanced at high temperatures, thereby, confirming that the nature of the lead adsorption process is endothermic (Fig. 6). The increase in the removal of lead at high temperatures is attributed to the reasons mentioned above; the increase in both sizes of the active sites and the diffusion of lead ions, which enhances the removal of lead. Additionally, some studies indicated that increasing the *St* expands the size of the adsorbent particles that result in the breaking of some internal bonds near the surfaces of the particles, which produces more binding sites (Alquzweeni & Alkizwini, 2020).

Effects of MgAl-LDH-biochar dose

Adsorption of lead has been carried out at three different doses of MgAl--LDH-biochar (0.1, 0.2, and 0.3 $g \cdot L^{-1}$) at initial pH: 5.0, *Ct*: 80 min, *St*: 45°C, *Lc*: 30 $mg \cdot L^{-1}$, and stirring speed of 150 rpm. The effects of the MgAl-LDH-biochar

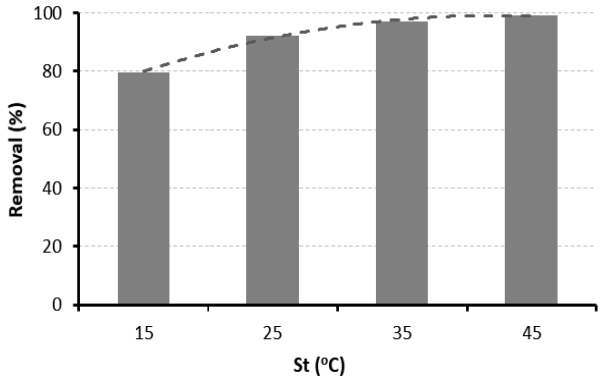

FIGURE 6. Effects of *St* on lead adsorption on the MgAl-LDH-biochar

dose on the removal of lead are shown in Figure 7, which indicates that the lead removal is positively influenced by the increase of the MgAl-LDH-biochar dose. It was noticed that the removal of lead increased vicinity from 72 to 100% when the MgAl-LDH-biochar dose increased from 0.1 to 0.3 $g \cdot L^{-1}$, respectively. The enhancement of lead removal with the increase of the MgAl-LDH-biochar dose is related to the increase in the number of the adsorption sites; the more the dose of the MgAl-LDH-biochar, the higher the number of active sites, which results in better removal of lead. However, increasing the dose of MgAl-LDH-biochar from 0.2 to 0.3 $g \cdot L^{-1}$ increased the removal of lead by only 1%. Thus, to maintain the cost-effectiveness of the treatment method, MgAl-LDH-biochar dose of 0.2 $g \cdot L^{-1}$ was used to run the rest of the experiments.

Effects of *Lc*

Basing on the fact that the discharged concentration of any pollutant is varying according to the season and/or the industrial activity. Thus, a set of experiments were commenced to measure the effects of

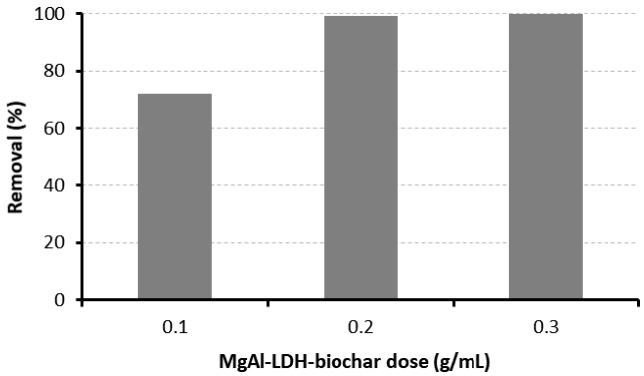

FIGURE 7. Effects of MgAl-LDH-biochar dose on lead removal

different *Lc* (10, 20, 30, 40 and 50 mg·L^{-1}) using the optimum conditions obtained in the previous sets of experiments (pH: 5.0, *St*: 45°C, Ct: 80 min, MgAl-LDH-biochar dose: 2 g·L^{-1} and stirring speed: 150 rpm). Figure 8 depicts the effect of the *Lc* on the removal of lead using the MgAl-LDH--biochar; it can be seen that the higher the Lc, the lower the removal of lead, where, it was noticed that increasing the *Lc* from 10 to 50 mg·L^{-1} has decreased the removal of lead by about 30%. This decrease in the removal of lead is related to the availability of the active sits on the surfaces of the MgAl-LDH-biochar. Simply, a constant amount of MgAl-LDH-biochar (0.2 g·L^{-1}) is available for the adsorption process, therefore, at high lead concentrations, it is not sufficient to absorb all lead ions, i.e. the available active sites will not be enough to occupy all lead ions. Generally, these obtained results in this study follow the same trends in the published literature (Gong et al., 2012).

Conclusions

In conclusion, the present study explored the adsorption of lead ions on green absorbent that was made by coating biochar particles with MgAl-LDH. The results of this study revealed that the MgAl-LDH-biochar is suitable for adsorbing of lead ions. Generally, it was observed that the performance of the MgAl-LDH-biochar was enhanced when the solution pH became slightly acidic, and also when the solution temperature increased. Additionally, it was noticed that increasing the dose of the MgAl--LDH-biochar more than 2 g·L^{-1} was not beneficial for the studied concentrations of lead. In contrast, increasing lead concentration has negatively influenced the performance of the MgAl-LDH-biochar. Thus, based on the obtained results from the commenced experiments, the efficiency of the MgAl-LDH-biochar could be enhanced by keeping the pH of the solution at the vicinity of the neutral range and by avoiding low water temperatures. The kinetic study confirmed a good affinity between lead ions and the MgAl--LDH-biochar. In summary, it could be concluded that the MgAl-LDH-biochar is a potential eco-friendly partial solution for two manger environmental concerns, which are the municipal solid wastes and water/wastewater pollution.

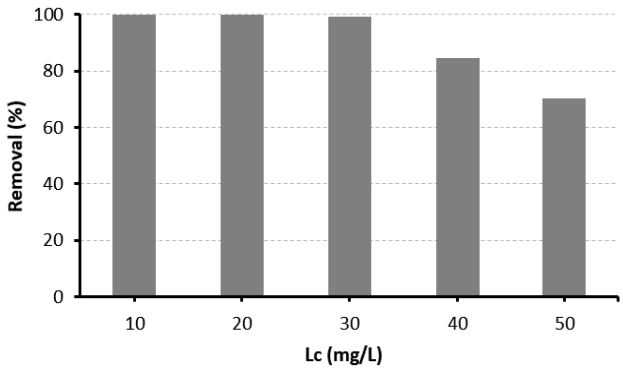

FIGURE 8. Effects of *Lc* on lead removal by MgAl-LDH-biochar

References

Abdulhadi, B., Kot, P., Hashim, K., Shaw, A., Muradov, M. & Al-Khaddar, R. (2021). Continuous-flow electrocoagulation (EC) process for iron removal from water: Experimental, statistical and economic study. *Science of the Total Environment*, *756*(2), 1-16.

Abdulla, G., Kareem, M.M., Khalid, H.S., Muradov, M., Kot, P., Mubarak, H.A., Abdellatif, M. & Abdulhadi, B. (2020). Removal of iron from wastewater using a hybrid filter. *Materials Science and Engineering*, *888*(2), 1-11.

Al-Marri, S., AlQuzweeni, S.S., AlKizwini, R.S., Zubaidi, S.L. & Al-Khafaji, Z.S. (2020). Ultrasonic-Electrocoagulation method for nitrate removal from water. *Materials Science and Engineering*, *888*(1), 1-9.

Al-Saati, N., Hussein, T., Abbas, M., Al-Saati, Z., Sadique, M., Aljefery, M. & Carnacina, I. (2019). Statistical modelling of turbidity removal applied to non-toxic natural coagulants in water treatment: a case study. *Desalination and Water Treatment*, *150*(1), 406-412.

Alattabi, A.W., Harris, C.B., Alkhaddar, R.M., Hashim, K.S., Ortoneda-Pedrola, M. & Phipps, D. (2017). Improving sludge settleability by introducing an innovative, two-stage settling sequencing batch reactor. *Journal of Water Process Engineering*, *20*, 207-216.

Alenazi, M., Hashim, K., Hassan, A., Muradov, M., Patryk, K. & Abdulhadi, B. (2020). Turbidity removal using natural coagulants derived from the seeds of strychnos potatorum: statistical and experimental approach. *Materials Science and Engineering*, *888*(1), 408-416.

Alenezi, A.K., Hasan, H.A., Amoako-Attah, J., Gkantou, M. & Abdulhadi, B. (2020). Zeolite-assisted electrocoagulation for remediation of phosphate from calcium-phosphate solution. *Materials Science and Engineering*, *888*(2), 22-31.

Alhendal, M., Nasir, M.J., Amoako-Attah, J., Al-Faluji, D., Patryk, K. & Bareq, A. (2020). Cost-effective hybrid filter for remediation of water from fluoride. *Materials Science and Engineering*, *888*(1), 43-51.

Alquzweeni, S.S. & Alkizwini, R.S. (2020). Removal of Cadmium from Contaminated Water Using Coated Chicken Bones with Double-Layer Hydroxide (Mg/Fe-LDH). *Water*, *12*(8), 1-13.

Alyafei, A., AlKizwini, R.S., Yeboah, D., Gkantou, M., Al Khaddar, R., Al-Faluji, D. & Zubaidi, S. (2020). Treatment of effluents of construction industry using a combined filtration-electrocoagulation method. *Materials Science and Engineering*, *888*(2), 60-71.

Aqeel, K., Mubarak, H.A., Amoako-Attah, J., Abdul-Rahaim, L.A., Al Khaddar, R., Abdellatif, M. & Al-Janabi, A. (2020). Electrochemical removal of brilliant green dye from wastewater. *Materials Science and Engineering*, *888*(1), 122-132.

Dada, A., Olalekan, A., Olatunya, A. & Dada, O. (2012). Langmuir, Freundlich, Temkin and Dubinin–Radushkevich isotherms studies of equilibrium sorption of Zn^{2+} unto phosphoric acid modified rice husk. *IOSR Journal of Applied Chemistry*, *3*(1), 38-45.

Emamjomeh, M., Kakavand, S., Jamali, H., Alizadeh, S., Safdari, M., Mousavi, S. & Mousazade, M. (2020a). The treatment of printing and packaging wastewater by electrocoagulation–flotation: the simultaneous efficacy of critical parameters and economics. *Desalination and Water Treatment*, *205*(2), 161-174.

Emamjomeh, M., Mousazadeh, M., Mokhtari, N., Jamali, H., Makkiabadi, M., Naghdali, Z. & Ghanbari, R. (2020b). Simultaneous removal of phenol and linear alkylbenzene sulfonate from automotive service station wastewater: Optimization of coupled electrochemical and physical processes. *Separation Science and Technology*, *55*(17), 3184-3194.

Goel, P. (2006). *Water pollution: causes, effects and control*. Delhi, India: New Age International Inc.

Gong, J., Wang, X., Shao, X., Yuan, S., Yang, C. & Hu, X. (2012). Adsorption of heavy metal ions by hierarchically structured magnetite-carbonaceous spheres. *Talanta*, *101*(2), 45-52.

Han, D., Currell, M.J. & Cao, G. (2016). Deep challenges for China's war on water pollution. *Environmental Pollution*, *218*(6), 1222-1233.

Khalid, H., Ali, S.M., AlRifaie, J.K., Kot, P., Andrew, S., Rafid, A., Idowu, I. & Gkantou, M. (2020a). *Escherichia coli* inactivation using

a hybrid ultrasonic–electrocoagulation reactor. *Chemosphere*, *247*(4), 868-875.
Khalid, H., Patryk, K., Zubaid, S., Alwash, R., Rafid, A., Shaw, A., Al-Jumeily, D. & Aljefery, M. (2020b). Energy efficient electrocoagulation using baffle-plates electrodes for efficient *Escherichia coli* removal from wastewater. *Journal of Water Process Engineering*, *33*(20), 79-86.
Hashim, K.S., Andrew, S., Al-Jumeily, D., Alwash, R. & Aljefery, M.H. (2020a). Electrocoagulation as an eco-friendly river water treatment method. In R. AlKhaddar et al. (eds.), *Advances in Water Resources Engineering and Management*. Berlin: Springer.
Hashim, K.S., Ewadh, H.M., Muhsin, A.A., Zubaidi, S.L., Aljefery, M. & Al-Khaddar, M.R. (2020b). Phosphate removal from water using bottom ash: Adsorption performance, coexisting anions and modelling studies. *Water Science and Technology*, *82*(11), 1-17.
Hashim, K.S., Shaw, A. & Al-Shamma'a, A. (2021). Water purification from metal ions in the presence of organic matter using electromagnetic radiation-assisted treatment. *Journal of Cleaner Production*, *280*(2), 1-17.
Idowu, I.A., Atherton, W., Alo, B.I. & Shaw, A. (2019). An analyses of the status of landfill classification systems in developing countries: Sub Saharan Africa landfill experiences. *Waste Management*, *87*(1), 761-771.
Iriarte-Velasco, U., Sierra, I., Zudaire, L. & Ayastuy, J.L. (2016). Preparation of a porous biochar from the acid activation of pork bones. *Food and Bioproducts Processing*, *98*(2), 341-353.
Meili, L., Lins, P., Zanta, C., Soletti, J., Ribeiro, L., Dornelas, C., Silva, T. & Vieira, M. (2019). MgAl-LDH/Biochar composites for methylene blue removal by adsorption. *Applied Clay Science*, *168*(5), 11-20.
Ozaki, H., Ichise, H., Kitaura, E., Yaginuma, Y., Yoda, M., Kuno, K. & Watanabe, I. (2019). Immutable heavy metal pollution before and after change in industrial waste treatment procedure. *Scientific Reports*, *9*(1), 1-12.
Salah, Z., Ortega-Martorell, S., Abdellatif, M., Gharghan, S.K. & Ahmed, M.S. (2020). A method for predicting long-term municipal water demands under climate change. *Water Resources Management*, *34*(3), 1265-1279.
Zhang, Y., Han, S., Liang, D., Shi, X., Wang, F., Liu, W., Zhang, L., Chen, L., Gu, Y. & Tian, Y. (2014). Prenatal exposure to organophosphate pesticides and neurobehavioral development of neonates: a birth cohort study in Shenyang, China. *Egyptian Journal of Petroleum*, *27*(4), 1275-1290.

Summary

MgAl-LDH-biochar composites as a green sorbent for lead removal from water. The present study aims at the development of a green sorbent (MgAl-LDH-biochar) from the municipal solid wastes (cow bones) to remediate water from heavy metals. MgAl--LDH-biochar was characterized using X-ray diffraction (XRD), and it was used to remove lead at different pH, doses, contact time (*Ct*), and solution temperatures (*St*). The obtained results proved MgAl-LDH-biochar removes 99% of lead when the initial pH, *Ct*, *St*, and dose were 5.0, 80 min, 45°C, and 0.2 $g \cdot L^{-1}$, respectively.

Authors' address:
Intidhar J. Idan – corresponding author
(https://orcid.org/0000-0002-2791-4932)
University of Babylon
Faculty of Engineering
Department of Environmental Engineering
Hilla, 51001, Babylon
Iraq
e-mail: jabiridan@gmail.com

Jawad K. Al-Rifaie
Al-Furat Al-Awsat Technical University
Hilla, 51015, Babylon
Iraq
e-mail: alrifaie2010@gmail.com

Hind M. Ewadh
University of Babylon
Environmental Research and Studies Centre
Hilla, 51001, Babylon
Iraq
e-mail: hindewadh2021@gmail.com

Scientific Review – Engineering and Environmental Sciences (2021), 30 (2), 261–270
Sci. Rev. Eng. Env. Sci. (2021), 30 (2)
Przegląd Naukowy – Inżynieria i Kształtowanie Środowiska (2021), 30 (2), 261–270
Prz. Nauk. Inż. Kszt. Środ. (2021), 30 (2)
http://iks.pn.sggw.pl
DOI 10.22630/PNIKS.2021.30.2.22

Elanda FIKRI[1,2], Nanny DJUHRIAH[3], Neneng Yetty HANURAWATY[3]

[1] Diponegoro University, Doctorate Program of Environmental Studies
[2] Bandung Health Polytechnic, Center of Excellence
[3] Bandung Health Polytechnic, Department of Environmental Health

Study on the utilization of electrocoagulation concept as a disinfectant substitute in hospital wastewater

Key words: electrocoagulation, disinfectants, contact time, number of electrode plates, Coliforms, hospital wastewater

Introduction

Hospital as a place or service facility to handle, take care of, and treat will produce a large amount of wastewater and its quality needs attention because it has ingredients that are hazardous to health of the society and its environment (Tchamango, Nanseu-Njiki, Ngameni, Hadjiev & Darchen, 2010; Deepak, 2014; Rad & Lewis, 2014; Jagadal, Hiremath & Shivayogimath, 2017; Ahmad et al., 2019).

In addition to having a positive impact on society, namely as a place to heal the sick, hospital also has the possibility of having a negative impact (Akansha, Nidheesh, Gopinath, Anupama & Kumar, 2020). All medical service activities in the hospital will produce by-products in the form of garbage and waste that can be indicated as a reservoir, which can have a negative impact on health (Hakim & Hardianti, 2017). One of them can be in the form of pollution from an activity process, that is, if the resulting waste is not managed properly considering all hospital wastewater is likely to contain chemicals (toxic), infectious and radioactive (Niati & Widarto, 2006). Based on the results of Rapid Assessment in 2002 by the Directorate General of the Pemberantasan Penyakit Menular dan Penyehatan Lingkungan (P2MPL), there were 648 hospitals out of 1,476 hospitals which 49% of them had new incinerators and 36% of them had wastewater treatment plants (WWTP). Based on this amount, the quality of wastewater that has gone through management process that meets the requirements has only reached 52% (Djaja & Maniksulistya, 2006).

Waste management in hospitals is generally done to reduce the level of pollution both physically, chemically, and microbiologically. Specifically, for microbiological management, the waste management unit in this hospital uses Coliform bacteria as an indicator of its parameters. These bacteria are a large and heterogeneous group of Gram-negative rods that are within certain limits similar to *Escherichia coli* (Tapotubun, Savitri & Matrutty, 2016).

There are various methods used in deriving microbiological parameters in wastewater. Most hospitals in Indonesia use chlorine (chlorination) in the process of disinfection of waste water, because it is considered the cheapest on the market. However chlorine is beneficial for human life, and toxic to the environment and human health. The chlorine nature as a strong oxidizer makes it easy to bind to other compounds, forming toxic compounds such as organochlorine which has a carcinogenic effect. Therefore, there needs to be other alternatives that are more environmentally friendly and have minimal impact on human health. One method that can be developed is the electrocoagulation system.

Electrocoagulation is a water purification method (Liu et al., 2019). The working principle of electrocoagulation is to use two electrode plates inserted into a vessel filled with water to be purified. Furthermore, the two electrodes are electrified with direct current so that an electrochemical process occurs which causes the cation to move toward the cathode and the anion to move toward the anode (Hakizimana et al., 2017). Flocculants are eventually formed which will bind contaminants or particles from the raw water. There are anodes and cathodes in electrocoagulation. At the anode occurs the release of active coagulant in the form of metal ions into the solution, while at the cathode an electrolysis reaction occurs in the form of hydrogen gas release (Miwa, Malpass, Machado & Motheo, 2006; Önder, Koparal & Öğütveren, 2007).

Electrocoagulation requires simple equipment and is easy to operate (Chen, Chen & Yue, 2002; Cañizares, Jiménez, Martínez, Sáez & Rodrigo, 2007; Lakshmanan, Clifford & Samanta, 2010). Electrocoagulation can reduce colloidal/ /smallest particle content faster, and can provide high enough process efficiency for various conditions, no pH regulation is needed, without the use of chemical additives, deposits formed from the electrocoagulation process are more easily separated from water, can move particles smaller colloidal particles, and the electric current can be regulated (Van Genuchten, Addy, PenÞa & Gadgil, 2012; Lu, Li, Yin, Ma & Lin, 2015).

Existing researches related to electrocoagulation are limited to decreasing physical and chemical parameters of wastewater (Silva, Graca, Ribeiro & Rodrigues, 2018), phosphates (Dura & Breslin, 2019), suspended solids (Sadeddin, Naser & Firas, 2011), Cu, Ni, Zn, and Cr (Kim, Kim & Zoh, 2020), oil (Chen, Chen & Yue, 2000; Fajardo, Rodrigues, Martins, Castro & Quinta-Ferreira, 2015), and arsenic contaminated water (Nidheesh & Singh, 2017; Syam & Nidheesh, 2020), they are not applied to microbiological parameters. Research conducted by Wiyanto et al. (2014) shows that the electrocoagulation process can reduce the percentage of sulfide

levels in water. Research conducted by Setianingrum, Agus and Sarto (2016) shows that at 10-volt electricity voltage and contact time for 60 min can reduce the color parameters in batik waste water reaching 80% and COD of 71.3% (distance between electrode plates is 3 cm). Whereas the research of Darmawanti, Suhartana and Widodo (2010) shows that a contact time of 180 min and a current of 2.5 A can reduce the color of waste reaching 88.51%. Furthermore, research from Ni'am, Caroline and Afandi (2017) shows that using a 12-volt voltage, 4 electrodes, and a 45-minute contact time, can reduce COD level to 61% in wastewater.

Based on these limitations, it is necessary to conduct a research by applying electrocoagulation in reducing microbiological parameters in wastewater. Anodes and cathodes use aluminum (Al) because aluminum is a reactive electrode, a good reductant, resistant to corrosion, cheap, and easy to obtain.

Material and methods

Research type and strategies

An experimental type of research with factorial randomized design, namely looking for an effect of certain treatments on others, under controlled conditions (Notoatmodjo, 2010). Variables controlled in the study were:

- Current of 5 A and 12 V voltage.
- In order to overcome the absorption effect of electrodes, the type of electrode plate used was aluminum electrodes.
- Distance between the electrodes was 8 cm.
- Thickness of the electrode plate was 1 mm.
- The pH should be less than 9.0.

Population and sample

Population is a generalization area consisted of objects/subjects that have certain quantities and characteristics determined by researchers to be studied and then drawn conclusions. The population in this study was wastewater from effluent hospital in Bandung City (Standar Nasional Indonesia [SNI], 2008). The number of hospitals sampled in this study is one sample, namely Kebon Jati Hospital, Bandung City.

The sample size was based on the number of treatments and repetitions in the study (Gomez & Gomez, 2007). The treatments used in this study were 3 treatments using a ratio of contact time for 30, 60, and 90 min, and the number of plates (4, 6, and 8 electrode plates). The sample size calculation used the Gomez formula:

$$t(r-1) \geq 15$$

where:
t (treatment) – many treatments,
r (replica) – many repetitions.

Then:

$$t(r-1) \geq 15$$
$$3(r-1) \geq 15$$
$$3r-3 \geq 15$$
$$3r \geq 18$$
$$r \geq 6$$

The number of repetitions in this study was 6 times. The amount of wastewater needed in a repetition was 12.5 l, so the sample size for 3 treatments was:

3 treatments × 6 repetitions = 18 samples
18 samples × 12.5 l = 225 l of wastewater sample × 2 = 450 l

The volume of the wastewater sample was adjusted to the needs of examination and analysis parameters in the laboratory, which was 100 ml (the minimum sample for Coliform examination in wastewater). The sampling technique used was grab sampling.

Data analysis

Bivariate analysis was carried out on the variables suspected to be related or influence, and saw the magnitude of the influence of independent variable on dependent variable. Bivariate analysis used was two-way ANOVA (with $\alpha = 5\%$).

Results and discussion

Average temperature and pH of wastewater based on number of plates and contact time

Based on Table 1, it shows that the highest average temperature (26.3°C) occurred in the electrocoagulation process with 8 plates in 60 min contact time, while the lowest temperature (25.67°C) occurred in the electrocoagulation process with 4 plates in 90 min contact time.

The results of this study also showed an increase in temperature from 25.75 to 26.0°C, and the highest average temperature (26.0°C) was in the electrocoagulation process with 8 plates. Likewise, with the contact time variable, it also showed an increase in temperature from 25.83 to 25.94°C, and the highest average temperature (25.94°C) was in the electrocoagulation process with 60 min contact time.

The use of electrocoagulation method can increase temperature. This is in line with the increasing number of plates and

TABLE 1. Average temperature of wastewater based on number of plates, contact time and average pH

Number of plates	Contact time [min]	Average temperature [°C]	Average pH
4	30	25.833	7.750
	60	25.750	7.617
	90	25.667	7.583
6	30	25.833	7.750
	60	25.750	7.500
	90	25.917	7.733
8	30	25.833	7.717
	60	26.333	7.583
	90	25.833	7.767

contact time used. The increase in temperature is due to the strong electric current that spreads to the aluminum plate and direct contact with the wastewater to be treated. Another factor that can affect the high and low temperature is the temperature of the air during processing, the higher the air temperature will affect the temperature in the wastewater.

Table 1 also shows that the highest average pH (7.767) occurred in the electrocoagulation process with 8 plates in 90 min contact time, while the lowest average pH (7.5) occurred in the electrocoagulation process with 6 plates in 60 min contact time. The increase in pH value is caused by the accumulation of OH in the electrocoagulation process. Rindatami, Bangun and Prayitno (2016) states that cathode in the electrocoagulation process produces OH^- ions which will increase the pH value. The pH value of the solution also affects the number of ions in the solution as well as the solubility of the formed product. The pH of the solution affects the overall efficiency and effectiveness of electrocoagulation. This is consistent with research conducted by Kobya and Demirbas (2015) which states that the range of $6 < pH < 9$ is effective in reducing COD in textile wastewater by electrocoagulation. The number of electrodes and the amount of voltage used affect the electrocoagulation pro-cess. Flocks that bind the contaminant are produced by interaction between the electrode and the voltage in the electrocoagulation process. The more flocks produced the better the electrocoagulation process (Hanif, Khai & Adin, 2012). This increase in pH is normally attributed to the water reduction reaction at the cathode, and this in turn will depend on the rate of the alloy dissolution reaction. The pH will influence the nature of the aluminum hydroxy species. It is evident that the monomeric hydroxyaluminum cations are stable at low pH, while increasing the pH to values close to 7 leads to the production of cationic aluminum hydroxy species, and the $Al(OH)_3$ precipitate (Dura & Breslin, 2019).

Table 2 shows that there was no significant difference between the number of plates ($p = 0.628$), contact time ($p = 0.856$), and the number of plates and contact time ($p = 0.814$) and the temperature in electrocoagulation process. The same results were also shown in pH analysis. The results showed that there was no significant difference between the number of plates ($p = 0.89$), contact time ($p = 0.108$), and the number of plates and contact time ($p = 0.664$) and the pH in electrocoagulation process.

TABLE 2. Analysis of differences in temperature and pH values based on the number of plates and contact time in electrocoagulation process

Source	Sig.(temperature)	Sig.(pH)
Corrected model	0.940	0.514
Intercept	0.000	0.000
Number of plates	0.628	0.890
Contact time	0.856	0.108
Number of plates × Contact time	0.814	0.664

Total Coliforms in electrocoagulation process

The results related to total Coliforms in this study showed that the total Coliforms was in the range of 2–2.735 colonies, with an average of 333 colonies and a standard deviation of ±572,102. Based on Table 3, the lowest average total Coliform occurred in the electrocoagulation process was with 6 plates at 90 min (138 colonies), and the highest was at 4 plates at 60 min contact time (669 colonies).

TABLE 3. Average total Coliforms in wastewater based on number of plates and contact time

Number of plates	Contact time [min]	Mean
4	30	294.167
	60	669.167
	90	580.000
6	30	183.333
	60	300.000
	90	138.333
8	30	140.667
	60	228.667
	90	463.333

TABLE 4. Bivariate analysis of total Coliforms differences based on number of plates and contact time in electrocoagulation process

Source	Sig.
Corrected model	0.727
Intercept	0.000
Number of plates	0.269
Contact time	0.537
Number of plates × Contact time	0.863

The results of bivariate analysis (two-way ANOVA) shown in Table 4 showed that there was no significant difference between the number of plates (p = 0.269), contact time (p = 0.537), and the number of plates and contact time (p = 0.863) and the total Coliforms in electrocoagulation process.

The interaction between variables number of plates and contact time showed that the lowest average total Coliforms occurred in the electrocoagulation process with 6 plates at 90 min, i.e. only 138 Coliform colonies. Although the results of the bivariate analysis showed no significant difference between the number of plates (p = 0.269), contact time (p = 0.537), and number of plates and contact time (p = 0.863), these results indicate effectiveness in using the concept of electrocoagulation compared to the use of other disinfectants. This result can be seen in the figure, which shows that the use of other disinfectants commonly used in hospitals is not very effective in reducing total Coliforms, this is indicated by the presence of a value that exceeds the quality standards for wastewater set by the government, namely at the first inspection with a total Coliforms of 11,067 colonies and a fifth examination with a total Coliforms of 12,009 colonies (maximum standard is 3,000 colonies). Whereas in the use of electrocoagulation, everything is below the environmental quality standard set by the government. This means that this concept is quite effective in use, as a substitute for disinfectants.

Table 5 shows effectiveness of the use of electrocoagulation concept based on the number of plates and contact time. The results showed that by using 6 plates

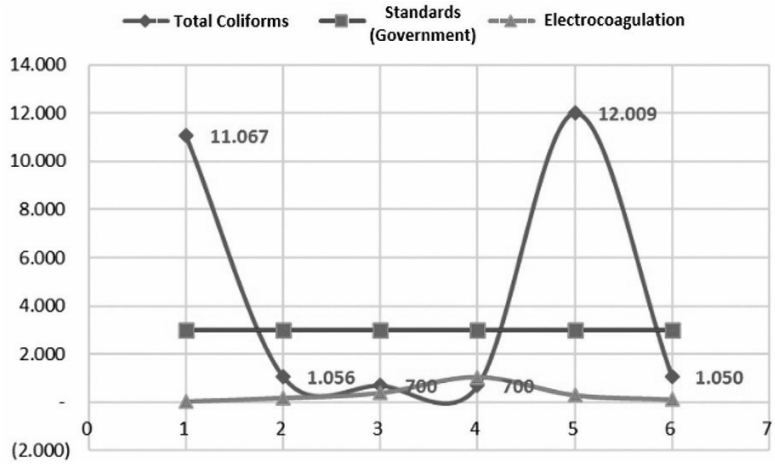

FIGURE. Comparison of total Coliforms based on the use of disinfectants and electrocoagulation concept

TABLE 5. Effectiveness of the use of electrocoagulation in reducing Coliforms [%]

Number of plates	Contact time		
	30 min	60 min	90 min
4	80.49	76.78	48.06
6	73.87	82.68	88.38
8	78.30	78.01	84.45

and 90 min contact time showed the best results in reducing Coliforms (effectiveness of 88.38%). While the lack of effectiveness was shown in the electrocoagulation process using 4 plates with 90 min contact time.

The mechanism of Coliform death in wastewater after electrocoagulation treatment is when hospital wastewater flows through the electrodes. Electron jumps in the electric field from the cathode (negative) to the anode (positive) will "shoot" Coliform bacteria in wastewater. Electric shock in the electrocoagulation system will break down cell walls, which will eventually kill the bacteria.

Conclusions

There is no significant difference between the contact time (p = 0.537), number of electrode plates (p = 0.269) and the total Coliforms in electrocoagulation process. The use of 6 plates and 90 min contact time shows the best results in reducing total Coliforms in the electrocoagulation process with an effectiveness reaching 88.38%. The concept of electrocoagulation can be used as a substitute for disinfectants in reducing total Coliforms in hospital wastewater. Recommendations for the policy makers or end users is to try implement this method as a substitute for disinfectant. Because so far, chemical disinfectants used to reduce microbiological parameters (total Coliforms) have a negative impact on humans and the environment.

Acknowledgements

This study was financially supported by Unit Penelitian dan Pengab-

dian Masyarakat (UPPM) Poltekkes Kemenkes RI Bandung, Ministry of Health, Indonesia scheme.

References

Ahmad, T., Aadil, R.M., Ahmed, H., Rahman, U., Soares, B.C., Souza, S.L., Pimentel, T.C., Scudino, H., Guimaraes, J.T., Esmerino, E.A. & Freitas, M.Q. (2019). Treatment and utilization of dairy industrial waste: a review. *Trends in Food Science & Technology*, *88*, 361-372.

Akansha, J., Nidheesh, P.V., Gopinath, A., Anupama, K.V. & Kumar, M.S. (2020). Treatment of dairy industry wastewater by combined aerated electrocoagulation and phytoremediation process. *Chemosphere*, *253*, 126652. https://doi.org/10.1016/j.chemosphere.2020.126652

Cańizares, P., Jiménez, C., Martínez, F., Sáez, C. & Rodrigo, M.A. (2007). Study of the electrocoagulation process using aluminum and iron electrodes. *Industrial & Engineering Chemistry Research*, *46*(19), 6189-6195.

Chen, X., Chen, G. & Yue, P.L. (2000). Separation of pollutants from restaurant wastewater by electrocoagulation. *Separation and Purification Technology*, *19*(1-2), 65-76.

Chen, X., Chen, G. & Yue, P.L. (2002). Novel electrode system for electroflotation of wastewater. *Environmental Science & Technology*, *36*(4), 778-783.

Darmawanti, T., Suhartana, S. & Widodo, D.S. (2010). Pengolahan Limbah Cair Industri Batik dengan Metoda Elektrokoagulasi Menggunakan Besi Bekas Sebagai Elektroda [Batik industry liquid waste treatment by electrocoagulation method uses scrap metal as an electrode]. *Jurnal Kimia Sains dan Aplikasi*, *13*(1), 18-24.

Deepak, S. (2014). Treatment of dairy waste water by electro coagulation using aluminum electrodes and settling, filtration studies. *International Journal of ChemTech Research*, *6*(1), 591-599.

Djaja, I.M. & Maniksulistya, D. (2006). Gambaran pengelolaan limbah cair di Rumah Sakit X Jakarta Februari 2006 [Hospital Wastes Water Management in Jakarta February 2006]. *Makara Kesehatan*, *10*(2), 60-63.

Dura, A. & Breslin, C.B. (2019). The removal of phosphates using electrocoagulation with Al−Mg anodes. *Journal of Electroanalytical Chemistry*, *846*, 113161. https://doi.org/10.1016/j.jelechem.2019.05.043

Fajardo, A.S., Rodrigues, R.F., Martins, R.C., Castro, L.M. & Quinta-Ferreira, R.M. (2015). Phenolic wastewaters treatment by electrocoagulation process using Zn anode. *Chemical Engineering Journal*, *275*, 331-341.

Gomez, K.A. & Gomez, A.A. (2007). *Statistical Procedures for Research.* Jakarta: Universitas Indonesia Press.

Hakim, A.R. & Hardianti, B.D. (2017). Pendekatan Aplikasi DEWATS Dalam Manajemen Limbah Cair Rumah Sakit [DEWATS application approach in hospital wastewater management]. *Jurnal Biologi Tropis*, *17*(2), 28-34.

Hakizimana, J.N., Gourich, B., Chafi, M., Stiriba, Y., Vial, C., Drogui, P. & Naja, J. (2017). Electrocoagulation process in water treatment: a review of electrocoagulation modeling approaches. *Desalination*, *404*, 1-21.

Harif, T., Khai, M. & Adin, A. (2012). Electrocoagulation versus chemical coagulation: coagulation/flocculation mechanisms and resulting floc characteristics. *Water Research*, *46*(10), 3177-3188.

Jagadal, C.B., Hiremath, M.N. & Shivayogimath, C.B. (2017). Study of dairy wastewater treatment using monopolar series system of electrocoagulation process with aluminium electrodes. *International Journal of Innovative Research in Science, Engineering and Technology*, *6*(7), 12891-12898.

Kim, T., Kim, T-K. & Zoh, K-D. (2020). Removal mechanism of heavy metal (Cu, Ni, Zn, and Cr) in the presence of cyanide during electrocoagulation using Fe and Al electrodes. *Journal of Water Process Engineering*, *33*, 101109. https://doi.org/10.1016/j.jwpe.2019.101109

Kobya, M. & Demirbas, E. (2015). Evaluations of operating parameters on treatment of can manufacturing wastewater by electrocoagulation. *Journal of Water Process Engineering*, *8*, 64-74.

Lakshmanan, D., Clifford, D.A. & Samanta, G. (2010). Comparative study of arsenic re-

moval by iron using electrocoagulation and chemical coagulation. *Water Research*, *44*(19), 5641-5652.

Liu, F., Zhang, Z., Wang, Z., Li, X., Dai, X., Wang, L., Wang, X., Yuan, Z., Zhang, J., Chen, M. & Wang, S. (2019). Experimental study on treatment of tertiary oil recovery wastewater by electrocoagulation. *Chemical Engineering and Processing-Process Intensification*, *144*, 107640. https://doi.org/10.1016/j.cep.2019.107640

Lu, J., Li, Y., Yin, M., Ma, X. & Lin, S. (2015). Removing heavy metal ions with continuous aluminum electrocoagulation: A study on back mixing and utilization rate of electrogenerated Al ions. *Chemical Engineering Journal*, *267*, 86-92.

Miwa, D.W., Malpass, G.R.P., Machado, S.A.S. & Motheo, A. (2006). Electrochemical degradation of carbaryl on oxide electrodes. *Water Research*, *40*(17), 3281-3289.

Ni'am, A.C., Caroline, J. & Afandi, M.H. (2017). Variasi jumlah elektroda dan besar tegangan dalam menurunkan kandungan COD dan TSS limbah cair tekstil dengan metode elektrokoagulasi. *AL-ARD: Jurnal Teknik Lingkungan*, *3*(1), 21-26.

Niati, P.D. & Widarto (2006). Penentuan kandungan unsur pada instalasi Pengolahan air limbah (IPAL) RSUP dr. Soeradji Tirtonegoro Klaten dengan metode Aanalisis Aktivasi Neutron Reaktor Kartini. *Jurnal Pendidikan Fisika Indonesia*, *4*(2), 120-125.

Nidheesh, P.V. & Singh, T.S.A. (2017). Arsenic removal by electrocoagulation process: recent trends and removal mechanism. *Chemosphere*, *181*, 418-432.

Notoatmodjo, S. (2010). *Health Research Methodology*. Jakarta: Rineka Cipta.

Önder, E., Koparal, A.S. & Öğütveren, Ü.B. (2007). An alternative method for the removal of surfactants from water: Electrochemical coagulation. *Separation and Purification Technology*, *52*(3), 527-532.

Rad, S.J. & Lewis, M.J. (2014). Water utilization, energy utilization and waste water management in the dairy industry: a review. *International Journal of Dairy Technology*, *67*(1), 1-20.

Ridantami, V., Bangun, W., Prayitno (2016). Pengaruh tegangan dan waktu pada pengolahan limbah radioaktif uranium dan torium dengan proses elektrokoagulasi [Effects of voltage and time on uranium and thorium liquid radioactive waste treatment using electrocoagulation process]. *Jurnal Forum Nuklir (JFN)*, *10*(2), 102-107.

Sadeddin, K., Naser, A. & Firas, A. (2011). Removal of turbidity and suspended solids by electro-coagulation to improve feed water quality of reverse osmosis plant. *Desalination*, *268*(1), 204-207.

Setianingrum, N.P., Prasetya A. & Sarto dan (2017). Pengurangan Zat Warna Remazol Red Rb Menggunakan Metode Elektrokoagulasi secara *Batch* [Reduction of remazol red Rb dyes using a batch electrocoagulation method]. *Jurnal Rekayasa Proses*, *11*(2), 78-85.

Silva, J.F.A., Graça, N.S., Ribeiro, A.M. & Rodrigues, A.E. (2018). Electrocoagulation process for the removal of co-existent fluoride, arsenic and iron from contaminated drinking water. *Separation and Purification Technology*, *197*, 237-243.

Standar Nasional Indonesia [SNI] (2008). *Water and wastewater*. *Part 59: Methods for sampling wastewater* (SNI 6989.59:2008). Jakarta: Badan Standardisasi Nasional.

Syam B.D. & Nidheesh, P.V. (2020). A review on electrochemical treatment of arsenic from aqueous medium. *Chemical Engineering Communications*, *11*, 1-22.

Tapotubun, A.M., Savitri, I.K.E. & Matrutty, T.E.A.A. (2016). Panghambatan bakteri patogen pada ikan segar yang diaplikasi *Caulerpa lentillifera* [The Inhibitor Pathogen Bacteria's of Sea Grape *Caulerpa lentillifera* Applies on Fresh Fish]. *Jurnal Pengolahan Hasil Perikanan Indonesia*, *19*(3), 299-308.

Tchamango, S., Nanseu-Njiki, C.P., Ngameni, E., Hadjiev, D. & Darchen, A. (2010). Treatment of dairy effluents by electrocoagulation using aluminium electrodes. *Science of the Total Environment*, *408*(4), 947-952.

Van Genuchten, C.M., Addy, S.E., PenÞa, J. & Gadgil, A.J. (2012). Removing arsenic from synthetic groundwater with iron electrocoagulation: an Fe and As K-edge EXAFS study. *Environmental Science & Technology*, *46*(2), 986-994.

Wiyanto, E., Harsono, B., Makmur, A., Pangputra, R., Julita, J. & Kurniawan, M.S. (2017). Penerapan elektrokoagulasi dalam proses penjernihan limbah cair [Application of electrocoagulation in the process of clarifying wastewater]. *Jetri: Jurnal Ilmiah Teknik Elektro*, *12*(1), 19-36.

Summary

Study on the utilization of electrocoagulation concept as a disinfectant substitute in hospital wastewater. The purpose of this study is to identify differences in variations of contact time and number of electrode plates in electrocoagulation process on the decrease of total Coliforms in Bandung City hospital wastewater. An experimental research with factorial randomized design. The volume of wastewater sample to check the total Coliforms was a minimum of 100 ml, using 3 treatments and 6 repetitions. Data analysis used was two-way ANOVA test. The results showed that there was no significant difference between the number of plates ($p = 0.269$), contact time ($p = 0.537$), and the number of plates and contact time ($p = 0.863$) with the total Coliforms in electrocoagulation process. The use of 6 plates and 90 min contact time showed the best results in reducing total Coliforms, with effectiveness reaching 88.38%. This means that the concept is quite effective to use as a substitute for disinfectant.

Authors' address:
Elanda Fikri – corresponding author
(https://orcid.org/0000-0001-7196-6011)
Diponegoro University
Doctorate Program of Environmental Studies
Semarang, 50241
Indonesia
e-mail: elandafikri@yahoo.com

Scientific Review – Engineering and Environmental Sciences (2021), 30 (2), 271–282
Sci. Rev. Eng. Env. Sci. (2021), 30 (2)
Przegląd Naukowy – Inżynieria i Kształtowanie Środowiska (2021), 30 (2), 271–282
Prz. Nauk. Inż. Kszt. Środ. (2021), 30 (2)
http://iks.pn.sggw.pl
DOI 10.22630/PNIKS.2021.30.2.23

Abdulamir Hussein QASIM

University of Kirkuk, College of Engineering

Causes and side effects of changing water quality in Khassa-Chai river in Kirkuk, Iraq

Key words: water quality assessment, water availability, surface water, physiochemical characteristics

Introduction

Thanks to water, human civilization has been found and developed on our planet. Due to the water crisis, the source of life has become a major concern in recent years. In the face of population growth and industrial developing water demand increased and safe water supply been a pre-requisite. The impact of climate change is evident in reducing the natural flow of seasonal rivers in Iraq (Qasim, 2017; Pham & Tran, 2020).

The river's flow in an urban area is often highly variable and much polluted (Covarrubia, Rayburg & Neave, 2016; Joshua & Adeniyi, 2020). Due to human activities, a significant decrease in water quantity alongside dramatic deterioration of water level is still increasing. In Iraq, there is evidence that the decline in water quantity is still seen in Iraqi main rivers. In addition to that, there is sufficient evidence of a decline in the water quality of the rivers and their tributaries that enter the country since 1990 (Qasim, 2017). As a consequence, the changes in the physicochemical parameters of the water (i.e. temperature, pH, electrical conductivity, turbidity, salinity, suspended solids, etc.) will surely affect the living conditions of aquatic organisms.

One of the important steps in achieving an effective pollution control of surface water is the monitoring and assessment of water quality. Water quality changes may be due to climate change and due to anthropogenic activities. The solubility of salts and minerals in the water may originate by weathering and erosion of fractured bedrock into water bodies. Therefore, there is a need to reduce or prevent activities that can increase the pollution level of the rivers. Various investigations and studies have shown that

anthropogenic activities will negatively impact on changes in water availability (Izonfuo & Bariweni, 2001; Akpan-Idiok, Ibrahim & Udo, 2012; Taiwo, Arowolo, Adekunle & Adetunji, 2013; Taiwo, Beddows, Shi & Harrison, 2014; Awomeso, Taiwo, Idowu, Gbadebo & Oyetunde, 2019). Urban runoff was recognized as one of the ordinary causes of water pollution. Municipal and agricultural wastes such as food processing, textile making, poultry, and abattoir wastes would be put at the top of these activities (Ayantobo, Awomeso, Oluwasanya, Bada & Taiwo, 2014; Ojekunle et al., 2014).

In Iraq, as a result of the discharge of untreated wastewater, many rivers, and urban streams are polluting (Qasim, 2019). Washing, bathing, and periodic watering of livestock are considering other sources of pollutions. The lack of development and maintenance programs is causing water crisis. It is therefore a multipurpose dam (58 m high with a total length of 2.36 km) designed to maintain water supply into the Khassa-Chai river during all seasons (Zedan, Faris & Abdulsattar, 2017; Khassaf & Madhloom, 2019).

However, over the past three decades, the subsequent absence of funds led to contamination of the Khassa-Chai river by urban, industrial and agricultural activities. In addition, no academic environmental research has been done to explain the serious deterioration in the river's condition. The lack of research and studies in this area has not helped decision-makers to react adequately to protect the river environment. In order to call for quick action and cooperation with local government and individuals, this research will bring further attention to river safety.

Material and methods

Study area

Khassa-Chai river is a seasonal tributary of Zaghaitun river, which is in turn flowing into the Al-Adhaim dam reservoir (10 km) northeast of Kirkuk near Kuchuk village. The section of the river studied lies within latitude 35°21.010′––35°35.103′N and longitude 44°18.107′––44°39.045′E (Fig. 1). The study was carried out in Khassa-Chai river located in Kirkuk, Northeast Iraq. The water in the river and the reservoir behind the dam may allow for recreational activities such as boating and fishing. In addition to recreation and leisure purposes, major human activities within the study area are farming and gravel dredging. To determine the characteristics of the river and evaluate its water quality, eight sites have been identified along the Khassa--Chai river. The results of these eight sites may highlight the concept of water pollution and its effects. Consequently, the results will determine how the river was affected by the pollution associated with the urban development of the city of Kirkuk.

Observation point 1 is located in village Dollowar (15 km north Kirkuk city). Several small buildings and rehabilitation activities are going on in the watershed. Thanks to land topography, the storm-waters from the mountains discharge towards the river. At this point, the Khassa-Chai river is relatively shallow with rocky bed, banks, and reaches with sandy or muddy bottoms. Observation point 2 is located in the village of Coran, 3 km downstream of the first point. Activities like irrigation

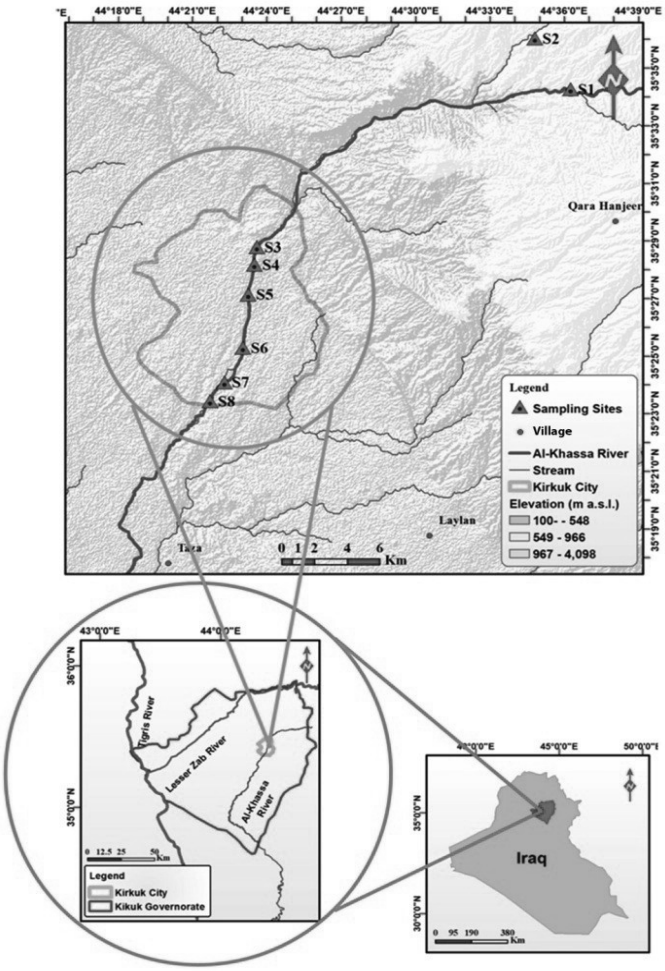

FIGURE 1. Map of Khassa-Chai river shows water observation points

and periodic watering of livestock were observed during the whole year. To provide potable water to the villagers and their domestic animals, several drinking water compact units have been started in construction by non-governorate organizations (NGOs) after 2005 but without enough preliminary research studies on the river. Thus, this point was abandoned as a drinking water source yet. Observation points 3–8 are located inside Kirkuk city along 18 km. These points are relatively shallow with sandy or muddy bottoms. In the absence of minimum maintenance flow and insufficient wastewater treatment plants, the Khassa-Chai river is affected by changes in water characteristics. Therefore, gray-water discharges into these points from multiple and single residences and building sectors along the edge of the river.

Sampling technique

To ensure the conservation of a stretch of water of the Khassa-Chai, it is necessary to study the importance of the river, its connection to the health and enjoyment of Aboriginal people who live here. Thus, this seasonal river has two important roles for Kirkuk citizens. The first role is depending on the water quantity. During the winter and spring seasons, the Khassa-Chai river provides sufficient water amounts for agricultural lands. More than 74 ha of agricultural land play the sole subsistence income for more than 38 multiple families. These lands produced various types of agricultural products like onions, cabbage, celery, etc. which can be sold locally by the villagers, or sold through local distribution facilities and markets or directly along the interior roads of the city.

The second important role of the Khassa-Chai river is represented in receiving municipal wastewater and residual runoff from agricultural land. In addition to those two important roles, the river coast turns of a free wide disposal site for solid waste during dry seasons (summer and autumn). This uncontrolled disposing of solid waste, such as garbage, glass, plastic, etc. is adding more challenge to the local government in Kirkuk. However, these roles could represent a conflicting interest with the recreational purposes and presence of natural aquatic life in the Khassa-Chai river.

To study and analysis those vital topics, 37 water samples were collected from eight monitoring points along the Khassa-Chai river. Two of these points are outside of Kirkuk city in, while the other six points located inside the city as illustrated schematically in Figure 1. To achieve reliable results, the study covered both rainy and dry seasons between April 2017 and January 2018. Two types of parameters have been considered here: physical and chemical. These physicochemical parameters are including temperature, color, pH, total suspended solids (TSS), total dissolved solids (TDS), electrical conductivity (EC), and dissolved oxygen (DO). These two types of water quality parameters (chemical and physical) are determined by using the standard procedures of the American Public Health Association (APHA). The water samples are collected from the eight mentioned points in prewashed one- and two-liter plastic bottles along the Khassa-Chai river.

Water temperature was determined in-situ. To determine the other mentioned physicochemical parameters, water samples were brought to the Sanitary Engineering Laboratory of the College of Engineering (Department of Civil Engineering) and the scientific laboratory of the Environmental Research Unit (ERU) in the College of Sciences – Kirkuk University. The Sanitary Engineering Laboratory is an important laboratory that concerns with the physicochemical analysis of water samples in the university. The water parameters were measured electronically by using various types of tools and devices. For example, Hanna HI 98130 (Hanna Instruments) was used to determine TDS and EC, whereas TSS was determined gravimetrically. Color and turbidity values were determined by using Hanna HI 98130. Colorimeter MD 600 (Lovibond) device was used to determine DO. To examine the water pH levels, the collected water samples were tested by

using the device MultiMeter Instrument SensoDirect 150 (Lovibond).

Statistical analysis

The Statistical Package for Social Science 22.0 was used to analyze the collected data. In this study, the SPSS was assigned to simplify the statistical analysis of the physiochemical measures were performed on all observation points. To achieve a consistent analysis appropriately, the data was entered into pre-prepared tables based on the Microsoft Office Excel 2007. These programs provide users with a good possibility to change statistical requirements according to site data, also to give a measure of how the data distributes itself about the expected value.

By analyzing water samples, the quality of the water, and the causes of environmental degradation which are directly related to the health inside the city of Kirkuk will be able to determine easily. Despite the vast size of the mass of information collected in this study, the predictive nature of the data and outcome produces a minimum probability of error. For future studies, many locations of the Khassa-Chai river could provide promising possibilities to obtain further results on the river's self-purification and existing of hazards ions and heavy metals in the river. Thus, the statistical analysis will simplify the path to better define the expected outcomes of both new and existing outcomes.

Results and discussion

Analytical results

Seasonal variations in the physicochemical parameters of river water quality at different points are shown in Figure 2. During the survey and the case study period, the average monthly temperature was 21.4°C (70.5°F), ranging from an average minimum of 13.2°C (52.2°F) to a maximum of 24.8°C (76.6°F). This wide variation in water temperature has a significant influence on the activity of many types of aquatic organisms. Aquatic organisms are generally more sensitive

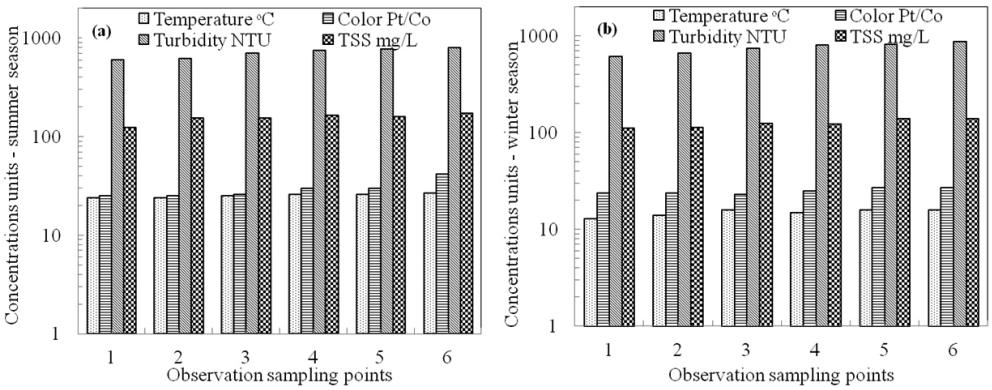

FIGURE 2. Average seasonal concentrations of physicochemical parameters (first group) of Khassa--Chai river during summer (a) and winter (b) season

to the temperature fluctuations than the other terrestrial counterparts (Brown, Le Tissier & Bythell, 1995; Snydner & Rossi, 2004; Hains, 2010; Wałkuska & Wilczek, 2010). Further, seasonal temperature changes often affect the rate of fish eggs development. These changes are a signal to begin the development of the life cycle in the environment.

The concentration of turbidity was ranging between 610 and 882 (±6) NTU during winter and summer seasons respectively. Levels of TSS were ranging between 155 and 130 (±5) $mg \cdot L^{-1}$ during the same period (Fig. 2). Loading of sediment, mud, silt material, and other pollutants from the landscape might compromise the purity of the waters waters (Hunsaker & Levine, 1995; Dodds & Oakes, 2008; Hall & Hossain, 2020). The highest concentration of turbidity during the summer is evidence of a considerable reduction in flow rate compared to the winter season. These high values of turbidity and TSS, especially during the dry season, refer to water pollution dramatically. Hence, as a consequence of this, aquatic ecosystems are affected by increased turbidity due to reduced photosynthesis (Henley, Patterson, Neves & Dennis, 2000; Holliday, Rasmussen & Miller, 2003).

Upstream sampling sites are offering less sediment quantity. By increasing the flow rate of water, small water vortex leads the river to become more turbid due to fine mud practices, and therefore, turbidity levels of the river water are increasing towards the Khassa-Chai river downstream in the southwest of Kirkuk city.

In terms of color, the most common cause of color is usually the presence of minerals. Although there were no significant changes in color during summer and winter, the data showed a slight change in color between several observation points located outside and inside of Kirkuk city (Fig. 2). However, this variation in color might refer to changes taking place in soil types and composition.

Figure 3 brings out the variation of physicochemical parameters of the Khassa-Chai river during the study period. The mean concentration levels of EC were ranging between 961 and

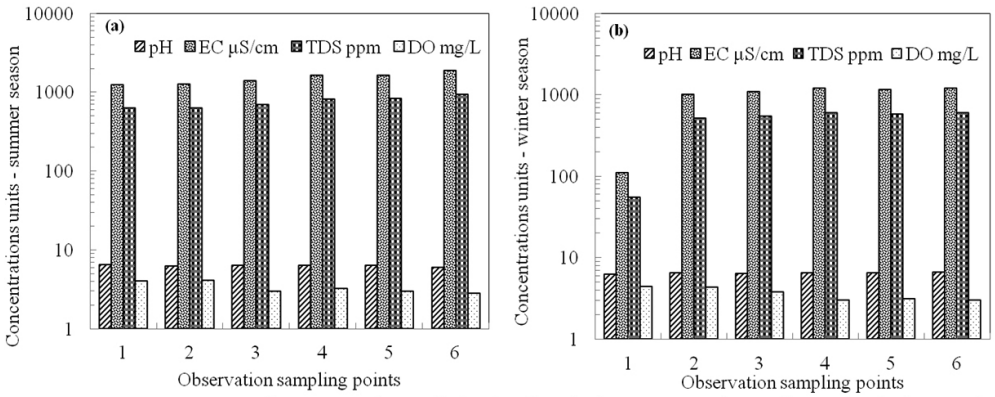

FIGURE 3. Average seasonal concentrations of physicochemical parameters (second group) of Khassa--Chai river during summer (a) and winter (b) season

1,509 (±5) $\mu S \cdot cm^{-1}$ during the winter and the summer seasons respectively; and TDS was ranging between 480 and 755 (±4) $mg \cdot L^{-1}$. The results show that the pH values were ranging from 6.29 to 6.51 (±0.29). The pH values of the Khasa-Chai river did not change significantly over the two seasons. The variation of pH values is due to the buildup of organic material from plant leaves and animals, in addition to other pollutant resources, such as water mixed with chemicals, paints, and hot water that discharge from various local factories along the river. However, the results showed that the pH values did not exceed the specific standard of the World Health Organization (WHO) and are almost acceptable.

The results presented in Figure 4 of this study is showing that, in most cases, the water quality of the Khassa-Chai river towards the south of Kirkuk city does not meet the WHO guidelines of the water quality. These values are greatly exceeding the recorded level in the north of the city. To summarize the results, three main findings can be drawn from figures described above.

Factor 1 is related to the turbidity of water. This factor is linked to the visible problems due to suspended waste and the pollutant that producing from the point and non-point sources. By the accumulation of large amounts of solid waste on the bank of the Khassa-Chai river, the surface water will be subject to the collected pollutant from various kinds of toxic wastes. Subsequently, during the rainfall, different materials including soil, leaves, solid and liquid wastes, pesticides, and chemicals are washed into the surface water bodies. As known, the presence of high levels of turbidity will contribute to increasing the microorganisms and germs in the river. So, degraded water quality in the southwest of Kirkuk can no longer regulate its self-purification and self-recovery capacity; thereby this problem risks accelerating the decline in water quality and availability.

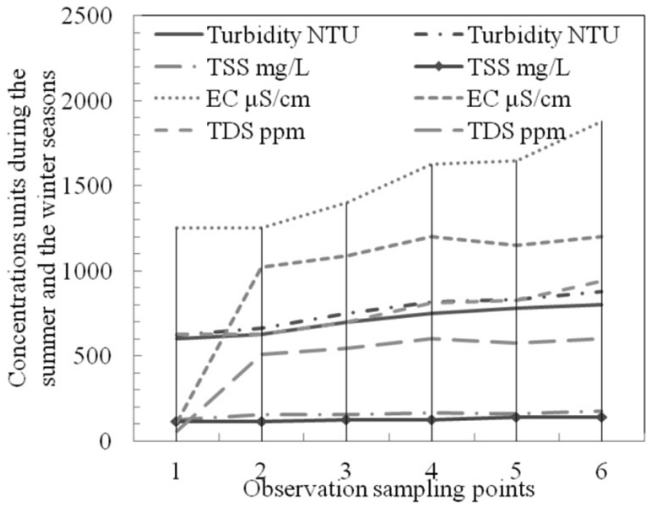

FIGURE 4. Spatial variation of physicochemical parameters (first and second group) of the Khassa-Chai river

Increasing concentrations of TDS and EC toward the south side of Kirkuk is highlighted by Factor 2. Mixing of the river with untreated wastewater is one of the reasons for increasing the EC and TDS (Cole & Ryan, 2003; Taiwo et al., 2014; Ondoo et al., 2019). Anthropogenic sources of water pollution are resulting from farming activities, the use of composted animal manures for soil amendment in addition to other sources such as domestic, and restaurant pollution sources. Increasing population density towards the south of the city (fourth, fifth and sixth locations) will contribute to increasing the accumulation rate of TDS and EC.

Factor 3 refers to small fluctuations in the concentration of TSS at various locations along the river. The results in Figure 4 showed increases in the concentration of total suspended solids from 121 to 143 $mg \cdot L^{-1}$. The result of this factor indicates that most of the contaminants are due to the suspended particles, which are not dissolved in water. These suspended particles, including but not limited to, any minerals, salts or metals in the given watercourses. As a result, the particles could attach to sediment particles and clay minerals that have settled on the river bed and could be carried into water bodies.

Climate change concerns in water quality

Increased climate variability has made both rainfall and dryness patterns more inconsistent and unpredictable in many areas. The variations in temperature have increased since 1975 and affected the frequent recurrence of severe drought and floods (Pantula, 2016; Abed, Bouarbi, Hamidou & Bouzit, 2017; Qasim, 2017; Paredes, Castillo, Viteri, Fuentes & Bodero, 2019). Over the past dedicates, the Khassa-Chai river was experienced a serious drought. As Iraq shows high sensitivity to climate change concerns, it is interesting to assess and discuss some negative side effects. Although this serious problem has become more specific with the formation of different disciplines, it is interesting to assess and discuss some negative side effects. Additionally, the impact of climate change may be hard to isolate it from changes in natural water characteristics.

The effect of climate change on the Khassa-Chai river does not much different from the aggregate effect of climate change on the two main rivers in Iraq (the Tigris and the Euphrates). Historical information and photos show that the water volume of the Khassa-Chai river. The water was so abundant that it was able to help in increasing the amount of water of the tributaries of the Tigris river, especially the tributaries near the southwest of the city of Kirkuk. On the contrary to the previous years, evidence of the impact on water amount in the Khassa--Chai river can already be seen from the frequent drought that has been occurring over the past two decades.

Over the past decade, between the years 2005 and 2015, the lands around the Khassa-Chai river has strongly influenced by seasonal and climatic fluctuations. The impact of climate change on the river is varied between periods of severe drought and floods. The crop with the largest proportion of the cultivated area (more than 65%) was affected by severe and moderate floods. Afterward,

the areas that were severely affected by the floods had up to that point been affected by drought.

In 2012, for example, the torrential rain and flood led to a 1.5 m (5 ft) rise in river levels. The flood led to the collapse of many riverbanks stamens in the upper course of the river. Consequently, the upper soil layers have been eroded that made muddy stream along Khassa-Chai river course toward the river downstream. Returning to the accumulated waste beside the river, it was easy to imagine the amount of pollution caused by drift these pollutants into the riverbed during the rains. This matter led to a considerable loss for the farmers due to the destruction that takes place on their agricultural lands.

The rains and dry seasons have been changing over the years. The influence of high-temperature and low-humidity in Iraq will absolutely lead to higher evaporation rates. Towards its mouth, the drought of the river was a result of high temperatures and low precipitation. Because of these reasons, the climate challenge currently carries serious problems.

As a consequence, the significant elongated dryness pattern has added negative impacts on hundreds of people and increased the negative financial consequences of this problem for the families who are already suffering from the loss of their only financial income that has taken place over the last 15 years. As a result, this situation has caused crops to fail. This situation forced farmers to abandon their lands either due to lack of water (when the plants are young) or due to the extra water amount of irrigation when the plants do not need watering or rarely need water. Thus, although a good amount of water body in Iraq, there is a clear indication of the changes in water quality and quantity (De Stefano, Jacob, Eric, Jim & Aaron, 2017; Qasim, 2017). So, the local government needs to given more attention to water resources management.

Conclusions

The assessment of water quality from different locations in the Khassa-Chai river in Kirkuk showed a significant variation in many of the physicochemical parameters. As a result of human activities, the observed locations of inside the city area are already deteriorating. Four of the observation points inside the city have become a landfill and an accumulation field of solid waste and debris of demolished buildings during urban transformation. The impact of pollution on water quality toward the river downstream has recently become more observant amongst the different location changes. However, northeast of the city of Kirkuk, may provide a good source of irrigation water for defining agricultural activities, but not wholesome for drinking.

Acknowledgements

The researchers gratefully acknowledge the assistance of the Civil Engineering Department and the Environmental Research Unit of the Kirkuk University for their support in the research. The researchers would also like to express their gratitude towards the Faculty of Sciences at the University of Kirkuk for its full support and cooperation provided during the research period.

References

Abed, B., Bouarbi, L., Hamidou, M.K. & Bouzit, M. (2017). A numerical analysis of pollutant dispersion in street canyon: influence of the turbulent Schmidt number. *Scientific Review Engineering and Environmental Sciences*, *26*(4), 423-436.

Akpan-Idiok, A.U., Ibrahim, A. & Udo, I.A. (2012). Water quality assessment of Okpauku River for drinking and irrigation uses in Yala, cross river state, Nigeria. *Journal of Environmental Sciences*, *6*(6), 210-221.

Alex, J.H., Rodney, J., Hubert, L., Bill, F. & Marc, B. (2019). Hypolimnetic oxygenation 2: oxygen dynamics in a large reservoir with submerged down-flow contact oxygenation (Speece cone). *Journal Lake and Reservoir Management*, *35*(3), 323-337.

Awomeso, J.A., Taiwo, A.M., Idowu, O.A., Gbadebo, A.M. & Oyetunde, O.A. (2019). Assessment of water quality of Ogun River in southwestern Nigeria. *IFE Journal of Science*, *21*(2), 375-388.

Ayantobo, O.O., Awomeso, J.A., Oluwasanya, G.O., Bada, B.S. & Taiwo, A.M. (2014). Non-cancer human health risk assessment from exposure to heavy metals in surface and groundwater in Igun Ijesha, southwest Nigeria. *Journal of Environmental Sciences*, *10*(3), 301-311.

Brown, B.E., Le Tissier, M.D. & Bythell, J.C. (1995). Mechanisms of bleaching deduced from histological studies of reef corals sampled during a natural bleaching event. *Journal of Marine Biology*, *122*(2), 655-663.

Cao, X. & Liu, L. (2015). Ecological toxicity of engineered nano materials to the organisms in the environment. *Journal of Advanced Materials Research*, *1094*, 437-440.

Cole, J.M. & Ryan, M.C. (2003). Arsenic source and fate at a village drinking water supply in mexico and its relationship to sewage contamination. In J. Bundschuh, P. Bhattacharya, Chandrasekharam (eds.), *Natural Arsenic in Groundwater; Occurrence, Remediation and Management Conference* (pp. 67-71). London: Taylor & Francis Group.

Covarrubia, J.C., Rayburg, S. & Neave, M. (2016). The influence of local land use on the water quality of urban rivers. *International Journal of GEOMATE*, *11*(23), 2155-2161.

De Stefano, L., Jacob, D.P., Eric, A.S., Jim, E. & Aaron, T.W. (2017). Assessment of transboundary river basins for potential hydro-political tensions. *Journal of Global Environmental Change*, *45*, 35-46.

Dodds, W. & Oakes, R. (2008). Headwater influences on downstream water quality. *Journal of Environmental Management*, *41*(3), 367-377.

Hains, H. (2010). A review of "Freshwater ecology: concepts and environmental applications of limnology". *Journal Lake and Reservoir Management*, *26*(4), 347-348.

Hall, J. & Hossain, A.K. (2020). Mapping Urbanization and Evaluating Its Possible Impacts on Stream Water Quality in Chattanooga, Tennessee, Using GIS and Remote Sensing. *Journal of Sustainability*, *12*(5), 2-46.

Harmon, W.M. (2018). *Estimating watershed mercury contribution to Lake Fort Smith State Park, University of Arkansas, Fayetteville, USA* (MSc thesis). *Theses and Dissertations*, *2833*. Retrieved from: https://scholarworks.uark.edu/etd/2833 [access 20.06.2020].

Henley, W.F., Patterson, M.A., Neves, R.J. & Dennis, L.A. (2000). Effects of sedimentation and turbidity on lotic food webs: a concise review for natural resource managers. *Journal of Reviews in Fisheries Science*, *8*(2), 125-139.

Holliday, C.P., Rasmussen, T.C. & Miller, W.P. (2003). Establishing the relationship between turbidity and total suspended sediment concentration. In K.J. Hatcher (ed.), *Proceedings of the 2003 Georgia Water Resources Conference*. Athens: University of Georgia.

Hunsaker, C.T. & Levine, D.A. (1995). Hierarchical approaches to the study of water quality in rivers. *Bioscience Journal*, *45*(3), 193-202.

Izonfuo, L.W. & Bariweni, A.P. (2001). The effect of urban runoff water and human activities on some physico-chemical parameters of the Epie Creek in the Niger Delta. *Journal of Applied Science and Environmental Management*, *5*(1), 47-55.

Joshua, I.O. & Adeniyi, A. (2020). A comprehensive review of water quality monitoring and assessment in Nigeria. *Chemosphere*, *260*, 127569. https://doi.org/10.1016/j.chemosphere.2020.127569

Khassaf, S.I. & Madhloom, A.M. (2019). Stability analysis of zoned earth dam under effect of the most dangerous conditions (case study: Khassa Chai dam). *International Journal of Scientific & Engineering Research*, *10*(12), 110-118.

Ojekunle, Z.O., Ufoegbune, G.C., Oyebamiji, F.F., Sangowusi, R.O., Taiwo, A.M. & Ojekunle, V.O. (2014). Assessment of the effect of commercial activities on the surface water quality of Ogun River, Nigeria. *Merit Research Journal*, *2*(9), 196-204.

Ondoo, K.O., Kiptoo, J.K., Onditi, A.O., Shivaji, S.M., Omondi, B. E. & Ogilo, J.K. (2019). Determination of selected water quality parameters in river Sio, Busia County, Kenya. *International Research Journal of Pure and Applied Chemistry*, *18*(3), 1-16.

Pantula, M.R. (2016). *Drought early warning system: Identification of onset end magnitude (SPI and SPEI) and composite index*. Chennai: Notion Press.

Paredes, M., Castillo, T., Viteri, R., Fuentes, G. & Bodero, E. (2019). Microplastics in the drinking water of the Riobamba city, Ecuador. *Scientific Review Engineering and Environmental Sciences*, *28*(4), 653-663.

Pham, H.T. & Tran, T.K. (2020). The Effect of Urbanization on Temperature Trend in Some Regions across Vietnam during the Past Decade. *International Journal of Environmental Science and Development*, *11*(9), 419-424.

Qasim, A.H. (2017). *Impact du changement climatique et qualité de l'eau sur les bassins du Tigre et de l'Euphrate en Irak: effets sur la polution croissante de l'eau douce* [*Impacts of climate change on water resources (quantity and quality) in the Tigris and Euphrates basins in Iraq*] (PhD thesis). Poitiers: Université de Poitiers.

Qasim, A.H. (2019). International water model under productivity conditions: the case of the Tigris and the Euphrates. *International Journal of GEOMATE*, *17*(62), 29-34.

Shields, F.D., Lizotte, R.E. & Knight, S.S. (2013). Spatial and temporal water quality variability in aquatic habitats of a cultivated floodplain. *River Research and Applications Journal*, *29*(3), 313-329.

Snydner, M.J. & Rossi, S. (2004). Stress protein (HSP70 family) expression in intertidal benthic organisms: The example of Anthopleura elegantissima (Cnidaria: Anthozoa). *Journal of Marine Science*, *68*(1), 155-162.

Taiwo, A.M., Arowolo, T.A., Adekunle, I.M. & Adetunji, M.T. (2013). Evaluating the environmental impacts of poultry farming on stream water quality: A study from Abeokuta, Nigeria. *Journal of Environmental Quality Management*, *22*(4), 79-93.

Taiwo, A.M., Beddows, D.C., Shi, Z. & Harrison, R.M. (2014). Mass and number size distributions of particulate matter components: comparison of an industrial site and an urban background site. *Science of the Total Environment Journal*, *475*, 29-38.

Wałkuska, G. & Wilczek, A. (2010). Influence of discharged heated water on aquatic ecosystem fauna. *Polish Journal of Environmental Studies*, *19*(3), 547-552.

World Health Organization [WHO] (2016). *Guidelines for Drinking-Water Quality (Fourth edition incorporating the first addendum)*. Geneva: World Health Organization.

Zedan, A.J., Faris, M.R. & Abdulsattar, A.A. (2017). Seepage analysis through an earth dam (Khasa-Chai Dam) as a case study. *Engineering and Technology Journal*, *35*(2), 172-181.

Summary

Causes and side effects of changing water quality in Khassa-Chai river in Kirkuk, Iraq. Water quality of seasonal water rivers is on a quick decline due to various human activities arising as a result of urbanization and population growth. This study assessed the water quality of the Khassa-Chai river in Kirkuk during two seasons: winter and summer (wet and dry). Thirty-seven water samples were collected from eight monitoring observation points along the Khassa-Chai river during October 2019 and March 2020. Water samples were analyzed for various parameters such as temperature, pH, electrical conductivity (EC), turbidity, total suspended solids (TSS), total dissolved solids (TDS), color, and dissolved oxygen

(DO). These physicochemical parameters were analyzed using standards methods demonstrated by the American Public Health Association (APHA). To determine the significant difference, all the results obtained were statistically analyzed. In most results, higher concentrations are out of the indicated permissible limits of the World Health Organization (WHO). It can be concluded that the most domestic wastewater effluents are discharged into the river, such as sewage coming from nearby houses and restaurants in addition to the solid waste produced from close commercial stores. To reduce the negative impact on water and human health, pollution sources need to be properly managed. The paper calls for further research to figure out the ability of the Khassa-Chai river to make the use of city water in improving the environment.

Author's address:
Abdulamir Hussein Qasim – corresponding author
(https://orcid.org/0000-0002-4695-3021)
University of Kirkuk
College of Engineering
Department of Civil Engineering
Environmental Research Unit
36013, Kirkuk
Iraq
e-mail: aqasim01@uokirkuk.edu.iq

Scientific Review – Engineering and Environmental Sciences (2021), 30 (2), 283–292
Sci. Rev. Eng. Env. Sci. (2021), 30 (2)
Przegląd Naukowy – Inżynieria i Kształtowanie Środowiska (2021), 30 (2), 283–292
Prz. Nauk. Inż. Kszt. Środ. (2021), 30 (2)
http://iks.pn.sggw.pl
DOI 10.22630/PNIKS.2021.30.2.24

Muna H. AHMED, Ali M. Al-SALIHI, Hazim H. HUSSAIN

Mustansiriyah University, College of Sciences

Testing the performance of a solar energy cooling system in Baghdad city

Key words: cool buildings, solar chimney, ground heat exchanger, weather conditions

Introduction

The search for alternative ways to cool the air in the hot long season instead of using the electric power has become an important issue due to the severe shortage of electric power generation in the last two decades due to the deterioration of the infrastructure. According to Iraqi Meteorological Organization, the air temperature recordings in 2018 have exceeded 50°C. Hence, adopting renewable energy technologies such as solar cooling is one of the good solutions to the power problem in the country. In addition to this good feature, using the renewable energy would reduce fossil fuel consumption and pollutant gas emissions into the atmosphere. The energy can have many forms such as kinetic, potential, electromagnetic, nuclear, sound, light or photo-energy, and gravitational (Mohamed, 2017). Energy is important issue for human development, and acts as a key factor in determining the economic development of all countries (Atwan, Kasim, Jasim & Hameed, 2020). Fossil fuels are burned by power plants, transportation methods and by different industries. This results in emitting large amounts of pollutants, which endanger human health, has a negative impact on the economy and destroys the natural environment.

While most of today's energy is derived from fossil fuels, new technologies offer a range of electricity generation and cooling and heating options where they are required. These new options contain renewable energy technologies (Haghighi & Maerefat, 2015). Internal conditions in most buildings are uncomfortable because of extreme outdoor weather conditions and the incorrect locations of windows and doors that implements natural ventilation (Zaidan,

Abed & Jasim, 2019). Consumption of high-grade energy has risen considerably with growing needs to obtain thermal comfort conditions inside buildings, residential complexes, greenhouses, cattle buildings, etc. (Bisoniya, 2015). Passive system terminology is applied to buildings that have, as integral parts, elements that admit, absorb, store, and emit solar energy; thus, reducing the need for more energy for comfort heating. These elements have something to do with the right orientation of the buildings, the right dimensions of openings, the use of terrace and other shading devices, and the use of insulation and thermal mass (Kalogirou, 2014). A passive strategy for cooling buildings can be obtained from natural ventilation. Effective ventilation and thermal comfort are of great significance in rural areas and in hot climate. One of the natural ventilation techniques that are used for conditioning buildings and which can participate to progress the energy efficiency of facilities are solar chimneys (Saifi, Settou, Dokkar, Negrou & Chennouf, 2012). Solar chimney has been frequently adopted in buildings to save energy by enhancing the natural ventilation (Shi et al., 2019). It can be defined as a natural-draft system that uses solar radiation to move air upward and thus transforms solar energy into kinetic energy of air. The use of constant pressure air density decreases with the increase in temperatures. Air with higher temperature than that of ambient air is driven upwards by the buoyancy forces. A solar chimney makes use of this physical phenomenon (Charvat, Jicha & Stetina, 2014). A second technique called ground heat exchanger, can be utilized which is a heat transfer device that exchanges heat between two or more process fluids (Zohuri, 2017). This technique is known by many different names such as the buried pipe system, underground air tunnel, earth tube heat exchanger and earth air tunnel. A variety of applications such as building thermal comfort, animal residence and agricultural greenhouses utilizes this system (Taib, Anuar & Ibrahim, 2015). It is an ancient technique that has been used for thousands of years with high efficiencies especially in the hotter and drier climates (Ariffin, Sanusi & Noor, 2014). The cooling tubes system consists of long pipes buried underground with one end connected to the house and the other end to the outside (Zaki, Amjad & Almssad, 2007). Passive techniques are used to decrease the effect of the climate impacts on buildings by using insulating materials and air control system, which mean saving energy and reducing the demanded for cooling (Abed, Zaidan & Jasim, 2019). This system works automatically as a result of the pressure difference between hot and cold air as the air flows from areas of higher pressure (cold air) to areas of lower pressure (hot air).

Our research aims to design a cooling system that depends on water and solar energy that can be used to cool houses or poultry fields and other facilities in areas adjacent to rivers, lakes, marshes and other water bodies.

Correlation in the broadest sense is a measure of an association between variables. In correlated data, the change in the magnitude of one variable is associated with a change in the magnitude of another variable, either in the same (positive correlation) or in the opposite (negative correlation) direction. Most

often, the term correlation is used in the context of a linear relationship between two continuous variables and expressed as Pearson product–moment correlation (Schober, Boer & Schwarte, 2018). The correlation coefficient (r) is a test of the linear relationship between the calculated and measured value which is defined by:

$$r = \frac{\sum_{i=1}^{N}\left(y_i - \overline{y}\right)\quad\left(x_i - \overline{x}\right)}{\left[\left\{\left[\sum_{i=1}^{N}\left(y_i - \overline{y}\right)\right]\right\}\quad\left\{\left[\sum_{i=1}^{N}\left(x_i - \overline{x}\right)\right]\right\}\right]^{0.5}} \tag{1}$$

where:
N – number of the values,
y_i – estimated value,
x_i – measured value,
$\overline{y}$ – mean value of the estimated values,
$\overline{x}$ – mean value of the measured values.

Material and methods

The current study was carried out in Baghdad during April and May 2020. The constructed design is an innovative cooling system that consists of a test room, a chimney and a heat exchanger (Figs. 1 and 2). The test room (1 m^3 size volume) was built by using sandwich

FIGURE 1. Images of the system

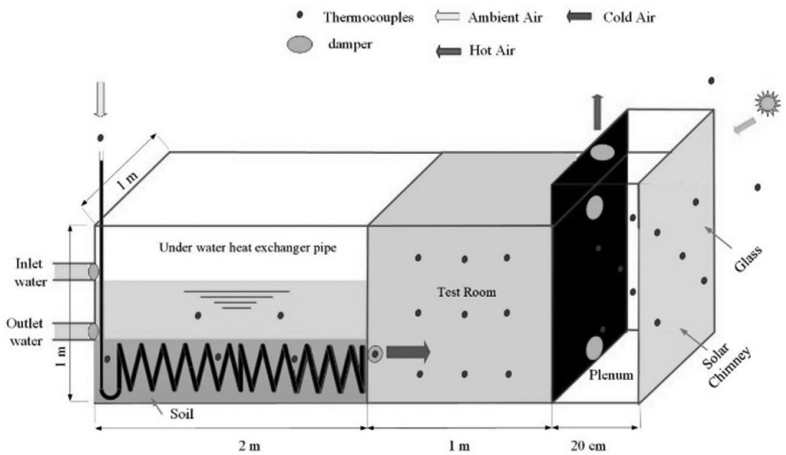

FIGURE 2. The system diagram

panel material with a thickness of 5 cm. This room is connected to a solar chimney (20 cm length, 1 m width and 1 m height). The front side of the chimney was made of glass panels facing the geographical South. The other side consists of a metal plate painted black to enhance the absorption of solar energy during daytime. The heat exchanger was made of aluminum pipe (16 m length, 20 cm diameter).

The air inside the chimney heats up, rises and floats to the top of the chimney and exits from the ventilation hole. This movement of air will lead to an imbalance in air pressure causing to draw the cold air from the test room through the heat exchanger. The latter was buried with a layer of 20 cm thick mixed soil placed at the bottom of a submerged basin. The heat exchanger inlet exposed to the outside air and the outlet is connected to the test room. The basin that contains the water and the heat exchanger was made of galvanized iron plates of 1 mm thick. It was surrounded from outside by a layer of mixed soil 5 mm thick. It is also insulated with a sandwich panel material (2 m length, 1 m width, 1 m height). To study the effect of weather conditions on the performance of the system, the weather parameters such as solar radiation, ambient air temperature, wind speed and relative humidity were measured using an automatic weather station. In addition, a grid of 20 thermocouples were used to measure the temperature at the various parts of the system during test process. These parts include water and soil in the bottom of the water basin, inlet and outlet air, heat exchanger, test room and solar chimney. The measurements were recorded by Data Locker that stores data and which powered by solar energy.

The efficiency of the cooling system (E_{ff}) was calculated using the following equation (Zaidan et al., 2019):

$$E_{ff} = \frac{(T_{in} - T_{out})}{T_{in} - T_w} \cdot 100 \qquad (2)$$

where:

T_{in} – inlet air temperature of the heat exchanger,

T_{out} – outlet air temperature of the heat exchanger+,

T_w – water temperature.

Results and discussion

The changes in temperatures of test room, chimney, water, air at heat exchanger inlet and outlet and the solar radiation for April are visualized in Figure 3. The results show that temperatures begin to rise gradually. Maximum temperatures were recorded to be 23.5°C in test room at 3 pm, 56.95°C in chimney at 2 pm, 30.57°C for inlet air at 2 pm, 18.36°C for water at 5 pm, and 19.43°C for outlet air at 5 pm. By the same approach, the results of May were also visualized in Figure 4. Maximum temperatures were recorded to be 27.01°C at 3 pm at test room 56.76°C in the chimney at 2 pm, 33.97°C for in let air at 2 pm, 21°C for water at 5 pm and 22.08°C for outlet air at 5 pm. It is clear that the temperature of the system was changing according to the change in solar radiation. Those changes in the temperature are identical to those published in 2012 study (Saifi et al., 2012).

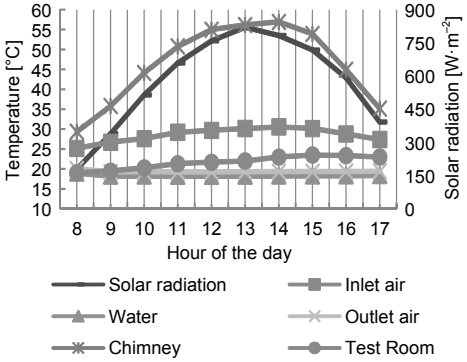

FIGURE 3. Temperature changes and solar radiation with the time in April 2020

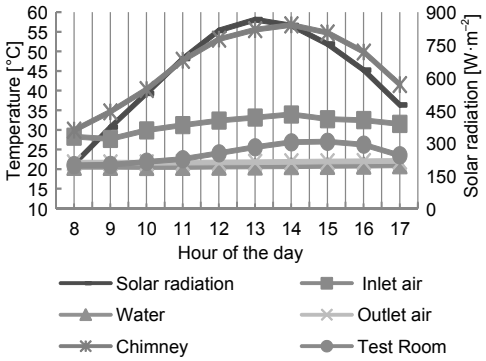

FIGURE 4. Temperature changes and solar radiation with time in May 2020

The difference between test room temperature and ambient air temperature during April is shown in Figure 5. The minimum difference was recorded to be 3.2°C at 8 am while the maximum difference (8.35°C) was recorded at 4 pm, it was during May. The minimum and maximum values of temperature were recorded to be 4.63 and 9.49°C at 8 am and 5 pm, respectively (Fig. 6). Thus, it is obvious that temperature of the test room was less than that of the ambient air.

The effectiveness of the system was calculated as the rate during the period (April and May 2020) using Eq. (2) and data in Table 1. The results of effectiveness for April and May were 89.01 and 89.5%, respectively. The results are almost identical to those stated by Zaidan et al. (2019) where the cooling efficiencies were 92.6 and 90.05%. A relationship was found between the cooling efficiencies and the factors related to the weather conditions by finding Pearson correlation coefficient in Eq. (1). Table 2 shows the weather data during study period. This relationship is seen in Figure 7 between the intensity of solar radiation and the efficiency of the system during daytime in April. A 0.91 correlation coefficient was obtained from the relationship between

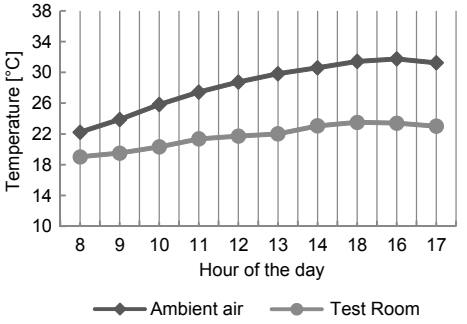

FIGURE 5. The difference in ambient air and test room temperature in April 2020

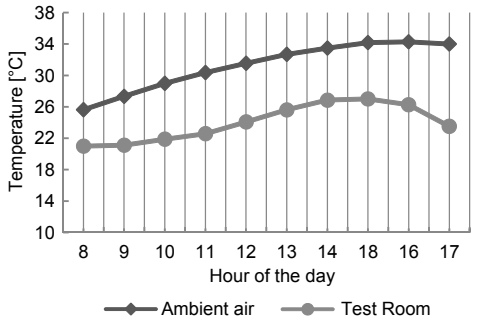

FIGURE 6. The difference in ambient air and test room temperature in May 2020

TABLE 1. Temperatures of inlet air, water, outlet air and efficiency for April and May 2020

Time	April				May			
	inlet air temperature [°C]	water temperature [°C]	outlet air temperature [°C]	temperature efficiency [%]	inlet air temperature [°C]	water temperature [°C]	outlet air temperature [°C]	temperature efficiency [%]
08:00	25.20	18.98	20.03	83.11	28.30	20.60	21.66	86.23
09:00	26.75	18.21	19.28	87.47	27.72	20.59	21.65	85.13
10:00	27.66	18.25	19.33	88.52	29.91	20.57	21.64	88.54
11:00	29.21	18.18	19.27	90.11	31.24	20.58	21.67	89.77
12:00	29.73	18.18	19.27	90.56	32.40	20.63	21.72	90.73
13:00	30.16	18.21	19.31	91.79	33.17	20.69	21.78	91.26
14:00	30.57	18.25	19.35	90.07	33.97	20.77	21.87	91.66
15:00	30.19	18.27	19.37	90.77	32.75	20.84	21.94	91.47
16:00	28.82	18.30	19.39	89.63	32.48	20.91	22.00	90.57
17:00	27.39	18.36	19.43	88.15	31.52	21.00	22.08	89.73

TABLE 2. Weather data for April and May 2020

Time	April				May			
	ambient air [°C]	wind speed [$m \cdot s^{-1}$]	solar radiation [$W \cdot m^{-2}$]	relative humidity [%]	ambient air [°C]	wind speed [$m \cdot s^{-1}$]	solar radiation [$W \cdot m^{-2}$]	relative humidity [%]
08:00	22.22	0.74	179.9	63.7	25.63	0.61	203.9	51.7
09:00	23.87	0.87	339.1	60.3	27.34	0.97	372.8	49.4
10:00	25.81	1.22	514.8	55.4	28.98	1.33	527.6	47.1
11:00	27.44	1.68	659.4	52.0	30.36	1.51	687.0	43.7
12:00	28.74	1.77	759.0	47.0	31.54	1.87	816.0	40.4
13:00	29.82	1.59	821.0	43.4	32.68	2.05	866.1	38.0
14:00	30.60	1.37	783.7	41.1	33.48	2.04	839.3	35.7
15:00	31.42	1.32	718.1	38.5	34.18	1.99	754.1	33.4
16:00	31.75	1.33	592.1	37.1	34.28	1.86	634.5	33.8
17:00	31.24	1.33	392.2	36.1	34.00	2.59	474.4	33.0

them. This indicates that the relationship is very strong, which means that solar radiation is the most important element of the weather condition affecting the system. The results also proved that there is a direct relationship between the intensity of solar radiation and the efficiency of the system's efficiency in May during daylight hours, correlation coefficient reached 0.89, as seen in Figure 8.

Figure 9 shows the relationship between temperature and system effective-

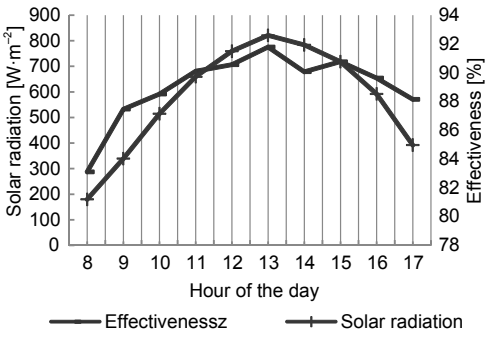

FIGURE 7. The relationship between solar radiation and cooling efficiency in April 2020

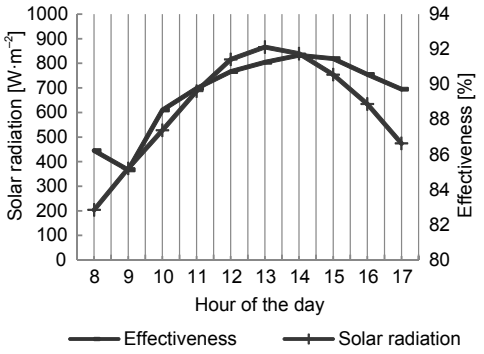

FIGURE 8. The relationship between solar radiation and cooling efficiency in May 2020

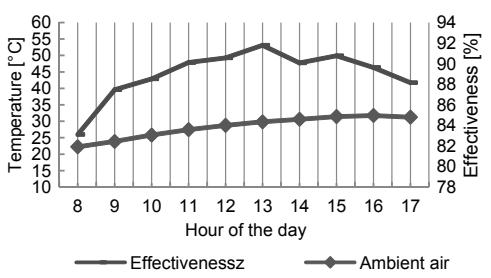

FIGURE 9. The relationship between temperature and cooling efficiency in April 2020

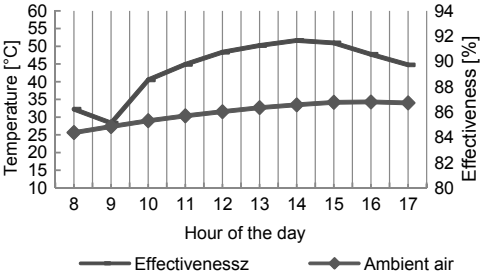

FIGURE 10. The relationship between temperature and cooling efficiency in May 2020

ness changes in April. This relationship has a positive direct correlation coefficient of 0.747. Another relationship between the system's efficiency and temperature in May can be established (Fig. 10). This relationship was positive, and the correlation coefficient of 0.882. This indicates that the increase in temperature lead to the increased of evaporation documenting the efficiency of the system.

Moreover, another relationship between the efficiency and wind speed in April was established as seen in Figure 11. The relationship was found to be direct and the correlation coefficient is 0.82. Figure 12 demonstrates the relationship between system efficiency and wind speed in May. The relationship is direct and the correlation coefficient is 0.814. The increase in wind speed leads to increase in evaporation and hence enhances the efficiency.

Figure 13 shows the relationship between system efficiency and relative humidity in April. The relationship was found to be negative, and the correlation coefficient of –0.665. Finally, the relationship between system efficiency and relative humidity in May were analyzed as shown in Figure 14. The figure indicates that the relationship was of a negative nature, and the correlation coefficient of –0.843.

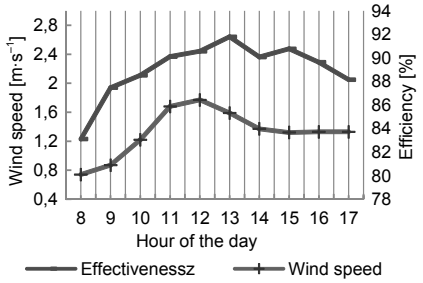

FIGURE 11. The relationship between wind speed and cooling efficiency in April 2020

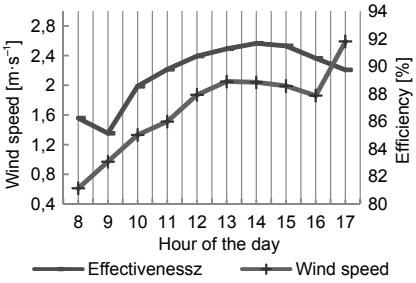

FIGURE 12. The relationship between wind speed and cooling efficiency in May 2020

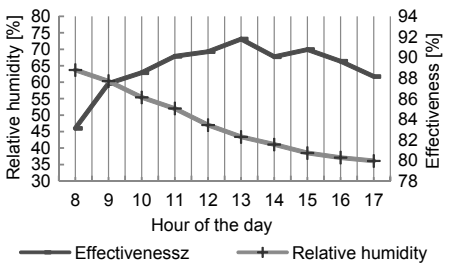

FIGURE 13. The relationship between relative humidity and cooling efficiency in April 2020

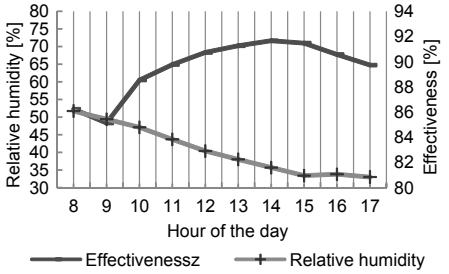

FIGURE 14. The relationship between relative humidity and cooling efficiency in May 2020

The reason for the negative relationship is the relative humidity reduces evaporation which occurs in the water basin. This process is inertial as it does not increase the water temperature (cooling). The heat that water gains from ambient air is lost by evaporation, which makes the water maintain its relative temperatures.

Conclusions

1. The system showed a significant difference in the air temperatures between the test room and the ambient air for April and May 2020. The maximum difference was 8.35°C at 4 pm in April and 9.49°C at 5 pm in May.
2. The cooling efficiency of the system reached maximum values of 89.01% in April and 89.5% in May.
3. There was a positive direct relationship between cooling efficiency and the weather elements such as solar radiation, temperature and wind speed, the correlation coefficient was 0.91, 0.747, 0.82 in April and 0.89, 0.882, 0.814 in May. However, there was a negative relationship between the system efficiency with relative humidity, the correlation coefficient was –0.665 in April and –0.84 in May.

Acknowledgements

Thanks for Mustansiriyah University (https://uomustansiriyah.edu.iq), Baghdad, Iraq for its support to complete this work.

References

Abed, F.M, Zaidan, M.H. & Jasim, A.K. (2019). Cooling building using a geothermal and underwater piping systems techniques (hot and dry weathers). *Journal of Advanced Sciences and Engineering Technologies*, *2*(1), 13-28.

Ariffin, N.A.M., Sanusi, A.N.Z. & Noor, A.M. (2014). Materials for the earth air pipe heat exchanger (EAPHE) system as a passive ground cooling technology for hot-humid climate. In *Handbook on the Emerging Trends in Scientific Research* (pp. 88-98). Singapore: PAK Publishing Group.

Atwan, A.F., Kasim, N.K., Jasim, N.A. & Hameed, J.S. (2020). Improvement the PV solar module cooling systems by using shallow geothermal. *AIP Conference Proceedings*, *2290*(1), 050028. https://doi.org/10.1063/5.0028808

Bisoniya, T.S. (2015). Design of earth–air heat exchanger system. *Geothermal Energy*, *3*(1), 1-10.

Charvat, P., Jicha, M. & Stetina, J. (2004). Solar chimneys for ventilation and passive cooling. In A.A.M. Sayigh (ed.), *Proceedings of the 8th World Renewable Energy Congress (WREC VIII)*: 28th August – 3rd September 2004, Denver, Colorado, USA. Retrieved from: https://www.researchgate.net/profile/Pavel-Charvat/publication/264882993_SOLAR_CHIMNEYS_FOR_VENTILATION_AND_PASSIVE_COOLING/links/53fdd93c0cf22f21c2f85410/SOLAR-CHIMNEYS-FOR-VENTILATION-AND-PASSIVE-COOLING.pdf [access 29.03.2020].

Haghighi, A.P. & Maerefat, M. (2015). Design guideline for application of earth-to-air heat exchanger coupled with solar chimney as a natural heating system. *International Journal of Low-Carbon Technologies*, *10*(3), 294-304.

Kalogirou, S.A. (2014). *Solar energy engineering processes and systems*. Cambridge (MA): Academic Press.

Mohamed, E.L.S. (2017). *Economics of variable renewable sources for electric power production*. Sunnyvale (CA): Lambert Academic Publishing.

Saifi, N., Settou, N., Dokkar, B., Negrou, B. & Chennouf, N. (2012). Experimental study and simulation of airflow in solar chimneys. *Energy Procedia*, *18*, 1289-1298.

Schober, P., Boer, C. & Schwarte, L.A. (2018). Correlation coefficients: appropriate use and interpretation. *Anesthesia & Analgesia*, *126*(5), 1763-1768.

Shi, L., Cheng, X., Zhang, L., Li, Z., Zhang, G., Huang, D. & Tu, J. (2019). Interaction effect of room opening and air inlet on solar chimney performance. *Applied Thermal Engineering*, *159*, 113877. https://doi.org/10.1016/j.applthermaleng.2019.113877

Taib, M.Y., Anuar, S. & Ibrahim, H. (2015). A review of ground heat exchangers for cooling application in the Malaysian climate. *Journal of Mechanical Engineering and Sciences*, *8*, 1426-1439.

Zaidan, M.H., Abed, F.M. & Jasim, A.K. (2019). Air-conditioning of buildings by using ground and water effects to drop down the inlet air temperature. *Journal of Advanced Research in Fluid Mechanics and Thermal Sciences*, *54*(2), 165-174.

Zaki, A.K., Amjad, A.M. & Almssad, A. (2007). Cooling by underground earth tubes. In M. Santamouris, P. Wouters (eds.), *2nd PALENC Conference and 28th AIVC Conference. on Building Low Energy Cooling and Advanced Ventilation Technologies in the 21st Century*, 27-29 September 2007, Crete island, Greece. Book of Proceedings. Vol. 1 (pp. 517-520). Dafni-Athens: Heliotopos Conferences.

Zohuri, B. (2017). Heat exchanger types and classifications. In *Compact Heat Exchangers: Selection, Application, Design and Evaluation* (pp. 19-56). Cham: Springer.

Summary

Testing the performance of a solar energy cooling system in Baghdad city. Renewable energy resources have become a promissory alternative to overcome the problems related to atmospheric pollution and limited sources of fossil fuel energy. The

technologies in the field of renewable energy are used also to improve the ventilation and cooling in buildings by using the solar chimney and heat exchanger. This study addresses the design, construction and testing of a cooling system by using the above two techniques. The aim was to study the effects of weather conditions on the efficiency of this system which was installed in Baghdad for April and May 2020. The common weather in these months is hot in Baghdad. The test room of the design which has a size of 1 m^3 was situated to face the geographical south. The test room is thermally insulated and connected to a solar chimney which generates a convection current to draw the air out of the room through a heat exchanger. The heat exchanger was submerged in a water tank of 2 m length, 1 m width and 1 m height. It was also covered with a layer of soil mixture with a thickness of 10 cm. The experiment simulates the natural conditions of a shallow water surface, connected to the room from the other side. The study results revealed that the air temperature inside the test room was lower than that of the ambient air outside. Pearson correlation coefficient showed that there was a strong direct relationship between solar radiation, temperature and wind speed from one side and the cooling efficiency from the other side. Also, there was a negative correlation between relative humidity and cooling efficiency.

Authors' address:
Muna H. Ahmed
Ali M. Al-Salihi
(https://orcid.org/0000-0002-6945-767X)
Hazim H. Hussain
(https://orcid.org/0000-0002-5588-8030)
Mustansiriyah University
College of Science
Atmospheric Sciences Department
Baghdad, Iraq
e-mail: mahmed@uomustansiriyah.edu.iq
alialsalihi.atmsc@uomustansiriyah.edu.iq
dr.hazim@uomustansiriyah.edu.iq

Scientific Review – Engineering and Environmental Sciences (2021), 30 (2), 293–303
Sci. Rev. Eng. Env. Sci. (2021), 30 (2)
Przegląd Naukowy – Inżynieria i Kształtowanie Środowiska (2021), 30 (2), 293–303
Prz. Nauk. Inż. Kszt. Środ. (2021), 30 (2)
http://iks.pn.sggw.pl
DOI 10.22630/PNIKS.2021.30.2.25

Manar Al-JETHELAH, Hussam DEYAB, Tadahmun YASEEN

Tikrit University, College of Engineering

Thermal performance of novel indirect passive solar dryer

Key words: solar dryer, passive, flat collector, efficiency

Introduction

Drying crops under the sun is a popular method among farmers due to its low cost (Sreekumar, Manikantan & Vijayakumar, 2008; Montero, Blanco, Miranda, Rojas & Celma, 2010; Puglia, Rizzo, Morselli & Tartarini, 2019). However, drying under sun is uncontrolled, and time-consuming. Furthermore, the sun-dried products could be damaged by animals and contaminated (Bansal, 1987). As a result, the need for solar dryers is key. The concept of solar dryer is to heat air that is passed over/through a wet crop. The moisture concentration difference between the heated air and the wet crop results in moisture evaporation from the wet crop to the heated air. Solar dryers are categorized into direct solar dryer, indirect solar dryer, and mixed solar dryer. This classification is based on the way that the solar dryer receives the solar radiation. The solar dryer performance and improving it have become under consideration of many researchers. Othieno, Grainger and Twidell (1982) dried maize in indirect solar dryer. The moisture content of the maize was decreased 8% in three days. Ameri, Hanini, Benhamou and Chibane (2018) found that the indirect solar dryer showed better thermal performance than the direct one. Lingayat, Chandramohan and Raju (2017) concluded that the humidity and velocity of the drying air played a significant role to improve the solar dryer performance. Maiti, Patel, Vijas, Eswaran and Ghosh (2011) added to the solar dryer reflectors which improved the efficiency by 18.5%. El-Sebaii, Aboul-Enein, Ramadan and El-Gohary (2002) added a storage system to indirect solar dryer. Twelve hours earlier, the equilibrium moisture content of seedless grapes, 18%, was gained by using the storage system.

The present experimental investigation proposes a novel solar dryer design. The proposed solar dryer design has two

connected units. The first unit is a solar air heater, flat plate collector. The second unit is a drying chamber. Three walls of the drying chamber were designed as solar radiation receivers, i.e. flat plates covered with glass. Using this design not only ensures larger receiving area, but also the solar dryer faces the sun from three directions; the east, the south, and the west; rather than only from the South. As a reference, a conventional indirect solar dryer was also constructed and studied. The conventional indirect solar dryer consists of a solar air heater, flat plate collector, and an opaque drying chamber. The experimental study was performed in Tikrit city – Iraq (34°40′ N, 43°39′ E).

Construction of the solar dryers and measuring devices

The components of the studied solar dryers are described in this section. Furthermore, the details of the measuring devices are reported.

Solar dryer design

Both the proposed and conventional solar dryers consist of two main apparatuses, i.e. solar collector and drying chamber (Fig. 1). The novel proposed design is represented in the drying chamber walls. In the conventional solar dryer, the drying chamber walls are opaque and thermally insulated. While three walls of the proposed drying chamber; left, front, and right walls; are solar collectors.

Solar collector

The design of the solar collector for both dryers was similar. The solar collector was a flat plate of area 0.75 m^2 directed to the south. The solar collectors were fixed in front of the drying chambers. The collector was 40° inclined from horizon facing the south. The collector consists of a flat plate made from a sheet of aluminium as an absorber. The absorber was painted with a matt black colour to enhance its ability to absorb thermal radiation. The absorber was covered with a glass, 0.004 m thickness. To give the drying air space to naturally flow over the absorber through the collector, a gap of 0.05 m was left between the absorber and the glass. The sides and bottom of the solar collector were thermally insulated with a 0.05 m thickness of cork. The internal and external dimensions of the solar collector were 1 × 0.75 × 0.07 m and 1 × 0.85 × 0.12 m, respectively. The role of the solar collector is to provide heat, by absorbing solar radiation, to warmth the drying air before entering the drying chamber.

Drying chamber

Both solar dryers had a drying chamber. The drying chamber specifications are listed in Table 1. The drying chamber was constructed from light aluminium sheets and frames. To connect the drying chamber to the solar collector, a rectangular duct was used. In each chamber, three movable trays, wire-mesh, were used. At the top of each chamber, a cylindrical galvanized chimney was attached. The back of the drying chamber was used as a door. The other drying chamber walls;

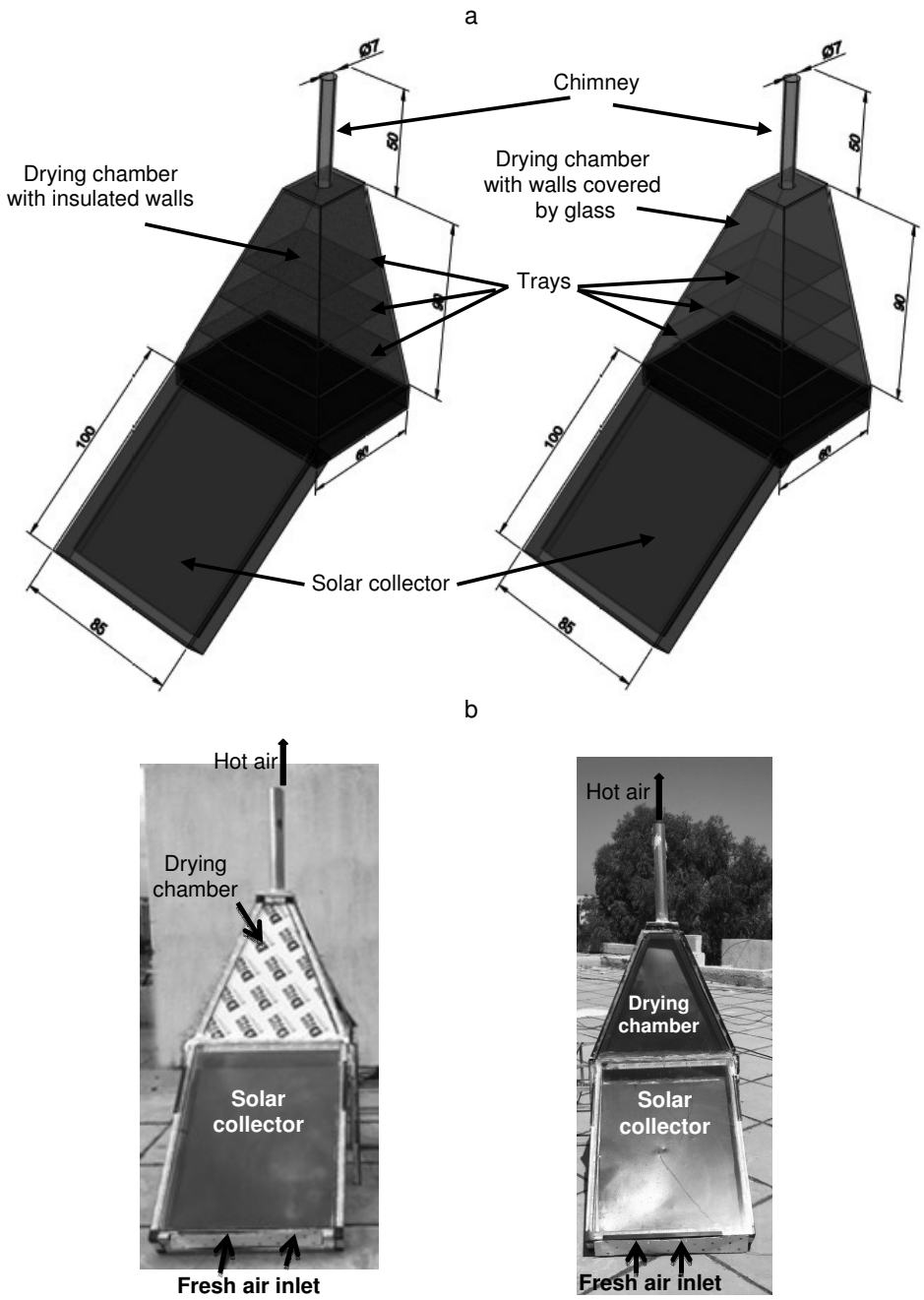

FIGURE 1. Novel solar dryer: a – three-dimensional configuration and dimensions (all dimensions in cm); b – the experimental test rig

TABLE 1. Drying chamber specifications

Component	Dimensions [m]			Material
	base	top	width	
Conventional dryer drying chamber walls:				
front and back	0.85	0.21	0.93	aluminium sheets covered by 20-mm thick of cork
right and left	0.60	0.28	0.93	
Novel dryer drying chamber walls:				
back	0.85	0.21	0.93	aluminium sheets covered by 20-mm thick of cork
front	0.85	0.21	0.93	aluminium sheets coated with black and covered by 4-mm thick of glass
left and right	0.60	0.28	0.93	
Duct, connects the solar collector with the drying chamber	0.75 × 0.07			aluminium
Chimney	0.07-diameter, 0.5-height			aluminium

left, front, and right walls; were inclined by 75°. For the conventional solar dryer, all the drying chambers walls including the door were thermally insulated with cork. For the novel solar dryer, only the door was thermally insulated with cork. The left, front, and right walls were coated with matt black colour and covered with 4 mm thick glass. A space of 5 mm was left between the wall and the glass (Dheyab, Al-Jethelah, Yassen & Khalil, 2019). As a result, the three walls became solar collectors.

Measuring devices

The measured data in the present work were solar radiation and temperatures. The solar radiation was measured using a solar digital meter daystar. inc DS-05A type was used with a relative uncertainty of ±3%, resolution of 1 $W \cdot m^{-2}$, and range of 0–1,200 $W \cdot m^{-2}$. The velocity of air leaving the drying chamber was measured using BENETECH GM8 16C anemometer with an accuracy of ±0.1 $m \cdot s^{-1}$. To measure the temperatures, K-type thermocouple wires with an uncertainty of ±0.1°C were used. The used data logger was of type Applent AT4808 with an uncertainty of ±0.2% +1°C, resolution of 0.1°C, and temperature range from –200 to 1,300°C. The relative uncertainties of the measured and calculated parameters are listed in Table 2.

TABLE 2. The relative uncertainty of the measured and calculated parameters

Parameter	Relative uncertainty [%]
Temperature-thermocouple	0.10
Temperature – data logger	1.15
Air velocity	5.56
Solar radiation meter	3.00
Thermal efficiency	0.03

Experimental procedure

The experimental set-ups were oriented toward the south. The solar collector was always exposed and never been covered. In this way, the solar collector absorber was heated by the solar radiation before starting the experiments. The experiments were conducted from 9:00 to 15:00. At the head of each hour, the solar radiation, air velocity leaving the drying chamber, and the temperatures at the aforementioned locations were recorded.

Energy analysis

The solar dryers are used to produce hot air, from the solar radiation, then use it to dry crops. The thermal an energy balance of the solar dryer is

$$I = Q_u + Q_{st} + Q_l \tag{1}$$

where:
I – solar radiation,
Q_u – useful thermal energy,
Q_{st} – stored energy,
Q_l – thermal loss.

Since the stored energy in this work is zero, Eq. (1) becomes

$$Q_u = Q_s - Q_l \tag{2}$$

The useful heat is expressed as

$$Q_u = \dot{m}\, c_p\, \left(T_o - T_i\right) \tag{3}$$

where:
$\dot{m}$ – drying air mass flow rate,
c_p – specific heat,
T_o – temperature leaving the dryer,
T_i – temperature entering the dryer.

The efficiency of the indirect solar dryer (η) is expressed as (Karoua et al., 2018)

$$\eta = \frac{Q_u}{\tau\, \alpha\, A\, I} \tag{4}$$

where:
τ – covering glass optical coefficient of transmission,
α – thermal diffusivity of the absorber,
A – total absorber area.

The relative uncertainty of the thermal efficiency is listed in Table 2.

Results and discussion

The experiments of the present work were conducted in Tikrit – Iraq (34°40' N 43°39' E) form 10th to 12th of March 2019 from 9:00 to 15:00. The presented results are for both the proposed and conventional solar dryers for sake of comparison.

Conventional indirect solar dryer

The conventional indirect solar dryer was experimented on 10 March 2019 (9:00–15:00). The recorded solar radiation, the ambient, absorber, and the drying chamber entrance, lower space, and upper space temperatures are depicted in Figure 2. The dryer entrance temperature increased as the solar radiation increased. The highest dryer entrance temperature was 62°C at 12:00. Between 11:00 and 14:00, the dryer entrance temperature was ranging around 60°C. Then it decreased after 14:00 as the solar radiation and ambient temperature decreased.

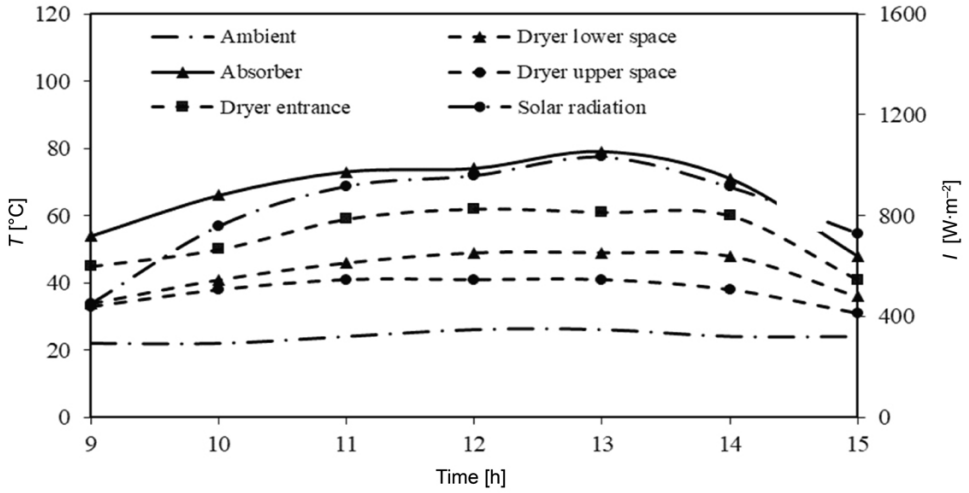

FIGURE 2. Conventional indirect solar dryer parameters

At the drying chamber lower space, the temperature raised with the solar radiation increase. The highest recorded temperature at the lower space was 49°C between 12:00 and 13:00. The lower space temperature was 24°C higher than the ambient at 14:00. The drying chamber upper space temperature increased with increasing the solar radiation and reached its highest value, i.e. 41°C, between 11:00 and 13:00. The upper space temperature was 17°C higher than the ambient at 11:00. As the drying air flow along the drying chamber, its temperature decreased. The temperature difference between the lower and upper spaces was decreased up to 10°C at 14:00. This temperature difference indicates an ununiform drying environment.

Novel indirect solar dryer

The novel indirect solar dryer was experimented on 12 March 2019 (9:00––15:00). Figure 3 shows the recorded solar radiation, the ambient, absorber, and the drying chamber walls; i.e. facing the east (left), the south (front), and the west (right); temperatures besides the drying chamber entrance, lower, and upper spaces. The highest recorded temperature of the left wall was 97°C at 10:00, the front wall was 105°C at 13:00, and the right wall was 92°C at 15:00. Each wall reached its highest temperature when it was directly to the sun as the sun moved from the east to the west. The highest entrance temperature was 74°C at 13:00 when the highest solar radiation was reached. In the lower space, the highest recorded temperature was 67°C between 12:00 and 13:00. At the same time, i.e. between 12:00 and 13:00, also the highest temperature of the upper space was recorded, i.e. 68°C. The air temperature difference between the entrance and the lower space was from 33 to 50°C. This difference is due to flowing the drying air through long and large absorbing area, i.e. the solar collector. Then the drying air lost part of its heat to the connected duct between the solar collector and the drying

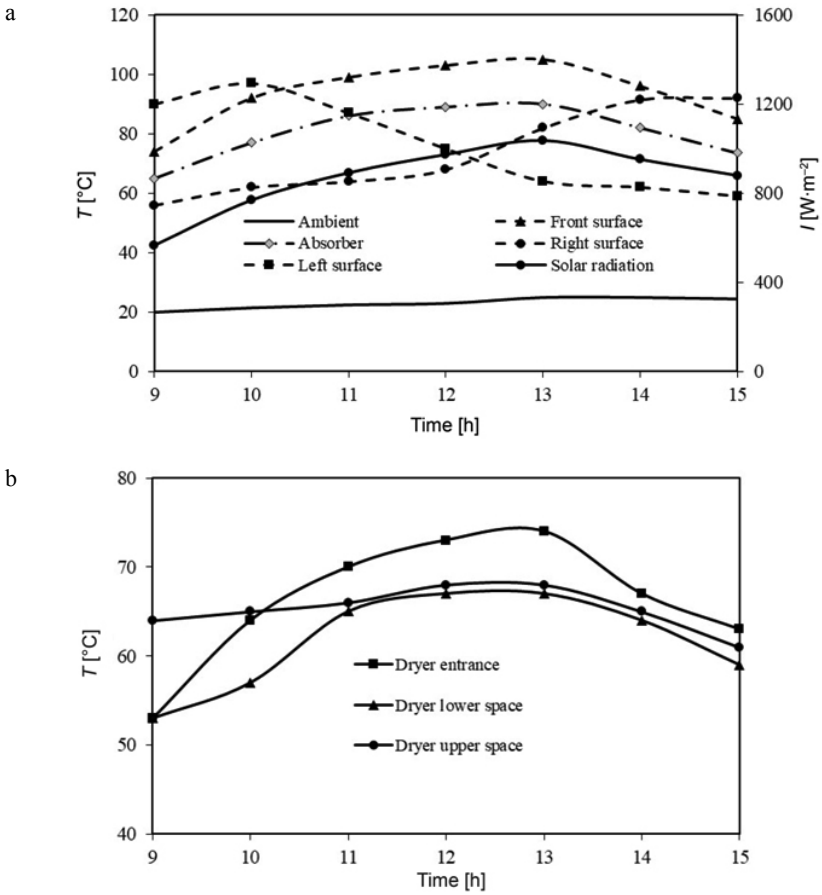

FIGURE 3. Novel indirect solar dryer parameters

chamber. At the beginning of the experiment, 9:00, the lower space temperature was 11°C below the upper space temperature. Two reasons caused this reduction. First, the hot drying air at the drying chamber entrance lost part of its thermal energy to the relatively cold chamber components. Second, at this early time of the day, the solar radiation was not sufficient to heat the drying chamber. With time progress, the solar radiation went up causing higher temperature at the lower space of the drying chamber. As a result, a decrease in the temperature difference between the upper and lower spaces can be noticed, i.e. ~1°C. This low temperature difference was a result of designing the left, front, and right walls of the drying chamber as solar collectors. The low temperature difference through the drying chamber offers a uniform drying.

Comparison between the conventional and novel solar dryers

Figure 4 shows a comparison between the novel and the conventional indirect solar dryers temperatures. The

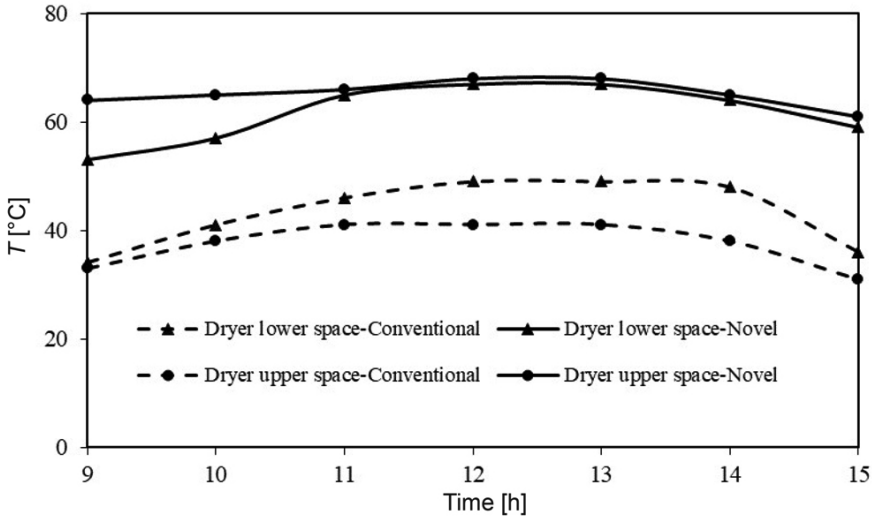

FIGURE 4. Comparison between the novel and the conventional indirect solar dryers temperatures

drying air at the entrance of the drying chamber was from 33 to 50°C (61–68%) above the ambient.

The temperature of the lower space of the novel dryer chamber was from 33 to 44°C (58–66%) above the ambient, while for the conventional dryer chamber it was from 12 to 24°C (35–50%) above the ambient. The novel dryer chamber lower space temperature was from 16 to 23°C (25–39%) above the conventional one.

The temperature of the upper space of the novel dryer chamber was from 36.5 to 45°C (60–69%) above the ambient, whereas for the conventional dryer chamber it was from 7 to 17°C (23–42%) above the ambient. The novel dryer chamber upper space temperature was from 25 to 31°C (38–49%) above the conventional one.

The temperature of the drying air in the upper space of the novel dryer chamber was 1 to 11°C (1–17%) higher than that of the lower space. It should be pointed out that the low difference, i.e. 1–3%, was for five hours out of seven hours of the experiment time. While for the conventional dryer, the difference between the upper and lower spaces temperature was from –10 to –1°C (from –26 to –3%).

Figure 5 shows a comparison between the novel and the conventional indirect solar dryers thermal efficiencies. The novel dryer thermal efficiency was 46–71%, while the conventional thermal efficiency was 7–16%. In other words, the novel dryer thermal efficiency was higher than that of the conventional one by 37–55%. A comparison between the present work efficiencies and others from literature is tabulated in Table 3. The proposed novel solar dryer achieved the highest efficiency among the other designs.

It can be concluded that the thermal performance of the proposed design was better than that for the conventional design.

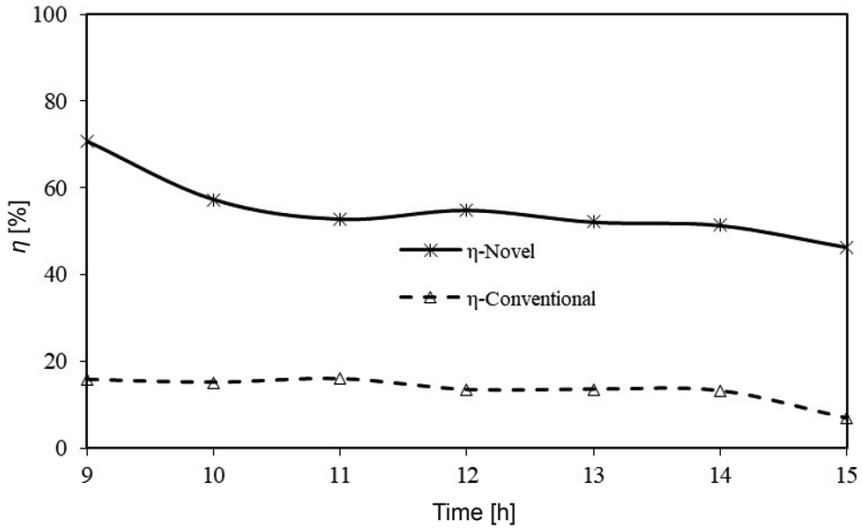

FIGURE 5. Comparison between the novel and the conventional indirect solar dryers thermal efficiencies

TABLE 3. Comparison between the present investigated solar dryers and with previous works

Reference	Average ambient temperature [°C]	Average solar radiation [W·m^{-2}]	Efficiency [%]
Lingayat et al. (2017)	42	724.0	31.5
Miri et al. (2002)	30	825.0	40.0
Madhlopa, Jones and Saka (2002)	30	246.5	21.0
Present conventional indirect solar dryer	24	823.6	19.0
Present novel indirect solar dryer	23	866.1	55.0

Conclusions

A novel indirect solar dryer design was proposed and tested in the present experimental work. In this innovative design, besides the solar collector, three of the drying chamber walls were designed to be solar collector as well. A conventional indirect solar dryer was also tested for sake of comparison. Based on the recorded and calculated data, it can be concluded that:

- Using a solar collector elevated the temperature of the drying air at the drying chamber inlet up to 68% in the novel dryer and 60% in the conventional dryer above the ambient.
- In the novel dryer chamber lower space, the drying air was warmer than that in the conventional dryer up to 39% due to the solar collector and the drying chamber walls.
- In the novel dryer chamber upper space, the drying air was warmer

than that in the conventional dryer up to 49% as a result of the solar collectors on the drying chamber walls.
– A thermal uniformity was achieved through the novel solar dryer, as only 3% temperature difference between the drying chamber upper space and lower space temperatures was recorded. While in the conventional solar dryer, a –26% difference was found.
– The novel indirect solar dryer achieved a thermal efficiency of 55% above that of the conventional one.

References

Ameri, B., Hanini, S., Benhamou, A. & Chibane, D. (2018). Comparative approach to the performance of direct and indirect solar drying of sludge from sewage plants, experimental and theoretical evaluation. *Solar Energy*, *159*, 722-732. https://doi.org/10.1016/j.solener.2017.11.032

Bansal, N.K. (1987). Solar crop drying. In *Physics and Technology of Solar Energy* (pp. 413-445). Berlin: Springer.

Dheyab, H.S., Al-Jethelah, M.S.M., Yassen, T.A. & Khalil, T. (2019). Experimental Study of The Optimum Air Gap of a Rectangular Solar Air Heater. *Journal of Advanced Research in Fluid Mechanics and Thermal Sciences*, *59*(2), 318-329.

El-Sebaii, A.A., Aboul-Enein, S., Ramadan, M.R.I. & El-Gohary, H.G. (2002). Experimental investigation of an indirect type natural convection solar dryer. *Energy Conversion and Management*, *43*(16), 2251-2266. https://doi.org/10.1016/S0196-8904(01)00152-2

Karoua, H., Moummi, A., Hamidat, A., Moummi, N., Aoues, K., Benchabane, A. & Benchatti, A. (2018). Experimental investigation and exergy analysis of an air heater with a solar concentrator used for drying processes. *International Journal of Heat and Technology*, *36*(3), 791-800. https://doi.org/10.18280/ijht.360303

Lingayat, A., Chandramohan, V.P. & Raju, V.R.K. (2017). Design, development and performance of indirect type solar dryer for banana drying. *Energy Procedia*, *109*, 409-416. https://doi.org/10.1016/j.egypro.2017.03.041

Madhlopa, A., Jones, S.A. & Saka, J.K. (2002). A solar air heater with composite–absorber systems for food dehydration. *Renewable Energy*, *27*(1), 27-37.

Maiti, S., Patel, P., Vyas, K., Eswaran, K. & Ghosh, P.K. (2011). Performance evaluation of a small scale indirect solar dryer with static reflectors during non-summer months in the Saurashtra region of western India. *Solar Energy*, *85*(11), 2686-2696. https://doi.org/10.1016/j.solener.2011.08.007

Miri, R., Mokrani, O., Siad, F. & Belhamel, M. (2002). Étude expérimentale d'un séchoir solaire. *Revue Des Énergies Renouvelables*, *2002*, 41-48.

Montero, I., Blanco, J., Miranda, T., Rojas, S. & Celma, A.R. (2010). Design, construction and performance testing of a solar dryer for agroindustrial by-products. *Energy Conversion and Management*, *51*(7), 1510-1521. https://doi.org/10.1016/j.enconman.2010.02.009

Othieno, H., Grainger, W. & Twidell, J.W. (1982). Application of small scale solar crop driers to maize drying in Kenya. In *Energy for rural and island communities* (pp. 377-386). Amsterdam: Elsevier. https://doi.org/10.1016/B978-0-08-027606-9.50047-7

Puglia, M., Rizzo, A., Morselli, N. & Tartarini, P. (2019). Efficiency and economical assessment of a solar powered dryer combined with a biomass gasification system. *International Journal of Heat and Technology*, *37*(3), 705-709.

Sreekumar, A., Manikantan, P.E. & Vijayakumar, K.P. (2008). Performance of indirect solar cabinet dryer. *Energy Conversion and Management*, *49*(6), 1388-1395. https://doi.org/10.1016/j.enconman.2008.01.005

Summary

Thermal performance of novel indirect passive solar dryer. An experimental investigation was conducted to study the performance of a novel indirect type free convection solar dryer. The novel and a conventional indirect passive solar dryer were built. Solar irradiation and temperature of different locations were recorded. The air at the drying chamber entrance, lower space, and upper space temperatures besides the thermal efficiency of the novel dryer were 68, 39, 49 and 85%, respectively, higher than the conventional one.

Authors' address:
Manar Al-Jethelah – corresponding author
(https://orcid.org/0000-0001-5383-7216)
Tadahmun Yaseen
(https://orcid.org/0000-0003-2377-6787)
Tikrit University
College of Engineering
Mechanical Engineering Department
Tikrit, Iraq
e-mail: m.aljethelah@tu.edu.iq
hussam.sami@tu.edu.iq
tadahmunahmed@tu.edu.iq

Scientific Review – Engineering and Environmental Sciences (2021), 30 (2), 304–314
Sci. Rev. Eng. Env. Sci. (2021), 30 (2)
Przegląd Naukowy – Inżynieria i Kształtowanie Środowiska (2021), 30 (2), 304–314
Prz. Nauk. Inż. Kszt. Środ. (2021), 30 (2)
http://iks.pn.sggw.pl
DOI 10.22630/PNIKS.2021.30.2.26

Hiba D. SALEEM, Asad H. ALDEFAE, Wissam H. HUMAISH

University of Wasit, College of Engineering

Verification of strength resistance of sandy soil using small scale penetrometer tests

Key words: cone penetration, tip resistance, sleeve resistance, relative density, angle of internal friction

Introduction

To study a problem concerning with geotechnical aspect, one of the main factor that should be considered by the geotechnical engineer during model preparation experimentally is obtaining soil strata properties in the prepared model close to that property of natural soil in-situ. Cohesionless soil can be defined clearly by its relative densities whereas the cohesive soil is defined by compressibility. Many verified methods to prepare sandy soil specimens model in the laboratory are widely used at different geotechnical laboratories and research center around the world (Presti, Pedroni & Crippa, 1992; Dave & Dasaka, 2012; Gade & Dasaka, 2016; Aldefae, Shamkhi & Khalaf, 2019; Aldefae & Saleem, 2020). One of the main characteristic and advantage of sandy soil specimen is "can be prepared experimentally in the laboratory at dry state". Different techniques are performed and followed to verify the soil strata characteristics of the prepared model and even in-situ (Juang, Huang, Holtz & Chen, 1996; Lunne, Powell & Robertson, 2002; Sivrikaya & Tođrol, 2006; Schneider, Randolph, Mayne & Ramsey, 2008; Al-Aayedi, Aldefae & Shamkhi, 2020).

Cone penetration resistance is very well known parameters that reveal the actual soil strength. It can be determined using the cone penetration test in which very important soil properties intended to help the engineers in the design earthworks and foundation for any structure. Direct results can be obtained in-situ as no borehole is required to perform this test. Based on the description detailed in the ASTM D3441--98 standard (American Society for Testing and Materials [ASTM], 2012), the diameter of the exterior wall of the cone tube is about 3.6 cm with projected (base) area 10 cm^2 and it has an inclined side slope cone of 60°. Cone tip resistance (q_c)

represents the developed soil resistance by the cone to the penetration (the governed force divided by the projected area) whereas the frictional (sleeve) resistance (f_c) represents the frictional force developed along the sleeve (above the cone) due to local surrounding soil divided by the surface area of the sleeve. Both forces and stresses are the main two forces and stresses components that represent the total cone resistance.

Experimentally, the different cone models were designed and many tests are performed to investigate the sandy soil resistance under 1 g (Zhuang & Yu, 2018) and even in a centrifuge using controlled installation system (Kim et al., 2014; Darby, Bronner, Para Bastidas, Boulanger & De Jong, 2016; Zhou et al., 2019). Six millimeter small scale penetrometer model was designed, manufactured and tested new 6 mm cone penetrometer (Kutter et al, 2017; Carey et al., 2018).

There are many correlations have been developed to investigate the cone resistance from main soil properties. For cohesionless soil, and because the mean particle size and the relative density plays a significant role in the soil resistance. The frictional resistance ratio (i.e. the sleeve resistance divided by the tip resistance – f_c/q_c), for both electrical and mechanical cone from the mean particle size of the soil particles (i.e. D_{50}) is computed by Anagnostopoulos, Koukis, Sabatakakis and Tsiambaos (2003) as follows:

$$F_r = 1 \cdot 45 - 1 \cdot 36 \log D_{50}$$
(for electrical cone) (1)

$$F_r = 0 \cdot 7{,}811 - 1 \cdot 611 \log D_{50}$$
(for mechanical cone) (2)

From Eqs. (1) and (2), it was observed that the sandy soil has large tip resistance with small frictional ratio (Zervogiannis, Bouckovalas & Christoulas, 1987). Similar behavior has been concluded by Carey, Gavras and Kutter (2020).

New empirical equation to determine the relative density from the cone resistance has been proposed after many experimental tests (Campanella, Robertson & Gillespie, 1983) as follows:

$$D_r\,[\%] = A + B \log_{10}\left(\frac{q_c}{\sqrt{\sigma'_o}}\right) \tag{3}$$

where:
A, B – imperial correlations coefficient as proposed by Jamiolkowski, Lo Presti and Manassero (2003),
σ'_o – vertical effective stress.

Other correlation equation between the relative density of sandy soil and the cone resistance has been proposed by Kulhawy and Mayne (1990) as follows:

$$D_r\,[\%] = 68\left[\log\left(\frac{q_c}{\sqrt{P_a * \sigma'_o}}\right) - 1\right] \tag{4}$$

where:
P_α – atmospheric pressure (≅ 100 kPa).

The drained angle of internal friction of sandy soil has been determined also using Eq. (5) as described by Campanella et al. (1983).

$$\varphi' = \tan^{-1}\left[0.1 + 0.38 \log\left(\frac{q_c}{\sigma'_o}\right)\right] \tag{5}$$

Other two empirical correlations equations between the drained friction angle for poorly graded sandy soil with silt (SP-SM) and the cone resistance have been presented by Ricceri, Simonimi and Cola (2002) and Lee, Salgado and Carraro (2004) respectively, as follows:

$$\varphi' = \tan^{-1}\left[0.38 + 0.27 \log\left(\frac{q_c}{\sigma'_o}\right)\right] \quad (6)$$

$$\varphi' = 15.575\left(\frac{q_c}{\sigma'_h}\right)^{0.1714} \quad (7)$$

In this paper, mini cone penetration test is performed on different relative densities models to investigate how the cone penetration resistance of sandy soil are significantly influenced by the some physical and drained shear strength. The experimental tests were performed at the University of Wasit, geotechnical laboratories of the Engineering Faculty. New equations are proposed based on the obtained results and were compared with well-presented previous studies which were explained in the introduction above.

Small scale cone penetrometer model

Small scale penetrometer is designed and manufactured at the geotechnical laboratory of engineering faculty to achieve 50 cm embedded length within the soil layers model. It has 10 mm diameter and 0.5 kN mini load cell is connected at the end (tip) of the cone to investigate the tip or bearing cone resistance. The cone is manufactured from similar steel properties that were used in designing of the in-situ penetrometer. Another load cell (5 kN in diameter) is connected at the top of the penetrometer which connected within the installation and loading machine to inspect the behavior of the total cone resistance (including the frictional resistance and the tip resistance). Figure 1 shows the small scale penetrometer model with load cells and slip ring (used in screw piles test which is not mentioned in this paper).

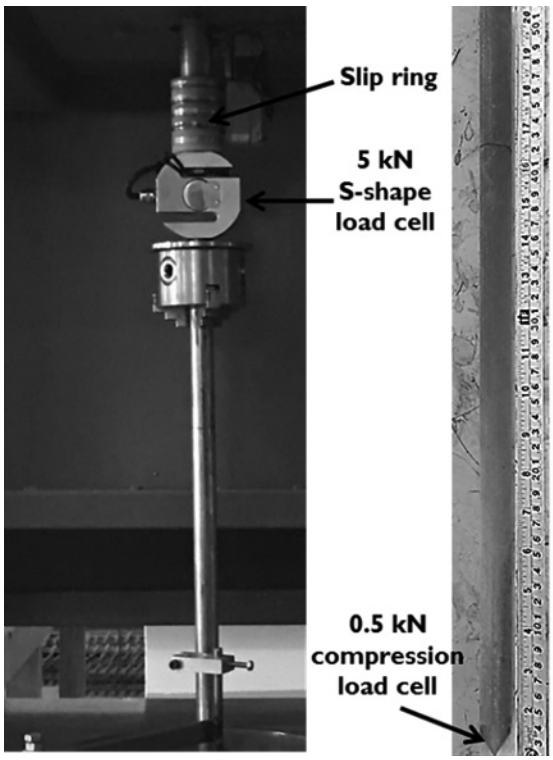

FIGURE 1. Small scale penetrometer

Model preparation and loading machine

Fine silica sand has 0.17 mm mean diameter size (i.e. D_{50}) is used in the model preparation utilizing $0.8 \times 0.8 \times 0.7$ m steel container that was designed and fabricated by Aldefae et al. (2019) previously (Fig. 2). To achieve the desired relative density for each test in cohesionless soil, mechanical pluviator that was designed and manufactured in the geotechnical laboratory at the University of Wasit by Aldefae and Saleem (2020) is used. Similar procedure during the model preparation that was commonly used in the pluviation technique is followed here (Al-Aayedi et al., 2020). The prepared and tested models under many relative densities are inspected during the cone penetration tests to investigate how the soil strength is strongly influenced by the relative density. The tested models relative density ranges between loose to dense states. A universal loading machine (ULM) is used to perform the CPT tests under a displacement rate of 4 mm·min^{-1} (Fig. 2). In the prototype scale, the standard displacement rate for CPT tests is around 1,000 mm·min^{-1}, as described in the ASTM D3441-98 standard, which is totally different from the displacement rate in the model scale here. In spite of that, the cone penetration resistance in cohesionless soils is not strongly influenced by the displacement of the penetration machine as investigated carefully by Dayal and Allen (1975).

Soil strength in term of the penetrometer resistance (q_u) and the relationships between both the ultimate cone resistance with the relative density (D_r %) and the drained angle of internal friction (φ') have been determined and simple empirical equations are introduced between these parameters. Then, comparisons with dis-

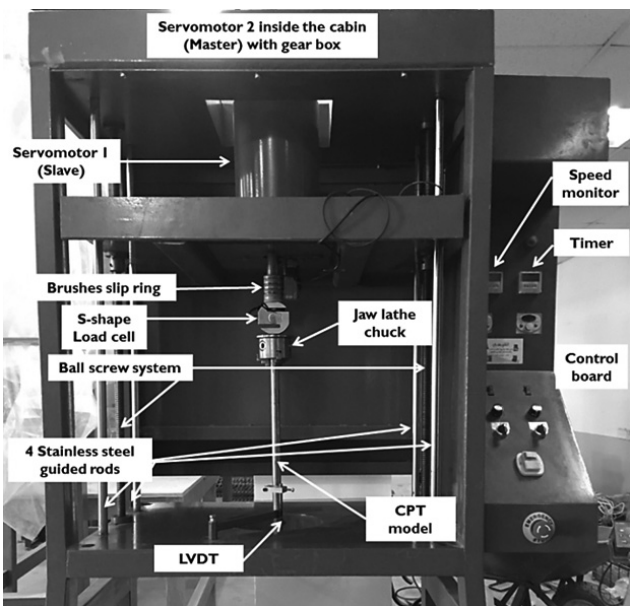

FIGURE 2. Loading rig machine and cone penetrometer

covered parameters from previous studies have been conducted with the parameters that were obtained from this paper.

Results and discussion

Penetrometer resistance results

Seven cone penetration tests are conducted in on cohesionless soil (sandy soil). Wide ranges of relative density are considered in the test procedure by preparation the models using the pluviator technique that was mentioned earlier in this paper. These relative densities have been represented the full density status for sandy soil (loose, medium, dense and very dense state). One cone penetration test is conducted for each test and the cone penetrates the soil at the center of the container and far from the container's side walls to prevent any boundary effect may develop due to the soil deformation. The penetration resistance results for identifying the variation of the soil strength within different soil relative density is illustrated in Figure 3. It should be noticed from the figure that the cone element penetrates the soil layer in the container up to 45 cm. Maximum penetrometer stroke is limited to be 47 cm and the machine is controlled to be stopped suddenly using digital draw wire to prevent any damages that may occur for the ball screw system.

The relative density effect is shown clearly as the cone resistance increases with depth once the relative density increases. High relative density has maximum cone resistance and it was three times the cone resistance in case of loose state (low density). This behavior can be attributed to the large void ratio in case of loose state and the downward and lateral movement of the soil particles occurs in low resistance while this resistance is going to increase sharply because of the soil particle interlocks when the cone penetrates the soil layers.

This behavior is compared with what was observed by Gade and Dasaka (2017) at dense state (i.e. 40 and 80% D_r) though the depth of penetration was 35 cm at previous study. Very close variation with depth of cone resistance between the measured and the art-of-literature values and this support what was discovered here in this paper. It can be seen that there is the slightly different trend in the measured value at low density (i.e. 40% D_r) at moderate stress level (i.e. 25 cm depth as shown in Fig. 3) whereas very close for the measured ultimate value at the final depth (i.e. 38 cm).

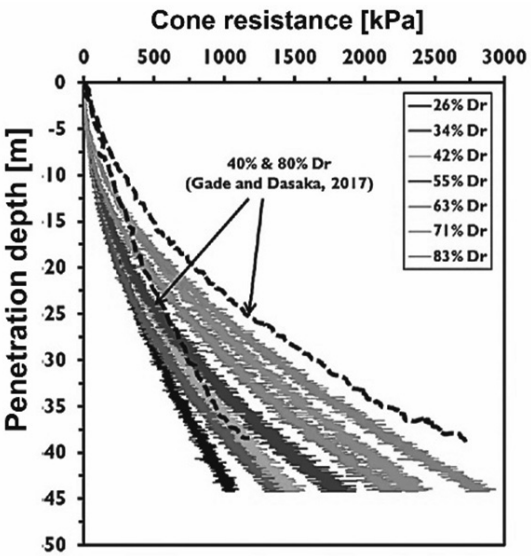

FIGURE 3. Cone penetration results of full range of relative density

Sleeve (frictional) resistance results

To determine the sleeve or frictional resistance (f_c) for different relative densities in this study, Eq. (2) is used as the cone model represents a mechanical cone. Frictional resistance ratio is calculated first which is constant because it is a function of the mean particle size (D_{50}). The measured ultimate cone resistances from the tested models at the maximum penetration are used then to calculate the sleeve or frictional resistance for each case (i.e. the wide range from low to dense state). Figure 4 shows the effect of the relative density on the calculated sleeve resistance. It can be seen also that the calculate sleeve resistance, tacitly, is small comparing with the measured cone resistance for all the range of the tested densities. This finding is consistent with what was discovered by Anagnostopoulos et al. (2003) when they noticed that the sandy soil has small frictional resistance. Accordingly, as shown in Figure 4, the frictional resistance ratio is (14%) approximately; thus, the calculated sleeve resistance is around 14% of the ultimate cone resistance at maximum penetration.

Angle of internal friction effect on the cone resistance

The angles of internal friction are determined using the basic direct shear test for dry sandy soil according to the wide range of the selected relative density (to cover the sandy soil status as mentioned before). It can be seen from Figure 5 that the cone penetration resistance increases from 1,000 to approximately 2,800 kPa as the angle of internal friction increase from 31.6 to 41.8°. It could be seen also that the variation of the cone resistance was about 180% and this is not surprising us as the sandy soil changed from the critical state (i.e. low strain level) to the peak state (i.e. at large strain level) and we have to say here that the dilation for the sandy soil effect has a significant effect on the measured cone resistance.

It is not true to say that both the internal friction angle and the dilation effect

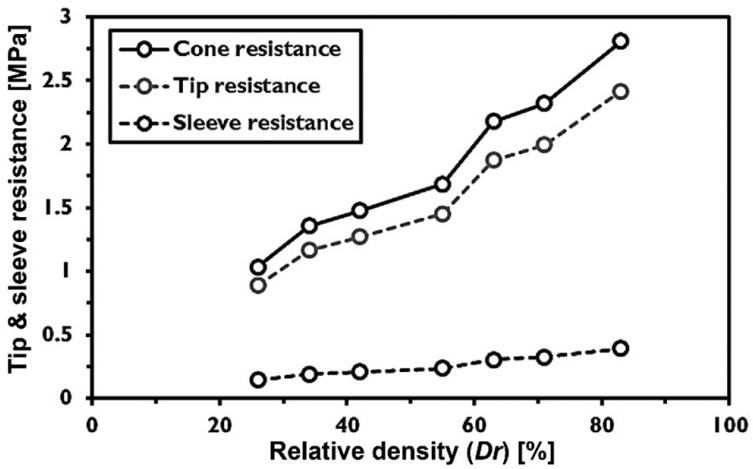

FIGURE 4. Effect of relative density variation on tip and sleeve cone resistance

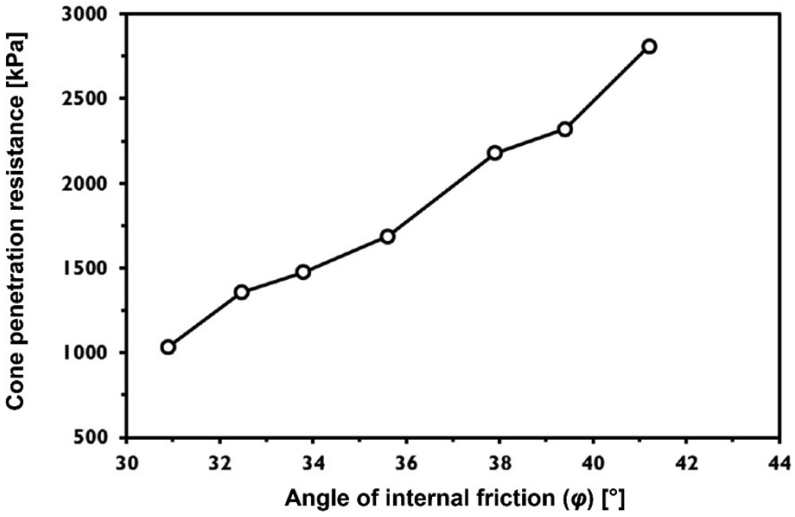

FIGURE 5. Effect of angle of internal friction on cone resistance

on the cone resistance are detached as discovered by Puebla, Byrne and Philips (1997). The overlapping between two parameters are significant and the most increasing in the cone penetration resistance as a results of the developing of the dilation which is very important parameter in sandy soils.

Calculated and measured cone penetration resistance

To predict the obtained results of the cone resistance, Eq. (5) is used in this paper. Excellent agreement can be seen in Figure 6 between the measured and calculated cone resistance. It should be seen noticed that this agreement between the calculated cone resistance and measured values cannot say it is under predicted or over predicted and it can only say that its slightly over predicted at low cone resistance (low to medium dense state) and under predicted at high cone resistance (dense state). This can be attributed to the confinement stresses increasing at large cone resistance (2,000 kPa and above). This behavior is consisted with

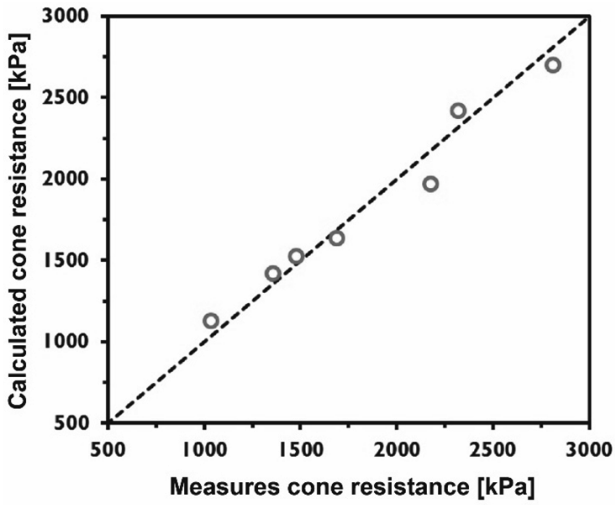

FIGURE 6. Measured and calculated cone resistance

the main finding discovered by Ahmadi, Byrne and Campanella (2005).

On the other hand, the over prediction of the measured cone resistance (i.e. below 1,500 kPa) can be attributed to the difficulties of achieving the boundary condition as the radial displacement cannot be controlled to be zero at the container boundary during the test and this behavior is exactly with what Salgado, Jamiolkowski and Mitchell (1998) came up with.

Comparison of the measured cone resistance

The obtained experimental results from the cone model penetration tests are compared with three different fields, numerical and experimental results selected carefully from many previous studies as shown in Figure 7.

It can be seen from Figure 7 that the cone resistance increases as the angle of internal friction increase. Actually this is not surprising as the relative density increases with the angle of internal friction. The "very well" finding here is the trend of the results in this paper comparing with results of field test (Campanella et al., 1983) and experimental (Ricceri et al., 2002) as well as numerical study (Lee et al., 2004). The convergence of these results with slightly under or over predicting can be attributed to the boundary condition of the problem that have been considered very well during the test particularly the cone penetration rate, the sandy soil layers model preparation as well as the boundary effects from the walls of container to the cone model.

Conclusions

The cone penetration test is one of the quick geotechnical tests that are widely used to investigate the soil layers strength characteristics for non-cohesive soil. The main conclusions can be listed as follows:

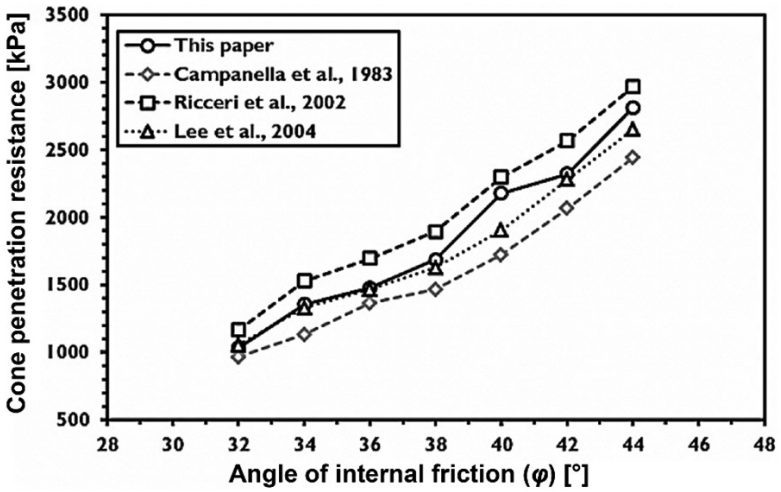

FIGURE 7. Comparison of measured cone resistance with previous obtained values

1. The small scale penetrometer model tests results replicated the actual strength behavior of sandy soil by comparing the experimental results with art-of-literature or previous field and numerical results.
2. The cone resistance results are increased up to 160% when the soil density changed from loose to medium dense state (1 MPa at loose state to 1.6 MPa at dense state). Whereas it increased to 280% when the density characteristics changed to dense state (2.8 MPa at dense state).
3. The cone resistance is strongly influenced by the angle of internal friction as the values increased sharply when the soil changed from the low density (i.e. $\varphi \cong 31 \cdot 5°$) to dense state (i.e. $\varphi \cong 42°$).
4. The sleeve resistance is small comparing with the tip cone resistance (around 15%) and this is consistence with fact of cohesion-less soil.

References

Ahmadi, M.M., Byrne, P.M. & Campanella, R.G. (2005). Cone tip resistance in sand: modeling, verification, and applications. *Canadian Geotechnical Journal*, *42*(4), 977-993.

Al-Aayedi, H.K., Aldefae, A.H. & Shamkhi, M.S. (2020). Seismic performance of bridge piers. *IOP Conference Series: Materials Science and Engineering*, *870*(1), 012069. https://doi.org/10.1088/1757-899X/870/1/012069

Aldefae, A.H. & Saleem, H.D. (2020). Design, manufacturing and testing of biaxial mechanical travelling pluviator. *IOP Conference Series: Materials Science and Engineering*, *870*(1), 012071. https://doi.org/10.1088/1757-899X/870/1/012071

Aldefae, A.H., Shamkhi, M.S. & Khalaf, T. (2019). Design and manufacturing of geotechnical laboratory tools used in physical modeling. *Cogent Engineering*, *6*(1), 1637622. https://doi.org/10.1080/23311916.2019.1637622

American Society for Testing and Materials [ASTM] (2012). *Standard test method for electronic friction cone and piezocone penetration testing of soils (ASTM D3441-98).* West Conshohocken (PA): American Society for Testing and Materials.

Anagnostopoulos, A., Koukis, G., Sabatakakis, N. & Tsiambaos, G. (2003). Empirical correlations of soil parameters based on cone penetration tests (CPT) for Greek soils. *Geotechnical & Geological Engineering*, *21*(4), 377-387.

Campanella, R.G., Robertson, P.K. & Gillespie, D. (1983). Cone penetration testing in deltaic soils. *Canadian Geotechnical Journal*, *20*(1), 23-35.

Carey, T., Gavras, A., Kutter, B., Haigh, S.K., Madabhushi, G.S.P., Okamura, M., Kim, D.S., Ueda, K., Hung, W-Y., Zhou Y-G., Liu, K., Chen, Y.M., Zeghal, M., Abdoun, T., Escoffier, S. & Manzari, M. (2018). A new shared miniature cone penetrometer for centrifuge testing. In *Physical Modelling in* Geotechnics. Vol. 1 (pp. 293-298). London: CRC Press.

Carey, T., Gavras, A. & Kutter, B. (2020). Comparison of LEAP-UCD-2017 CPT Results. In *Model Tests and Numerical Simulations of Liquefaction and Lateral Spreading* (pp. 117-129). Cham: Springer.

Darby, K.M., Bronner, J.D., Parra Bastidas, A.M., Boulanger, R.W. & DeJong, J.T. (2016). Effect of shaking history on the cone penetration resistance and cyclic strength of saturated sand. In *Geotechnical and Structural Engineering Congress 2016* (pp. 1460-1471). Reston (VA): American Society of Civil Engineers.

Dave, T.N. & Dasaka, S.M. (2012). Assessment of portable traveling pluviator to prepare reconstituted sand specimens. *Geomechanics and Engineering*, *4*(2), 79-90.

Dayal, U. & Allen, J.H. (1975). The effect of penetration rate on the strength of remolded clay and sand samples. *Canadian Geotechnical Journal*, *12*(3), 336-348.

Gade, V.K. & Dasaka, S.M. (2016). Development of a mechanized traveling pluviator to prepare reconstituted uniform sand specimens. *Journal of Materials in Civil Engineering*, *28*(2), 04015117. https://doi.org/10.1061/(ASCE)MT.1943-5533.0001396

Gade, V.K. & Dasaka, S.M. (2017). Assessment of air pluviation using stationary and movable pluviators. *Journal of Materials in Civil Engineering*, *29*(5), 06016023. https://doi.org/10.1061/(ASCE)MT.1943-5533.0001798

Jamiolkowski, M., Lo Presti, D.C.F. & Manassero, M. (2003). Evaluation of relative density and shear strength of sands from CPT and DMT. In *Soil behavior and soft ground construction* (pp. 201-238). Reston (VA): American Society of Civil Engineers.

Juang, C.H., Huang, X.H., Holtz, R.D. & Chen, J.W. (1996). Determining relative density of sands from CPT using fuzzy sets. *Journal of Geotechnical Engineering*, *122*(1), 1-6.

Kim, J.H., Kim, S.R., Lee, H.Y., Choo, Y.W., Kim, D.S. & Kim, D.J. (2014). Miniature cone tip resistance on silty sand in centrifuge model tests. In Ch. Gaudin, D. White (eds.), *Proceedings of the 8th International Conference on Physical Modelling in Geotechnics 2014* (pp. 1301-1306). London: CRC Press.

Kulhawy, F.H. & Mayne, P.W. (1990). *Manual on estimating soil properties for foundation design.* Palo Alto (CA): Electric Power Research Institute.

Kutter, B., Carey, T., Stone, N., Zheng, B.L., Gavras, A., Manzari, M.T., Zeghal, M., Abdoun, T., Korre, E.,Escoffier, S., Haigh, S.K., Madabhushi, G.S.P., Madabhushi, S.S.C., Hung, W-Y., Liao, T-W., Kim, D-S, Kim, S-N., Ha, J-G., Kim, N.R., Okamura, M., Sjafruddin, A.N., Tobita, T., Ueda, K., Vargas, R., Zhou, Y-G. & Liu, K. (2020). LEAP-UCD-2017 comparison of centrifuge test results. In B. Kutter, M. Manzari, M. Zeghal (eds.), *Model Tests and Numerical Simulations of Liquefaction and Lateral Spreading* (pp. 69-103). Cham: Springer.

Lee, J., Salgado, R. & Carraro, J.A.H. (2004). Stiffness degradation and shear strength of silty sands. *Canadian Geotechnical Journal*, *41*(5), 831-843.

Lunne, T., Powell, J.J. & Robertson, P.K. (2002). *Cone penetration testing in geotechnical practice.* Boca Raton (FL): CRC Press.

Presti, D.L., Pedroni, S. & Crippa, V. (1992). Maximum dry density of cohesionless soils by pluviation and by ASTM D 4253-83: a comparative study. *Geotechnical Testing Journal*, *15*(2), 180-189.

Puebla, H., Byrne, P.M. & Phillips, R. (1997). Analysis of CANLEX liquefaction embankments: prototype and centrifuge models. *Canadian Geotechnical Journal*, *34*(5), 641-657.

Ricceri, G., Simonini, P. & Cola, S. (2002). Applicability of piezocone and dilatometer to characterize the soils of the Venice Lagoon. *Geotechnical & Geological Engineering*, *20*(2), 89-121.

Salgado, R., Jamiolkowski, M. & Mitchell, J.K. (1998). Penetration resistance in sand: analysis and applications to liquefaction potential assessment and estimation of pile base resistance. *Rivista Italiana di Geotecnica*, *32*(4), 5-17.

Schneider, J.A., Randolph, M.F., Mayne, P.W. & Ramsey, N.R. (2008). Analysis of factors influencing soil classification using normalized piezocone tip resistance and pore pressure parameters. *Journal of Geotechnical and Geoenvironmental Engineering*, *134*(11), 1569-1586.

Sivrikaya, O.S.M.A.N. & Tođrol, E. (2006). Determination of undrained strength of fine-grained soils by means of SPT and its application in Turkey. *Engineering Geology*, *86*(1), 52-69.

Zervogiannis, H., Bouckovalas, G. & Christoulas, S. (1987). Correlation of mechanical characteristics and classification of soil deposits. *Bulletin of Central Public Works Laboratory*, *4*, 255-265.

Zhou, Y.G., Liang, T., Chen, Y.M., Ling, D.S., Kong, L.G., Shamoto, Y. & Ishikawa, A. (2019). A two-dimensional miniature cone penetration test system for centrifuge modelling. In Ch. Gaudin, D. White (eds.), *Physical Modelling in Geotechnics* (pp. 301--307). London: Taylor & Francis Group.

Zhuang, P.Z. & Yu, H.S. (2018). Size effects in cone penetration tests in sand. In W. Wu, H.S. Yu (eds.), *Proceedings of China-Europe Conference on Geotechnical Engineering* (pp. 283-287). Cham: Springer. https://doi.org/10.1007/978-3-319-97112-4_64

Summary

Verification of strength resistance of sandy soil using small scale penetrometer tests. This study focuses on utilizing cone penetrometer models to determine strength (resistance) of sandy soil and also assessment how the relative density and the angle of friction effects on the measured cone penetration resistance in sandy soil. Simple empirical equations are used also to determine the cone penetration resistance components such as the sleeve resistance and the tip resistance. Simple comparison is performed between the measured and calculated soil strength and well agreement is noticed between them.

Authors' address:
Asad H. Aldefae – corresponding author
(https://orcid.org/0000-0002-8725-4470)
University of Wasit
College of Engineering
Hay Al-Rabe', Wasit, Kut
Iraq
e-mail: asadaldefae@uowasit.edu.iq

Scientific Review – Engineering and Environmental Sciences (2021), 30 (2), 315–326
Sci. Rev. Eng. Env. Sci. (2021), 30 (2)
Przegląd Naukowy – Inżynieria i Kształtowanie Środowiska (2021), 30 (2), 315–326
Prz. Nauk. Inż. Kszt. Środ. (2021), 30 (2)
http://iks.pn.sggw.pl
DOI 10.22630/PNIKS.2021.30.2.27

Mohammed KADHUM[1], Zainab MAHDI[2], Yousif FUNFAKH[1], Zaid MOHAMMED[3], Mustafa ABDULRAHEEM[1, 4], Michaela GKANTOU[5]

[1] University of Babylon, College of Engineering
[2] Middle Technical University – Baghdad, Technical Engineering College
[3] University of Technology – Baghdad, Engineering College
[4] Department of planning and development, General Company of electricity distribution for the middle region, Karbala branch
[5] Liverpool John Moores University, School of Civil Engineering and Built Environment

Experimental investigation on the post-fire performance of reactive powder concrete columns

Key words: post-fire, concrete, behavior, third term, fourth date, fifth date, max sixth

Introduction

Reactive powder concrete (RPC) is gaining increasing attention, from both academia and the construction industry, because of its favourable characteristics, such as good dynamic mechanical properties (Tuama, Kadhum, Alwash, Al-Khafaji & Abdulraheem, 2020). Therefore, RPC, since it was developed during the 1990s, has been widely applied in different construction industry fields, such as bridges, roads, military shelters, and municipal works (Yan, 2009; Kadhum, Alwash, Tuama & Abdulraheem, 2020). Numerous studies (Liu & Huang, 2009; Tai, Pan & Kung, 2011) have been performed to investigate the performance of concrete members exposed to fire in two phases; the first, investigate the impact of fire on the main mechanical characteristics as a construction material, and the second, focuses on the analysis of the structural behavior during the fire. Suddenly exposure of RPC to elevated temperatures might cause a spalling incident; this is probably due to the internal gas pore pressure increments while heating (Hager, Zdeb & Krzemień, 2013). "Spalling that caused by the rapid concrete loss after the fire temperatures reach to the inner concrete's layers core, thus increment in the transmission rate of concrete heat to the deeper member's layers" (Abdulraheem & Kadhum, 2018). The

temperature range of fire could be subdivided into two strength loss terms in RPC: 23–200°C and 300–500°C. Within the range 23–200°C, RPC maintains or maybe gains an increase in the original strength. In the range 300–500°C, RPC loses abundant amounts of genuine strength (Kadhum, 2015). Based on their position in the structure, columns may be exposed to fire on one side, two sides, three sides, or all four sides, which is an extremely critical situation. It can be seen so far that experimental studies relating to this new ultra high strength fiber reinforced concrete are still limited. According to that, the information available on the fire performance of RPC columns need to be conducted further. The purpose of the present study is to an extremely critical situation (Kodur & Raut, 2012), quantify some of the parameters influencing the residual strength and surface spalling of RPC columns to provide recommendations for fire-safe constructions. Experiments on RPC columns were performed through the manufacturing of a special smart system to represent the real condition of fire. The following parameters are considered: reinforcement ratio, temperature levels, and duration of exposure to fire. This research aims to compare the structural behavior of the concentrically loaded RPC and NSC column specimens after exposure to fire at various temperature levels.

Experimental program

The experimental work consists of two stages. The first stage includes the materials utilized, preparation, casting, and curing of the test samples. The second stage comprises (i) loading up to 25% of the ultimate load before heating, and (ii) heating with keeping the 25% loading constant (iii) loading after the heating process is finished and until failure, whereas the results for columns that are not heated are measured after the applied load only.

Depiction of the tested column specimens

The tested columns have dimensions of 900 mm long and a square cross-section of 100 × 100 mm, as demonstrated in Figure 1. The experimental program consists of 21 reduced-scale columns, which were cast, and tested up to failure under concentric compression loading. These columns were categorized into three groups according to their variables: the first group consisted of seven columns of RPC reinforced with 4∅6 mm as longitudinal reinforcement and ∅5 mm bars were utilized for ties (lateral reinforcement), the second group consisted of seven columns of RPC that were without reinforcement to investigate the impact of column reinforcement after the fire at different heating levels, and the third group consisted of seven columns of NSC reinforced with 4∅6 mm as longitudinal reinforcement and ∅5 mm bars were utilized for ties.

Constituent materials and fabrication

Two kinds of concrete were investigated in this investigation: the RPC for the specimens of the first and the second group and the NSC mix for the

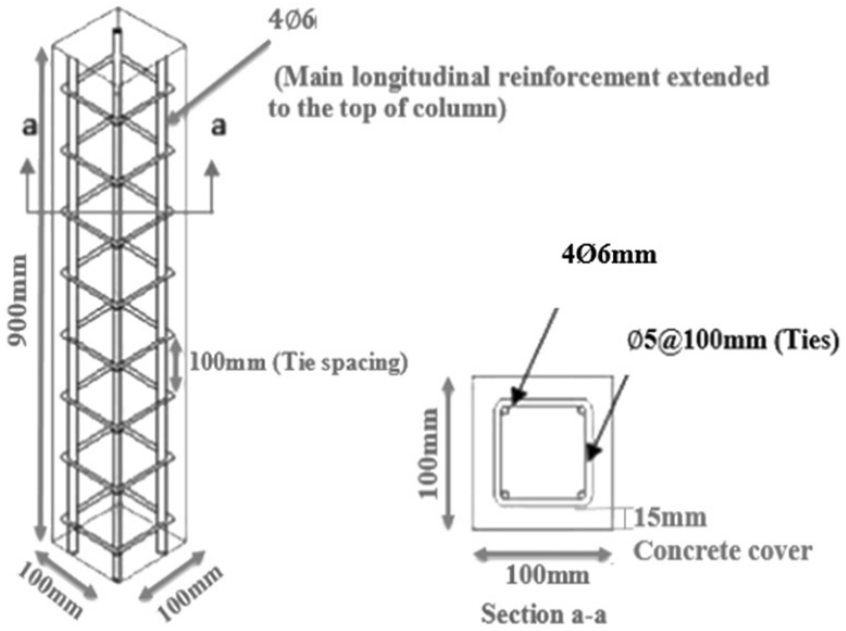

FIGURE 1. Characterization of the columns

specimens of the third group. The RPC mix consisted of 230 kg·m^{-3} of silica fume and 950 kg·m^{-3} of ordinary Portland cement (OPC). The physical and chemical compositions were depending on the requirement of the ASTM C1240--05 standard (ASTM International, 2005). The specific surface and chemical compositions of silica fume and cement are presented in Table 1. A 0.175 water-cementitious ratio was produced using a dosage (4% by weight of cementitious) of high-performance super-plasticizer (SP) which is known commercially as Hyperplastic PC200. Sand amount of 1,050 kg·m^{-3} with a maximum particle size of 600 μm and 230 kg·m^{-3} of brass--coated steel micro-fibers (0.18 mm in diameter and 13 mm long) and tensile strength of 2,300 MPa were used for all RPC mixes. The NSC mix consisted of 550 kg·m^{-3} of OPC, 730 kg·m^{-3} of natural sand, 810 kg·m^{-3} of rounded gravel with a maximum size of 10 mm, whilst the w/c was 0.45. The physical properties of fine and coarse aggregate

TABLE 1. Chemical characteristics of silica fume and cement

Material	CaO [%]	SiO_2 [%]	Al_2O_3 [%]	Fe_2O_3 [%]	SO_3 [%]	MgO [%]	Fineness [$m^2 \cdot kg^{-1}$]
OPC	62.23	19.86	4.88	3.48	2.47	2.47	340
Silica fume	0.41	94.84	0.55	0.05	0.11	0.21	19 980

TABLE 2. Physical characteristics of fine and coarse aggregate

Fine aggregate	Coarse aggregate
Fineness modulus = 2.6	Fineness modulus = 7.87
Sulphate content = 0.09%	Bulk density = 1 405 kg·m^{-3}
Fine material passing from sieve (75 μm) = 4.2%	Max. size used = 10 mm
Specific gravity = 2.65	Specific gravity = 2.75
Water absorption = 0.74%	Water absorption = 1.2%

were determined as per the Iraqi Standard Specification IQS 45/1984 (Central Organization for Standardization and Quality Control [CCSQC], 1984) and are listed in Table 2. The mixing process utilized a horizontal rotary mixer of 0.09 m^3 capacity for the column samples. The mixing method was adopted by our previous research (Abdulraheem, 2018) and approved to give satisfying workability and good dispersion of the materials.

Heating process and testing methodology

The slab specimens were tested under increasing concentric load up to failure at the age of 60 days utilizing a frame of 200 t capacity. For each of the three groups, one specimen was used as a reference, which was tested up to the failure, without any fire exposure, while the other six specimens were initially loaded to 25% of the ultimate load; subsequently, they were subjected to fire temperature under 25% constant loading, assuming three different temperatures (300, 400 and 500°C) and two durations (30 and 60 min) for fire exposure, and finally were tested until failure after the exposure to fire is finished. For the columns, which were subjected to fire under loading, the target heating temperature was reached utilizing a sliding arm to control the fire distance to the surface of the columns and by monitoring the fire intensity thru controlling the liquefied petroleum gas pressure in the burners by utilizing an electric gas regulator control. A gas regulator control is an electronic valve used to supply a very fast and straight gas flow. The target temperatures were 300, 400, and 500°C for the exposed columns, while the reference columns were not exposed to fire (at room temperature). The duration of the temperature loading was either 30 or 60 min, which was enough to warm up the sample to a uniform temperature (Abdulraheem, 2018; Abdulraheem & Kadhum, 2018). The structural behavior of the RPC columns exposed to fire results from loading each column to 25% of the ultimate load before heating, utilizing load control at a loading rate of 1 kN·s^{-1}, and then heating these columns with keeping the 25% loading constant after that is loading them until failure. For columns that have not been heated, the results come solely from the applied load (Fig. 2). The vertical and lateral deformations were measured using two dial gauges with an accuracy of 0.001 mm per deviation to measure the deformations for each load increment.

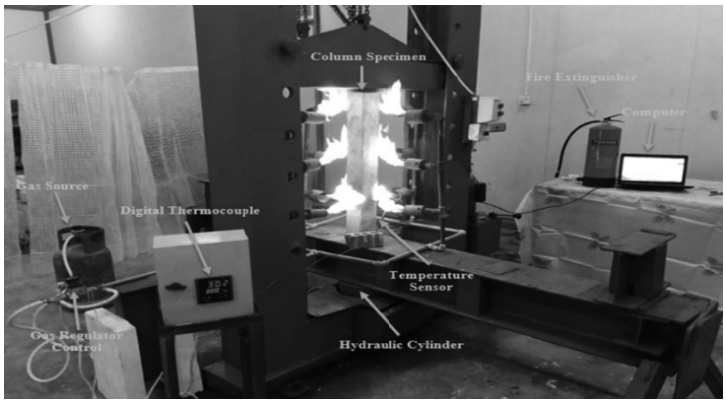

FIGURE 2. Experimental set-up

Test results and discussion

Axial load and deformation

The results in Table 3 showed that, after exposure to fire at 300°C for 30 min, the ultimate strength of the RPC columns slightly increased, by 0.35% for the first group and 1.27% for the second group, which can be attributed to the further hydration of cementitious materials activated by elevated temperature (Abdulraheem, 2018; Abdulraheem & Kadhum, 2018), while for NSC columns the bearing strength is decreased by 1.88%. Exposure for 60 min shows a slight decrease in the ultimate strength of the RPC columns, by 0.58% for the first group and 0.954% for teh second, while the NSC continued to decrease by 3% of its ultimate load capacity. After 3–6 min, a crack propagation sound was heard, and small chunks from the surface layer fell out. The bearing strength started to decrease for the RPC columns after exposure to fire temperature of 400°C because thermal gradients developed in the concrete cross-section, and the moisture in the concrete was transformed to vapor and thus created pore pressure (Abdulraheem, 2018; Abdulraheem & Kadhum, 2018). When pore pressure exceeded the tensile strength of the concrete, pieces of the concrete peeled off, and the ultimate loading capacity of the RPC columns decreased after 30 min of heating, by 28.52% for the first group and 35.29% for the second group, and after 60 min the ultimate load of the RPC decreased, by 31.92% for the first group and 37.28% for the second group. The ultimate load of the NSC column decreased by 5.64% and 11.9% after half an hour and an hour of exposure to fire, respectively. After 9–12 min of exposure to fire at 500°C, the RPC specimens started to spall, big parts fell out, and the ultimate strength clearly decreased after 30 min, by 48.78% for the first group and 71.55% for the second group, and after 60 min, by 54.37% for the first group and 78.53% for the second group. These results demonstrate the effect of steel reinforcement, which contributes to saving the core of the column from the internal pressure that results from heating. The ultimate strength of

TABLE 3. The results and details of the tested columns

Group	Column designation	Fire duration [min]	Ultimate load capacity [kN]	Failure mode
1	RPC-1-25	–	1 070.5	compression
	RPC-1-300	30	1 074	compression
	RPC-1-300	60	1 064	compression
	RPC-1-400	30	765	compression
	RPC-1-400	60	728.5	flexural
	RPC-1-500	30	548	compression
	RPC-1-500	60	488.5	flexural and compression
2	RPC-0-25	–	872	compression
	RPC-0-300	30	883	compression
	RPC-0-300	60	864	compression
	RPC-0-400	30	564.5	compression
	RPC-0-400	60	547	flexural
	RPC-0-500	30	248	flexural
	RPC-0-500	60	187	flexural and compression
3	NSC-1-25	–	399	compression
	NSC-1-300	30	391.5	compression
	NSC-1-300	60	387	compression
	NSC-1-400	30	376.5	compression
	NSC-1-400	60	351.5	compression
	NSC-1-500	30	365	compression
	NSC-1-500	60	326.5	compression

the NSC columns was reduced by 8.52% after 30 min and 18.2% after 60 min.

The residual strength with the fire temperature level is shown in Figure 3. The results of the ultimate capacity of the columns with and without exposure to fire are given in Table 3. It could be observed from Figure 3 that with increasing the fire duration from 30 to 60 min, the decrement in the load-carrying capacity is not highly affected. However, when the column capacity is reached, the column fails either by crushing or flexural buckling.

The results proved that the resistance of NSC to fire is greater than that of RPC, which is severely spalled at elevated temperatures. The internal cracks are the main cause of spalling. There is, however, some doubt surrounding whether the surface layer is split partially or completely at various depths at the core of the column, taking into account that there is no considerable damage on the surface (Kadhum & Mohammed, 2017). The vertical displacement of the reinforced RPC and NSC columns, as shown in Figure 4, has a similar trend

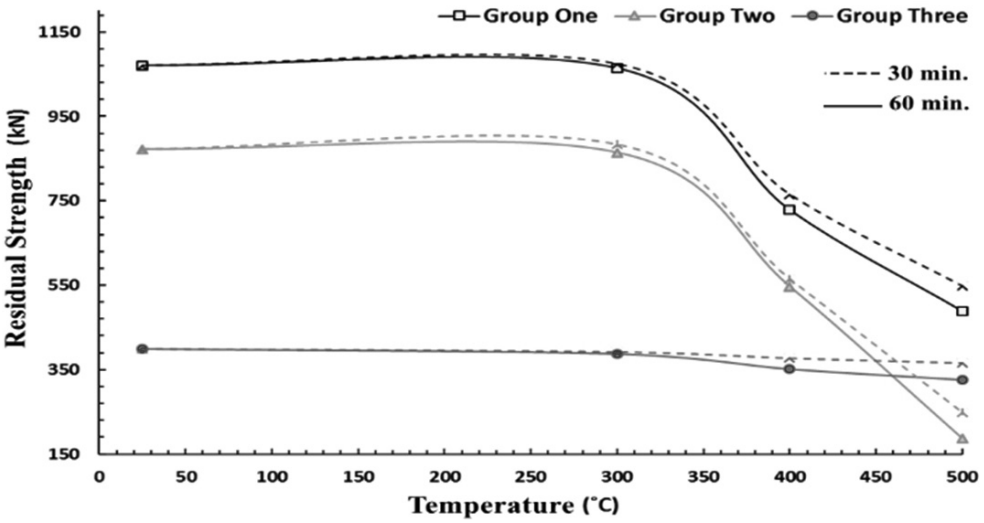

FIGURE 3. The residual strength with the change of temperature after half an hour and an hour of fire exposure

for all columns, but the maximum vertical displacement values of 4.21 and 2.54 mm for RPC and NSC columns, respectively, were reached after fire exposure at 400°C and for 60 min. The vertical deformation during exposure to fire results from many reasons, such as thermal expansion, applied load, and creep. The positive and negative vertical deformation values indicate expansion and contraction, respectively, of the concentric column specimens. RPC and NSC column specimens exposed to fire at 300, 400, and 500°C exhibited a small contraction when loaded to 25% of the ultimate load; the initial deforma-

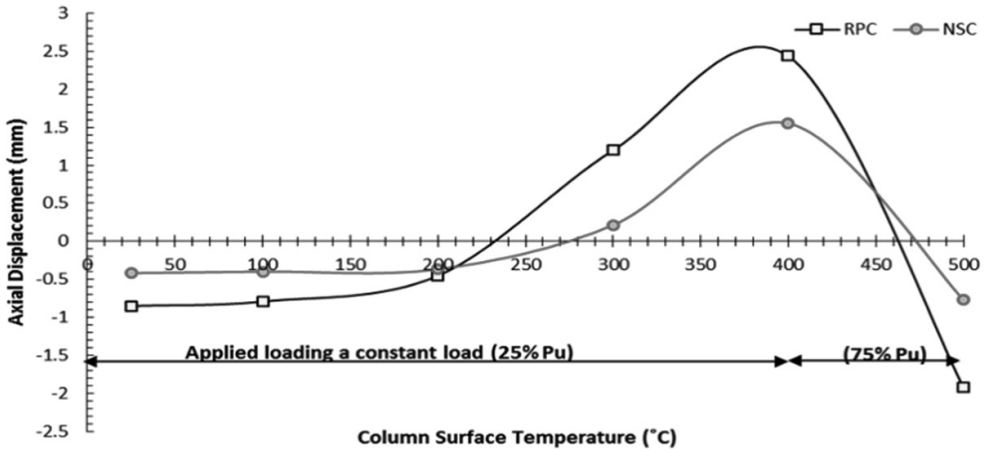

FIGURE 4. Comparison of vertical displacements of RPC and NSC columns after exposure to fire

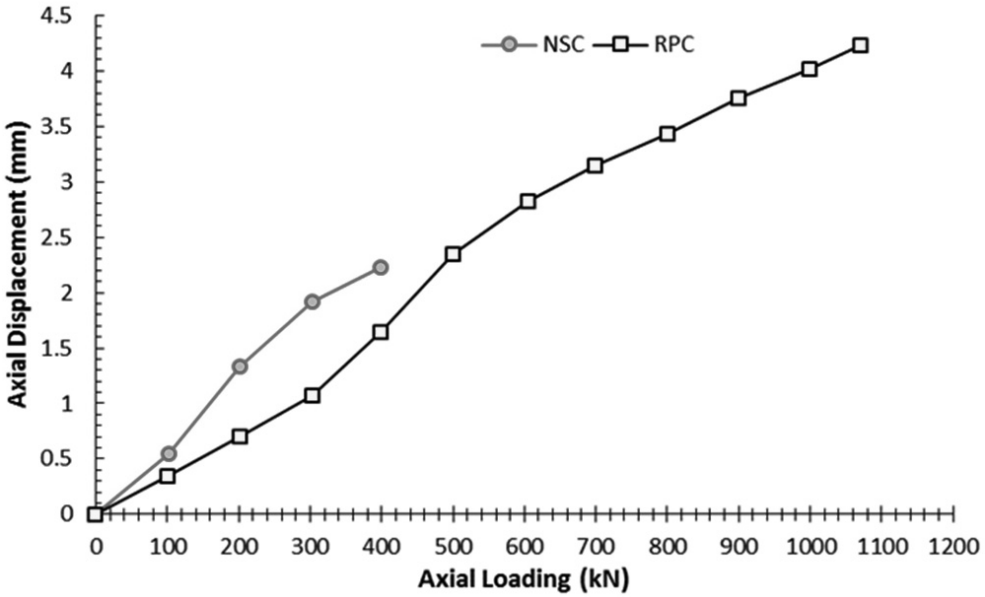

FIGURE 5. Comparison of vertical displacements of the reference RPC and NSC columns

tion (expansion) of the RPC and NSC column specimens was mostly because of the thermal concrete expansion and steel, though in the intermediate stages both load and thermal expansion had a substantial influence. In the succeeding stages, the creep influence becomes clear due to the high temperature. The contraction of the RPC and NSC columns after the exposure duration is finished could be attributed to the loss in stiffness and strength of the steel and concrete. Finally, Figure 3 shows the column surface temperature versus the vertical deformation in the y-direction (elongation or contraction) for RPC and NSC columns at different stages during loading and heating, while Figure 5 shows the vertical displacement for RPC and NSC columns due to loading at the normal temperature of the room (25°C).

Pattern of cracks and spalling

By inspecting each case, it is clear that, despite the good agreement in the measured parameters, an obvious aberration in the values of the extent of the cracks may be noticed between the tested columns in each instance. The cracks, which appeared in the columns, can be classified according to the acting loading condition, as: pure axial concentric load; pure thermal stress; combined thermal stress and axial load.

Pure axial concentric load. In this study, one column from each group was tested at room temperature in order to be the reference for the other columns. The columns failed by compression mode (crushing) and the cracks appeared in a conical pattern like the failure of the cylinder in a compression test, as shown in Figure 6.

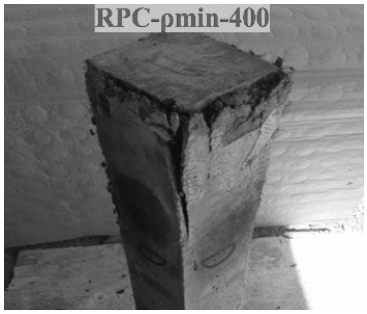

FIGURE 6. Typical crack pattern of pure axial concentric load columns

Pure thermal stress. In this study, the thermal stress that resulted when the columns were exposed to fire differed in intensity. Different cracks appeared in each stage (stages A, B, C, D):

A. During 30–45 min of exposure to fire at 300°C, hairline cracks appeared at the middle portion of the column specimens.
B. During 21–36 min of exposure to fire at 400°C, hairline cracks and surface spalling appeared in the RPC column; before that, the sound of crack propagation was heard. The surface spalling occurs due to the pore pressure (Klingsch, 2014).
C. Sloughing-off spalling (non-violent breaking off of concrete fragments) and corner spalling (removal of the concrete cover from the corner) occurred during 40–55 min of exposure to fire at 400°C. Sloughing-off spalling occurs due to longer exposure, corner spalling occurs due to the temperature impact from two sides (Klingsch, 2014).
D. Explosive spalling took place in RPC columns at 500°C. An assumption is proposed that the combined thermal stresses and pore pressure caused this explosive spalling (Khoury & Anderberg, 2000). The pore pressure ensuing from explosive spalling may, in short, be defined as follows: moisture is created within the pore concrete system along with temperature increases. This moisture increases when the temperature is above 100°C, water as liquid and vapor are present inside the pore system. The presence of pressure occurs due to the pore saturation degree and the building temperature. A part of this vapor is liberated through the voids and pores depending on the concrete permeability; nevertheless, pore pressure rises as long as adequate moisture is obtainable.

Combined thermal stress and axial load. The present research focuses on the structural behavior of the columns exposed to burning under loading, which is a real situation that represents the chemical changing of the microstructure of a building by raising the temperature levels during the burning of the member and as follows:

A. All NSC columns failed by compression mode; diagonal cracks appeared at the middle third of columns at 75–80% of the failure load, followed by crushing and rupture of certain ties.
B. At 300°C, the RPC failed by compression mode. A set of cracks appeared on the column faces, approximately 80% of the failure load; the cracks seen on the columns were vertical and diagonal.
C. At 400°C, the unreinforced RPC column failed by flexural mode, while the reinforced RPC column failed in compression mode.

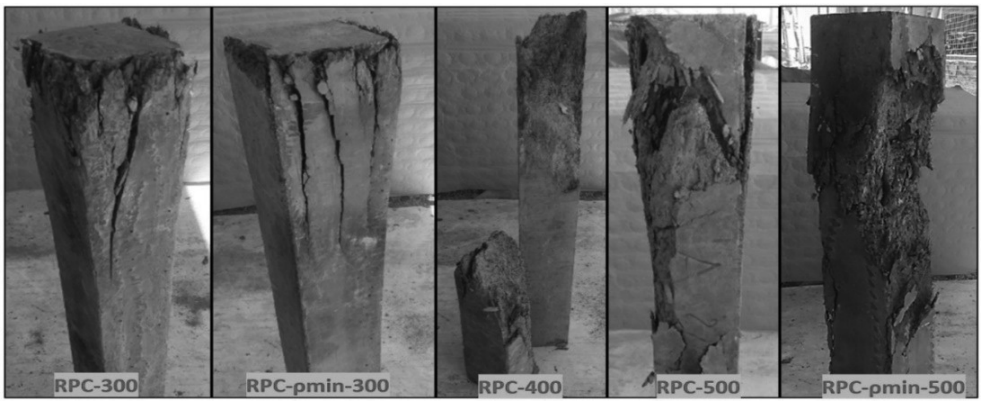

FIGURE 7. Failure mode of RPC columns due to combined thermal stress and axial load at different temperature levels

D. The deterioration of the RPC at 500°C appeared in two forms: local damage (cracks) in the material itself, and global damage resulting from flexural failure at the first third of the column.

The mode of failure of the RPC columns due to combined thermal stress and axial load is shown in Figure 7.

Finally, the authors recommend, basing on the successful use of electromagnetic sensors in many fields (Gkantou, Muradov, Kamaris, Atherton & Kot, 2019; Ryecroft et al., 2019a; Ryecroft et al., 2019b; Teng et al., 2019), using of embedded sensors in the concrete members to monitor the progress of temperature that helps to have a better understanding for the effects of fire on concrete structures.

Conclusions

This research has studied the post-fire performance of reactive powder concrete columns exposed to fire at different temperature levels (300, 400 and 500°C) and for two durations (30 and 60 min). From the outcome of our investigation, it is possible to conclude that:

- The residual strength of RPC columns drops with increasing temperature starting at 300°C.
- Based on the experimental results, explosive spalling occurred in a period of up to 30 min of heating. At all times, minor spalling took place first, followed by major and severe spalling.
- The deterioration of the RPC at 500°C appeared in two forms: local damage (cracks) in the material itself and global damage resulting from failure in the column.
- Compared to the fire resistance of NSC, RPC has a higher susceptibility to fire-induced spalling. This is possibly due to the low permeability and the high density of RPC, which prevents water vapor from escaping at elevated temperatures and leads to high pore pressure, which produces spalling.
- Explosive spalling took place in RPC columns at 500°C due to pore pressure.

– The residual strength of reinforced RPC columns is greater than that of the unreinforced columns at high temperatures because the longitudinal reinforcement confined the core of the column and prevent it from spalling.

References

Abdulraheem, M.S. (2018). Experimental investigation of fire effects on ductility and stiffness of reinforced reactive powder concrete columns under axial compression. *Journal of Building Engineering*, *20*, 750-761.

Abdulraheem, M.S. & Kadhum, M.M. (2018). Experimental and numerical study on post--fire behaviour of concentrically loaded reinforced reactive powder concrete columns. *Construction and Building Materials*, *168*, 877-892.

ASTM International (2005). Standard specification for silica fume used in cementitious mixtures (ASTM C1240-05). West Conshohocken, PA: ASTM International.

Central Organization for Standardization and Quality Control [CCSQC] (1984). Aggregate from natural sources for concrete and construction (IQS 45/1984). Baghdad: Central Organization for Standardization and Quality Control.

Gkantou, M., Muradov, M., Kamaris, G.S., Atherton, W. & Kot, P. (2019). Novel electromagnetic sensors embedded in reinforced concrete beams for crack detection. *Sensors*, *19*(23), 5175-5189.

Hager, I., Zdeb, T. & Krzemień, K. (2013). The impact of the amount of polypropylene fibres on spalling behaviour and residual mechanical properties of Reactive Powder Concretes. *MATEC Web of Conferences*, *6*(1), 02003-02016.

Kadhum, M. (2015). Prediction of Mechanical Properties of Reactive Powder Concrete by Using Artificial Neural Network and Regression Technique after the Exposure to Fire Flame. *Jordan Journal of Civil Engineering*, *9*(3), 1-15.

Kadhum, M.M., Alwash, N.A., Tuama, W.K. & Abdulraheem, M.S. (2020). Experimental and numerical study of influence of crude oil products on the behavior of reactive powder and normal strength concrete slabs. *Journal of King Saud University – Engineering Sciences*, *32*(5), 293-302.

Kadhum, M.M. & Mohammed, Z.A. (2017). Predict the Ultimate Moment Capacity of Reactive Powder Concrete Beams Exposed to Fire Flame Using Artificial Neural Network and Multiple Linear Regression Models. *International Journal of Engineering and Technology (IJET)*, *9*(3), 2637-2649.

Khoury, A. & Anderberg, Y. (2000). *Fire Safety Design – Concrete Spalling Review*. Swedish Borlänge: National Road Administration.

Klingsch, E.W. (2014). Explosive spalling of concrete in fire. *IBK Bericht*, *356*(1), 1-13.

Kodur, V. & Raut, N. (2012). A simplified approach for predicting fire resistance of reinforced concrete columns under biaxial bending. *Engineering Structures*, *41*, 428-443.

Liu, C-T. & Huang, J-S. (2009). Fire performance of highly flowable reactive powder concrete. *Construction and Building Materials*, *23*(5), 2072-2079.

Ryecroft, S., Shaw, A., Fergus, P., Kot, P., Hashim, K., Moody, A. & Conway, L. (2019a). A First Implementation of Underwater Communications in Raw Water Using the 433 MHz Frequency Combined with a Bowtie Antenna. *Sensors*, *19*(8), 1813-1823.

Ryecroft, S., Shaw, A., Fergus, P., Kot, P., Hashim, K. & Conway, L. (2019b). A Novel Gesomin Detection Method Based on Microwave Spectroscopy. In D. Al-Jumeily et al. (eds.), *12th International Conference on Developments in eSystems Engineering (DeSE 2019)* (pp. 429-433). IEEE Computer Society Conference Publishing Services. https://doi.org/10.1109/DeSE.2019.00085

Tai, Y-S., Pan, H-H. & Kung, Y-N. (2011). Mechanical properties of steel fiber reinforced reactive powder concrete following exposure to high temperature reaching 800°C. *Nuclear Engineering and Design*, *241*(7), 2416-2424.

Teng, K.H., Kot, P., Muradov, M., Shaw, A., Hashim, K., Gkantou, M. & Al-Shamma'a, A. (2019). Embedded Smart Antenna for

Non-Destructive Testing and Evaluation (NDT&E) of Moisture Content and Deterioration in Concrete. *Sensors*, *19*(3), 547-559.
Tuama, W., Kadhum, M., Alwash, N., Al-Khafaji, Z. & Abdulraheem, M. (2020). RPC Effect of Crude Oil Products on the Mechanical Characteristics of Reactive-Powder and Normal--Strength Concrete. *Periodica Polytechnica Civil Engineering*, *64*(2), 422-429.
Yan, G. (2009). Application of reactive powder concrete in highway barriers. In Q. Peng et al. (eds.), *International Conference on Transportation Engineering 2009* (pp. 7–12). American Society of Civil Engineers. https://doi.org/10.1061/9780784410394

Summary

Experimental investigation on the post-fire performance of reactive powder concrete columns. The increased use of reactive powder concrete (RPC) in concrete structures has attracted attention towards the structural behavior of RPC in fires. This work examines experimentally the performance of RPC and NSC columns subjected to 25% of the ultimate load and exposed to direct fire flame for a period of 30 and 60 min at various temperature levels. The paper aims to evaluate the maximum temperature level and fire duration that can be withstood by this type of concrete columns. The results show that the failure mode of RPC columns without reinforcement is a sudden shear failure, whereas the failure mode of reinforced RPC columns is a crushing failure with rupture of certain ties. The RPC columns at high temperatures spall intensively; additionally, the ultimate strength clearly decreases compared to the NSC columns at the same conditions.

Authors' address:
Mohammed M. Kadhum
(https://orcid.org/0000-0002-4732-3646)
University of Babylon
College of Engineering
Department of Civil Engineering
Al Hilla, 51001
Iraq
e-mail: eng.mohammed.mansour@uobabylon.edu.iq

Zainab H. Mahdi
Middle Technical University
Technical Engineering College
Baghdad, 10001
Iraq
e-mail: zaideng.2004@yahoo.com

Yousif Taha Funfakh
University of Babylon
College of Engineering
Department of Civil Engineering
Al Hilla, 51001
Iraq
e-mail: eng.mohammed.mansour@uobabylon.edu.iq

Zaid Mohammed
University of Technology
Building and Construction Engineering Department
Baghdad, 10001
Iraq
e-mail: zainabengineeringcollege@yahoo.com

Mustafa Abdulraheem – corresponding author
General Company of electricity distribution for the middle region, Karbala branch
Karbala, 5600
Iraq
e-mail: mostfa_seham@yahoo.com

Michaela Gkantou
Liverpool John Moores University
School of Civil Engineering and Built Environment
Liverpool, L3 3AF
UK
e-mail: M.Gkantou@ljmu.ac.uk

Scientific Review – Engineering and Environmental Sciences (2021), 30 (2), 327–336
Sci. Rev. Eng. Env. Sci. (2021), 30 (2)
Przegląd Naukowy – Inżynieria i Kształtowanie Środowiska (2021), 30 (2), 327–336
Prz. Nauk. Inż. Kszt. Środ. (2021), 30 (2)
http://iks.pn.sggw.pl
DOI 10.22630/PNIKS.2021.30.2.28

Volodymyr SNITYNSKYY[1], Ivan KERNYTSKYY[2], Bohdan DIVEYEV[3], Orest HORBAY[3], Yevhen FORNALCHYK[3], Ruslan HUMENUYK[1], Yaroslav SHOLUDKO[1]

[1] Lviv National Agrarian University – LNAU, Faculty of Mechanical and Power Engineering
[2] Warsaw University of Life Sciences – SGGW, Institute of Civil Engineering
[3] Lviv Polytechnic National University – LPNU, Institute of Engineering Mechanics and Transport

Optimization of the semi-active vibration absorbers

Key words: dynamic vibration absorber, semi-active, adaptive schemes, optimization, robustness, design

Introduction

Given the diversity of types of dynamic processes that cause increased vibrations and increased operational requirements, the development of methods and means of vibration protection, in particular – passive ones or controlled remains relevant. Among them, a special place is occupied by dynamic vibration absorber (DVA), which are joined to the design in order to reduce its vibration load. A special feature of DVA is that their use can be foreseen at the design and construction stage, and in case of elimination of unsatisfactory characteristics of the structure already in the process of its operation.

DVAs differ in the methods of energy dissipation. The most well-known are DVAs with a viscoelastic element or a combination of an elastic element and a damper. Electromagnetic and electrostrictive processes are also used in all types of DVAs with electromagnets or piezoelectric elements. Such DVAs usually belong to the class of active, because with the help of electrical processes it is easier to control processes.

One of the main directions of the development of the theory of fading oscillations is to evaluate their efficiency and to select optimal parameters with different disturbing loads. To date, the theory of single-mass linear DVA with viscous and independent friction with harmonic oscillations with stable or fixed frequency (which varies in time) is most fully developed.

The semi-active DVA uses control to adjust the device configuration based on the actual structure of the vibration. As

is typical for structural control, there are many types of devices and management laws, some of them are more realistic than others of varying degrees of complexity. A considerable number of practical implementations of semi-active DVA's can be found in the literature, some of which are described in Seiler, Fischer and Huber (2002), Casciati, Magonette and Marazzi (2006), Setareh, Ritchey, Murray, Koo and Ahmadian (2007), Nagarajaiah (2009), Shena and Ahmadian (2013), Weber and Distl (2013).

A broad description of the control algorithms that can be used to control these devices can be found in Setareh et al. (2007), which in turn are divided into two groups. Some of them are based on strategies that constantly change the parameters of the DVA in dynamic mode, and the other – on the ON/OFF control strategy. The latter option, though not as impressive as the first one, tends to result in algorithms that are simpler, more realistic, and easier to implement.

For realization of semi-active control various mechanisms for controlling the movement of DVA are offered. The mechanism based on the magneto-rheological (MR) control method has recently gained popularity in the structural control zone (Spencer & Nagarajaiah, 2003). The application of a magnetic field causes changes in the structure of the liquid MR inside the damper, which is used to control the damping force, in these elements. The simplicity of its mechanical functioning is associated with low direct constructive costs and low running costs for their operation. DVA can simultaneously reduce amplitude of oscillations at several frequencies. In Pinkaew and Fujino (2001) based on the optimal control theory, it has been found that a semi-active DVA can extinguish the vibration of the primary in both the transient and in steady-state modes. In Hu and Jin (1997) and Qian and Hu (2001) a semi-active vibration absorber with piecewise linear elastic components is presented, which may have an adjustable the operating frequency, which follows the frequency variation of the excitation. In Koo and Ahmadian (2004) numerically studied two kinds semi-active skyhook DVA, and then magnetic resonator (MR) damper is tapped and experimentally confirmed the improved control efficiency. The conventional DVA are presented in Diveyev, Horbay, Kernytskyy, Pelekh and Velhan (2017), Kernytskyy et al. (2017), Pelekh et al. (2017).

Semi-active DVA

Consider the frequency response and vibrograms of uncontrolled and controlled damping of DVA (Fig. 1).

The DVA equations in this case will be:

$$m_1 \frac{d^2 x_1}{dt^2} + k_1 x_1 + c_1 \frac{dx_1}{dt} - k_2 (x_2 - x_1) - c_2 \left(\frac{dx_2}{dt} - \frac{dx_1}{dt} \right) - c_{t2}\, sign\left(\frac{dx_2}{dt} - \frac{dx_1}{dt} \right) = k_1 x_0 + c_1 \frac{dx_0}{dt} \quad (1)$$

$$m_2 \frac{d^2 x_2}{dt^2} + k_2 (x_2 - x_1) + c_2 \left(\frac{dx_2}{dt} - \frac{dx_1}{dt} \right) + c_{t2}\, sign\left(\frac{dx_2}{dt} - \frac{dx_1}{dt} \right) = 0$$

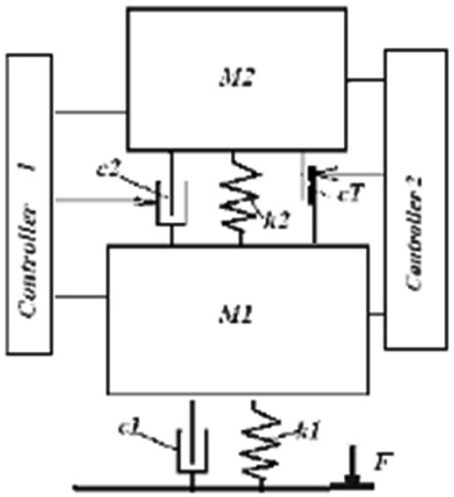

FIGURE 1. Semi-active DVA with the damping and friction control

Here a kinematic perturbation with a certain frequency is considered. The coefficients are now variables in time and change according to some rules with the help of controllers (Fig. 1). Here the rule ON-OFF of semi-active DVA's can be found in the literature, some of which are described in Hu and Jin (1997), Pinkaew and Fujino (2001), Qian and Hu (2001), Seiler et al. (2002), Spencer and Nagarajaiah (2003), Koo and Ahmadian (2004), Casciati et al. (2006), Setareh et al. (2007), Nagarajaiah (2009), Weber and Distl (2013), for viscous friction is applied:

$$sign\left(x_1\left(\frac{dx_2}{dt}-\frac{dx_1}{dt}\right)\right)>0,\ c_2=c_{2A}$$
$$sign\left(x_1\left(\frac{dx_2}{dt}-\frac{dx_1}{dt}\right)\right)\le 0,\ c_2=c_{2B} \quad (2)$$

The complexity and high dimensionality of some models lead to the use of a heuristic search method.

DVA optimization

Wide application for optimization found algorithms of random search, namely genetic algorithms (Allen & Karjalainen, 1999). The problem of solving such problems is the direction in the computer sciences, which is called artificial intelligence (AI). For application of GA mathematical models should adequately reproduce the real dynamic processes in machines and structures with DVA. They must satisfy the following basic requirements:

1. Adequate reproduction of dynamic processes in structures.
2. To include in the set of calculation parameters the determining design and technological parameters.
3. To be adapted to the next transformation into machine codes (there is somewhat absurd idea that designs should be designed not only on the basis of their functional characteristics, but also on the requirements of their maximum simplification, from the conditions of their simplest mathematical modeling).
4. Interact with known software application packages of computer design and computer-based production training.
5. Have an information correlation with world-wide patent knowledge bases (for example, from espacenet.com) and with accessible "open" software on the Internet. There are concepts of local and global object search. The complexity and high dimensionality of some models lead to the use of a heuristic search method. In this matter, random search methods (genetic algorithms – GA) were used to optimize DVA.

The optimization function is

$$F_{CIL} = \max\left(\ddot{x}_1(f)\right),\ f_1 < f < f_2 \qquad (3)$$

Results of optimization of the frequency response for DVA (frequency response function – FRF) with constant damping and controlled damping are presented in Figure 2a, the corresponding vibration for the frequency inside the optimization interval are presented in Figure 2b. Here x_1 – vibration level of base, f_1, f_2 – boundaries of observed frequency domain, P – weight function, f – first eigen-frequency. Parameters of optimization are m_2, k_2, c_2. Just as a viscous friction, let us consider a variable dry friction (4).

$$sign\left(x_1\left(\frac{dx_2}{dt} - \frac{dx_1}{dt}\right)\right) > 0,\ c_{t2} = c_{T2A}$$
$$sign\left(x_1\left(\frac{dx_2}{dt} - \frac{dx_1}{dt}\right)\right) \le 0,\ c_{t2} = c_{T2B} \qquad (4)$$

[The ordinate units are not specified here (as well in Figs. 5, 6, 8, 10) as all problems are linear. The appearance of the graphs will be identical, regardless of the intensity of the load].

In Figure 3 the results of optimization for DVA with controlled viscous damping, friction damping and both simultaneously are shown. In the narrower range, active friction is more effective (Fig. 4).

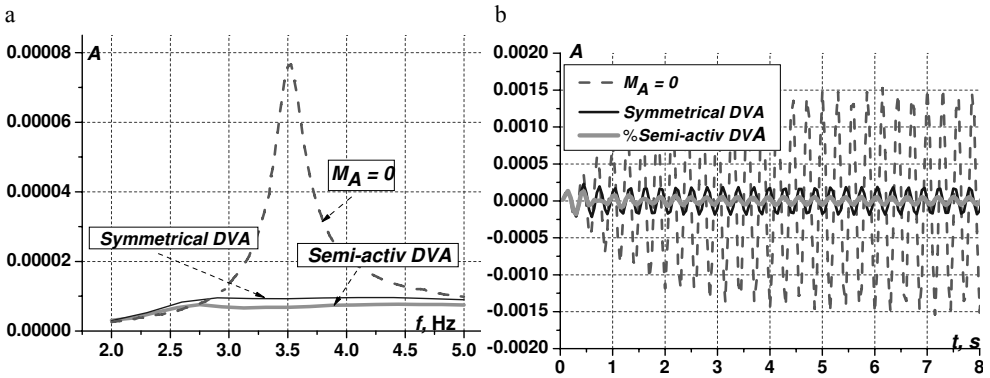

FIGURE 2. Results of optimization of the frequency response for DVA with constant damping and controlled damping (a); the corresponding vibration for the frequency inside the optimization interval (b)

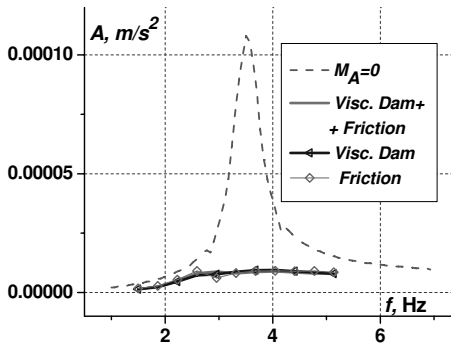

FIGURE 3. Optimized FRF's for controlled viscous, dry friction and both controlled simultaneously

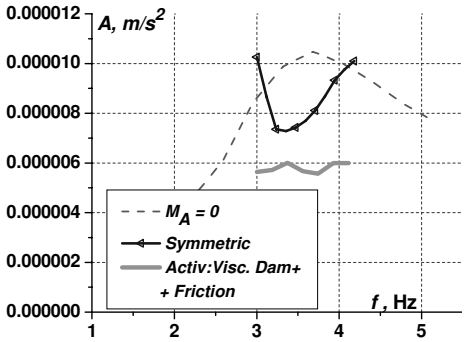

FIGURE 4. Narrower range of optimization

Pulse optimization

Consider the optimization of the DVA by parameters, with impulse disturbance

$$CiL = \max\left(\left|u_1(t)\right|\right),\ t > T_0 \qquad (5)$$

Here, for the target function, the maximum deviation of the amplitude of the basis is taken after some initial period of time. Figures 5 and 6 show the results of optimization in the control of viscous and dry friction and without control.

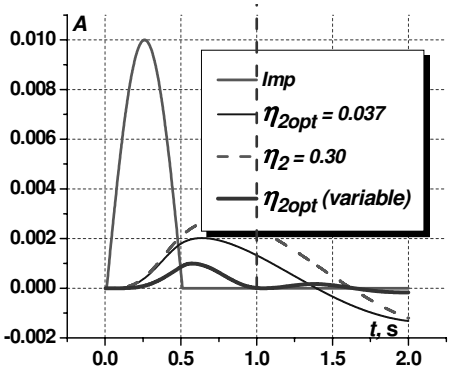

FIGURE 5. Results of optimization in the control of viscous friction and without control

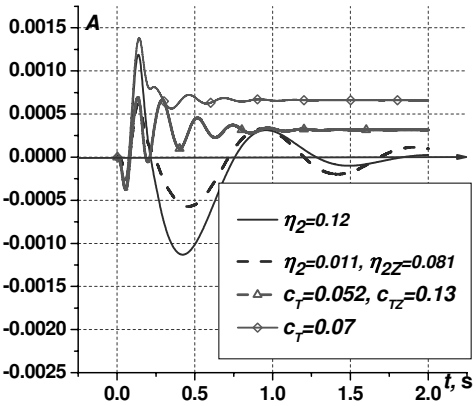

FIGURE 6. Optimization results in the management of viscous and dry friction and without control

DVA robust optimization

The fundamental definition of robust design is described as a product or process is said to be robust when it is insensitive to the effects of sources of variability, even through the sources themselves have not been eliminated (Fowlkes & Creveling, 1995). The questions of robustness are discussed in Zang, Friswell and Mottershead (2005) at optimization of DVA. As the main criterion the weighted sum of deviation of the basic design and the gradient module of this deviation is considered. A set of random values of such parameters as mass and stiffness of DVA is used for graphically constructing a shell of optimal DVA with the deviation of parameters.

In our optimization method, genetic methods are used that give a sequence of points of parameters that coincide with the optimal value. On the basis of intermediate results of calculations, it is possible to construct not shells of plane charts, but map parameters, which is more informative. For this purpose, one or two start-ups of the optimization process, preferably with diametrically opposite points of permissible values, prevail. The criterion of robustness is the convexity of these maps in the vicinity of the optimum. Although this is not a sufficient condition, only necessary. For a more complete study, we introduce the following indicator – the radius of deviation (R_Δ).

$$R_\Delta = \min(R),\ CiLa = (1+\alpha)CiL \qquad (6)$$

This is the minimum distance from the points with the indicators $(1 + \alpha)$ at

the higher (worst) points from the optimal point. For optimization in a linear case, only two parameters are depicted in Figure 7 for $\alpha = 2$. In this case, this condition is also sufficient. In the case of a lot of parametric optimization, the convexity of all maps across all parameters pairs is a necessary, but not sufficient condition. In a multidimensional space, the behavior of the target function can be complex. However, the criterion that finds the nearest point with some deviation of the point to the optimum remains effective. For optimization in a linear case only for two parameters (frequency and damping) are depicted in Figure 7 for $\alpha = 2$.

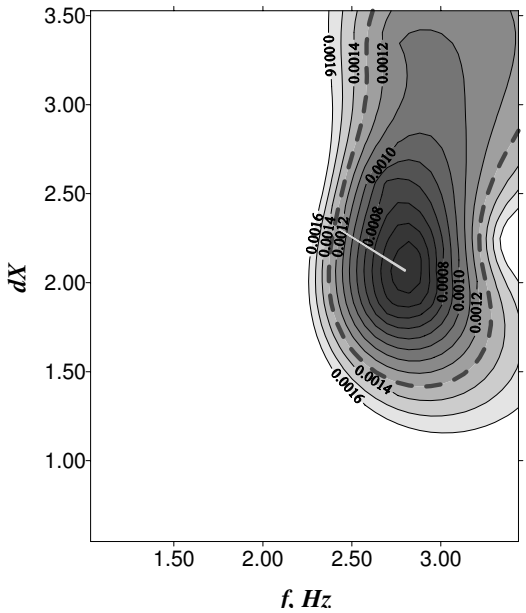

FIGURE 7. Map of optimization in by two parameters, and the indicator of robustness

Different types of control management

Consider some simple control algorithms. This is, first of all, the rule (2) is known as sky-hook or ON-OFF (Hu & Jin, 1997; Pinkaew & Fujino, 2001; Qian & Hu, 2001; Seiler et al., 2002; Spencer & Nagarajaiah, 2003; Koo & Ahmadian, 2004; Casciati et al., 2006; Setareh et al., 2007; Nagarajaiah, 2009; Weber & Distl, 2013) for viscous friction. The effectiveness of this rule in the wide-frequency range is shown in Figure 7. But there are similar rules of management (Shen & Ahmadian, 2013; Moutinho, 2015):

$$sign\left(\frac{dx_1}{dt}\left(\frac{dx_2}{dt}-\frac{dx_1}{dt}\right)\right)>0,\ c_2=c_{2A}$$

$$sign\left(\frac{dx_1}{dt}\left(\frac{dx_2}{dt}-\frac{dx_1}{dt}\right)\right)\le 0,\ c_2=c_{2B}$$

or (7)

$$sign\left(\frac{d^2x_1}{dt^2}\left(\frac{dx_2}{dt}-\frac{dx_1}{dt}\right)\right)>0,\ c_2=c_{2A}$$

$$sign\left(\frac{d^2x_1}{dt^2}\left(\frac{dx_2}{dt}-\frac{dx_1}{dt}\right)\right)\le 0,\ c_2=c_{2B}$$

We shall also investigate the effectiveness of different control rules in the classical case in the vicinity of the resonance (Fig. 8).

Just like outside the resonance zone, ON-OFF control is effective only. Other management is just a bit better than an uncontrollable process.

Let us consider the process of optimization DVA with the fewer notions

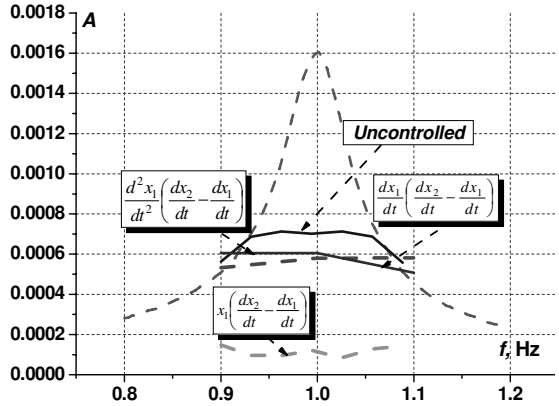

FIGURE 8. The effectiveness of different control rules in the vicinity of the resonance

m_2 / m_1 = 0.06 (ON-OFF algorithm). In Figure 9 the process of genetic optimization is shown.

In Figure 10 the results of optimization are shown. In Figure 11 variation of controlled damping and in Figure 12 the map of optimal parameters are presented.

Let us consider less DVA mass (m_2 / m_1 = 0.02). In Figure 13 the vibration of base is shown by optimal DVA.

a

N = 1
fx.804E+00 dx.560E+00 dx2.254E-01 Av.249E+00 dv.131E+00 CiL.444E-02

N = 13
fx.799E+00 dx.682E+00 dx2.243E-01 Av.238E+00 dv.131E+00 CiL.431E-02

N = 15
fx.804E+00 dx.682E+00 dx2.169E-01 Av.249E+00 dv.131E+00 CiL.407E-02

N = 70
fx.979E+00 dx.532E+00 dx2.191E-02 Av.764E+00 dv.957E-01 CiL.293E-02

N = 75
fx.950E+00 dx.716E+00 dx2.379E-02 Av.763E+00 dv.119E+00 CiL.224E-02

N = 3343
fx.965E+00 dx.964E+00 dx2.552E-03 Av.344E+00 dv.502E+00 CiL.177E-02

N = 3544
fx.966E+00 dx.963E+00 dx2.558E-03 Av.683E+00 dv.502E+00 CiL.173E-02

b

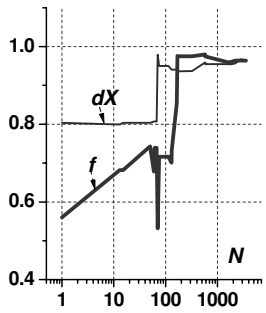

FIGURE 9. The process of genetic optimization is shown: a – step by step date; b – graphical representation of frequency and damping

a

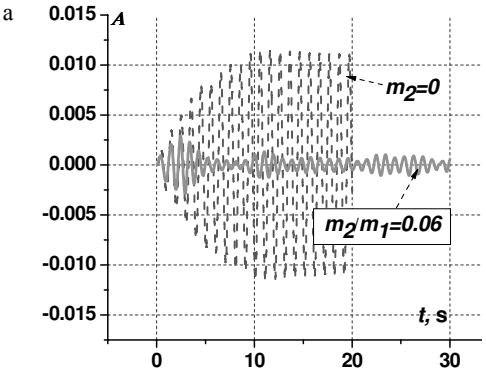

b

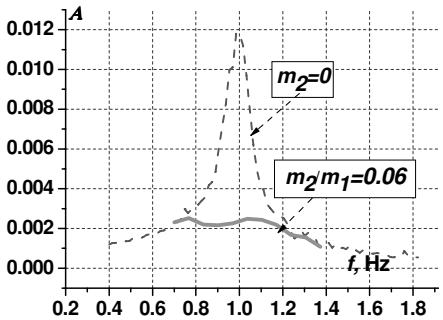

FIGURE 10. Results of optimization: a – in the time domain; b – optimal FRF

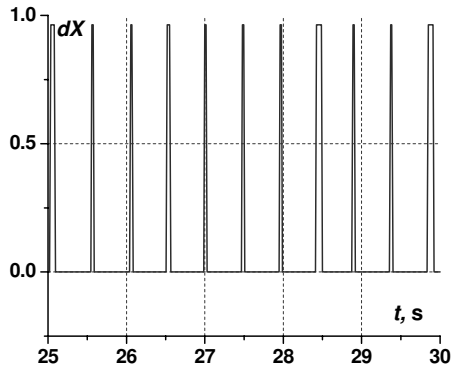

FIGURE 11. Variation of controlled damping

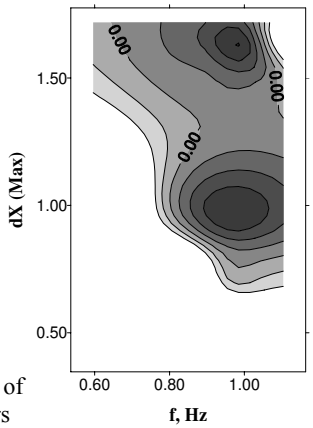

FIGURE 12. Map of optimal parameters

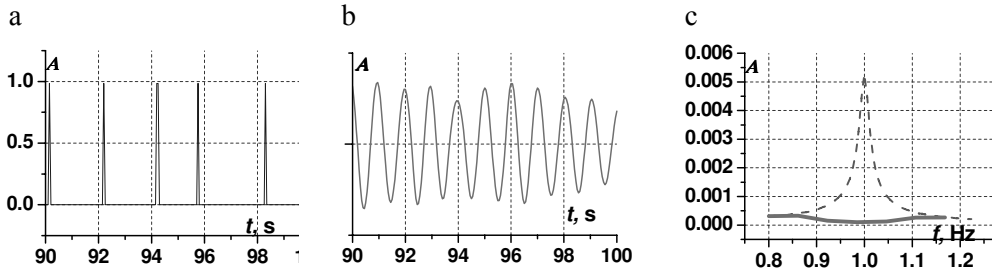

FIGURE 13. Vibration of base: a – changing damping (after 90 s); b – time domain; c – optimal FRF

Conclusions

The semi-active DVAs, which are controlled both by damping and frequency, are considered. The new methods of DVA optimization by impact and narrow frequency excitation are considered. On the basis of the simple models, it is possible to optimize different types of DVA in the range of the first resonance of the basis, where, as a rule, the greatest amplitudes of oscillations. Separately, various types of DVA control: skyhook (different types), ON-OFF, are investigated. It has been found that ON-OFF control is only effective with the measurements of the relative speed of the DVA and the displacement of the basic design.

References

Allen, F. & Karjalainen, R. (1999). Using genetic algorithms to find technical trading rules. *Journal of Financial Economics*, *51*(2), 245-271.

Casciati, F., Magonette G. & Marazzi F. (2006). *Technology of semiactive devices and applications in vibration mitigation*. New York: Wiley.

Diveyev, B., Horbay, O., Kernytskyy, I., Pelekh, R. & Velhan, I. (2017). Dynamic properties and damping predictions for laminated micro-beams by different boundary conditions. In *13th International Conference on Perspective Technologies and Methods in MEMS Design*: Lviv 20-23 April 2017 (pp. 30-34). New York: IEEE.

Fowlkes, W.Y. & Creveling, C.M. (1995). *Engineering methods for robust product design: using Taguchi methods in technology and*

product development. Reading, MA: Addison-Wesley Publishing Company.

Hu, H. & Jin, D. (1997). A semi-active vibration control strategy based on piecewise linear vibration absorbers. *Journal of Vibration Engineering*, *10*(2), 125-130.

Kernytskyy, I., Diveyev, B., Horbaj, O., Hlobchak, M., Kopytko, M. & Zachek, O. (2017). Optimization of the impact multi-mass vibration absorbers. *Scientific Review Engineering and Environmental Sciences*, *26*(3), 394-400.

Koo, J.H. & Ahmadian, M. (2004). In search of suitable control methods for semi-active tuned vibration absorbers. *Journal of Vibration and Control*, *10*(2), 163-174.

Moutinho, C. (2015). Testing a simple control law to reduce broadband frequency harmonic vibrations using semi-active tuned mass dampers. *Smart Materials and Structures*, *24*(5), 055007. https://doi.org/10.1088/0964-1726/24/5/055007

Nagarajaiah, S. (2009). Adaptive passive, semiactive, smart tuned mass dampers: identification and control using empirical mode decomposition, Hilbert transform, and short-term Fourier transform. *Structural Control and Health Monitoring: The Official Journal of the International Association for Structural Control and Monitoring and of the European Association for the Control of Structures*, *16*(7-8), 800-841.

Pelekh, Y., Konyk, I., Hlobchak, M., Cherchyk, G., Opalko, V. & Diveyev, B. (2017). Optimization of the particle vibration absorbers as SDOF system. In *13th International Conference on Perspective Technologies and Methods in MEMS Design*: Lviv 20-23 April 2017 (pp. 30-34). New York: IEEE.

Pinkaew, S.T. & Fujino, Y. (2001). Effectiveness of semi-active tuned mass dampers under harmonic excitation. *Engineering Structures*, *23*(7), 850-856.

Qian, X. & Hu, H. (2001). A semi-active vibration absorber with an adjustable clearance and its realization. *Journal of Vibration Engineering*, *14*(4), 378-381.

Seiler, G., Fischer, O. & Huber, P. (2002). *Semi-active MR dampers in TMD's for vibration control of footbridges: II. Numerical analysis and practical realization*. Paris: Footbridge Conference.

Setareh, M., Ritchey, J.K., Murray, T.M., Koo, J.H. & Ahmadian, M. (2007). Semiactive tuned mass damper for floor vibration control. *Journal of Structural Engineering*, *133*(2), 242-250.

Shen, Y. & Ahmadian, M. (2013). Nonlinear dynamical analysis on four semi-active dynamic vibration absorbers with time delay. *Shock and Vibration*, *20*(4), 649-663.

Spencer Jr, B.F. & Nagarajaiah, S. (2003). State of the art of structural control. *Journal of Structural Engineering*, *129*(7), 845-856.

Weber, F. & Distl, H. (2013). Real-time controlled tuned mass dampers for Wolgograd Bridge. *Beton-und Stahlbetonbau*, *108*(6), 362-372.

Zang, C., Friswell, M.I. & Mottershead J.E. (2005). A review of robust optimal design and its application in dynamics. *Computers and Structures*, *83*(4-5), 315-326.

Summary

Optimization of the semi-active vibration absorbers. In this paper, an efficient numerical approach is proposed to maximize the minimal damping of modes in a prescribed frequency range for general viscous tuned-mass systems. Methods of decomposition and numerical synthesis are considered on the basis of the adaptive schemes. The influence of dynamic vibration absorbers and basic design elastic and damping properties is under discussion. A technique is developed to give the optimal DVA's for the elimination of excessive vibration in sinusoidal and impact forced system. One task of this work is to analyze parameters identification of the dynamic vibration absorber and the basic structure. The questions of robustness at optimization of DVA are considered. Different types of control management for semi-active DVA's are applied. Examples of DVA's practical implementation are presented.

Authors' address:
Ivan Kernytskyy – corresponding author
(https://orcid.org/0000-0001-6084-1774)
Warsaw University of Life Sciences – SGGW
Institute of Civil Engineering
Department of Mechanics and Building Structures
Nowoursynowska 159, 02-776 Warsaw
Poland
e-mail: ivankernytskyy@ukr.net

Volodymyr Snitynskyy
(https://orcid.org/0000-0001-9633-1004)
Bohdan Diveyev
(https://orcid.org/0000-0001-5184-499X)
Orest Horbay
(https://orcid.org/0000-0002-0915-5637)
Ruslan Humenuyk
(https://orcid.org/0000-0001-7511-3673)
Yaroslav Sholudko
(https://orcid.org/0000-0001-5588-0066)

Scientific Review – Engineering and Environmental Sciences (2021), 30 (2), 337–353
Sci. Rev. Eng. Env. Sci. (2021), 30 (2)
Przegląd Naukowy – Inżynieria i Kształtowanie Środowiska (2021), 30 (2), 337–353
Prz. Nauk. Inż. Kszt. Środ. (2021), 30 (2)
http://iks.pn.sggw.pl
DOI 10.22630/PNIKS.2021.30.2.29

Anatoliy MOKIY[1], Yuriy PYNDA[2], Olha ILYASH[3], Mariia PIKH[4], Rostyslav PYNDA[5]

[1] Dolishniy Institute of Regional Research of National Academy of Sciences of Ukraine
[2] Lviv University of Business and Law
[3] National Technical University of Ukraine "Igor Sikorsky Kyiv Polytechnic Institute", International University of Finance
[4] National University of Food Technologies, Lviv State College of Food and Processing Industry
[5] Lviv University of Business and Law

Characteristics of interconnections of construction sector and environment: regional study of Ukraine

Key words: construction sector, environment, ecosystem, interconnections, reveal systemic interconnections, regions

Introduction

The results of the global trends analysis in the construction industry confirm its evolving nature, namely through the prism of socio-economic priorities at to conserving energy and respecting the environment. For several decades, there have been three stages in the evolutionary development of construction, where each successive stage contains all the positive components of the previous one, enhancing and refining them. These stages include: energy efficient construction, especially in the context of the adopted Directive on energy efficiency of new buildings (Gumbarević, Milovanović, Bagarić, Gaši & Dunović, 2020), according to which EU Member States must be provided with zero energy buildings by 31 December 2020 – the attention of scientists, designers, engineers was paid, first of all, to the reduction in the costs of heat and power supply of buildings and structures (Harvey, 2009; Sandvall, Ahlgren & Ekvall, 2017; Hummel et al., 2021); green building construction, as to energy conservation and harmful emissions, the concept of an "active building" with a positive energy balance is rationally reasonable (Ksit & Majcherek, 2016; Eze, Ugulu, Egwunatum & Awodele, 2021) and innovative sustainable development-oriented

construction, which means the life-sustaining or stable development without reducing the resources and capabilities of future generations (Lu, 2012; Kauskale, Geipele, Zeltins & Vanags, 2018). However, given a significant impact of construction on socio-economic development, the construction sector should be viewed as a complex subsystem in interaction with the environment (Zolfagharian, Nourbakhsh, Irizarry, Ressang & Masoud, 2012; Teriö and Honkanen, 2013; Enshassi, Kochendoerfer & Rizq, 2014).

Literature review

The studies of trends in the relationship between economic and environmental systems indicate the need to adapt the construction sector to dynamic innovative technologies. The concept of Industry 4.0, an innovative platform for environmental protection, is noteworthy. According to the authors, the development of Construction 4.0 using Industry 4.0 as an example will change the ways of interaction and the impact of the construction industry on the ecosystem (Sawhney, Riley & Irizarry, 2020). The researchers note that the prospects for sustainable development will be an effective way of using resources for future generations and they can help to reduce environmental degradation (Weißenberger, Jensch & Lang, 2014; Rostami, Khoshnava, Rostami & Lamit, 2015; Khoshnava, Rostami, Zin, Štreimikienė, Mardani & Ismail, 2020).

In recent scientific developments, scholars show great interest in the problems of the construction sector growth and its impact on the environment. According to some scientists, the fact of pressure of the construction sector on the environment is highly convincing (Yilmaz & Bakış, 2015; Razkenari, Fenner, Shojaei, Hakim & Kibert, 2020). In this context, the authors emphasize the importance of justifying the interaction of green building with the ecosystem (Kauškale & Riemenschneider, 2016; Olukoya & Atanda, 2020). If strategies of process integration are compared, it will help to make optimal decisions about integrating processes in construction networks outside a building site and about introducing changes in the ecosystem (Shen et al., 2008; Ruan, Ochieng, Price & Egbu, 2012; Arashpour, Wakefield, Blismas & Minas, 2015).

In spite of the availability of these research results, there are currently no scientific publications in which authors would try to empirically assess the relationship between the construction infrastructure development and sustainability of the ecosystem. Given the clear local concentration of construction (resource provision, construction and placement of finished construction products), it is essential to note the specifics of its development in the regional context.

In order to determine the regional specifics of the spatial and component structure of the integrated relationships between the construction sector and the ecological system, it is vital to pay attention to energy productivity. For example, in Australian regions, a group of scientists identified regional centres of effective strategies of energy consumption and defined patterns of energy productivity growth in the construction industry (Ma, Hosseini, Jiang, Martek & Mills, 2018). In addition, Australian scientists expanded their research on the benefits of reverse

logistics (RL) in the construction industry. The study identified 12 barriers to the implementation of reverse logistics (RL), including the regulatory environment, unforeseen costs and non-recognition of the importance of the impact of the construction chain on the ecosystem (Rameezdeen, Chileshe, Hosseini & Lehmann, 2016).

In Ukraine and abroad, there is a scientific controversy about research on the dynamic relationship between the development of the construction sector and the growth of the regional economy. It is represented by three aspects: (1) a study of the role of the construction sector in socio-economic development of the country (Tatar, 2016; Kalinichenko & Sidorova, 2017; Fisunenko, 2018; Krysovatyy, Mokiy, Zvarych & Zvarych, 2018; Frolova, Zhadko, Ilyash, Yermak & Nosova, 2021); (2) a comprehensive study of the impact of the relationship between the construction industry and other industries on economic development of the region (Bogdan, 2012; Ilyash, Hrynkevych, Ilich, Kozlovskyi & Buhaichuk, 2020); (3) modelling the impact of the construction sector development on economic growth of the region (Momot, Filatova & Tofanyuk, 2011; Pynda, 2018; Mokiy & Antonyuk, 2019; Ilyash, Vasyltsiv, Lupak & Get'manskiy, 2021).

Despite the presented research on dynamic interrelations between the development of the subjects of the construction sector and the economy growth of regions (Mokiy, Ilyash, Pynda, Pikh & Tyurin, 2020), there are no studies on the role of intersystem relations in regional sectors of the economy and ecological system. In particular, a methodological approach to assessing the state and prospects of the construction system and its connection with the ecosystem in the regional context needs to be tested, the construction system structure requires formalization and components such as labour resources, industry productivity and its raw material and resource, financial and investment components have to be aggregated. Taking into account these components will help to qualitatively and quantitatively measure the indicators of integration of the spatial and sectoral subsystem of the construction sector and the ecosystem into a complex socio-economic macrosystem, as well as to assess the development of the construction and ecological system in the regional aspect. The whole range of outlined problems is presented in this scientific research.

Material and methods

Since the construction sector of the national economy consists of a number of functionally interconnected components (vertically and horizontally integrated), designed to ensure the implementation of common socio-economic goals and objectives, it can be considered to have all signs of systemicity.

A number of existing methods to determine the integrated indicators are accompanied by various complications or excessive subjectivism while justifying and determining the values of the weight components. The method of main components, deprived of these shortcomings which could be easily applied in studying of different in quality and content of hierarchical socio-economic systems. This methodological approach to the integrated assessment of the components of the construction sector involves the

use of a multiplicative form of the integrated index, determines the corresponding dependencies of nonlinear relations often occuring in economic processes and phenomena than linear ones. One of its advantages should also be stated the possibility of simultaneous rationing and integrated assessment of indicators and their thresholds; the formalized justification of weights.

Baseline indicators for the calculation of integrated indexes in the construction sector are selected on the basis of expert analysis and displayed in Annex 1. Using the method of main components, the calculation of integrated indexes in the construction sector of the economy is carried out according to the following sequence of calculations:

$$I_t = \prod_{i=1}^{n} z_{it} * a_i ; \ \sum_{i=1}^{n} a_i = 1; \ a_i \geq 0 \qquad (1)$$

where:
I_t – integral indicator of system development dynamics,
z_{it} – normalized annual values of the indicators t,
$t = 1, T$,
a_i – weight annual coefficients,
$i = 1, n$.

The indicators of de-stimulants are converted into stimulants by normalization. The calculation of weight coefficients involves the design of a correlation matrix, the emphasizing of the main components, the calculation of load factor and the identification of the main components. The relationship between primary features and components is described by the following dependency (Kharazishvili & Dron, 2014):

$$y_t = \sum_{i=1}^{m} c_{it} G_t \qquad (2)$$

where:
y_t – standardized values,
i – component with single variances within a year t,
$t = 1$,
T – years of the researched period; total variance is equal to the number of features m,
c_{it} – contribution of i-component in total variance set of indicators within a year t,
$i = 1$,
m – number of features.

Component G_t is defined as:

$$G_t = \sum_{i=1}^{n} d_{it} x_{it} \qquad (3)$$

where:
d_{it} – load factors,
x_{it} – in-data,
$i = 1$,
n – number of features,
$t = 1$,
T – years of the researched period.

Weight coefficients a_i are calculated as:

$$a_i = \frac{c_i \left| d_i \right|}{\sum_{i=1}^{n} c_i \left| d_i \right|} \qquad (4)$$

The methodical approach to the integral evaluation of system elements provides for the use of a multiplicative form of the integral index, which reflects nonlinear relationships, as well as normalization and integral evaluation of indicators, their threshold values; formalized

justification of the weight factor (Sukhorukov & Kharazishvili, 2013).

Methodological approaches to identifying the interconnections of systems should be based on the targeted use of a set of interrelated methods, united by common principles to test the assumptions of determining the evaluation criteria related to particularities of the studied relations, as well as to determine the criteria of evaluating the accuracy of the results obtained for system-dynamic modeling of development of such systems of different kinds (socio-economic, technical, informational etc.) (Ilyash et al., 2020). A large number of links between systems are difficult to quantify, which limits modeling possibilities (O'Connor & McDermott, 2006; Krysovaty, 2018; Mokiy et al., 2019). The impact of the indices and factors of a complex system cannot be clearly predicted because of their variability and the transition of the system to a state of "disturbance" which requires a balance of the system. The works of Zadeh (1976), Kaufmann (1982), Zhukovin (1983), Borisov, Alekseev and Merkurieva (1989), Leonenkov (2005), Shtovba (2007) are devoted to this problem and related issues. Given the complexity of determining the relationship between complex systems, the formalization of such fuzzy, indefinite interconnections requires a description of the process of forming the complex system based on a fuzzy assessment of the state of the system using the fuzzy set method (O'Connor & McDermott, 2006; Mokiy, Pikh & Pynda, 2019; Pawlik & Shaposhnykov, 2019).

In terms of sets and state space, the notion of the set of the initial state and the set of the final (specified) state of a complex system is applied. In these terms, the stability of the subsystems is defined as a transition from an initial growth to a given growth and it occurs so that none of many factors exceed the allowable limits of a given change path of state of the complex system (Khodjayan, 2012).

Due to complexity, and in some cases impossibility to take a quantitative measurement, one of the atypical research methods, in particular the fuzzy set method (fuzzy logic), was used to identify the level of impact of the components of the construction sector on the environment. The tool for studying fuzzy models was the MATLAB package, in which the formation of a fuzzy logic classification and derivation system was carried out using the Fuzzy Logic Toolbox module.

Methodological approaches to identifying the dynamic characteristics of interconnections between systems and the complex system should take into consideration the existence of direct and indirectly hidden (according to Fritjof Capra) connections between the components (Fridtjof, 2004) and the dependence of the effective indicators of the development dynamics on factors of various degrees of influence (Antonyuk, 2016).

Let's consider the dynamics of the development of a complex system on the basis of fuzzy sets. In the general case, the definition of a set of S would have the form:

$$S = \mu_i(x) \tag{5}$$

where:

$\mu_i(x)$ – function of the assessment rating of the situation with the i-parameter which reflects factors to determine belonging to fuzzy sets (Gil, 2001).

The automation of the fuzzy simulation process of estimating the state of a complex system is done using a software product MATLAB and package Fuzzy Logic Toolbox. The components of complex system are characterized by a set of n indicators: $X = (x_i)$, $i = 1, n$ where is the number of indicators.

Results and discussion

The approbation of the described methodological approach is based on the example of the spatial-sector subsystem of construction in the complex socio-economic macro system (Pynda, 2018). The very subsystem of the high-spatial sector includes functionally interconnected subsystems (vertically and vertically integrated) to achieve socio-economic goals and solve problems.

The assessment of the state and prospects of the development of the construction system and its relationship with the country's ecosystem requires the formalization of its structure. System features of the functioning and the presence of problems connected with the development of the construction system allow us to aggregate such important components as (Annex 2): (1) labour-resource (personnel and social productivity) (x_1); (2) productive component (results of the functioning of the construction system are reflected by indicators of commissioning of housing) (x_2); (3) raw material resource component (state of the system and related branch subsystems of the construction industry, reflected by indicators of the volumes of extracted building raw materials and building materials production) (x_3); (4) finance and investment component (financial elements of the construction system (enterprises) and sector investment capacity) (x_4); (5) foreign trade (volumes of import-export operations in the construction subsystem) (x_5).

The following conditions are important for displaying the components listed by the relevant indicators: (1) qualitative and quantitative measurement of indicators; (2) report presentation to the official statistics; (3) opportunity to assess the development of the construction system at the macro level and meso levels of the management hierarchy.

Formalization of the set of indicators provides a systematic approach to diagnosis, reduces the risk of overloading and "clogging" of unnecessary data (Klimenko, Feshchenko & Voznyuk, 2010). For each of the components there is a different degree of impact on the development of construction, and, moreover, in the regions, the indicators reflect the specificity of the subsystem of the lower (second) level of the system hierarchy. Thus, the labour-resource component is characterized by the greatest values of integrated indices, namely, the most significant influence on the development of the construction subsystem in the regions; the largest values are observed in Dnipropetrovsk (integrated index is 0.565), Zaporizhya (0.544), Rivne (0.582), Sumy (0.639), Kharkiv (0.616) and Chernivtsi (0.672) regions.

The integral indicators for the development of major components of the construction process are calculated in the dynamics of the years 2013 and 2018, and the environmental index, taking into account its relative stability, for 2018 (Annex 2).

Thus, for each component we define a subset of indicators $X_r = (x_{ir})$, $i = 1.5$;

r = 1.28. Given that the study took place from 2013 to 2018, the subset of the indicators has the form $X_{rt} = (x_{irt})$, where x – is a complex construction parameter in the region, i = 1.5 and t = 1.6 (Marushchak, 2014).

Therewith:

$$\forall i = \overline{1, 5}; X_i \subset X; \forall t = \overline{1, 5}; X_{it} \subset X_r \quad (6)$$

The complete set of levels of the construction system development in the i^{th} region consists of five fuzzy subsets of the species: Extremely Low (EL), Low (L), Medium (M), High (H), Very High (VH). Subsets of this type are given as linguistic changes in accordance with the formed term-sets. It is defined that five components form the term-set of the linguistic variable "Level of development of the construction system" in the region. To form a fuzzy set, we used the Mamdani algorithm, which describes several successive steps, each receiving the input values obtained in the previous step. At the "input" and "output" arrive the quantitative values. In the intermediate stages, the fuzzy logic apparatus is used for fuzzy set theory (Shtovba, 2007).

The rules consist of conditions and conclusions which, in their turn, are vague statements, and include the linguistic variable and the term represented by fuzzy terms. When forming a rule base, each condition is given a weighting factor (*Ri*) or a degree of certainty about the truth of the result (prerequisites) {EL – «Extremely Low»), L – «Low»; M – «Medium»; H – «High»; VH – «Very High» level}, i = 1.5 (Fig. 1). It is assumed that the weight factor is equal to 1. The linguistic variables, written in condition, are called incoming and outgoing, the values of which are calculated by setting the range of changes with the corresponding gradation (Fig. 2).

Fuzzy output of the studied results is based on the formation of sets. At the phasing stage, the values of the incoming variables are converted to the values of linguistic type variables with the help of a membership function of a fuzzy number. At the stage of elaborating conditions, solutions and defazification,

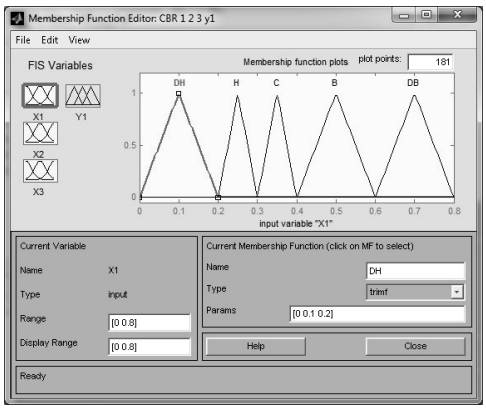

FIGURE 1. Graphical representation of the x_1 variable through the triangular membership function using Membership Function Editor

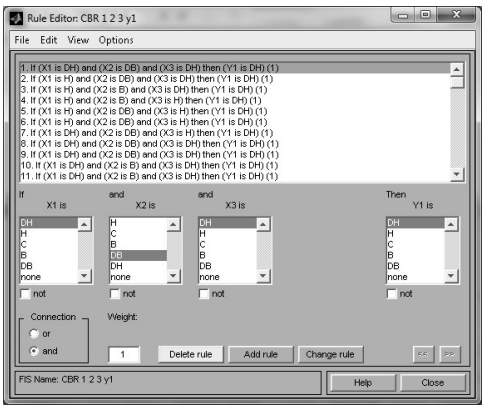

FIGURE. 2. Fuzzy Mamdani knowledge base in Rule Editor

there is a shift from fuzzy values to the specified parameters. A fuzzyfication stage of incoming variables leads to fuzziness (Leonenkov, 2005). To the "input" arrive the base of rules and an array of input data $X = (x_i)$ that contains values of all the "incoming" (x_i) variables $i = \overline{1, 5}$ and of the "outgoing" (y) variable. The goal of the stage is to obtain truth values for all conditions from the rule base. The value of the weighting factor of the rules is taken equal to one.

The accuracy of the evaluation depends on the completeness of the knowledge base. The achievement of the flexibility of the process of assessing the development of the subsystem in construction is achieved through the task of key decision-making rules, the logical conclusion for each of these rules is formed at the defuzzification, which turns fu ozzuio ccy data from the output block of solutions to a clear value (Babets, 2013).

While setting conditions, the minimum value of the all true prerequisites is searched

$$a = \min\{x_i\} \tag{7}$$

where:
$i = 1$,
n – prerequisites numbers.

Thus, the purpose of this stage is to obtain a set of "activated" membership functions

$$\mu_i'(x) = \min\{x\} = \{d_i\ ,\ \mu_i\ (x)\} \tag{8}$$

where:
$\mu_i'(x)$ – "activated" membership function,
$\mu_i(x)$ – term membership function,
d_i – degree of truth of i-prerequisite.

The purpose of defuzzification is to obtain quantitative values for each of the "outgoing" linguistic variables, using the i "source" of variable and the set X_i, which refers to it and takes into consideration the total value of the outgoing variable.

$$y_i = \frac{\int_{\min}^{\max} x \cdot \mu_i\ (x)\,\mathrm{d}x}{\int_{\min}^{\max} \mu_i\ (x)\,\mathrm{d}x} \tag{9}$$

where:
$\mu_i(x)$ – membership function to the corresponding fuzzy set X_i,
min, max – limits of the entirety fuzzy variables,
y_t – result of defuzzification (Kaufmann, 1982).

The simulation of the optimal development of the construction system is done on the basis of the objective function:

$$f_j = \max_t \left\{ \max_i \left\{ \sup_{x \in X_i} \left(\min\left\{ \mu_{x_i}(x), \mu_{x_i}(x) \right\} \right) \right\} \right\} \tag{10}$$

where:
X_i – values range of i^{th} parameter $\left(i = \overline{1, 5}\right)$,
$\mu_{x_i t}$ – functions of the membership of fuzzy subsets of the main elements of the construction subsystem of the region, where $i = \overline{1, 5}$; $i = \overline{1, 6}$.

According to the obtained results, the surfaces of their predicted relationship values are formed. The closest connection can be traced in the following combinations (Fig. 3). The revealed interconnections of the construction system with the ecosystem are the basis for their optimization (Fig. 3, the table).

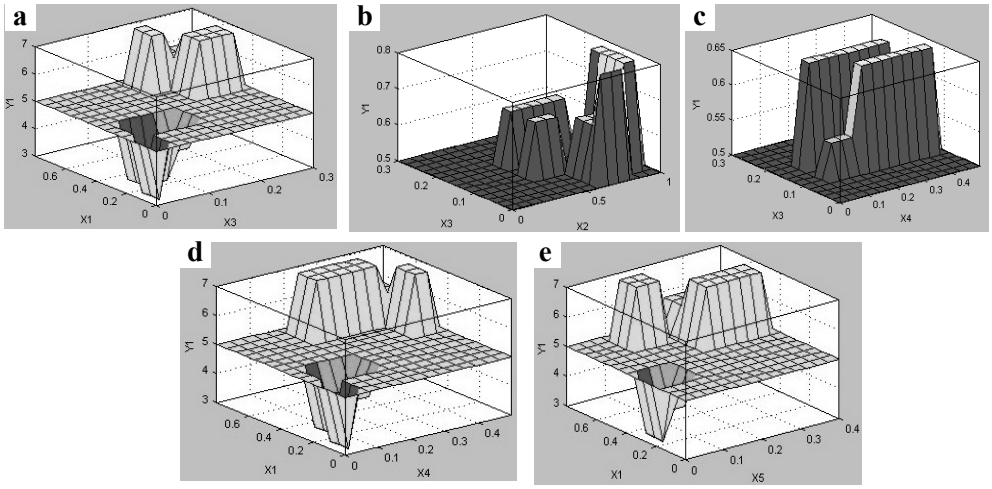

FIGURE 3. Fragment of three-dimensional surfaces of the predicted values of interconnections of the construction sector and the environment: a – interconnection between labour-resource (x_1), interconnection between raw material resource (x_3), components and environment (Y); b – interconnection between productive (x_2), raw material resource (x_3) components and environment (Y); c – interconnection between raw material resource (x_3), finance and investment (x_4) components and environment (Y); d – interconnection between labour-resource (x_1), finance and investment (x_4) components and environment (Y); e – interconnection between labour-resource (x_1), foreign trade (x_5) components and environment (Y)

TABLE. Fragment of the interconnections model between the construction sector components and the environment (Y)

Integral indicator of					Ecological index (Y)	Level
labour--resource component (x_1)	productive component (x_2)	raw material resource component (x_3)	finance and investment component (x_4)	foreign economic component (x_5)		
0.101	0.717	0.0669			0.2	EL
0.111	0.681	0.0163			0.2	
0.101	0.717	0.0669			0.2	
0.246	0.717	0.0669			0.3	
0.255	0.693	0.0596			0.3	
0.246	0.5	0.132			0.55	L
0.467	0.38			0.19	0.65	M
	0.5	0.179	0.25		0.65	
	0.524	0.168	0.334		0.65	
	0.596	0.175	0.304		0.65	
	0.741	0.175	0.304		0.65	
	0.753	0.0849	0.304		0.65	
	0.753	0.168	0.334		0.65	
0.602	0.38			0.19	0.8	H
0.699	0.452		0.232		0.8	

H – «High»; M – «Medium»; L – «Low»; EL – «Extremely Low» level.

The obtained results (Fig. 3, the table) reflect the relationship between the construction system and the environment over the 2013–2018 period.

Thus, the scientific hypothesis of the relationship between building systems and the environment is confirmed, which can be applied when determining such rationally feasible parameters, as:

1. A significant effect on the high level of the environmental index (0.8) is observed through the following combination:
   – when x_1, x_2, $x_5 \rightarrow Y$ – an integral indicator of the labour and resource component equals 0.602, that is true only for Sumy, Kharkiv and Chernivtsi regions; an integral indicator of the productive component at 0.38 is traced only in Ivano-Frankivsk, Kyiv, Lviv and Odesa regions.; An integral index of the foreign economic component at the level of 0.19 takes place only in Kherson region.
2. The average level of the environmental index (0.65) is influenced by the following optimal combinations:
   – when x_1, x_2, $x_5 \rightarrow Y$ – an integral indicator of the labour and resource component at the level of 0.467 is observed in Dnipropetrovsk, Transcarpathian, Zaporizhia, Mykolaiv, Poltava, Rivne, Sumy, Kharkiv, Cherkasy and Chernivtsi regions; the value of an integral indicator of the productive component is 0.38; an integral index of the foreign economic component at the level of 0.19, respectively;
   – when x_2, x_3, $x_4 \rightarrow Y$ – an integral indicator of the productive component at the level of 0.5 is peculiar only to Kyiv region; the value of an Integral indicator of the raw material component 0.179 is also observed only in Kyiv region; an integral index of the financial and investment component 0.25 is observed only in Mykolaiv and Ternopil regions.

According to the simulation results, the current state of the construction sector in most regions of Ukraine shows the relationship of its components with the lowest level of the environmental index, which confirms the hypothesis of a significant negative impact of construction on the country's ecosystem.

The results of the study confirm the different levels of impact (described by different diagrams) of the development components of construction sector on the environment. The obtained model will enable predicting the impact of components of the construction sector on the environment according to the optimal values calculated in terms of regions of Ukraine, taking into account their specificity and importance, based on the results of the principal component method.

Conclusions

The construction system development is closely related to the ecosystem and requires constant adaptation of the construction sector to rapid changes in scientific and technological progress in order to reduce the negative impact on the environment. However, given the long payback period, high cost and multi-component nature of construction products, as well as the connection

of construction with other sectors of the economy, the ability to innovate in the construction sector depends on the intersystem relations of the regional economy and the environment. Due to the use of fuzzy logic methods to study the relationship between the building system and the ecosystem, this research developed a methodological approach to the integral assessment of system elements based on the creation of a multiplicative form of the integral index that reflects nonlinear connections with the environment.

The approbation of the used methodological approach is based on the example of the spatial and sector subsystem of construction in a complex socio-economic macrosystem. The results presuppose the formalization of its structure and aggregation of five components (labour, productive, raw material and resource, financial and investment components, as well as foreign trade) and the study of the development of the construction system at the regional level. Based on the results, the labour component has a significant impact on the development of the construction subsystem in the regions; the largest values of integral indices are observed in Dnipropetrovsk (0.565), Zaporizhzhia (0.544), Rivne (0.582), Sumy (0.639), Kharkiv (0.616) and Chernivtsi (0.672) regions.

The simulation of the optimal development of the building system in the macrosystem is carried out based on the objective function and defuzzification. The results showed the existing three types of relationships between the construction sector and the ecosystem: (1) between labour resources and the components of raw materials and the environment; (2) between the productive component and the components of raw materials and the environment; (3) between the financial and investment component and the components of raw materials and the environment. Consequently, the study helped to build models of the relationships between the components of the construction sector and the environment and calculate their predicted values. Due to the low level of initial results in the regions of Ukraine, the target parameter (the environmental indicator) had the value above the average level (3%).

This study provides a selection of optimal models for studying the relationship between the construction sector and its components with the lowest level of the environmental index in the country's regions. In addition, the study is a guide for further research to discuss ways of reducing the negative impact of construction on the ecosystem.

References

Antonyuk, D. (2016). *Modernizatsiya instytutsional'noyi infrastruktury pidpryyemnytstva rehionu v protsesi yevropeys'koyi intehratsiyi Ukrayiny* [*Modernization of the institutional infrastructure of entrepreneurship in the region in terms of European integration of Ukraine*] (doctoral dissertation). Natsionalna Akademiya Nauk Ukrayiny, Lviv.

Arashpour, M., Wakefield, R., Blismas, N. & Minas, J. (2015). Optimization of process integration and multi-skilled resource utilization in off-site construction. *Automation in Construction*, *50*, 72-80. https://doi.org/10.1016/j.autcon.2014.12.002

Babets, I.H. (2013). *Stratehiya ekonomichnoyi bezpeky interrehional'noho spivrobitnytstva Ukrayiny v umovakh yevrointehratsiyi* [*Stra-*

tegy of economic security of interregional cooperation of Ukraine in terms of European integration] (doctoral dissertation). Natsionalnyy instytut stratehichnykh doslidzhen, Kyiv.

Bogdan, N. (2012). Teoretychni aspekty zabezpechennya ekonomichnoyi bezpeky pidpryyemstv budivel'noho kompleksu v protsesi vzayemodiyi iz zovnishnim seredovyshchem. *Efektyvna ekonomika*, *10*. Retrieved from: http://www.economy.nayka.com.ua/?op=1&z=1434 [access 17.06.2021].

Borisov, A., Alekseev, A. & Merkurieva, G. (1989). *Obrabotka nechetkoy informatsii v sistemakh prinyatiya resheniy*. Kyiv: Radio i svyaz.

Enshassi, A., Kochendoerfer, B. & Rizq, E. (2014). Evaluación de los impactos medioambientales de los proyectos de construcción [An evaluation of environmental impacts of construction projects]. *Revista ingeniería de construcción*, *29*(3), 234-254.

Eze, C.E., Ugulu, R.A., Egwunatum, S.I. & Awodele, I.A. (2021). Green building materials products and service market in the construction industry. *Journal of Engineering, Project, and Production Management*, *11*(2), 89-101. https://doi.org/10.2478/jeppm-2021-0010

Fisunenko, N.O. (2018). Pidkhody do doslidzhennya stanu budivelnoyi haluzi. In M.M. Palinchak et al. (eds.), *Zabezpechennya staloho rozvytku ekonomiky: problemy, mozhlyvosti, perspektyvy: materialy dopovidey* (pp. 40-43). Uzhhorod: Vydavnychyy dim "Helvetyka".

Fridtjof, C. (2004). *Skrytyye svyazi.* Kyiv: OOO Izdatelskiy dom "Sofiya".

Frolova, L., Zhadko, K., Ilyash, O., Yermak, S. & Nosova, T. (2021). Model for opportunities assessment to increase the enterprise innovation activity. *Business: Theory and Practice*, *22*(1), 1-11. https://doi.10.3846/btp.2021.13273

Gil, C. (2001). *International business: competition in the global market.* New York: Publishing House "Osnovy".

Gumbarević, S., Milovanović, B., Bagarić, M., Gaši, M. & Dunović, I.B. (2020). Improving competences of engineers and workers in the AEC industry for delivering NZEBs. *Organization, Technology and Management in Construction: an International Journal*, *12*(1), 2256-2274. https://doi.org/10.2478/otmcj-2020-0021

Harvey, L.D.D. (2009). Reducing energy use in the buildings sector: measures, costs, and examples. *Energy Efficiency*, *2*, 139-163. https://doi.org/10.1007/s12053-009-9041-2

Hummel, M., Büchele, R., Müller, A., Aichinger, E., Steinbach, J., Kranzl, L., Toleikyte, A. & Forthuber, S. (2021). The costs and potentials for heat savings in buildings: Refurbishment costs and heat saving cost curves for 6 countries in Europe. *Energy and Buildings*, *231*, 110-454. https://doi.org/10.1016/j.enbuild.2020.110454

Ilyash, O., Hrynkevych, S., Ilich, L., Kozlovskyi, S. & Buhaichuk, N. (2020). Economic assessment of the relationship between housing and communal infrastructure development factors and population quality of life in Ukraine. *Montenegrin Journal of Economics*, *16*(3), 93-108. https://doi.org/10.14254/1800-5845/2020.16-3.8

Ilyash, O., Vasyltsiv, T., Lupak, R. & Get'manskiy, V. (2021). Models of efficiency of functioning in trading enterprises under conditions of economic growth. *Bulletin of Geography. Socio-economic Series*, *51*(51), 7-24. https://doi.org/10.2478/bog-2021-0001

Kalinichenko, L. & Sidorova, Y. (2017). Analiz tendentsiy rozvytku budivel'noyi haluzi ta budivel'noyi produktsiyi Ukrayiny [Analysis of trends in the construction industry and construction products of Ukraine]. *Molodyy vchenyy – Young Scientist*, *4.4*(44.4), 64-69. http://molodyvcheny.in.ua/files/journal/2017/4.4/15.pdf [access 17.06.2021].

Kauskale, L., Geipele, I., Zeltins, N. & Vanags, J. (2018). Sustainable construction industry development and green buildings: a case of Latvia. *Latvian Journal of Physics and Technical Sciences*, *55*(1), 44-52. https://doi.org/10.2478/lpts-2018-0005

Kauškale, L. & Riemenschneider, F. (2016). The environmental and economic substantiation of investments in green buildings. *Baltic Journal of Real Estate Economics and Construction Management*, *4*(1), 126-144. https://doi.org/10.1515/bjreecm-2016-0010

Kharazishvili, Yu. & Dron, Ye. (2014). *Prohnozuvannya indykatoriv, porogovikh znachen' ta rivnya ekonomichnoyi bezpeky Ukrayiny*

v serednostrokoviiperspektivi. Analitychna dopovid' [*Forecasting of indicators, threshold values and level of economic security of Ukraine in the medium-term perspective*: *Analytical report*]. Kyiv: Natsionalnyy Instytut Stratehichnykh Doslidzhen. Retrieved from: https://niss.gov.ua/sites/default/files/2014-12/prognoz-5238c.pdf [access 17.06.2021].

Khodjayan, A. (2012). Metodolohichni *zasady formuvannya derzhavnoyi polityky, oriyentovanoyi na pidvyshchennya rivnya konkurentospromozhnosti natsionalnoyi ekonomiky* [*Methodological principles to form the state policy aimed at increasing the competitiveness of the national economy*] (doctoral dissertation). Nauchno-issledovatelskiy ekonomicheskiy institut Ministerstva ekonomicheskogo razvitiya i torgovli Ukrainy, Kyiv.

Khoshnava, S.M., Rostami, R., Mohamad, Z.R., Štreimikienė, D., Mardani, A. & Ismail, M. (2020). The role of green building materials in reducing environmental and human health impacts. *International Journal of Environmental Research and Public Health*, *17*(7), 25-89. https://doi.org/10.3390/ijerph17072589

Klimenko, M., Feshchenko, V. & Voznyuk, N. (2010). *Osnovy ta metodolohiya naukovykh doslidzhen: navchalnyy posibnyk*. Kyiv: Aharna osvita.

Kaufmann, A. (1982). *Vvedeniye v teoriyu nechetkikh mnozhestv* (Russian transl.) [*Introduction to the theory of fuzzy subsets*]. Moskva: Radio i svyaz.

Krysovatyy, A., Mokiy, A., Zvarych, R. & Zvarych, I. (2018). Alterglobalization via the inclusive circular economy paradigm. *Economic Annals-XXI*, *174*, 11-12.

Ksit, B. & Majcherek, M. (2016). Green construction in building renovation. *Civil and Environmental Engineering Reports*, *21*(2), 63-70. https://doi.org/10.1515/ceer-2016-0022

Ma, L., Hosseini, M. R., Jiang, W., Martek, I. & Mills, A. (2018). Energy productivity convergence within the Australian construction industry: a panel data study. *Energy Economics*, *72*, 313-320.

Lu, Y. (2012). Sustainability and innovative construction: green building with concrete. Journal of *Civil and Environmental Engineering*, *2*, e107. https://doi.org/10.4172/2165-784X.1000e107

Leonenkov, A. (2005). *Nechetkoye modelirovaniye v srede MATLAB i fuzzyTECH*. Sankt-Petersburg: BHV-Petersburg.

Mokiy, A. & Antonyuk, K. (2019). Theoretical and methodological principles of security through an inclusive model of development of Ukrainian regions. *Strategic Priorities*, *51*(3-4), 83-93.

Mokiy, A., Pikh, M. & Pynda, Yu. (2019). Methodological approach for detecting dynamic characteristics of interconnections of subsystems and complex systems. In *IEEE 2019 14th International Scientific and Technical Conference on Computer Sciences and Information Technologies (CSIT)* (pp. 122-127). Lviv: National University of Lviv Polytechnic.

Mokiy, A., Ilyash, O., Pynda, Yu., Pikh, M. & Tyurin, V. (2020). Dynamic characteristics of the interconnections urging the construction enterprises development and regions economic growth. *TEM Journal*, *9*(4), 1550--1561. https://doi.org/10.18421/TEM94-30

Momot, T.O., Filatova, I.O., Tofanyuk, O.V. (2011). Ekonomichna bezpeka korporatyvnykh pidpryyemstv budivelnoyi haluzi [The economic security of corporate building enterprises]. *Ekonomika ta upravlinnya pidpryyemstvamy mashynobudivnoyi haluzi: problemy teoriyi ta praktyky*, *2*(14), 14-26.

O'Connor, J. & McDermott, L. (2006). *The art of systems thinking. Essential skills for creativity and problem solving*. Moscow: Alpina Business Books.

Olukoya, O. & Atanda, J. (2020). Assessing the social sustainability indicators in vernacular architecture-application of a green building assessment approach. *Environments*, *7*(9), 67. https://doi.org/10.3390/environments7090067

Pawlik, A., Shaposhnykov, K. (eds.) (2019). *Strategic Management: Global Trends and National Peculiarities*. Kielce: Publishing House "Baltija Publishing".

Pynda, Yu.V. (2018). *Stratehiia rozvytku budivelnoi haluzi v Ukraini* [*Strategy of development of the building sector in Ukraine*]. Lviv: Izdatelstva "Rastr-7".

Rameezdeen, R., Chileshe, N., Hosseini, M.R. & Lehmann, S. (2016). A qualitative examination of major barriers in implementation of reverse logistics within the South Australian construc-

tion sector. *International Journal of Construction Management*, *16*(3), 185-196. https://doi.org/10.1080/15623599.2015.1110275

Razkenari, M., Fenner, A., Shojaei, A., Hakim, H. & Kibert, C. (2020). Perceptions of offsite construction in the United States: an investigation of current practices. *Journal of Building Engineering*, *29*, 101138. https://doi.org/10.1016/j.jobe.2019.101138

Rostami, R., Khoshnava, S.M., Rostami, R. & Lamit, H. (2015). Green and sustainability policy, practice and management in construction sector, a case study of Malaysia. *Research Journal of Applied Sciences, Engineering and Technology*, *9*(3), 176-188. https://doi.org/10.19026/rjaset.9.1393

Ruan, X., Ochieng, E.G., Price, A.D. & Egbu, C.O. (2012). Knowledge integration process in construction projects: a social network analysis approach to compare competitive and collaborative working. *Construction Management and Economics*, *30*(1), 5-19.

Sandvall, A.F., Ahlgren, E.O. & Ekvall, T. (2017). Cost-efficiency of urban heating strategies – Modelling scale effects of low-energy building heat supply. *Energy Strategy Reviews*, 18, 212-223. https://doi.org/10.1016/j.esr.2017.10.003

Sawhney, A., Riley, M. & Irizarry, J. (2020). *Construction 4.0: An Innovation Platform for the Built Environment.* London: Routledge, Taylor & Francis Group.

Shtovba, S. (2007). *Designing of fuzzy systems by means MATLAB*. Sao Paulo: Hot line-Telecom.

Shen, W., Hao, Q., Mak, H., Neelamkavil, J., Xie, H. & Dickinson, J. (2008). Systems integration and collaboration in construction: a review. In W. Shen et al. (eds.), *Proceedings of the 2008 12th International Conference on Computer Supported Cooperative Work in Design*. Vol. 1 (pp. 11-22). IEEE. https://doi.org/10.1109/CSCWD.2008.4536948

Sukhorukov, A. & Kharazishvili, Yu. (2013). On the methodology of integrated assessment of the components of the state economic security. *Strategic Priorities*, *3*(28), 5-15.

Tatar M.S. (2016). Doslidzhennya problem rozvytku resursnoho potentsialu budivelnykh pidpryyemstv Ukrayiny v umovakh aktyvizatsiyi faktoriv zovnishnoho seredovyshcha. [Research of the development problems of the Ukrainian construction companies resource potential in the activation conditions of the environmental factors]. *Naukovyy visnyk Uzhhorodskoho natsionalnoho universytetu*. *Mizhnarodni ekonomichni vidnosyny ta svitove hospodarstvo*, *6*(3), 81-86.

Teriö, O. & Honkanen, J. (2013). Environmental impact of Building Construction Projects in Northern Europe. *Construction Management*, *4*(2), 37-46.

Zadeh, L. (1976). *Ponyatiye lingvisticheskoy peremennoy i yego primeneniye k prinyatiyu priblizhennykh resheniy*. Moskva: Mir.

Zhukovin, V. (1983). *Mnogokriterialnyye modeli prinyatiya resheniy s neopredelennostyu*. Tbilisi: Metsniyereba.

Zolfagharian, S., Nourbakhsh, M., Irizarry, J., Ressang, A. & Masoud, G. (2012). Environmental impacts assessment on construction sites. In H. Cai et al. (eds.), *Construction Research Congress* 2012: *Construction Challenges in a Flat World* (pp. 1750-1759). American Society of Civil Engineers. https://doi.org/10.1061/9780784412329

Weißenberger, M., Jensch, W. & Lang, W. (2014). The convergence of life cycle assessment and nearly zero-energy buildings: The case of Germany. *Energy and Buildings*, *76*, 551-557. https://doi.org/10.1016/j.enbuild.2014.03.028

Yilmaz, M. & Bakış, A. (2015). Sustainability in Construction Sector. *Procedia – Social and Behavioral Sciences*, *195*, 2253-2262. https://doi.org/10.1016/j.sbspro.2015.06.312

ANNEX 1. Resource components indicators of the construction sector of the economy (own elaboration)

Labour component (x_1)	the number of people employed in construction per 1000 people of population level; average monthly nominal wages of construction workers; share in the structure of household cash expenditures on housing construction; the availability index of residential real estate.
Production component (x_2)	the volume of construction work carried out on residential buildings; the volume of construction work carried out on non-residential buildings; the volume of construction work carried out in the construction of engineering structures; commissioning of housing in cities per 1000 inhabitants; commissioning of apartments per 10,000 people; commissioning of housing in rural areas per 1000 inhabitants.
Raw material resources component (x_3)	production of non-refractory ceramic building bricks per 1000 people; production of blocks and bricks from cement, concrete or artificial stone for construction per 10,000 people; production of prefabricated structural elements for construction from cement, concrete or artificial stone per 1000 people; production of concrete solutions, ready for use per 1000 people; extraction of natural sands per 1000 people; mining pebbles, gravel, road metal and crushed stone per 1000 people; production of wooden windows, doors, their frames and thresholds per 10,000 people.
Financial and investment component (x_4)	Financial report (balance) of construction companies for 1 person; Profitability of operating activities of construction enterprises; The share of capital investment in construction; The share of capital investment in production of building materials.
Foreign economic component (x_5)	Exportation of stone, gypsum and cement products per 1000 people; Importation of stone, gypsum and cement products per 1000 people; Construction services export per 1000 people; Construction services import per 1000 people.

ANNEX 2. Spatial-component structure dynamics of integral indicators of subsystem development in construction and environment, 2013–2018 (own calculations and elaboration)

Region	Integral indicators of the development of the main elements in construction sector										Ecological index
	x_1		x_2		x_3		x_4		x_5		Y_1
	2013	2018	2013	2018	2013	2018	2013	2018	2013	2018	2018
Vinnytsia	0.469	0.397	0.159	0.262	0.108	0.018	0.095	0.092	0.025	0.012	0.856
Volyn	0.417	0.410	0.131	0.308	0.022	0.034	0.083	0.061	0.005	0.006	0.902
Dnipropetrovsk	0.440	0.565	0.105	0.185	0.071	0.047	0.049	0.110	0.004	0.002	0.361
Donetsk	0.504	0.290	0.101	0.022	0.052	0.004	0.032	0.100	0.035	0.032	0.467
Zhytomyr	0.452	0.417	0.109	0.146	0.147	0.109	0.142	0.085	0.004	0.071	0.883
Transcarpathian	0.558	0.499	0.124	0.200	0.024	0.021	0.074	0.061	0.012	0.036	0.853
Zaporizhia	0.522	0.544	0.082	0.081	0.048	0.035	0.011	0.010	0.012	0.017	0.844
Ivano-Frankivsk	0.089	0.061	0.247	0.413	0.027	0.026	0.111	0.158	0.064	0.019	0.785
Kyiv	0.492	0.450	0.420	0.828	0.141	0.212	0.023	0.048	0.007	0.015	0.842
Kirovohrad	0.522	0.451	0.028	0.281	0.058	0.048	0.034	0.085	0.009	0.005	0.875
Luhansk	0.533	0.372	0.070	0.020	0.015	0.001	0.047	0.019	0.012	0.042	0.811
Lviv	0.411	0.444	0.229	0.457	0.138	0.173	0.034	0.177	0.005	0.011	0.766
Mykolaiv	0.438	0.484	0.126	0.180	0.102	0.063	0.027	0.296	0.005	0.028	0.769
Odessa	0.434	0.365	0.294	0.420	0.017	0.010	0.015	0.185	0.005	0.005	0.838
Poltava	0.552	0.496	0.182	0.285	0.074	0.039	0.037	0.083	0.001	0.009	0.966
Rivne	0.528	0.582	0.143	0.283	0.039	0.034	0.028	0.138	0.008	0.012	0.870
Sumy	0.573	0.639	0.122	0.155	0.012	0.013	0.040	0.051	0.006	0.010	0.803
Ternopil	0.438	0.427	0.214	0.348	0.053	0.052	0.081	0.269	0.009	0.007	0.871
Kharkiv	0.466	0.616	0.159	0.232	0.028	0.028	0.039	0.204	0.036	0.020	0.863
Kherson	0.400	0.346	0.131	0.105	0.018	0.008	0.121	0.104	0.206	0.319	0.889
Khmelnytskyi	0.477	0.415	0.204	0.379	0.081	0.102	0.116	0.100	0.003	0.012	0.915
Cherkasy	0.515	0.474	0.134	0.127	0.068	0.030	0.017	0.045	0.031	0.101	0.914
Chernivtsi	0.558	0.672	0.226	0.313	0.024	0.030	0.074	0.039	0.045	0.035	0.902
Chernihiv	0.494	0.432	0.129	0.181	0.015	0.008	0.125	0.067	0.001	0.002	0.843

Summary

Characteristics of interconnections of construction sector and environment: regional study of Ukraine. The proposed modelling of the relationship between the spatial and component structure of the construction industry development and the environment helped to obtain combinations of high and medium levels of the impact of integral indicators of labour, productive and foreign economic components of the construction sector on the environmental index of the region. The high level of adaptability of the models used for the period 2013––2018 confirms the relationship between the development of the construction sector in most regions of Ukraine and the lowest level of the ecological index. This proves the scientific hypothesis about the negative impact of construction on the country's ecosystem. The study indicates that the dynamic characteristics of the relationship between the building system and the environment should take into account the existence of direct and indirect or even "hidden" relationships between the components. The scientific value of the study consists in using models of fuzzy sets to assess the relationship between the construction system and the ecosystem based on defuzzification, which preserves the flexibility of the process of assessing the development of subsystems in construction and making decisions as to reducing the negative environmental impact in regions.

Authors' address:
Anatoliy Mokiy
(https://orcid.org/0000-0001-8455-1421)
Dolishniy Institute of Regional Research of
National academy of Sciences of Ukraine
Kozelnytska St. 4, 79026 Lviv
Ukraine
e-mail: amokiy320@ukr.net

Yuriy Pynda
(https://orcid.org/0000-0002-1431-2318)
Lviv University of Business and Law
Kulparkivska St. 99, 79021 Lviv
Ukraine
e-mail: yuriy_p1@ukr.net

Olha Ilyash – corresponding author
(https://orcid.org/0000-0002-7882-3942)
International University of Finance
National Technical University of Ukraine "Igor Sikorsky Kyiv Polytechnic Institute"
Prospekt Peremohy 37, 03056 Kyiv
Ukraine
e-mail: oliai@meta.ua

Mariia Pikh
(https://orcid.org/0000-0003-4461-0364)
National University of Food Technologies
Lviv State College of Food and Processing Industry
Pulia St. 42, 79060 Lviv
Ukraine
e-mail: pmariyka@gmail.com

Rostyslav Pynda
(https://orcid.org/0000-0001-5326-9343)
Lviv University of Business and Law
Kulparkivska St. 99, 79021 Lviv
Ukraine
e-mail: rostyslav_p1@ukr.net

Scientific Review – Engineering and Environmental Sciences (2021), 30 (2), 354–364
Sci. Rev. Eng. Env. Sci. (2021), 30 (2)
Przegląd Naukowy – Inżynieria i Kształtowanie Środowiska (2021), 30 (2), 354–364
Prz. Nauk. Inż. Kszt. Środ. (2021), 30 (2)
http://iks.pn.sggw.pl
DOI 10.22630/PNIKS.2021.30.2.30

Firas N. Al-MASHHADANI[1], Qusay S. ALSAFFAR[2], Ibrahim A. Al-JADIR[3]

[1] Ministry of Education – Iraq, General Directorate of Vocational Education
[2] Ministry of Higher Education and Scientific Research – Iraq
[3] Murdoch University, PhD holder from the School of Engineering and Information Technology

An enhanced krill herd optimization technique used for classification problem

Key words: optimization, simulated annealing, standard krill herd

Introduction

Document classification (DC) has become one of the most important subjects in data mining and also it has gained a wide attention in the last few decades due to its important applications in various life aspects such as document filtering and dissemination, information retrieval, enterprise portals, business intelligence, text and summarization, etc. Consequently, vast document clustering algorithms have been suggested through the years, and an extensive survey of the most recent advances in document classification can be found in Kowsari et al. (2019). A couple of issues are pivotal for all the document classification algorithms which are: (i) the way that the discriminating features are extracted, and (ii) the way that the new coming document to be classified a according to the extracted feature in (i) the latent semantic indexing (LSI) (Yee, 2020) is considered as one of the most familiar representation and feature extraction method used for DC. Despite of the fact that the LSI is guaranteed to be handy in different text-related tasks, its objective is to discover the highly representative textual attributes, but it doesn't focus on the highly discriminative textual attributes in representing documents. Thus, the LSI would not be the best choice in the discrimination process of document into different classes. On the other hand, the linear discriminant analysis (LDA) (Li, Shao, Yin & Liu, 2019) is a different feature extraction method that which is famous in the pattern recognition mediums. Its objective is based on finding the

best features in terms of discriminability via the maximization of the ratio of the between inter class distances-to-the intra class distance of any set of data subject to a supervised learning criteria. The intra class means the distance of attributes within the class while the inter class represents the distance of the attributes within different classes. Currently, a number of studies have reported that the document data might be located in a non-linear sub-manifold. Nonetheless, each one of the LSI, and the LDA would only be considering to the Euclidean configuration. They don't successes to find out the actual configuration, if the document data resides on a non-linear sub-manifold incorporated within the document space. In terms of the DC, the selection of the classifier is different key factor after the extraction of the important documents' attributes. Presently, the neural networks, Bayesian algorithm, the k-nearest neighbor (KNN) classifier, and the support vector machines (SVM) are extensively utilized in a wide range of text-based applications but with the vast increment of the online availability of text documents on the Web environment, these methods have become insufficient to be capable of dealing with that huge information increase. The problem of classifying document automatically becomes a real challenge because of the large number of documents, the number of features and restricted awareness of human method to classify documents attributed to a number of factors (Jaya, Aulia, Hardi, Tarigan & Lydia, 2019). Thus, these traditional classification methods that used the exhaustive search in the search space become impractical solutions (Schaetti, 2019). In the last few years the KH method has invented as a global optimization method. It has considered as a novel metaheuristic inspired from nature herding process. It has allured text mining community. This algorithm has been used in a successful manner with different complicated optimization problems since its invention (Hofmann, Haskell, Klinck & Lascara, 2004; Gandomi & Alavi, 2012; Bolaji, Al-Betar, Awadallah, Khader & Abualigah, 2016). However, the usage of this algorithm for the DC in the regard of text mining is not yet well investigated. Therefore, in this paper we mainly focus on applying this method on document classification.

In this section an explanation of the proposed method based on the above information is explained in details as follows:

In this paper, the KH is used as a global search for DC problem which is used as an efficient way for an inter class-discrimination and is used for the attributes discrimination forming out the new classes while the simulated annealing (SA) approximation method is used as a krill modifier. The KH method is relatively a new global search. It simulates the behavior of the krill herd members in movement and foraging using Lagrange model (Hofmann et al., 2004). It is firstly proposed by Gandomi and Alavi (2012). As is mention before, global search methods are derivative-free methods, that is, they are stochastic-based. Thus, the KH can be robust in the exploration of the search space while it is weak in search of the local areas within the search space. Therefore, it is highly skeptical to be trapped in local optima like many other

global search methods. However, the advantage of the KH is that it has a few number of control parameters. More specifically, it has only one control parameter which is the time interval for the krill adjustment. By the combination of both the SA and the KH and producing the enhanced version of the KH method the we name our method the EKH, it becomes more likely to get a more robust method of document classification that trades-off between the exploration and the exploitation of the search space.

Krill herd algorithm

The KH algorithm is based on the idea of krill individual's movements and foraging. The objective function of the KH is calculated by measuring the minimum distance of each krill from the food source, at the same time, the entire herd density is also taken into account. The krill position is determined mainly by three factors, first its distance from the food, the impact of movement generated by other krill individuals and the krill physical diffusion. These three factors can be mathematically represented as:

- The movement of the KH that induced by other individuals from the herd with the aim of keeping the swarm as dense as possible.
- Forage activities.
- Random diffusion.

Lagrange model

Lagrange model can be used to generalize n-dimensional search space. The predation can remove krill from the herd and that reduces the density of the krill swarm. Also, that disturbs the way of the swarm to the food source. This is considered the initialization of the swarm. According to the three factors, a Lagrange model can be generated as is shown in Eq. (1). The time dependent position of krill individuals is selected according to the random diffusion controlled by N_i, foraging activity F_i, and movement made by the existence of the adjacent krills.

Foraging activity is made according to particular food criteria and is such that krill individuals move in slower motion and turn more frequently in regions of higher food densities. The existence/ /absence of neighboring krills might be dispersing, if the local food densities become very concentrated, or coalescing if food densities become very diluted, in a respective manner. Predation effect on krill individuals is incorporated and impacts the swarm structure by eliminating some individuals (Hofmann et al., 2004).

$$\frac{dX_i}{dt} = N_i + F_i + D_i \tag{1}$$

where:

N_i – parameter determining of the motion induced by other krill individuals,
F_i – foraging activity,
D_i – diffusion of the i^{th} krill.

Motion caused by other krills (N_i). Krill individuals strive to keep the swarm condense and move as one unit due to the impact of their mutual effects (Hofmann et al., 2004). The estimation of the swarm direction α_i can be determined by measuring the local swarm density, a target swarm density, and a repulsive swarm

density. Therefore, in Eq. (2) these three densities are used to calculate the motion induced by other krill individuals. For the first parameter N_i it can be updated by applying Eq. (2).

$$N_i^{\text{new}} = N^{\max} \cdot \alpha_i + N_i^{\text{old}} \cdot \omega_n \tag{2}$$

$$\alpha_i = \alpha_i^{\text{local}} + \alpha_i^{\text{target}} \tag{3}$$

where:
$N^{\max}$ – maximum speed induced,
N_i^{old} – final motion induced,
ω_n – inertia weight in the range [0, 1],
α_i^{local} – effect of the surrounding krill individuals on the motion of a particular krill,
α_i^{target} – effect of the best krill that has the best fitness value.

The effect of the surrounding krills α_i^{local} can be obtained from the following equations:

$$\alpha_i^{\text{local}} = \sum_{j=1}^{NN} \hat{K}_{ij} \hat{X}_{ij} \tag{4}$$

$$\hat{X}_{ij} = \frac{x_j - x_i}{\left\| x_j - x_i \right\| + \varepsilon} \tag{5}$$

$$\hat{K}_{ij} = \frac{K_i - K_j}{K^{\text{worst}} - K^{\text{best}}} \tag{6}$$

where:
X_i, X_j – locations of i^{th} and j^{th} krills,
ε – small positive value added to denominator to prevent any singularities,
k_i, k_j – fitness scores of the i^{th} and the j^{th} krills,
$k^{\text{worst}}, k^{\text{best}}$ – worst and best fitness scores in the swarn.

The target effect that determines the effect of the best krill that has the best fitness value can be calculated as follows:

$$\alpha_i^{\text{target}} = C^{\text{best}} \cdot \hat{K}_{i,\text{best}} \cdot \hat{X}_{i,\text{best}} \tag{7}$$

where:
$\hat{K}_{i,\text{best}}$ – computed as same as $\hat{k}_{ij}$, still the fitness value of j^{th} krill individual k_j, is substituted by the best fitness value,
$\hat{X}_{i,\text{best}}$ – computed as same as $\hat{X}_{ij}$, but X_j is substituted by the X_{best} that represents the best fitness value,
C^{best} – effective coefficient of the krill that has the best fitness value to the i^{th} krill; it be calculated as follows:

$$C^{\text{best}} = 2\left(rand + \frac{1}{I^{\max}}\right) \tag{8}$$

where:
$rand$ – random number in the range [0, 1],
I – iteration counter,
$I^{\max}$ – number of iterations.

Foraging motion (F_i). This factor can be computed in terms of food location and previous experience of where food was located. The foraging motion can be calculated as follows:

$$F_i = a \cdot \left(\beta_{ik}^{\text{food}} + \beta_{ik}^{\text{best}}\right) \tag{9}$$

where:
β^{food} – food attraction that is used to attract krills to global optimum,
β^{best} – effect of the current best krill individual and a is a constant value.

Physical diffusion. The physical diffusion is an arbitrary process which is computed as a function of the maximum diffusion speed and a random directional vector as follows:

$$D_i = D^{\max} \cdot \delta \tag{10}$$

where:

$D^{\max}$ – maximum diffusion speed,
δ – random directional vector with the values in the range [1, –1].

Motion process of krill herd. According to the N_i, F_i, and D_i, the krill positions can be calculated during the time interval Δt as is shown in the following equation.

$$x_i\left(t+\Delta t\right) = x_i\left(t\right) + \Delta t \frac{\mathrm{d}X_i}{\mathrm{d}t} \tag{11}$$

After the position updates of the krill individuals, the reproduction mechanisms are used, which are the crossover and the mutation.

Simulated annealing (SA)

It is inspired by the melting process of metals (Merendino & Celebi, 2013). After a particular heating degree, the metal liquid is cooled gradually, until it stabilizes by a decreased mobility of its atoms. This process continues until least energy is required. Because of the heating process allows atoms to move freely, the cooling process will have the time to let atoms to rearrange themselves to attain to the lower energy state (Wang, Guo, Gandomi, Alavi & Duan, 2013).

Like other approximation methods, this method has a local-based nature, it gradually improve the current state (solution) by small movements. The SA generates neighboring solutions and continues to generate other neighboring solutions in the same path that minimizes the objective function. In the exploration of the solution space, SA can accept the possibility of the worst solution in special cases to skip the local minima. More particularly, in every single iteration, the current solution x with an objective function value $f(x)$, there is a neighboring solution $\grave{x}$. Iteratively, the difference between the fitness of the current solution $f(x)$ and the neighboring solution $f(\grave{x})$ is used to calculate the probability of acceptance or rejection of the neighboring solution as follows:

$$\Delta f = f(\grave{x}) - f(x) \tag{12}$$

$$P_s = \exp\left(-\frac{\Delta f}{k \cdot T}\right) \tag{13}$$

$$T = T \cdot c \tag{14}$$

where:
P_s – probability of acceptance,
Δ – difference between the current and the neighboring solution,
k – Boltzmann constant,
T – initial temperature.

After the production of P_s probability, it is compared against a random value selection between zero and one (r). If $P_s > r$ the solution $\grave{x}$ will be accepted. Finally, T is decreased in every single iteration. In our proposed SA local search we used the single the Markov chain protocol (SMC) cooling schedule due to its equal efficiency in comparison to the Markov multi-chain protocol (Otranto, 2005).

Proposed simulated annealing krill herd

In this section an explanation of the proposed method based on the above information is explained in details as follows:

Document representation

Structured data contents the major sources for many text mining tasks. Nonetheless, many applications have unstructured data such as document collections. Therefore, to deal with unstructured data, text mining tasks must be performing many pre-processing steps for computing a structured model for the mining tasks. The pre-processing steps followed in this paper are listed below (Uysal & Gunal, 2014):

- Documents preparation: it involves the selection of the appropriate set of documents.
- Tokenization: it involves the identification of the words that would be pre-processed.
- Stop word removal: many words are not related to the classification tasks and these words must be deleted in this step. Often these words are commonly used in any text such as prepositions or articles.
- Stemming: here, each word is originated to its original grammatical form, by taking out the root of each word. For instance, the root form of "playing" is "play";
- Luhn-cut: this step is responsible of elimination of terms for which the frequency is less than a pre-defined threshold value.
- Weighting: is used for minimizing or maximizing the words contributions on mining tasks. For instance, a famous technique is used in this paper which is the term frequency-inverse document frequency (TF-IDF) (Christian, Agus & Suhartono, 2016).

The outcome of applying the pre-processing steps is a vector space model (Uysal & Gunal, 2014), also named as document-term-matrix. Here, each row is representing a document, while each column is representing an attribute, and each value represents a frequency (TF), or the term impact in that very document. Therefore, text mining methodologies like the classification would be employed in the structured document corpus. In addition, the majority of the information visualization applications need structured data, and for that reason, those pre-processing steps are suitable for the visualization of the document corpus (Saad, 2010).

Simulated annealing krill herd

For the native KH algorithm, because the search is only performed by random walks, the convergence cannot be expected easily. To enhance the performance of the native KH, the genetic reproduction operators have been combined to the native KH. Using the KH with the GA operators performed the best in comparison to the original version as is seen in publication by Abualigah, Khader and Hanandeh (2019). The KH uses three motions explained earlier, and that can guarantee the convergence to some extent with some simple optimization problems. Nonetheless, things could be harder, and convergence could be unreachable with more complicated optimization problems such

as document clustering. The KH can fail to discover the optimality with the document clustering as it is an NP-hard optimization problem.

In the current method, another component is added to the original KH that can modify the exploitation phase. This is the SA that resembles the local search in the schemes. As is explained earlier, the SA is based on the idea of the melting metals. In effect, in this paper, this physical concept of annealing metals under a particular degree is combined with the idea of krill herding. This is to generate a breed of modified individuals whose capability of exploitation of the search space is expected to exceed the ordinary individuals. The main distinction between the EKH and the KH is in the capability of the EKH to modify the best ordinary members in the herd to outperform themselves after the use of the SA concept.

To correct the premature convergence resulted from the slight changes at the end of the optimization process; the use of the SA can lift the curve where there might be stagnation points during the search in final stages. This can potentially suppress the possibilities of obtaining weak solutions (Wang et al., 2013).

The mechanism of the SA in that context is based on the acceptance of a small number of ordinary krill individuals with a low probability named a transition probability. This acceptance probability technique allows the population to be more diversified and that in return makes the premature convergence more preventable. Also, that would help the search to span wider areas in the solutions space leading to discover more promising areas (Mirjalili & Lewis, 2016). The proposed method can be summarized as shown in Algorithm 1.

ALGORITHM 1. The proposed hybrid krill herd and simulated annealing binary feature selection method

Begin
Step 1: Initialize. The generations counter t, the population-size P of N krill, the diffusion speed $D_{\max}$, the foraging speed V_f, and max speed $N_{\max}$, Boltzmann constant k, initial temperature T_0, cooling factor α, and an acceptance thresholding value f_n.
Step 2: Fitness computing. Compute the fitness for each individual krill according to the initial location of krills.
Step 3: While t less than maximum generation number **do**
arrange the entire krill herd based on their fitness.
Store the best krill so far.
for i := 1 to N (all krill population) **do**
conduct three motions as described earlier.
Updating locations for the krill individual i according to the simulated annealing operator (Algorithm 2).
Calculating the fitness value for each single krill according to its new location X_i+1.
end for i
Substituting the best krill individual with the worst one.
Sorting all the krill according to their fitness and find the current best.
$t := t + 1$;
Step 4: end for while
Step 5: best solution is found
End

ALGORITHM 2. Simulated annealing for krill individuals selection

Begin
$T := \alpha * T$;
$\Delta := f(X'_i) - f(X_i)$;
# Acceptance if become better
If $(-\Delta f > f_n)$ **is true then do**
$X_i+1 := X'$;
end if
% Acceptance with a lower probability if not become better
If $(\Delta f <= f$ and $\exp(-\Delta f$ div $(k\ X_T)) > r)$ **do**
$X_i+1 := X'$;
End if
End

The limited performance of the traditional KH method on with many scientific and engineering problems, made it necessary to modify the existing KH method in this paper we used the simulated annealing because of its capability to conduct the search in narrow search areas. In our proposed method, first, the traditional KH method is used to nominate promising candidates solutions set. Later, a krill selection using the simulated annealing method is applied. This method is considered as an operator incorporated with the traditional KH method. This operator has greedy technique and acceptance a not very good individual with a relatively small probability. This technique is used for accepting well-fit candidates solutions in order to enhance its reliability and efficiency and to solve optimization problems of a global numerical nature. Moreover, the simulated annealing operator is not only accepting modifications that enhance the fitness function. Rather it also retains some modifications in not very good individuals with a lower probability that is not ideally optimal. This could improve the diversity of the krill population; enhance the explorative aspect of the KH method, as well as avoiding prematurity of convergence. Moreover, this proposed method could speed up the global convergence ratio with no loss of the robust and strong features of the traditional KH method.

Parameter settings and evaluation measures

In this section an explanation of the test results is given. The parameters concerning the KH are used as follows, V_f = 0.02, the diffusion speed $D_{\max}$ = 0.005, the maximum induction $N_{\max}$ = 0.01, initial temp T_0 = 1.0, acceptance number $Accept_{\max}$ = 15, Boltzmann's factor k = 1, cooling parameter α = 0.95, and threshold of acceptance f_n = 0.01. All these parameters are replicated from the original KH paper.

After setting the of parameters, two evaluation measures were used to evaluate the results one is the F-measure external measure while the other classification error value is used as an internal measure which also serves as a clustering fitness function. Unlike the external measures such as those used in Forsati,

Keikha and Shamsfard (2015), the internal measure using the classification error is also used.

Datasets and test results

In this paper, five datasets were used which are diversified according to their number of classes, documents size, subjects and documents number. Table 1 shows the details of the used datasets that shows the number of instances (documents) and number of features for each dataset.

In this section, results obtained by EKH are described on five datasets shown in Table 1. A comparison of EKH is performed against a set of other clustering methods. Namely, these methods are the differential evolution (DE) (Opara & Arabas, 2019), the global artificial bee colony and Levenberq-Marquardt (GABC-LM) (Shah et al., 2017), the k-means, the harmony search (HS) (Sridharan & Komarasamy, 2020) and the standard KH (Gandomi & Alavi, 2012). For the GABC-LM the same parameter settings used in the original paper are also used in this paper. In the tests, 50 times each algorithm is run. This number is used by many other papers in this area.

Tables 2 and 3 report the values of the external and internal evaluation (fitness error values). The k-nearest neighbor has been used as a fitness function. The comparison of these methods is conducted using the comparing using the five datasets shown in Table 1. In Table 2 the EKH achieved better results in comparison to the other methods regarding the F-measure. This indicates that the use of the modified version of KH improved the performance of the classification as can be seen with the majority of datasets.

When it comes to the classification error, this criterion is used to measure the

TABLE 1. Datasets

Dataset	D#	#Classes	Instances	Attributes
6-event crimes	D-1	6	223	3 864
Classic3	D-2	3	3 893	13 310
TDT	D-3	53	6 738	1 445
Pair-20news	D-4	2	1 071	9 497
Reuters	D-5	8	4 195	6 738

TABLE 2. The classification results using the F-measure

Dataset	DE	GABC-LM	k-Means	HS	KH	EKH
6 Events crimes	0.7545	0.8265	0.6801	0.7697	0.8459	0.9689
Classic 3	0.9465	0.9428	0.7509	0.9049	0.9804	0.9956
TDT 5	0.6760	0.6617	0.0698	0.9194	0.7095	0.8728
Pair of 20news	0.0036	0.9896	0.6755	0.9816	0.9854	0.9987
Reuters	0.5865	0.5341	0.0698	0.5899	0.8551	0.9819

TABLE 3. The classification accuracy

Dataset	DE	GABC-LM	HS	KH	EKH
6 Events crimes	0.3039	0.2222	0.7188	0.7240	0.1232
Classic 3	0.4605	0.2606	0.7075	0.7438	0.1455
TDT 5	0.3450	0.3827	0.8214	0.6883	0.2894
Pair of 20news	0.2130	0.3450	0.7419	0.8449	0.1454
Reuters	0.2830	0.8306	0.7322	0.7345	0.2346

internal coherency of the resulted classes with no need to deal with the class labels. The classification error measures the distances between documents within the class. The error score should be minimized in contrast to the F-measure. The error rate and the F-measure relationship have been hardly studied. Idealistically, the error rate should be reduced while the F-measure increases. However, this is not always true. It is likely to happen that the internal measure remains the steady or slightly fluctuates whereas the F-measure changes largely. This case can give a positive indication as the F-measure change can show the positive or negative algorithm's performance despite the steadiness (or the slight changes) of the error rate. This case is clear in Table 3 where almost all the error rate results where nearly equal with all methods. At the same time the F-measure values shown in Table 3 are different among the algorithms. Therefore, despite the fact that with almost all the datasets, the error rate results are not equal.

Conclusions

In this paper, we propose the krill herd classification method named as the EKH. This method combines the KH with the SA approximation method. The SA is utilized because of its capability to enhance the solutions produced by the KH in a local manner using the synergy of the melting metals. The test results indicate that the EKH outperformed other document classification methods: these methods are the DE, the GABC-LM, the k-means, the HS, and the KH.

References

Abualigah, L.M., Khader, A.T. & Hanandeh, E.S. (2019). Modified krill herd algorithm for global numerical optimization problems. In S.K. Shandilya (eds.), *Advances in nature-inspired computing and applications* (pp. 205-221). Cham: Springer.

Mirjalili, S. & Lewis, A. (2016). The whale optimization algorithm. *Advances in Engineering Software*, *95*, 51-67.

Bolaji, A.L.A., Al-Betar, M.A., Awadallah, M.A., Khader, A.T. & Abualigah, L.M. (2016). A comprehensive review: Krill Herd algorithm (KH) and its applications. *Applied Soft Computing*, *49*, 437-446.

Christian, H., Agus, M.P. & Suhartono, D. (2016). Single document automatic text summarization using term frequency-inverse document frequency (TF-IDF). *ComTech: Computer, Mathematics and Engineering Applications*, *7*(4), 285-294.

Forsati, R., Keikha, A. & Shamsfard, M. (2015). An improved bee colony optimization algorithm with an application to document clustering. *Neurocomputing*, *159*, 9-26.

Gandomi, A.H. & Alavi, A.H. (2012). Krill herd: a new bio-inspired optimization algorithm. *Communications in Nonlinear Science and Numerical Simulation*, *17*(12), 4831-4845.

Hofmann, E.E., Haskell, A.E., Klinck, J.M. & Lascara, C.M. (2004). Lagrangian modelling studies of Antarctic krill (*Euphausia superba*) swarm formation. *ICES Journal of Marine Science*, *61*(4), 617-631.

Jaya, I., Aulia, I., Hardi, S.M., Tarigan, J.T. & Lydia, M.S. (2019). Scientific documents classification using support vector machine algorithm. *Journal of Physics: Conference Series*, *1235*(1), 012082. https://doi.org/10.1088/1742-6596/1235/1/012082

Kowsari, K., Jafari Meimandi, K., Heidarysafa, M., Mendu, S., Barnes, L. & Brown, D. (2019). Text classification algorithms: a survey. *Information*, *10*(4), 150. https://doi.org/10.3390/info10040150

Li, C.N., Shao, Y.H., Yin, W. & Liu, M.Z. (2019). Robust and sparse linear discriminant analysis via an alternating direction method of multipliers. *IEEE Transactions on Neural Networks and Learning Systems*, *31*(3), 915-926.

Merendino, S. & Celebi, M.E. (2013). A simulated annealing clustering algorithm based on center perturbation using Gaussian mutation. In Ch. Boonthum-Denecke, G.M. Youngblood (eds.), *Proceedings of the 26th International Florida Artificial Intelligence Research Society Conference* (pp. 456-461). Palo Alto: AAAI Press.

Otranto, E. (2005). The multi-chain Markov switching model. *Journal of Forecasting*, *24*(7), 523-537.

Opara, K.R. & Arabas, J. (2019). Differential evolution: a survey of theoretical analyses. *Swarm and Evolutionary Computation*, *44*, 546-558.

Saad, M.K. (2010). *The impact of text preprocessing and term weighting on Arabic text classification.* Gaza: Computer Engineering, the Islamic University.

Schaetti, N. (2019). Behaviors of reservoir computing models for textual documents classification. *2019 International Joint Conference on Neural Networks (IJCNN)*, *2019*, 1-7.

Shah, H., Tairan, N., Mashwani, W.K., Al-Sewari, A.A., Jan, M.A. & Badshah, G. (2017). Hybrid global crossover bees algorithm for solving boolean function classification task. In *International Conference on Intelligent Computing* (pp. 467-478). Springer: Cham.

Sridharan, K. & Komarasamy, G. (2020). Sentiment classification using harmony random forest and harmony gradient boosting machine. *Soft Computing*, *24*(10), 7451-7458.

Uysal, A.K. & Gunal, S. (2014). The impact of preprocessing on text classification. *Information Processing & Management*, *50*(1), 104-112.

Wang, G.G., Guo, L., Gandomi, A.H., Alavi, A.H. & Duan, H. (2013). Simulated annealing-based krill herd algorithm for global optimization. *Abstract and Applied Analysis*, *2013*, 213853. https://doi.org/10.1155/2013/213853

Yee, C.W. (2020). *Retrieving semantically relevant documents using Latent Semantic Indexing.* Yangon: Unversity of Computer Studies.

Summary

An enhanced krill herd optimization technique used for classification problem. In this paper, this method is intended to improve the optimization of the classification problem in machine learning. The EKH as a global search optimization method, it allocates the best representation of the solution (krill individual) whereas it uses the simulated annealing (SA) to modify the generated krill individuals (each individual represents a set of bits). The test results showed that the KH outperformed other methods using the external and internal evaluation measures.

Authors' address:
Firas N. Al-Mashhadani – corresponding author
(https://orcid.org/0000-0003-4537-7832)
Ministry of Education
D.G. Vocational Education
City Baghdad
Iraq
e-mail: firas.naziyah@vocational.edu.iq

Scientific Review – Engineering and Environmental Sciences (2021), 30 (2), 365–375
Sci. Rev. Eng. Env. Sci. (2021), 30 (2)
Przegląd Naukowy – Inżynieria i Kształtowanie Środowiska (2021), 30 (2), 365–375
Prz. Nauk. Inż. Kszt. Środ. (2021), 30 (2)
http://iks.pn.sggw.pl
DOI 10.22630/PNIKS.2021.30.2.31

Sabeeh Lafta FARHAN[1, 2], Daniel ANTÓN[2, 3], Venus Suleiman AKEF[4], Salah Lafta ZUBAIDI[5], Khalid Safaa HASHIM[6, 7]

[1] Wasit University, Engineering College
[2] Nottingham Trent University, School of Architecture, Design and the Built Environment
[3] Universidad de Sevilla, Escuela Técnica Superior de Ingeniería de Edificación
[4] University of Technology in Baghdad, Department of Architect Engineering
[5] Wasit University, College of Engineering
[6] University of Babylon, Environmental Research and Studies Centre
[7] Liverpool John Moores University, BEST Research Institute

Factors influencing the transformation of Iraqi holy cities: the case of Al-Najaf

Key words: urban transformation factors, traditional urban pattern, heritage, Al-Najaf, Iraqi holy cities, Islamic culture

Introduction

According to Hendrigan (2019), cities develop and change, and the fundamental role of changing cities is space. This is, or should be, usually aimed at improving residents' life conditions, but it could also be due to external factors such as social aspects, politics, war, etc. Paraphrasing Correia and Taher (2015), modern development, with its urban geometrical regularity, contrasts with the Islamic urban culture, which is significantly more related to social aspects of private life and religious practice.

For that reason, despite the diverse circumstances of each region, this research takes the Iraqi city of Al-Najaf as a case study to analyse the factors involved in the urban transformation of the historic centres of holy cities in the country. These changes, if forced and intrusive, may be associated with political and economic decisions instead of protecting the cities' great legacy and spiritual and urban significance (Farhan, Jasim & Al-Mamoori, 2019).

As stated by Abdelmonem (2017), whilst we cannot live in history or preserve the past, engaging with historic buildings or walking through traditional

urban fabric and alleyways becomes an essential asset of the contemporary urban experience. In this sense, understanding the human experiences, history and narratives is the aim of the archaeology of the built heritage, which analyses the historic fabric, structures and remains (Smith, 2006). Thereby, in order to understand the current situation of the city of Al-Najaf, it is worth describing first its geographical and historical context. Next, the methodological approach is explained to later depict the main traits and the conditions that led to the transformation of the city. The results of this study are presented and discussed, and the conclusions drawn.

Case study: the city of Al-Najaf

Geographical and historical context

The city of Al-Najaf is located on the southern border of western Iraq, 10 km west from the Euphrates river, 160 km south-west from Baghdad and 78 km east from Karbala (Al-Hakim, 2006). The coordinates of the Old City, Najaf's historic city centre, are approximately 31°59′45″N, 44°18′52″E, and the elevation is in the region of 65 m above sea level. In this way, the city overlooks the southwest on the lowlands of the Najaf Sea, which is a large area occupied by the Wadi-Al-Salam Cemetery (Valley of Peace) in the north-northwest, bordered by barren lands known as the Western Desert (Al-Maliki, 2011), and covers agricultural land in the east towards the city of Kofa (Ahmed, 1945; Matar, 2013). The harsh desert climate in this region (Fig. 1) had an impact on the style of the city's demarcation and reconstruction (Zubaidi, Al-Bugharbee, Muhsin, Hashim & Alkhaddar, 2020).

The city was far from geographical barriers and vulnerable to attacks, forcing its dwellers to fence it round through its changing historical stages (Al-Hakim, 2006; Fig. 2).

Consequently, Al-Najaf Old City could be considered a marginal site only connected to roads from the east, thus losing the advantages and characteristics of cities in central locations (Merzah, 2006).

Al-Najaf is one of the cities built, founded and expanded around a holy shrine of a well-known Islamic figure, Ali bin Abi-Talib (Abid, 2015). Ali bin Abi-Talib was the cousin and the son-in-law of Prophet Mohammed; he was born in Mecca (Makkah) in 598 BC inside the Kaa'bah, the holiest place for Muslims, and killed in 661 AD in Kufa, 10 km away from his grave. Shia Muslims know him as a Caliph or Imam, after the Prophet Mohammed (he ruled from 632 to 661 AD). However, Sunni Muslims account him as the fourth Caliph (656–661 AD) (Allan, 2012). This made Al-Najaf be considered an Islamic heritage city from its creation.

On the other hand, the city underwent difficult circumstances and challenges because of its surroundings and changes, thus bringing destruction and neglect due to unplanned and unstudied urban transformations (Farhan, Abdelmonem & Nasar, 2018). The current status of Al-Najaf Old City does not reflect the sanctity and holiness of the grave of Ali bin Abi-Talib or the many Islamic landmarks, nor the history of the science and culture in the city narration (Abid, 2016). Therefore,

FIGURE 1. Location of Najaf. Elevation map (Urutseg, 2011)

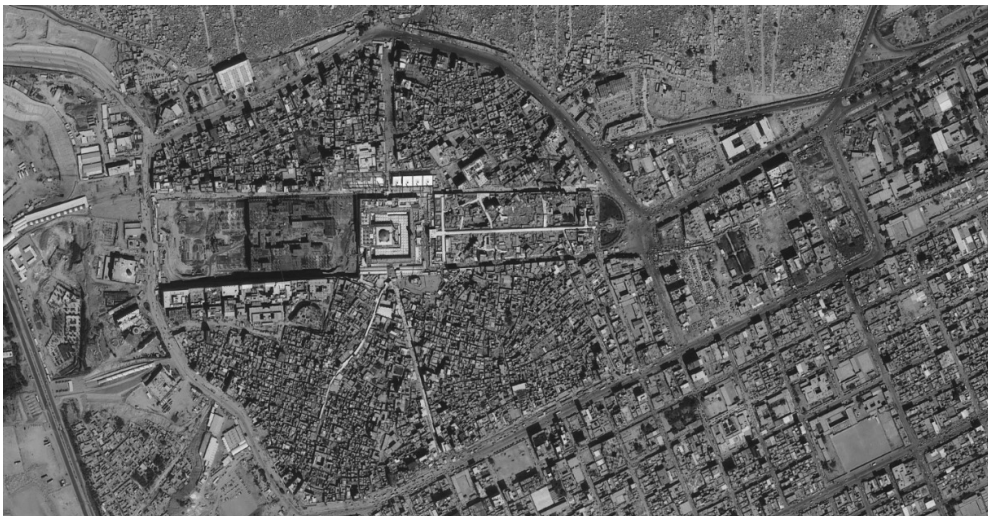

FIGURE 2. Arial view of Al-Najaf Old City (Nasar, 2015)

it is imperative to preserve the heritage assets of the city and the integrity and vitality of the sacred centre (Directorate of Urban Planning of Najaf Governorate, 2006).

Al-Najaf historic city centre

Al-Najaf was located near the city of Kufa (Al-Daraji, 2014) in a high desert plateau, where some tribes lived close

to springs (this was outside the current city), likewise nomads practiced grazing and agriculture (Batuta & Lee, 1829). Imam Ali was buried in this region after his martyrdom, but his sacred tomb remained hidden from the public for decades, as his will, to avoid desecration by his enemies. It remained secret until Imam Jaafar Al-Sadiq, sixth Imam of Shia and one of Imam Ali's grandsons, revealed it during the Abbasid Caliphate around mid-7th century BC (Shah-Kazemi, 2006).

Due the migration of some Islamic groups (Bosworth, 2007) to the city, it began to expand around the holy grave of Imam Ali to reach 2,500 m of perimeter. It was because of the increasing number of visitors (pilgrims) to the holy shrine that numerous houses were built around it. This marked the beginning of the civil and religious architecture in the region (Al-Ansari, 2007). Multiple factors such as those of religious, civilizational and political nature influenced the city's growth and development, thus leaving its features and identity on the urban fabric of the Al-Najaf (Al-Hakim, 2006). The most prominent factor was the religion, which added the religious character inherent in the city. Therefore, the phases of morphological development of the Old City (Fig. 3) can be summarised in two stages (Tabbaa, Mervin & Bonnier, 2014): (1) Phase I, from the establishment of the city until 1765 AD, with the

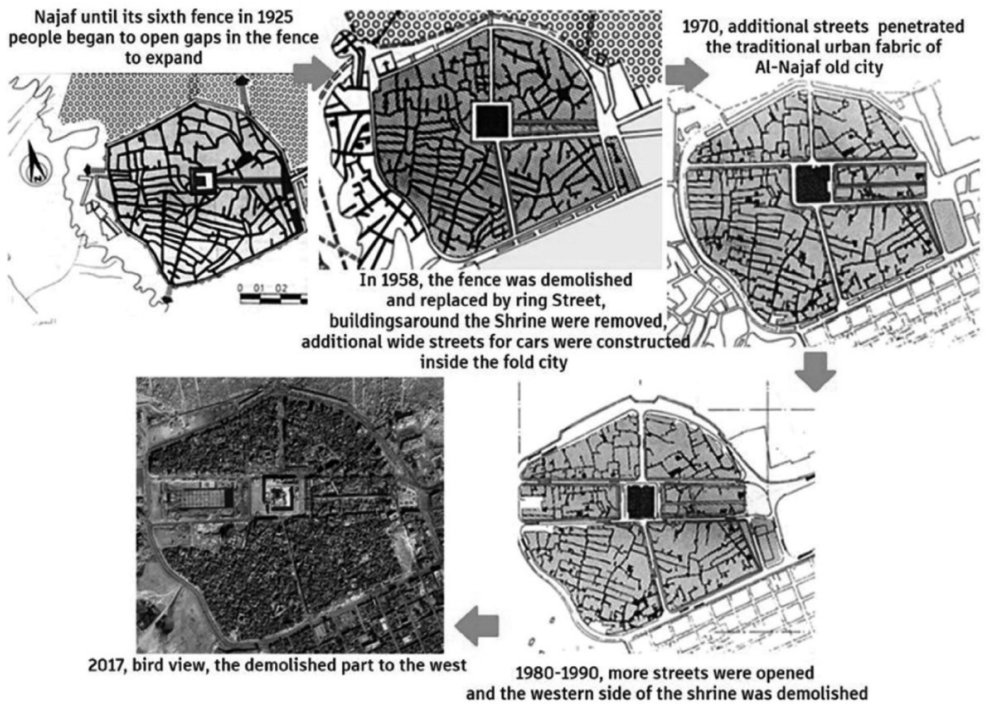

FIGURE 3. Phases of morphological development of Al-Najaf Old City (Farhan, Akef & Nasar, 2020, based on Al-Hakim, 2006)

construction of residential housing in the northern part adjacent to the holy shrine in 1787 AD (Al-Hakim, 2006), which is known as the Mishraq; and (2) Phase II, from 1765 to 1925 AD: Najaf developed and settled at the border of the sixth wall, which was built after the demolition of the fifth wall in 1811 AD (Farhan et al., 2018).

The historic city centre of Al-Najaf is characterised as a compact urban shape, with roads which delimited four neighbourhoods with irregular shapes (Fig. 4): Al Amara, Al-Ula, known as Mishraq; Al-Hawaysh, the smallest one; and Al-Buraq, the latest neighbourhood (Orbasli, 2007; Nasar, 2015).

Methodology

This paper examines the transformations happened in Al-Najaf, as well as their causes and implications, which require gathering specific data on the history, characteristics, circumstances and changing urban planning situation of the sacred city, concretely focusing on its historic city centre. In this sense, the Najaf archives do not contain enough information; therefore, this research had to resort to diverse sources to collect the data, e.g. governmental reports, official information, scientific publications, and analytical conversation with regional authorities, engineers and architects, urban

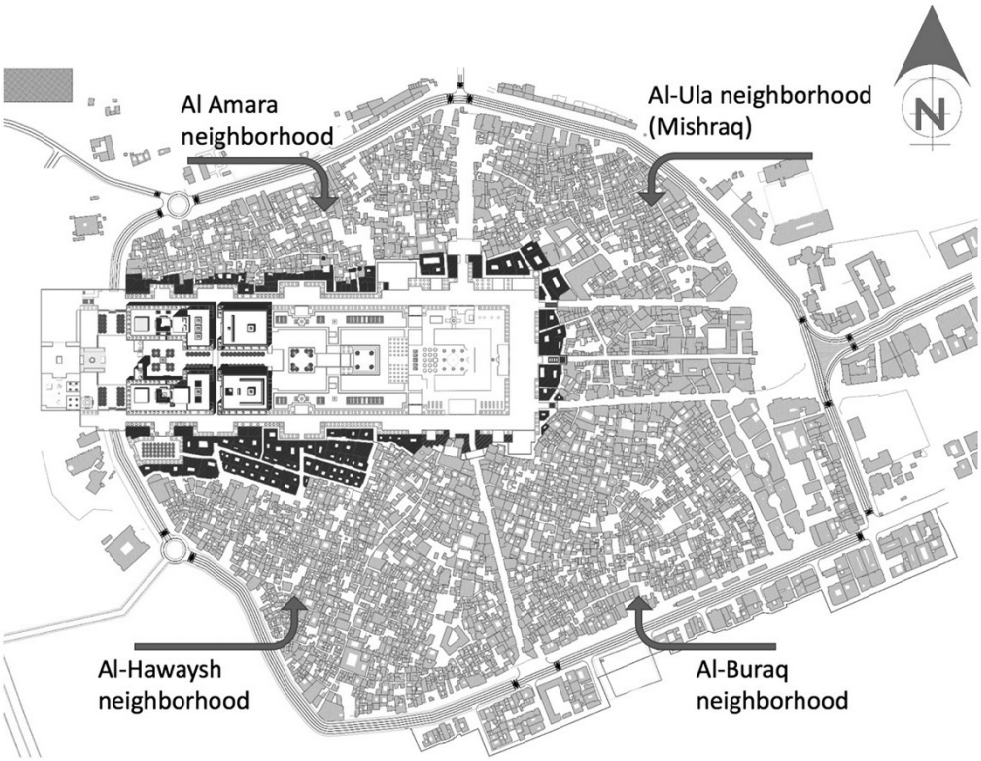

FIGURE 4. Neighbourhoods of Al-Najaf Old City (Department of Planning – Municipality of Najaf, 2020)

and regional planners, NGO members, Muslim seminarians, local citizens, and regular guests in the Old City.

The information gathered was analysed and classified into different categories, according to the nature of the urban transformations in Old Al-Najaf they correspond to.

Factors influencing the transformation of the city

Climate change clearly affects countries all over the world, and this impact can be detected in the local environment (Grimm et al., 2008), in residential areas in the cities, depending on the region and its characteristics, as well as on the short-medium and long-term gravity of the climate (Zubaidi, Kot, Alkhaddar, Abdellatif & Al-Bugharbee, 2018; Hashim et al., 2020), the availability of freshwater and its pollution by industries (Al-Marri et al., 2020; Alnaimi et al., 2020; Alyafei et al., 2020). Also, it was not previous urban planning nor spontaneous decision making that shaped the city of Najaf's urban fabric, but human interaction with the cultural and natural environment (Michell, 1978), which plays an essential role in constituting the composition of the city, its urban fabric, including its characteristics and features over time (Bender, 2006). Thus, the urban form and building typologies respond to the urban environment in which the cities expand (Bashir, 1995), which can be divided into two parts: (1) natural environment: it could be considered invariant beyond weather fluctuations, and (2) cultural environment: it changes throughout the years due to outside factors: the influence of Islamic faith, the impact of social aspects, customs and traditions, economy, politics, technology, and building materials (Kamona, 2010).

On the one hand, concerning the natural environment, the building typologies in Old Al-Najaf are directly determined by the natural environment in the region. This dense, intertwined urban fabric overlaps solid masses with flat surfaces and small openings to the outside (Al--Jibory, 2011) in buildings, thus avoiding direct sunlight on façades. The harsh climate also led to build basements in order to reduce heat transfer and increase humidity. There are various types of basements in Old Al-Najaf: basements located in most houses, with an average depth of approximately 6 m; the basements of the Hess have a depth of 10 m; Al-Qard with around 15 m; and Ras al-Tar, with an average depth of 25 m (this cool type is not usual) (Al-Ansari, 2013). Also, the use of other architectural solutions such as air conditioners, which present decorative and geometric patterns, now define the skyline of the city and have helped increase the hygrothermal comfort inside the buildings by bringing air and coolness into the aforementioned basements (Attia, 2016).

On the other hand, among cultural factors and interacting with environmental aspects, the Islamic religion represents the major factor that determines Old Al-Najaf's urban fabric and spatial composition, and is enhanced by the rest of factors which, in turn, affect the city in varying degrees (Mohammed & Hadi, 2011). The Islamic faith, together with moral values and spiritual principles deriving from it, influences the creation

of religious institutions and schools required to fulfil daily life needs, taking into consideration social aspects and economic efficiency. These are reflected in the city planning of Najaf, in the distribution of land use. The regular use of the transportation system (traffic system, vehicles and pedestrians) also confirms the importance of the locations of these institutions (Mustafa, 2010; Department of Planning – Municipality of Najaf, 2017).

Meanwhile, a closely interwoven organic tissue characterises the urban fabric surrounding the Holy Shrine, in such a way that the pedestrians walk through its human-scale narrow alleys. This design pattern allows the tension-attraction principle between the visitor and the Shrine, since the domes and lights of the houses between buildings can be seen from the alley. According to Al-Amely (2015), the visitor, once arrived at the Shrine, firstly get surprised by this vast, spacious courtyard before the building, which prepares them to be introduced to the holy place and feel the reverence and piety of it. Nevertheless, significant changes in the urban composition of the spaces surrounding the Holy Shrine have taken place due to design and planning practices. They have been removed to isolate the Shrine from the urban environment, which goes against the principle on which the area was designed. In addition, these interventions have brought about a great loss of both heritage characteristics and historic buildings. Moreover, new issues have arisen, such as more traffic around the Holy Shrine, thus causing visual and environmental pollution against the religious and spiritual status of this Shrine. The removal of these surrounding areas has reduced the predominance of the Sahn space on the composition of the city's public space, and has entailed the loss of the surprise element of the Sahn. Furthermore, occidental concepts were implemented in the area to make the Shrine be considered a monumental building. This was carried out by demolishing parts of it in order to create larger spaces to accommodate the new façades more clearly (Tabbaa et al., 2014), which in turn caused the façades of the Shrine to be exposed to the outside world. Also, the exotic architectural styles inserted do not sympathise with the features, traditions and identity of the region, nor they allow to highlight the unique architectural value of the Holy Haidarah Shrine, Imam Ali Shrine. All the above is considered a great loss in the Old City, and the weakening of the hegemony of the Shrine over the city's spatial configuration (Department of Planning – Municipality of Najaf, 2017).

Conclusions

The deterioration of the historic centre and the disappearance of heritage assets and value happened in Al-Najaf have threatened its cultural heritage and unique characteristics. This research, by gathering data from multiple and diverse sources, identified the factors that have brought about the transformations in the Old City. But it is the forced implementation of foreign concepts in the urban planning without respecting the original urban fabric and characteristics that significantly affects the identity and essence of the areas surrounding the Holy Shrine and tears down its unity. In this

sense, damage has been inflicted by removing large parts of the fabric of Najaf under various pretexts, which has brought about the loss of architectural features of heritage value and the isolation of the Shrine from its surroundings. Nonetheless, there is still an opportunity to preserve the authenticity of the city's composition and distinctive features which are part of the past we revere and cherish, although the desire to preserve the legacy of traditional architecture is not enough. Great efforts and effective measures such as urban planning and legal systems are needed to control the ongoing transformation of the Old City.

The policies for urban transformations should not be a reproduction of the past because this would be a cultural stalemate, nor be based on the traditions of others, since that diminishes the Arab Islamic personality and local character. Instead, modern technology and the rational heritage management should be combined to create a new personality that tells the story of this and future generations. The large transformations in the urban configuration of the historic city centre of Najaf have reduced the interaction between the locals, visitors, pedestrians and the urban environment, thus leading to the dispersion of society. Thus, the city is now overcrowded, and the routes are mostly used by vehicles in a way that neglects the needs of pedestrians.

The unique characteristics of the traditional urban fabric of Old Najaf are the result of the interaction of multiple factors, such as natural and cultural environmental factors, which remain the most determinant so far. However, as explained above, there is no justification for the introduction of strange systems or elements that lead to disruption in the balance between the content of the urban environment and its unique components. In other words, the traditional urban patterns cannot assimilate modern development as the traditional patterns were carefully and scientifically planned to preserve the Old City's splendour and identity. In this sense, the development projects should be aimed at preserving both the cohesion of the city's torn urban fabric and the visitor's experience – part of the basic visit to the city is an introduction to traditional city life, including religious schools, the work on textiles' transformation (renovation or restoration) and a visit to the Holy Shrine. This would certainly improve the visitors' appreciation and preserve the integrity of the value of Old Najaf's ancient heritage.

Acknowledgements

The authors wish to thank all the parties in the data collection for this research, including authorities, scholars, professionals, organisations members and individuals.

References

Abdelmonem, M.G. (2017). Architectural and urban heritage in the digital age: dilemmas of authenticity, originality and reproduction. *International Journal of Architectural Research: ArchNet-IJAR*, *11*(3), 5-15.

Abid, S.K. (2015). Imam Ali Shrine, institution and cultural monument: the implications of cultural significance and its impact on local conservation management. *Structural Studies, Repairs and Maintenance of Heritage Architecture XIV*, *153*, 87-98.

Abid, S.K. (2016). *An examination of heritage protection and conservation practices in the pilgrimage city of Najaf* (PhD thesis). University of Sheffield, Sheffield. https://etheses.whiterose.ac.uk/17278/1/Sadiq.Abid.pdf

Ahmed (1945). *The Euphrates Valley and the Siddh Indian Project*. Baghdad: Al-Ma'arif Press.

Al-Amely, M.F. (2015). *The impact of Kufa mosque in the urban growth of the Holy City*. Baghdad: University of Technology.

Al-Ansari, R.M. (2007). *Proposal for the development of the center of the city of Najaf and expansion of kindergarten Al-Haidariya, Mujahmah al-Muhajir*. London: Association for the Care of Iraqis.

Al-Ansari, R.M. (2013). *Najaf: past and present*. Baghdad: Al-Mamoon House for Translation and Publishing.

Al-Daraji, H.M. (2014). *The heritage buildings in Najaf: Characteristic between past and present*. Baghdad: Ministry of Tourism and Antiquities.

Al-Hakim, H. (2006). *Detailed of the history of Najaf: scientific and cultural*. Qom, Iran: The Hydrological Library.

Al-Jibory, K.S. (2011). Management of Imam Ali Shrine in Najaf. *Afaaq Najafiya*, *2011*, 70-147.

Al-Maliki, F. (2011). *Najaf heritage buildings under threat*.

Al-Marri, S., Alquzweeni, S.S., Hashim, K.S., Alkhaddar, R., Kot, P., Alkizwini, R.S., Zubaidi, S.L. & Al-Khafaji, Z.S. (2020). Ultrasonic-Electrocoagulation method for nitrate removal from water. *IOP Conference Series: Materials Science and Engineering*, *888*, 012073. https://doi.org/10.1088/1757-899X/888/1/012073

Allan, J.W. (2012). *The art and architecture of twelver Shi'ism: Iraq, Iran and the Indian Sub-continent.* London: Azimuth Editions.

Alnaimi, H., Idan, I.J., Al-Janabi, A., Hashim, K.S., Gkantou, M., Zubaidi, S.L., Kot, P. & Muradov, M. (2020). Ultrasonic-electrochemical treatment for effluents of concrete plants. *IOP Conference Series: Materials Science and Engineering*, *888*, 012063. https://doi.org/10.1088/1757-899X/888/1/012063

Alyafei, A., Alkizwini, R.S., Hashim, K.S., Yeboah, D., Gkantou, M., Al Khaddar, R., Al-Faluji, D. & Zubaidi, S.L. (2020). Treatment of effluents of construction industry using a combined filtration-electrocoagulation method. *IOP Conference Series: Materials Science and Engineering*, *888*, 012032. https://doi.org/10.1088/1757-899X/888/1/012032

Attia, A.N. (2016). *Protection and promotion of cultural heritage to enhance the Iraqi cultural identity*. Najaf: Dar Al-Turath.

Bashir, S. (1995). The renewal of islamic law: Muhammad Baqer as-Sadr, Najaf and the Shi'i International, Chibli Mallat. *Digest of Middle East Studies*, *4*(2), 64-67. https://doi.org/10.1111/j.1949-3606.1995.tb00552.x

Batuta, I. & Lee, S. (1829). *The travels of Ibn Batűta*. London: Oriental Translation Committee. Retrieved from: https://hdl.handle.net/2027/mdp.39015005211621

Bender, T. (2006). *Sacred space, sacred art*. Retrieved from: tombender.org/sustdesignarticles/SACRED_SPACE.pdf [access dd.mm.yr].

Bosworth, C.E. (2007). *Historic Cities of the Islamic World*. Leiden: Brill Academic Publishers.

Correia, J. & Taher, M. (2015). Traditional Islamic cities unveiled: the quest for urban design regularity. *Gremium*, *2*(4), 21-36.

Department of Planning – Municipality of Najaf (2017). *Foundation of physical planning of Najaf*. Najaf: Municipality of Najaf.

Department of Planning – Municipality of Najaf (2020). *Built areas in the Old City of Al-Najaf.* Najaf: Municipality of Najaf.

Directorate of Urban Planning of Najaf Governorate (2006). *Urban Renewal of the Najaf City Center*. Najaf: Directorate of Urban Planning of Najaf Governorate.

Farhan, S.L., Abdelmonem, M.G. & Nasar, Z.A. (2018). The urban transformation of traditional city centres: holy Karbala as a case study. *Archnet-IJAR*, *12*(3), 53-67. https://doi.org/10.26687/archnet-ijar.v12i3.1625

Farhan, S.L., Jasim, I.A. & Al-Mamoori, S.K. (2019). The transformation of the city of Najaf, Iraq: analysis, reality and future prospects. *Journal of Urban Regeneration and Renewal*, *13*(2), 160-171.

Farhan, S.L., Akef, V. & Nasar, Z. (2020). The transformation of the inherited historical urban and architectural characteristics of Al-Najaf's Old

City and possible preservation insights. *Frontiers of Architectural Research*, *9*(4), 820-836. https://doi.org/10.1016/j.foar.2020.07.005

Grimm, N.B., Faeth, S.H., Golubiewski, N.E., Redman, C.L., Wu, J., Bai, X. & Briggs, J.M. (2008). Global change and the ecology of cities. *Science*, *319*(5864), 756-760. https://doi.org/10.1126/science.1150195

Hashim, K.S., Ewadh, H.M., Muhsin, A.A., Zubaidi, S.L., Kot, P., Muradov, M., … Al-Khaddar, R. (2020). Phosphate removal from water using bottom ash: adsorption performance, coexisting anions and modelling studies. *Water Science and Technology*, *83*(1), 77-89. https://doi.org/10.2166/wst.2020.561

Hendrigan, C. (2019). *A future of polycentric cities: how urban life, land supply, smart technologies and sustainable transport are reshaping cities*. Singapore: Palgrave Macmillan. https://doi.org/10.1007/978-981-13-9169-9

Kamona, H.A. (2010). *Perception in the reconstruction of the city of Najaf as a capital of islamic culture 2012*. Najaf: Association Forum Posting in Najaf.

Matar, S. (2013). *Iraq: Seven thousand years of life*. Beirut: Arab Foundation for Publishing.

Merzah, M.S. (2006). *Heritage buildings in Najaf: the religious architecture and service architecture*. Baghdad: University of Baghdad.

Michell, G. (1978). *Architecture of the Islamic world: its history and social meaning*. London: Thames and Hudson.

Mohammed, M. & Hadi, E. (2011). The best way to deal with the centre of Najaf old town. In *Development and Planning* (p. 11). Baghdad: University of Baghdad.

Mustafa, M.H. (2010). *Information technology role in the development of Al-Najaf City*. Baghdad: University of Baghdad.

Nasar, Z. (2015). The sacred shrines on directing the movement axes within the urban fabric of the Islamic holy cities – An-Najaf Al-Ashraf as a case study. *Journal of University of Babylon for Engineering Sciences*, *23*(4).

Orbasli, A. (2007). Training conservation professionals in the Middle East. *Built Environment*, *33*(3), 307-322. https://doi.org/10.2148/benv.33.3.307

Shah-Kazemi, R. (2006). Ali Ibn Abi Talib. In J.W. Meri (ed.), *Medieval islamic civilization: an encyclopedia* (pp. 36-37). New York: Routledge Taylor & Francis Group. Retrieved from: http://opac.regesta-imperii.de/id/1429519

Smith, L. (2006). *Uses of heritage*. London: Routledge Taylor & Francis Group. https://doi.org/10.4324/9780203602263

Tabbaa, Y., Mervin, S. & Bonnier, E. (2014). *Najaf, the gate of wisdom. History, heritage & significance of the holy city of the Shi'a*. Paris: United Nations Educational, Scientific and Cultural Organization. Retrieved from: https://unesdoc.unesco.org/ark:/48223/pf0000228324

Urutseg (2011-03-16). *Iraq physical map*. Retrieved from: https://en.wikipedia.org/wiki/Najaf#/media/File:Iraq_physical_map.svg

Zubaidi, S.L., Al-Bugharbee, H., Muhsin, Y.R., Hashim, K. & Alkhaddar, R. (2020). Forecasting of monthly stochastic signal of urban water demand: Baghdad as a case study. *IOP Conference Series: Materials Science and Engineering*, *888*, 012018. https://doi.org/10.1088/1757-899X/888/1/012018

Zubaidi, S.L., Kot, P., Alkhaddar, R.M., Abdellatif, M. & Al-Bugharbee, H. (2018). Short-term water demand prediction in residential complexes: case study in Columbia City, USA. *2018 11th International Conference on Developments in eSystems Engineering (DeSE)*, *2018*, 31-35. https://doi.org/10.1109/DeSE.2018.0001

Summary

Factors influencing the transformation of Iraqi holy cities: the case of Al-Najaf. The historic centre of the Iraqi city of Al-Najaf embraces a seasonal pilgrimage to its holy sites that forces unusual urban conditions. This paper examines the impact of development projects and studies on the heritage integrity of the public (religious). This paper, therefore, recommends raising public awareness to adopt design approaches to face the overflow of visitors and the loss of heritage identity.

Authors' address:

Sabeeh Lafta Farhan – corresponding author

(https://orcid.org/0000-0002-4460-1268)
Wasit University
Engineering College
Department of Architectural Engineering
Al-Rabee Street, Al Kut, Wasit
Iraq
e-mail: drsabeeh@uowasit.edu.iq

Daniel Antón
(https://orcid.org/0000-0002-4267-2433)
Universidad de Sevilla
Escuela Técnica Superior de Ingeniería de Edificación
Departamento de Expresión Gráfica e Ingeniería en la Edificación
4A Reina Mercedes Avenue, 41012 Seville
Spain
Nottingham Trent University
School of Architecture, Design and the Built Environment
The Creative and Virtual Technologies Research Laboratory
50 Shakespeare Street, Nottingham NG1 4FQ
UK

Venus Suleiman Akef
(https://orcid.org/0000-0002-0822-8259)
University of Technology
Department of Architect Engineering
Baghdad
Iraq

Salah Lafta Zubaidi
(https://orcid.org/0000-0003-4229-9314)
Wasit University
College of Engineering
Department of Civil Engineering
Wasit
Iraq

Khalid Safaa Hashim
(https://orcid.org/0000-0001-9623-4060)
University of Babylon
Environmental Research and Studies Centre
Hill, Babylon City
Iraq
BEST Research Institute
Liverpool John Moores University
Liverpool
UK

Instruction for Authors

The journal publishes in English languages, peer-reviewed original research, critical reviews and short communications, which have not been and will not be published elsewhere in substantially the same form. Author of an article is required to transfer the copyright to the journal publisher, however authors retain significant rights to use and share their own published papers. The published papers are available under the terms of the principles of Open Access Creative Commons CC BY-NC license. The submitting author must agree to pay the publication charge (see Charges).

The author of submitted materials (e.g. text, figures, tables etc.) is obligated to restricts the publishing rights. All contributors who do not meet the criteria for authorship should be listed in an Acknowledgements section of the manuscript. Authors should, therefore, add a statement on the type of assistance, if any, received from the sponsor or the sponsor's representative and include the names of any person who provided technical help, writing assistance, editorial support or any type of participation in writing the manuscript.

Uniform requirements for manuscripts

Manuscript should be sent with tables, graphs and abstract on separate pages by e-mail: iks_pn@sggw.edu.pl. All figures and tables should be placed near their reference in the main text and additionally sent in a form of data files (e.g. Excel, Visio, Adobe Illustrator, Adobe Photoshop, CorelDRAW). Figures are printed in black and white on paper version of the journal (color printing is combined with an additional fee calculated on a case-by-case basis), while on the website are published in color.

The size of the manuscript should be limited up to 10 pages including overview, summary, references and figures (the manuscript more than 13 pages is unacceptable); Please set the text format in single column with paragraphs (A4 paper format), all margins to 25 mm, use the font Times New Roman, typeface 12 points and line spacing one and half.

The submitted manuscript should include the following parts:

- name and SURNAME of the author(s) – up to 5 authors
- affiliation of the author(s), ORCID Id (optional)
- title of the work
- key words
- abstract (about 500 characters)
- text of the paper divided into: Introduction, Material and Methods, Results and Discussion, Conclusions, References and Summary
- references in APA style are listed fully in alphabetical order according to the last name of the first author and not numbered; please find the details below
- post and mailing address of the corresponding author:

  Author's address:
  Name, SURNAME
  Affiliation
  Street, number, postal code, City
  Country
  e-mail: adress@domain

- Plagiarism statement (http://iks.pn.sggw.pl/Szablony/PublEth.pdf)

Reference formatting

In the Scientific Review Engineering and Environmental Sciences the APA 6th edition style is used.

Detailed information

More information can be found: http://iks.pn.sggw.pl